NAMIBIA UNIVERSITY OF SCIENCE AND TECHNOLOGY

TITLE

Integrating Field and Remote Sensing Approaches to Quantify Forest Structure and Biomass in the Miombo Ecoregion

Hermane Diesse Mwamba

Thesis/Dissertation submitted in fulfilment/ of the requirements for the Doctorate degree in PhD in Natural Resource Management and Ecology at the Namibia University of Science and Technology

Supervisor:

Professor Vera De Cauwer

Namibia University of Science and Technology

Co-Supervisors:

Dr. John L. Godlee

Smithsonian National Museum of Natural History

Dr. Nichola Knox

Downforce Technologies

March 2026

Declaration

I, *Hermane Diesse* hereby declare that the work contained in the thesis entitled: *Integrating Field and Remote Sensing Approaches to Quantify Forest Structure and Biomass in the Miombo Ecoregion* is my own original work and that I have not previously in its entirety or in part submitted to any university or higher education institution for the award of a qualification.

Signature:



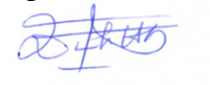
Date: 25 march 2026

Retention and Use of Thesis

I, Hermane Diesse, being a candidate for the degree of Doctor of Philosophy in Natural Resource Science, accept the requirements of the Namibia University of Science and Technology relating to the retention and use of theses deposited in the Library and Information Services.

In terms of these conditions, I agree that the original of my thesis deposited in the Library and Information Services will be accessible for purposes of study and research, in accordance with the normal conditions established by the Librarian for the care, loan or reproduction of theses.

Signature:



Date: 25 march 2026

Table of Contents

Table of Contents iii
List of Figures vii
List of Tables x
List of Acronyms xi
Acknowledgements xv
Abstract xvii
Chapter 1: General Introduction 1
1.1 Background 1
1.2 Research objectives 4
1.3 Significance of the Study 6
1.4 Limitations of the Study 6
1.5 Data sources 7
1.6 Thesis structure 8
1.7 References 11
Chapter 2: Rainfall shapes the dominance of large trees and forest biomass across tree-sizes in the Miombo ecoregion 17
Abstract 17
2.1 Introduction 18
2.2 Materials and methods 20
2.2.1 Study area 20
2.2.2 Data collection 20
2.2.3 Data analysis 22
2.2.4 Statistical analysis 27
2.3 Results 29
2.3.1 Stem diameter and biomass distribution across the rainfall gradient 29
2.3.2 Contribution of Large-Diameter Trees to Forest Biomass Structure 30
2.3.3 Patterns of AGB and structure along the rainfall gradient 32
2.3.4 Local drivers of biomass and structure 33
2.4 Discussion 37
2.4.1 Rainfall as a regional driver of forest biomass and structure 37
2.4.2 Local modulation by soils, topography, and fire disturbance 37
2.4.3 Hierarchical regulation and ecological implications 38

2.4.4 Uncertainty related to ancillary datasets 39
2.5 Conclusion 40
2.6 CRediT authorship contribution statement 41
2.7 References 42
Appendix 1 48
Chapter 3: Quantifying unseen woody biomass and diversity in understorey trees and shrubs at the extremes of rainfall in the Miombo ecoregion 52
Abstract 52
3.1 Introduction 54
3.2 Materials and Methods 57
3.2.1 Study area 57
3.2.2 Data collection 59
3.2.3 Data analysis 60
3.2.4 Statistical analysis 63
3.3 Results 65
3.3.1 Floristic composition of the understorey and overstorey layers 65
3.3.2 Distribution of species diversity and woody density across forest layers 65
3.3.3 Contribution of each layer to the total biomass 74
3.4 Discussion 78
3.4.1 Variation in AGB across layers and rainfall gradient 78
3.4.2 Variation in AGB across rainfall gradient 78
3.4.3 Contribution of each layer to the total AGB 79
3.4.4 Floristic composition, species diversity and woody density across forest layers and sites 79
3.4.5 Total species richness 80
3.4.6 Overstorey and Understorey species diversity 80
3.4.7 Variation in shrub and small tree species diversity across rainfall gradient 81
3.4.8 Future research and possible implications 83
3.5 Conclusion 84
3.6 CRediT authorship contribution statement 84
3.7 References 85
Appendix 2 93
Chapter 4: Linking subcanopy vegetation to canopy structure and forest attributes in dry Namibian woodlands 105
Abstract 106
4.1 Introduction 107

4.2 Materials and methods 110
4.2.1 Study area 110
4.2.2 Data collection 111
4.2.3 Inventory data 111
4.2.4 TLS data 112
4.2.5 TLS processing 115
4.2.6 TLS derived parameters 116
4.2.7 Statistical analysis 118
4.3 Result 121
4.3.1 Structural gradients of canopy metrics across plots 121
4.3.2 Influence of canopy structure on subcanopy vegetation 123
4.3.3 Influence of canopy metrics on key ecological attributes 126
4.4 Discussion 130
4.4.1 Influence of canopy structure on subcanopy vegetation 130
4.4.2 Canopy metrics differentiation and vegetation structure characterisation 131
4.4.3 Influence of canopy structure on field-measured ecological attributes 132
4.4.4 Methodological considerations and limitations 133
4.5 Conclusion 134
4.6 CRediT authorship contribution statement 134
4.7 References 135
Appendix 3 141
Chapter 5: Evaluating GEDI Canopy Height Accuracy Across Forest Structural Gradients in the Miombo Ecoregion 142
Abstract 142
5.1 Introduction 143
5.2 Materials and methods 146
5.2.1 Study area 146
5.2.2 Data 146
5.2.3 Statistical analysis 155
5.3 Results 158
5.3.1 Variation in GEDI Canopy Height Across Environmental Gradients 158
5.3.2 Accuracy of GEDI Canopy Height vs. Field-Measured Height 159
5.3.3 Environmental and Structural Drivers of GEDI Canopy Height Error 160
5.3.4 Modelling Field-Measured Tree Height using Random Forest 161
5.3.5 Variable Importance analysis 166

5.3.6 Comparison with Global Canopy Height Product 168
5.4 Discussion 169
5.4.1 Accuracy of GEDI height compared to the field height 169
5.4.2 Factors influencing GEDI error 170
5.4.3 Effects of National Forest Inventory Data 170
5.4.4 GEDI Canopy Height Across Environmental Gradients 171
5.4.5 Modelling Field Canopy Height 171
5.4.6 Residual Patterns of the Model 172
5.4.7 Comparison with Global Canopy Height Products 172
5.4.8 Limitations and future directions 173
5.5 Conclusion 173
5.6 CRediT authorship contribution statement 174
References 175
Appendix 4 182
Chapter 6: Synthesis and conclusion 184
6.1 Integrative Overview and Conceptual Foundations 184
6.2 Conceptual Framework 185
6.3 Synthesis of Results Across the Four Research Questions 186
6.3.1 Climatic Control of Vegetation structure and Biomass Allocation Across Tree Size Classes 186
6.3.2 Disturbance and Environmental Controls on Vegetation structure and Biomass Partitioning 188
6.3.3 GEDI Performance Across Structural Gradients and Calibration of Regional Canopy Height Models 189
6.4 Implications for Ecology, Remote Sensing, and Forest Monitoring in the Miombo Ecoregion 191
6.4.1 Ecological Implications: Rethinking Biomass Allocation and Large-Tree Dominance 191
6.4.2 Implications for Forest Dynamics: Fire as a Structural Filter 192
6.4.3 Implications for Remote Sensing: Structural Controls on Spaceborne LiDAR Performance 192
6.4.4 Implications for Management, Conservation, and Carbon Accounting 193
6.5 Limitations and Directions for Future Research 193
6.6 Concluding remarks 195
6.7 References 196

List of Figures

Figure 1.1. Thesis structure linking environmental gradients, vegetation structure, biomass allocation, and the accuracy of spaceborne LiDAR canopy height 10
Figure 2.1. Location of the plots across the vegetation types in Miombo ecoregion. Classification of vegetation type is adapted from the WWF Global 200 Ecoregions 22
Figure 2.2. Variation in Stem density and Mean total AGB across four rainfall classes. 29
Figure 2.3. Relationships between total above-ground biomass (AGB) and structural indicators of large-diameter tree dominance across Miombo forest plots 31
Figure 2.4.Relationships between mean annual precipitation and stand-level vegetation structure across the Miombo ecoregion. 33
Figure 2.5. Standardised coefficients (β) and 95 % confidence intervals from linear mixed-effects models predicting forest structural and biomass attributes across Miombo ecoregion biomes. 34
Figure 2.6. Partitioning of variance between and within Miombo vegetation types for each biomass-related attribute. Bars show the proportion of total variance explained by differences among vegetation types (green) and by within-vegetation types heterogeneity among plots (blue). 36
Figure 3.1. Typical representation of the understorey layer in dry and wet Miombo 55
Figure 3.2. Location of study sites in Namibia and DRC. 58
Figure 3.3. Plot design of the understorey subplots. 60
Figure 3.4. Variation in species richness, Shannon Equitability, woody plant density, and Shannon-Wiener index by site for understorey (small trees and shrubs) and overstorey (large trees and saplings) layers. Sites are ordered by mean annual precipitation: Kanovlei = 500 – 550 mm; Hamoye = 560 mm; Zambezi = 600 – 700 mm; Kibundu = 1200 mm; Mikembo = 1200 mm. 66
Figure 3.5. Changes in Diversity Indices and Woody Plant Density for Shrubs and Small Trees vs. Saplings and Large Trees.Sites are ordered by mean annual precipitation: Kanovlei = 500 – 550 mm; Hamoye = 560 mm; Zambezi = 600 – 700 mm; Kibundu = 1200 mm;Mikembo = 1200 mm. 70
Figure 3.6. Distribution of Woody Plant Density tand AGB across height classes. 73
Figure 3.7. Above-ground biomass (AGB) stored by each layer within each site with a threshold of DBH ≥ 5 cm. 74
Figure 3.8. Variation of understorey species richness (understorey shrub species richness and understorey tree species richness) with overstorey basal area 82

Figure 3.9. Variation of the percentage of the AGB stored in the understorey layer with the overstorey basal area 83
Figure 4.1 Study sites. Plots installed in Kanovlei and Hamoye State Forest are coloured in red. 111
Figure 4.2. Layout of the reflectors and TLS scanning position. 113
Figure 4.3. Reflectors used as tie points during the scanning. 114
Figure 4.4. Schematic diagram summarising the data processing and analysis workflow for the TLS data. 116
Figure 4.5. Vertical foliage structure derived from TLS data across forest plots. 117
Figure 4.6. Correlation matrix showing pairwise Spearman correlation coefficients among TLS-derived canopy structural metrics.Positive correlations are shown in red and negative in blue. Colour intensity of the squares indicates the strength of the correlation 122
Figure 4.7. Principal Component Analysis (PCA) biplot of TLS-derived canopy structural metrics across 5 × 5 m grid cells within plots (H1, H3, SK2). 123
Figure 4.8. Relationships between the Plant Density Index (PDI) of the subcanopy layer (0.1–3 m) and canopy structural metrics across plots. Green lines represent fitted trends using Generalised Additive Models (GAMs), while blue points show individual 5 x 5 m subplot values. Solid green lines indicate statistically significant relationships ($p < 0.05$), while dashed lines represent non-significant trends. Spearman's rank correlation coefficient and corresponding p-value are reported within each scatterplot 125
Figure 4.9. Relationships between TLS-[A1.1]derived canopy structure metrics and field-measured ecological attributes (species richness, tree density, and above-ground biomass) across plots. 127
Figure 5.1 Left: Major savanna vegetation types within southern Africa. Right: Plot locations within southern Africa across the gradient of mean annual precipitation (MAP, mm) 147
Figure 5.2 Visual example of filtered GEDI footprints for the study countries from 2019 to 2024. Zoomed insets show examples of plots with and without intersecting GEDI footprints. 151
Figure 5.3. Variation in GEDI-derived canopy height across environmental gradients in Miombo ecoregion. 158
Figure 5.4. Comparison between GEDI-derived canopy height and field-measured canopy height. 159
Figure 5.5 Distribution of GEDI error across field-measured height (n = 94). The annotation in red color represents the average underestimation at 10m and 20m canopy height. 160
Figure 5.6. Variation in GEDI canopy height error across vegetation structure and environmental gradients. 161

Figure 5.7. Observed versus predicted field-measured canopy height using Random Forest models. ... 163
Figure 5.8. Diagnostic plots for the Random Forest model predicting field canopy height (Model RF 1, RF 2, and RF 3). ... 164
Figure 5.9. Boxplots showing the distribution of prediction residuals in meter (Field Height − Predicted Height) ... 165
Figure 5.10. Variable importance ... 167

List of Tables

Table 2.1 . Structural dominance of large trees along rainfall gradient. Mean stand-level attributes are summarised for 25 rainfall classes (300 to above 1700) 26
Table 3.1. Comparison of species richness, Shannon-Wiener index, Shannon equitability index, above-ground biomass (AGB), and woody plant density between overstorey and understorey layers. . Here the growth forms are combined. Values are presented as mean ± standard deviation. Letters indicate significant differences among sites for each metric within each layer (overstorey or understorey), with different letters (e.g., "a," "b," "c") denoting statistically distinct groups ($p < 0.05$). 68
Table 3.2. Species richness and percentage contribution to total species richness of small trees, shrubs, and saplings and large trees across sites. 72
Table 3.3 Top five species contributing to overstorey and understorey above-ground biomass (AGB) at each site. 76
Table 4.1 TLS acquisition parameters 112
Table 4.2 Description of canopy structure metrics derived from TLS data used in this study 118
Table 4.3. Summary of the generalised linear mixed model (GLMM) examining the influence of the canopy metrics on the subcanopy PDI. 126
Table 4.4. Summary of Generalized Additive Models (GAMs) evaluating the influence of canopy structural metrics derived from TLS on field-measured ecological attributes. For each predictor, the deviance explained (%), estimated degrees of freedom (EDF), and p-value for the smooth term are reported. Models used a Poisson distribution for species richness and tree density, and a Gaussian distribution for biomass. 129
Table 5.1 Details of sampling sites used in this study, including sample sizes, dataset codes, principal investigators, associated projects, and whether the data originated from national forest inventories.. 148
Table 5.2 Variables used in the random forest to model canopy height 154
Table 5.3 Performance of global canopy height products and Random Forest models compared to field-measured canopy height (n = 14) 168

List of Acronyms

AGB: Above-Ground Biomass

BD: Basal Diameter

BEF: Biodiversity-Ecosystem Functioning

CD: Crown Diameter

CHM: Canopy Height Model

CSF: Cloth Simulation Function

CL: Coastal and Lowland forests

Cm: Centimetre

CPA: Canopy Projected Area

CV: Coefficient of Variation

CWD: Climatic water deficit

DBH: Diameter at Breast Height

DBH_CV: Coefficient of Variation in DBH

DBH_skew: Skewness

DBH_kurt: Kurtois

DBH_{50}%: diameter threshold above which trees cumulatively accounted for 50% of total plot AGB

DRC: Democratic Republic of the Congo

E: Environmental stress

EDF: Degrees Of Freedom

EVI: Enhanced Vegetation Index

FHD: Foliage Height Diversity

GAM: Generalised Additive Model

GDOP: Geometric Dilution of Precision

GEDI: Global Ecosystem Dynamics Investigation

GEE: Google Earth Engine

GFCH: Global Canopy Height Product

GLMM: Generalised Linear Mixed-Effects Model

GNSS: a Global Navigation Satellite System

GRD: Ground Range Detected

GS: Grassland and Savanna

H1: plot located in Hamoye state forest established before 2023 but re-measured in 2023

H3: plot 3 located in Hamoye state forest established in 2023

H4: plot 4 located in Hamoye state forest established in 2023

H': Shannon-Wiener index

HH: horizontal transmit/horizontal receive backscatter coefficients

HV: horizontal transmit/vertical receive backscatter coefficients

Ha: Hectare

Icesat: Ice, Cloud, and land Elevation Satellite

IW: Interferometric Wide

J: Shannon equitability index

JAXA: Japan Aerospace Exploration Agency

K1: plot located in Kanovlei state forest established before 2023 but re-measured in 2023

Kg: Kilogram

LiDAR: Light Detection And Ranging

LME: Linear Mixed-Effects Model

M1: plot 1 located in Mikembo reserve established before 2023 but re-measured in 2023

M2: plot 2 located in Mikembo reserve established in 2023

M3: plot 3 located in Mikembo reserve established in 2023

MAE: Mean Absolute Error

MAP: Mean Annual Precipitation

MAT: Mean Annual Temperature

MCD64A1: MODIS Monthly Burned Area Product

MDW: Mopane and dry Woodland

MERIT: Multi-Error-Removed Improved

Mg: Megagrams

Mm: millimetre

MM: Montane Forest and mosaic

MRV: Monitoring, Reporting and Verification

MW: Miombo woodland

NASA: National Aeronautics and Space Administration

NBR: Normalized Burn Ratio

NDMI: Normalised Difference Moisture Index

NDI: Normalised Difference Index

NDVI: Normalised Difference Vegetation Index

NDRI: Normalised Difference Radar Index

NDWI: Normalised Difference Water Index

NFI: National Forest Inventory

QMD: Quadratic Mean Diameter

PALSAR: Phased Array type L-band Synthetic Aperture Radar

PCA: Principal Component Analysis

PAI: Plant Area Index

PDI: Plant Density Index

PET: Monthly Potential Evapotranspiration

R^2: Coefficient of determination

Rh98: 98th percentile of GEDI canopy height

REDD+: Reducing Emissions from Deforestation and Forest Degradation Plus

RF: Radom Forest

RMSE: Root Mean Square Error

RVI: Radar Vegetation Index

SK1: plot 1 located in Kanovlei state forest established in 2023

SK2: plot 2 located in Kanovlei state forest established in 2023

SAVI: Soil-Adjusted Vegetation Index

SD: Standard deviation

SEOSAW: Socio-Ecological Observatory for Southern African Woodland

SOC: Soil Organic Carbon

SOR: Statistical Outlier Removal

TB: Thickets and Bushlands

TCC: Total Canopy Cover

TLS: Terrestrial Laser Scanning

UTM: Universal Transverse Mercator

VH: vertical transmit/horizontal receive backscatter coefficients

VV: vertical transmit/vertical receive backscatter coefficients WM: Wetlands and Mangroves

WWF: World Wide Fund for Nature

Z1: plot 1 located in Sachinga established in 2023

Z2: plot 2 located in Sachinga established in 2023

Acknowledgements

I would like to express my sincere gratitude to my supervision team for their support throughout this PhD. My deepest appreciation goes to my main supervisor, Prof. Vera De Cauwer. Thank you for accepting to supervise this work and for the countless ways in which you supported me, both academically and personally. Your encouragement, patience, and belief in me carried me through moments when I doubted myself. You pushed me to finish this thesis despite the challenges along the way, and I am truly grateful. I also extend my heartfelt thanks to Dr John Godlee, my first co-supervisor. Whenever I encountered difficulties, you were always available to help. I learned so much from you, from fieldwork techniques to statistical analysis. Your questions and comments improved my writing and strengthened the scientific quality of my work. My sincere thanks go as well to Dr Nichola Knox, my second co-supervisor. You welcomed me to Namibia at the very beginning, organised everything for my arrival, and supported me even after you left the University. Thank you for continuing to guide me and for facilitating my trip to Edinburgh for TLS training.

I gratefully acknowledge the FRAME Scholarship, funded by the European Union and the African Union, for supporting my academic mobility. I also thank the NERC-funded SECO Project (NE/T01279X/1) for sponsoring my fieldwork in Hamoye and Kanovlei, supporting the final months of my PhD, and funding the shipment of the RIEGL VZ-1000 terrestrial laser scanner from the University of Edinburgh to Namibia. I am thankful to the Conservation Action Research Network (CARN) through the ASPIRE Grant Programme for sponsoring my fieldwork in the Democratic Republic of the Congo, and to IDEA WILD for providing the laptop I used for my analyses. My appreciation goes to the NERC Geophysical Equipment Facility for approving my loan request and allowing me to use the TLS in Namibia. I am especially grateful to Alan Hobbs and his team for the intensive TLS training in Edinburgh and for preprocessing the TLS data.

I would like to thank Prof. Kyle Dexter for his remarkable involvement in my PhD. Thank you for welcoming me to the University of Edinburgh, integrating me into your research group, and making sure I had opportunities outside the academic environment as well during my stay in Edinburgh. Your support, your comments on my papers, and your efforts in coordinating the shipment of the TLS were invaluable. I also thank Prof. Jonathan Muledi for hosting me at the University of Lubumbashi and supporting my field campaigns, and Prof. Ajayi Oluibukun for his advice during this PhD study.

A special acknowledgement goes to the SEOSAW network and to all data owners who allowed me to use their plot data. This work depended on years of effort and collaboration by many researchers. I am particularly grateful to Penny Mograbi for facilitating every step of my access to SEOSAW data and ensuring that the process was smooth and supportive.

Fieldwork in Namibia and the DRC would not have been possible without dedicated teams. I thank my Namibian field team: Gabriel Uusiku, Emilia Haupindi, Lenna Naftal, Olivia Haikali, Naftal Cleophas, Vicky Takatu, Sikongo Kemba, Mr Kemba, Derrick Muyunda, and Hilma Amupolo. I also thank my Congolese field team: David Nkulu, Seraphin Irenge, Ben Nkomba, Henriette Lubo, Modeste, and Benedicte Hamba. Their hard work and perseverance made data collection possible in sometimes difficult conditions. I acknowledge the Kanovlei State Forest, Hamoye State Forest, Zambezi State Forest, Sachinga Livestock Development Centre, Kibundu village, and the Mikembo Reserve for their support and for granting permission to establish plots. I want to thank my fellow PhD colleagues, Nadege Versheri and Lenna Naftal, for their friendship and encouragement. Sharing challenges and progress with you both helped me stay motivated. I wish you every success as you continue your own journeys.

To my parents and brothers, thank you for always believing in me. To my wife, Michaelle, and my children, Charis, Furaha Joelle, and Faveur, I owe you more than words can express. Thank you for your patience, love, and sacrifices. I am sorry for my long absences and moments when my priorities seemed far from home. I hope to be more present now. I also take this opportunity to thank everyone that I have not mentioned here. Thanks for your support. Above all, I thank Almighty God. My life, my family, and this thesis are testimony to His grace. I am grateful to Jesus Christ for strength, guidance, and protection throughout this journey.

Abstract

Miombo ecoregion spans more than 3.8 million km² across eleven countries in eastern and southern Africa, forming the continent's largest tropical dry forest system. The vegetation structure (VS) is shaped by strong rainfall gradients, marked seasonality, and recurrent fires, resulting in a heterogeneous mosaic of tall trees, multi-stemmed shrubs, and dense understorey layers. This structural complexity creates challenges for interpreting above-ground biomass (AGB) patterns and for accurately monitoring VS using global remote-sensing products.

This thesis aimed to elucidate the influence of environmental gradients and VS on AGB partitioning and LiDAR canopy height estimation across the Miombo ecoregion using integrated field and remotely sensed data. I explored: (i) the influence of rainfall, disturbance, topography, and soils on biomass allocation across tree size classes and the contribution of large trees; (ii) the contribution of understorey vegetation (stem diameter < 5 cm) to total biomass and species diversity under contrasting rainfall conditions; (iii) the influence of canopy structural attributes on the subcanopy layer (vegetation height < 3 m) and associated ecological properties; and (iv) the extent to which structural and environmental gradients affect the accuracy of spaceborne LiDAR canopy height estimates.

Rainfall emerged as the dominant driver of AGB, increasing from 17 to 133 Mg ha^{-1} along a gradient of 345 to above 2000 mm mean annual precipitation. However, the biomass share of the largest 1% of stems indicated a slight decreasing trend along the gradient. AGB accumulation in Miombo, therefore, results from broad cohorts of medium and large stems rather than a few larger individuals as seen in humid forests. Elevation and fire reduced total AGB but did not diminish biomass stored in large trees, underscoring their resistance to disturbance.

Incorporating understorey into AGB assessments revealed a substantial and previously overlooked carbon pool in dry woodlands. Small trees, saplings, and shrubs contributed up to 28.2% of total AGB in Namibia, compared with only 2.5% in wet DRC. Understorey composition shifted along the rainfall gradient, from shrub-dominated in dry sites to sapling-dominated in wet forests, illustrating how rainfall, fire, and canopy closure shape biomass partitioning and recruitment.

Terrestrial laser scanning provided fine-scale insight into subcanopy patterns. Dense lower canopies promoted subcanopy density and biomass, whereas higher gap fraction reduced subcanopy density and

exerted non-linear effects on AGB. Greater variability in canopy cover reduced both species richness and biomass, highlighting the importance of canopy continuity in woodland.

These structural gradients also conditioned spaceborne LiDAR performance. The Global Ecosystem Dynamics Investigation (GEDI) systematically underestimated canopy height (mean bias -2.79 m), with stronger underestimation in dry woodlands and slight overestimation in wetforests. Regionally calibrated Random Forest models integrating GEDI metrics, climatic and structural variables improved height prediction (explained variance: 64%; bias: –0.27 m), outperforming existing global products.

This thesis demonstrates that Miombo biomass is distributed across broad demographic cohorts, that small-diameter vegetation constitutes an important yet overlooked carbon component, and that VS governs the performance of spaceborne LiDAR. These findings establish new empirical foundations for carbon accounting, forest monitoring, and remote-sensing applications in the region.

Keywords: Miombo ecoregion, Vegetation structure, Biomass, Understorey, Rainfall gradient, LiDAR

Chapter 1: General Introduction

1.1 Background

Vegetation structure refers to the spatial organisation of vegetation, both vertically and horizontally, within a stand (McElhinny et al., 2005; Shugart et al., 2010). It is commonly measured through attributes such as stem density, tree-size distribution, basal area, canopy cover, canopy height and the layering of vegetation from the understorey to the overstorey (Latifi, 2012). Together, these attributes define structural complexity (Pan et al., 2013), which develops over time under the influence of climate, soils, disturbance regimes and demographic processes (Ehbrecht et al., 2021; Gough et al., 2022). This structural arrangement, in turn, governs light distribution, species composition, the effective number of layers and the accumulation of above-ground biomass (AGB) (Balandier et al., 2022; Brüllhardt et al., 2020; Ehbrecht et al., 2016; Mensah et al., 2020), making it a key factor shaping ecological variation across landscapes.

The Miombo ecoregion is one of the world's largest tropical dry woodlands, spanning more than 3.8 million km² across the Democratic Republic of Congo (DRC), Angola, Malawi, Botswana, Zambia, South Africa, Namibia, Zimbabwe, Tanzania, Burundi and Mozambique (Byers, 2001; Mayaux et al., 2004; Timberlake & Chidumayo, 2011). It supports more than 100 million people, providing fuelwood, charcoal, timber, non-timber forest products and grazing resources (Chidumayo & Marunda, 2010; Marunda & Bouda, 2010; Ryan et al., 2016).

In addition to these provisioning services, Miombo ecoregion plays a broader role in ecological and biophysical processes. It contributes to agricultural production by enhancing soil fertility through nutrient inputs and by limiting soil erosion, which is important in areas with inherently low soil fertility (Ryan et al., 2016). It also forms a significant part of the global carbon cycle, storing an estimated 18-24 Pg C in both above and belowground (Ryan et al., 2016). Recent lidar-based studies suggest aboveground carbon stocks may be considerably higher than earlier estimates, pointing to substantial contributions to carbon sequestration in Miombo ecoregion (Demol et al., 2024). The extensive vertical and horizontal root systems of Miombo species confer high coppicing ability, enabling rapid vegetation recovery after disturbances and making the ecosystem highly productive (Handavu et al., 2017). Miombo ecoregion further sustains a wide range of plant and animal species, with a characteristic floristic composition dominated by *Brachystegia*, *Julbernardia* and *Isoberlinia*, and fauna including large herbivores and predators such as elephants, antelopes, giraffes and lions (Timberlake & Chidumayo, 2011).

These functions are increasingly influenced by growing anthropogenic pressures linked to the dependence of local populations on woodland resources. Rising demand for land, fuelwood and charcoal, together with agricultural expansion and resource extraction, can result in woodland degradation and conversion when use exceeds sustainable levels (Ribeiro et al., 2020). Such pressures modify vegetation composition, reduce biomass, and alter ecosystem functioning, with implications for both biodiversity and carbon dynamics.

As a consequence, the Miombo ecoregion exhibits marked spatial variation in vegetation structure, reflecting gradients in rainfall and disturbance regimes (Ribeiro et al., 2020; Timberlake & Chidumayo, 2011). While the floristic core of Miombo *sensu stricto* is dominated by *Brachystegia, Julbernardia* and *Isoberlinia* (Campbell, 1996), the broader ecoregion includes structurally related formations such as Mopane (dominated by *Colophospermum mopane*), *Burkea-Terminalia*, and *Baikiaea* woodlands (Campbell, 1996; De Cauwer, 2023; Strohbach & Petersen, 2007; Timberlake & Chidumayo, 2011; Van Wyk & Van Wyk, 2013). This mosaic reflects shared functional traits, such as strong seasonality, moderate canopy stature, and high disturbance frequency due to fire and herbivory.

Rainfall is a major driver of the Miombo structure, shaping species composition, tree growth and AGB (Davies et al., 2023; Godlee et al., 2021; Sankaran et al., 2005). Drier Miombo (mean annual precipitation; MAP below 1000 mm yr^{-1}) tends to be low-stature and open, whereas wetter Miombo (MAP above 1000 mm yr^{-1}) exhibits greater canopy height, higher basal area and greater vertical stratification (Frost, 1996; Mayaux et al., 2004; Ryan et al., 2012). These patterns indicate that rainfall not only governs total AGB but also likely influences how biomass is distributed among diameter classes and vertical layers. In humid tropical forests, AGB tends to increase with water availability (Mehta et al., 2014; Moore et al., 2018; Shackleton & Scholes, 2011), and a disproportionate share of biomass is concentrated in a small number of large-diameter trees (Bastin et al., 2015; Slik et al., 2013). Whether similar relationships occur in Miombo ecoregion remains unclear. The shorter stature, more open canopies, frequent fire and widespread resprouting strategies (Chidumayo, 2013; Frost, 1996) may produce fundamentally different size-class distributions and biomass allocation patterns along rainfall gradients. Empirical evidence on how large-tree dominance varies across the Miombo ecoregion remains limited.

Additionally, in humid tropical forests, the closed canopy reduces the relative influence of small trees on total AGB (Kindermann et al., 2022; Le et al., 2018), which partly explains why many field inventories exclude trees below 5 or 10 cm diameter at breast height (DBH) in different field inventories (Chave et al., 2014; SEOSAW partnership, 2021). In contrast, demographic and structural

characteristics across the Miombo ecoregion may amplify the importance of smaller trees. Recurrent fire and herbivory increase the abundance of shrubs, saplings and resprouting individuals, and promote multi-stemmed growth forms and high stem turnover (Mapaure, 2013; Ribeiro et al., 2008). These lower strata may contribute substantially to stand-level biomass, especially in the driest regions where large trees are less abundant, and the understorey comprises a major share of total stem density. Yet their contribution along rainfall gradients remains poorly quantified. This limits the understanding of how biomass is partitioned vertically and across size classes in these dry-woodland systems.

Accurately quantifying these multi-layered vegetation components remains challenging over large spatial extents when relying solely on traditional field-based approaches. The measurement of tree height, a key attribute of vegetation structure and an important predictor of biomass, is labour-intensive, spatially restricted and prone to significant errors, with reported inaccuracies ranging from 7% to 15% depending on the method used (Saliu et al., 2021). Remote sensing offers unprecedented opportunities to characterise vegetation structure at regional to global scales, overcoming many of the limitations inherent to field surveys (Knapp et al., 2020; Sexton et al., 2009).

Among recent advances in active remote sensing, spaceborne LiDAR (Light Detection and Ranging) has enabled detailed three-dimensional of forest canopy structure, at regional to global scales (Dubayah et al., 2020; Latifi, 2012; Lucas et al., 2015). The Global Ecosystem Dynamics Investigation (GEDI) mission, launched in 2018 aboard the International Space Station (ISS), represents a major step forward for mapping forest structure (Dubayah et al., 2020).

Unlike classical spaceborne LiDAR systems such as ICESat (Ice, Cloud, and land Elevation Satellite) and ICESat-2, GEDI is a multi-beam, full-waveform LiDAR sensor mounted on a low-Earth orbit platform, collecting data in discrete footprints (~25 m diameter, ~60 m along-track spacing) rather than continuous spatial fields (Duncanson et al., 2020). In addition, GEDI uses three lasers split into eight beams to record the complete vertical return signal within each footprint capturing canopy top, internal structure, and ground elevation (Dubayah et al., 2020; Hancock et al., 2019). GEDI samples the Earth's surface between 51.6° N and 51.6° S, producing non-wall-to-wall observations that require interpolation or data fusion approaches (e.g., Potapov et al., 2021). GEDI initially operated from 2019 to 2023 and resumed data acquisition in 2024, generating billions of waveform footprints and derived products of canopy height, vertical structure, and aboveground biomass.

Despite this progress, GEDI's performance in dry tropical woodlands remains poorly understood, and evaluations are limited to a few site-level studies (Atmani et al., 2022; Li et al., 2023, 2024; Liang et

al., 2023). Existing assessments suggest that GEDI may underestimates canopy height in Miombo and savanna ecosystems, but these findings stem from geographically isolated plots and do not encompass the full spectrum of environmental and structural variability across the region. To date, no study has evaluated GEDI canopy height accuracy across the Miombo ecoregion, leaving a critical gap in understanding the applicability of global height products in African dry forests.

1.2 Research objectives

This thesis aimed to elucidate the influence of environmental gradients and vegetation structure on biomass partitioning and LiDAR canopy height estimation across the Miombo ecoregion using integrated field and remotely sensed data. To achieve this aim, the research was structured around four specific objectives, each associated with a key research question and reference is made to the chapter that addresses it.

The specific research objectives are formulated as follows:

Specific objective 1: To assess the influence of rainfall, disturbance, topography, and soil characteristics on vegetation structure and biomass distribution across tree size classes, with particular emphasis on the contribution of large trees in the Miombo ecoregion.

Question 1: *How do rainfall, disturbance, topography, and soil characteristics influence vegetation structure and biomass distribution across tree size classes, and how do these factors affect the contribution of large trees in the Miombo ecoregion?* (chapter 2).

Rainfall is widely recognised as a major driver of woody biomass in tropical ecosystems (Godlee et al., 2021; Sankaran et al., 2005), yet the extent to which large-diameter trees dominate AGB under different climatic conditions remains poorly quantified in dry woodlands. While humid tropical forests show strong large-tree control of AGB (Slik et al., 2013), it is unclear whether similar patterns occur in Miombo ecoregion, where disturbance by fire strongly influences stand dynamics. Understanding how rainfall with associated environmental factors and local structure interact to shape AGB provides essential context for interpreting biomass distribution across the region.

Specific objective 2: To quantify the contribution of understorey vegetation (DBH < 5 cm) to total woody biomass and species diversity across contrasting rainfall conditions in the Miombo ecoregion.

Question 2: *To what extent does understorey vegetation (DBH < 5 cm) contribute to total woody biomass and species diversity across contrasting rainfall conditions in the Miombo ecoregion?* (Chapters 3)

Most woodland studies focus on stems ≥ 5 or 10 cm DBH, implicitly assuming that small trees and shrubs contribute little to total AGB or diversity. However, in disturbance-prone dry woodlands, open canopy, combined with recurrent fire and resprouting, creates dense understorey layers that may hold substantial biomass and species richness (Kindermann et al., 2022). Quantifying this overlooked component is essential for accurately characterising vegetation structure across rainfall gradients and for evaluating how traditional inventory thresholds may underestimate woody biomass and diversity.

Specific objective 3: To investigate the influence of canopy structural attributes on the subcanopy layer (tree height < 3 m), and associated ecological attributes such as species richness, tree density, and above-ground biomass, in the Miombo ecoregion

Question 3. *How do canopy structural attributes influence the subcanopy layer (tree height < 3 m) and associated ecological attributes, including species richness, tree density, and above-ground biomass?* (chapter 4)

Fine-scale canopy architecture regulates light distribution, microclimate and competitive interactions, which in turn shape subcanopy structure and community composition (Ehbrecht et al., 2016). Yet in dry woodlands, these relationships remain understudied. Advances in terrestrial laser scanning (TLS) offer new opportunities to quantify vertical complexity and canopy cover heterogeneity at high resolution. Understanding how canopy structure modulates subcanopy density and ecological attributes provides mechanistic insight into local-scale drivers of woodland dynamics.

Specific objective 4: To evaluate the impacts of structural and environmental gradients on the accuracy of spaceborne LiDAR canopy height estimates across the Miombo ecoregion.

Question 4. *How do structural and environmental gradients impact the accuracy of spaceborne LiDAR canopy height estimates across the Miombo ecoregion, and under which conditions does GEDI performance improve or decline?* (chapter 5)

Tree height is among the key attributes of vegetation structure and is widely used in allometric models for estimating AGB (Chave et al., 2014; Mugasha et al., 2013). Improving height accuracy is therefore essential for reliable biomass assessment. Although the Global Ecosystem Dynamics Investigation (GEDI) provides unprecedented global coverage of forest vertical structure, its performance in dry African woodlands remains uncertain (Li et al., 2023). Environmental factors such as slope, elevation, and vegetation structure may create systematic biases in canopy-height estimation (Adam et al., 2020). Evaluating GEDI's accuracy and developing regionally calibrated models is crucial for improving remote-sensing-based monitoring of vegetation structure and AGB in the Miombo ecoregion.

1.3 Significance of the Study

This study advances understanding of vegetation structure and biomass dynamics in the Miombo ecoregion, one of the world's most extensive yet understudied dry woodland. By integrating field inventories, terrestrial laser scanning, and spaceborne LiDAR, the thesis bridges local and regional perspectives on how environmental gradients and structural organisation shape biomass partitioning across forest layers. This approach challenges assumptions derived largely from closed-canopy tropical forests, where biomass is typically concentrated in a small number of large stems. By explicitly incorporating shrubs, saplings, and small trees alongside medium and large individuals, the study provides a more realistic basis for evaluating biomass and vegetation dynamics in Miombo ecosystems.

Beyond its ecological contributions, the research strengthens forest monitoring frameworks tailored to dry woodlands. By identifying the structural attributes that affect remote-sensing performance and exposing the limitations of conventional diameter-based inventory thresholds, it supports the refinement of models used for carbon accounting, climate reporting, and national forest assessments. These insights enhance the reliability of remote-sensing products calibrated with field data, which are increasingly used in resource management and Monitoring, Reporting and Verification (MRV) systems underpinning policy mechanisms such as REDD+.

1.4 Limitations of the Study

The scope of this thesis is shaped by both spatial and methodological constraints. Although the work integrates extensive regional datasets and detailed local measurements, certain parts of the Miombo ecoregion remain underrepresented, particularly sites along the intermediate rainfall gradient (between 700 mm and 1200 mm MAP), limiting a full characterisation of understorey contributions across the entire rainfall gradient. In addition, while terrestrial laser scanning and spaceborne LiDAR

provide unprecedented structural detail, their effectiveness is influenced by sampling distribution and field-data availability. For example, many field plots were not intersected by GEDI footprints, constraining the ability to validate spaceborne measurements at all locations.

Moreover, the thesis focuses on above-ground structure and does not examine below-ground biomass or long-term demographic processes such as growth, mortality, and recruitment, which also influence woodland dynamics. These limitations do not undermine the study's findings but instead delineate the point to promising avenues for future research, such as expanding plot coverage, integrating additional sensor platforms, and extending structural monitoring across temporal and environmental gradients.

1.5 Data sources

The research presented in this thesis draws on three complementary sources of information:

- Existing plot-based data
- Publicly available geospatial data including remote sensing
- New plot-based data collected in Namibia and DRC.

The existing plot-based data come from the SEOSAW network (A Socio-Ecological Observatory for Studying African Woodlands). About 2,749 forest inventory plots, which represent the most extensive standardised dataset available for African dry woodlands, were used. These data span major vegetation types and climatic gradients across seven countries, providing a robust basis for examining regional patterns of rainfall, vegetation structure and above-ground biomass.

In addition, full-census woody inventories were collected in 17 plots (0.5–1 ha) distributed across Namibia and the DRC. All woody individuals with a diameter of ≥ 1 cm were measured and identified, generating a detailed dataset that captures shrubs, small trees, and saplings (DBH < 5 cm) , which are generally omitted from conventional inventories and researches (Chave et al., 2014). This data offers a rare opportunity to quantify the biomass and species diversity contained in the understorey.

To characterise vertical structure with high precision, I acquired and processed terrestrial laser scanning (TLS) data across 24 subplots (25 × 25 m) from three plots of 0.5 ha in dry Namibian woodlands. The resulting point clouds provide sub-centimetre information on canopy architecture, gap structure and vegetation density, enabling fine-scale analysis of canopy–subcanopy interactions that cannot be obtained from traditional field measurements.

GEDI spaceborne LiDAR data were downloaded and processed to evaluate canopy height across southern Africa. Data acquisition spans 2019–2023. These measurements underpin the evaluation of canopy-height accuracy across the Miombo ecoregion and support the development of the first regionally calibrated GEDI height-correction models for these structurally heterogeneous dry woodlands.

Ancillary remote sensing and environmental datasets were compiled to provide predictors for canopy height and biomass models:

Climatic data: Mean Annual Precipitation (MAP) was extracted from ERA5-Land for the period 1960–2020.

Soil properties: Soil organic carbon (SOC), clay fraction, and cation exchange capacity (CEC) were obtained from ISRIC SoilGrids v2 at 250 m resolution.

Topography: Elevation and slope were derived from MERIT DEM v1.0.3 (~90 m resolution).

Fire and disturbance: Fire frequency was calculated using MODIS MCD64A1 Monthly Burned Area Product (500 m resolution) over the 10 years preceding field surveys. Additionally, the Normalized Burn Ratio (NBR) was derived from Sentinel-2 surface reflectance (10 m resolution, 2019–2024) to capture fire severity and recent burn scars.

Optical data: Sentinel-2A surface reflectance images (10 m resolution) were used to calculate vegetation and moisture indices, including NDVI, EVI, SAVI, NDMI, and NDWI, capturing canopy greenness, vigour, and water content.

Radar data: Sentinel-1A C-band backscatter (VV and VH) was used to derive VH+VV, VV/VH ratio, NDRI, and Radar Vegetation Index (RVI), while ALOS-2 PALSAR L-band SAR (HH and HV) was used to derive HH+HV, HV/HH, and Normalized Difference Index (NDI), capturing canopy volume and woody biomass structure.

1.6 Thesis structure

The thesis is organised into four data chapters, each addressing one of the main research questions. The core research chapters are presented in the style of stand-alone papers, as they are either published, in the process of revision, or intended for publication later (Figure 1.1). As such, there is some overlap among chapters in introductory, study sites and methodological material.

Chapter 1 provides the background and research questions that guide the thesis. It introduces the ecological context of the Miombo ecoregion, outlines the major knowledge gaps, and presents the overarching aim.

Chapter 2 corresponds to Research Question 1. It examines large-scale patterns of above-ground biomass and vegetation structure across the Miombo ecoregion using 2,749 SEOSAW plots. It evaluates how rainfall and stand structural attributes regulate biomass and large-tree dominance across major vegetation types.

Chapter 3 corresponds to Research Question 2. It investigates the contribution of small trees, saplings and shrubs to woody biomass and species diversity at the extremes of the rainfall gradient. Using plots in Namibia and the DRC, this chapter assesses how focusing only on stems ≥ 5 cm DBH affects our understanding of structural variation.

Chapter 4 corresponds to Research Question 3. It uses terrestrial laser scanning (TLS) to analyse fine-scale canopy architecture in dry Namibian woodlands. It evaluates how canopy cover, vertical complexity and gap structure influence subcanopy vegetation density, species richness and biomass.

Chapter 5 corresponds to Research Question 4. It assesses the accuracy of spaceborne LiDAR height measurements from the GEDI mission across structurally diverse Miombo forests. It analyses environmental and structural drivers of GEDI height error and develops regionally calibrated models to improve canopy height predictions.

Chapter 6 synthesises the major findings across all chapters, provides a conceptual framework, discusses their implications for forest ecology and biomass assessment in the Miombo ecoregion, and highlights directions for future research.

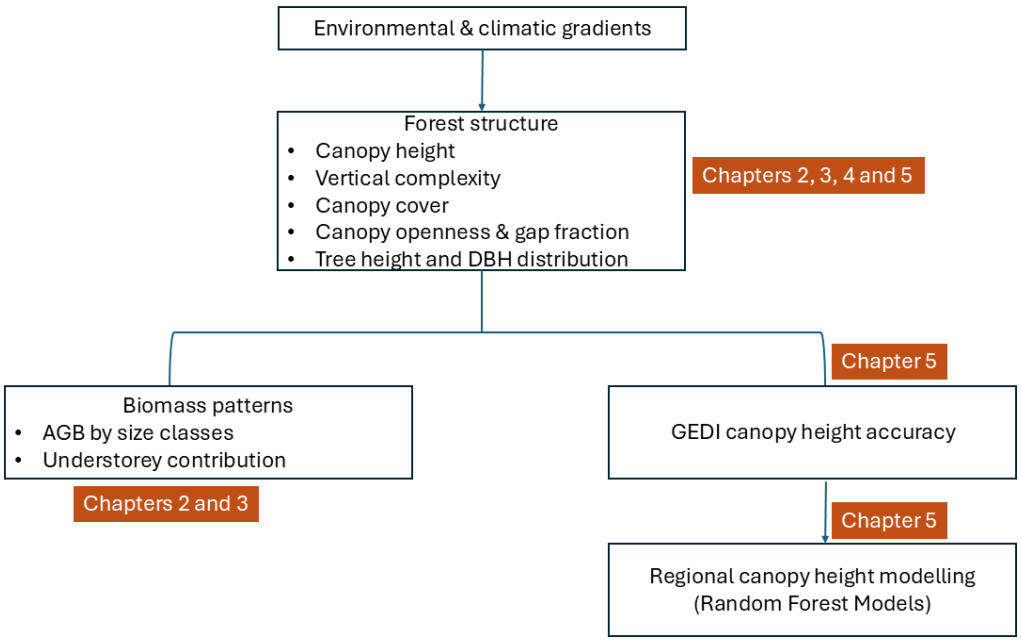


Figure 1.1. Thesis structure linking environmental gradients, vegetation structure, biomass allocation, and the accuracy of spaceborne LiDAR canopy height

1.7 References

Adam, M., Urbazaev, M., Dubois, C., & Schmullius, C. (2020). Accuracy Assessment of GEDI Terrain Elevation and Canopy Height Estimates in European Temperate Forests: Influence of Environmental and Acquisition Parameters. Remote Sensing, 12(23), 3948. https://doi.org/10.3390/rs12233948

Atmani, F., Bookhagen, B., & Smith, T. (2022). Measuring Vegetation Heights and Their Seasonal Changes in the Western Namibian Savanna Using Spaceborne Lidars. Remote Sensing, 14(12), 2928. https://doi.org/10.3390/rs14122928

Balandier, P., Mårell, A., Prévosto, B., & Vincenot, L. (2022). Tamm review: Forest understorey and overstorey interactions: So much more than just light interception by trees. Forest Ecology and Management, 526, 120584. https://doi.org/10.1016/j.foreco.2022.120584

Bastin, J.-F., Barbier, N., Réjou-Méchain, M., Fayolle, A., Gourlet-Fleury, S., Maniatis, D., De Haulleville, T., Baya, F., Beeckman, H., Beina, D., Couteron, P., Chuyong, G., Dauby, G., Doucet, J.-L., Droissart, V., Dufrêne, M., Ewango, C., Gillet, J. F., Gonmadje, C. H., … Bogaert, J. (2015). Seeing Central African forests through their largest trees. Scientific Reports, 5(1), 13156. https://doi.org/10.1038/srep13156

Brüllhardt, M., Rotach, P., Schleppi, P., & Bugmann, H. (2020). Vertical light transmission profiles in structured mixed deciduous forest canopies assessed by UAV-based hemispherical photography and photogrammetric vegetation height models. Agricultural and Forest Meteorology, 281, 107843. https://doi.org/10.1016/j.agrformet.2019.107843

Byers, B. (2001). Conserving the Miombo Ecoregion. WWF Southern Africa (p. 37).

Campbell, B. M. (1996). The miombo in transition: Woodlands and welfare in Africa (Center for International Forestry Research, Ed.). Center for International Forestry Research.

Chave, J., Réjou-Méchain, M., Búrquez, A., Chidumayo, E. N., Colgan, M. S., Delitti, W. B. C., Duque, A., Eid, T., Fearnside, P. M., Goodman, R. C., Henry, M., Martínez-Yrízar, A., Mugasha, W. A., Muller-Landau, H. C., Mencuccini, M., Nelson, B. W., Ngomanda, A., Nogueira, E. M., Ortiz-Malavassi, E., … Vieilledent, G. (2014). Improved allometric models to estimate the aboveground biomass of tropical trees. Global Change Biology, 20(10), 3177–3190. https://doi.org/10.1111/gcb.12629

Chidumayo, E. (2013). Forest degradation and recovery in a miombo woodland landscape in Zambia: 22 years of observations on permanent sample plots. Forest Ecology and Management, 291, 154–161. https://doi.org/10.1016/j.foreco.2012.11.031

Chidumayo, E., & Marunda, C. (2010). Dry Forests and Woodlands in Sub-Saharan Africa: Context and Challenges. In The Dry Forests and Woodlands of Africa (1st Edition).

Davies, R. W., Ryan, C. M., Harrison, R. D., Dexter, K. G., Ahrends, A., Te Beest, M., Benitez, L., Brade, T. K., Carreiras, J. M. B., Druce, D. J., Fayolle, A., Finckh, M., Godlee, J. L., Gonclaves, F. M., Grundy, I. M., Hoche, T., Holdo, R. M., Makungwa, S., McNicol, I. M., … Edwards, D. P. (2023). Precipitation gradients drive high tree species turnover in the woodlands of eastern and southern Africa. Ecography, e06720. https://doi.org/10.1111/ecog.06720

De Cauwer, V. (2023). Status quo of sustainable forest management in Namibia. Hanns Seidel Foundation and Desert Research Foundation of Namibia (DRFN).

Demol, M., Aguilar-Amuchastegui, N., Bernotaite, G., Disney, M., Duncanson, L., Elmendorp, E., Espejo, A., Furey, A., Hancock, S., Hansen, J., Horsley, H., Langa, S., Liang, M., Locke, A., Manjate, V., Mapanga, F., Omidvar, H., Parsons, A., Peneva-Reed, E., … Burt, A. (2024). Multi-scale lidar measurements suggest miombo woodlands contain substantially more carbon than thought. Communications Earth & Environment, 5(1), 366. https://doi.org/10.1038/s43247-024-01448-x

Dubayah, R., Blair, J. B., Goetz, S., Fatoyinbo, L., Hansen, M., Healey, S., Hofton, M., Hurtt, G., Kellner, J., Luthcke, S., Armston, J., Tang, H., Duncanson, L., Hancock, S., Jantz, P., Marselis, S., Patterson, P. L., Qi, W., & Silva, C. (2020). The Global Ecosystem Dynamics Investigation: High-resolution laser ranging of the Earth's forests and topography. Science of Remote Sensing, 1, 100002. https://doi.org/10.1016/j.srs.2020.100002

Duncanson, L., Neuenschwander, A., Hancock, S., Thomas, N., Fatoyinbo, T., Simard, M., Silva, C. A., Armston, J., Luthcke, S. B., Hofton, M., Kellner, J. R., & Dubayah, R. (2020). Biomass estimation from simulated GEDI, ICESat-2 and NISAR across environmental gradients in Sonoma County, California. Remote Sensing of Environment, 242, 111779. https://doi.org/10.1016/j.rse.2020.111779

Ehbrecht, M., Schall, P., Juchheim, J., Ammer, C., & Seidel, D. (2016). Effective number of layers: A new measure for quantifying three-dimensional stand structure based on sampling with terrestrial LiDAR. Forest Ecology and Management, 380, 212–223. https://doi.org/10.1016/j.foreco.2016.09.003

Ehbrecht, M., Seidel, D., Annighöfer, P., Kreft, H., Köhler, M., Zemp, D. C., Puettmann, K., Nilus, R., Babweteera, F., Willim, K., Stiers, M., Soto, D., Boehmer, H. J., Fisichelli, N., Burnett, M., Juday, G., Stephens, S. L., & Ammer, C. (2021). Global patterns and climatic controls of forest structural complexity. Nature Communications, 12(1), 519. https://doi.org/10.1038/s41467-020-20767-z

Frost, P. (1996). The ecology of miombo woodlands. In The Miombo in transition: Woodlands and Welfare in Africa (B. Campbell, pp. 11–57). Centre for International Forestry Research.

Godlee, J. L., Ryan, C. M., Bauman, D., Bowers, S. J., Carreiras, J. M. B., Chisingui, A. V., Cromsigt, J. P. G. M., Druce, D. J., Finckh, M., Gonçalves, F. M., Holdo, R. M., Makungwa, S., McNicol, I. M., Mitchard, E. T. A., Muchawona, A., Revermann, R., Ribeiro, N. S., Siampale, A., Syampungani, S., … Dexter, K. G. (2021). Structural diversity and tree density drives variation in the biodiversity–ecosystem function relationship of woodlands and savannas. New Phytologist, 232(2), 579–594. https://doi.org/10.1111/nph.17639

Gough, C. M., Atkins, J. W., Fahey, R. T., Curtis, P. S., Bohrer, G., Hardiman, B. S., Hickey, L. J., Nave, L. E., Niedermaier, K. M., Clay, C., Tallant, J. M., & Bond-Lamberty, B. (2022). Disturbance has variable effects on the structural complexity of a temperate forest landscape. Ecological Indicators, 140, 109004. https://doi.org/10.1016/j.ecolind.2022.109004

Hancock, S., Armston, J., Hofton, M., Sun, X., Tang, H., Duncanson, L. I., Kellner, J. R., & Dubayah, R. (2019). The GEDI Simulator : A Large-Footprint Waveform Lidar Simulator for Calibration and Validation of Spaceborne Missions. Earth and Space Science, 6(2), 294-310. https://doi.org/10.1029/2018EA000506

Handavu, F., Chirwa, P. W., Syampungani, S., & Mahamane, L. (2017). A review of carbon dynamics and assessment methods in the miombo woodlands. Southern Forests: A Journal of Forest Science, 79(2), 95-102. https://doi.org/10.2989/20702620.2016.1277643

Kindermann, L., Dobler, M., Niedeggen, D., & Linstädter, A. (2022). A new protocol for estimation of woody aboveground biomass in disturbance-prone ecosystems. Ecological Indicators, 135, 108466. https://doi.org/10.1016/j.ecolind.2021.108466

Knapp, N., Fischer, R., Cazcarra-Bes, V., & Huth, A. (2020). Structure metrics to generalize biomass estimation from lidar across forest types from different continents. Remote Sensing of Environment, 237, 111597. https://doi.org/10.1016/j.rse.2019.111597

Latifi, H. (2012). Characterizing Forest Structure by Means of Remote Sensing: A Review. In B. Escalante (Ed.), Remote Sensing—Advanced Techniques and Platforms. InTech. https://doi.org/10.5772/35143

Le, A., Paull, D., & Griffin, A. (2018). Exploring the Inclusion of Small Regenerating Trees to Improve Above-Ground Forest Biomass Estimation Using Geospatial Data. Remote Sensing, 10(9), 1446. https://doi.org/10.3390/rs10091446

Li, X., Wessels, K., Armston, J., Duncanson, L., Urbazaev, M., Naidoo, L., Mathieu, R., & Main, R. (2024). Evaluation of GEDI Footprint Level Biomass Models in Southern African Savannas using Airborne LiDAR and Field Measurements. Science of Remote Sensing. https://doi.org/10.1016/j.srs.2024.100161

Li, X., Wessels, K., Armston, J., Hancock, S., Mathieu, R., Main, R., Naidoo, L., Erasmus, B., & Scholes, R. (2023). First validation of GEDI canopy heights in African savannas. Remote Sensing of Environment, 285, 113402. https://doi.org/10.1016/j.rse.2022.113402

Liang, M., Duncanson, L., Silva, J. A., & Sedano, F. (2023). Quantifying aboveground biomass dynamics from charcoal degradation in Mozambique using GEDI Lidar and Landsat. Remote Sensing of Environment, 284, 113367. https://doi.org/10.1016/j.rse.2022.113367

Lucas, R. M., Mitchell, A. L., & Armston, J. (2015). Measurement of Forest Above-Ground Biomass Using Active and Passive Remote Sensing at Large (Subnational to Global) Scales. Current Forestry Reports, 1(3), 162–177. https://doi.org/10.1007/s40725-015-0021-9

Mapaure, I. (2013). Short-term responses of shrub layer communities to dry season fires and tree thinning in semi-arid miombo woodlands of north-western Zimbabwe. African Journal of Plant Science, 7(9), 414–425. https://doi.org/10.5897/ajps2013.0993

Marunda, C., & Bouda, H.-N. (2010). Environmental Services from the Dry Forests and Woodlands of Sub-Saharan Africa. In The dry forests and woodlands of Africa: Managing for products and services (1st edition, p. 231). Earthscan.

Mayaux, P., Bartholomé, E., Fritz, S., & Belward, A. (2004). A new land-cover map of Africa for the year 2000. Journal of Biogeography, 31(6), 861–877. https://doi.org/10.1111/j.1365-2699.2004.01073.x

McElhinny, C., Gibbons, P., Brack, C., & Bauhus, J. (2005). Forest and woodland stand structural complexity: Its definition and measurement. Forest Ecology and Management, 218(1–3), 1–24. https://doi.org/10.1016/j.foreco.2005.08.034

Mehta, N., Pandya, N. R., Thomas, V. O., & Krishnayya, N. S. R. (2014). Impact of rainfall gradient on aboveground biomass and soil organic carbon dynamics of forest covers in Gujarat, India. Ecological Research, 29(6), 1053–1063. https://doi.org/10.1007/s11284-014-1192-8

Mensah, S., Salako, V. K., & Seifert, T. (2020). Structural complexity and large-sized trees explain shifting species richness and carbon relationship across vegetation types. Functional Ecology, 34(8), 1731–1745. https://doi.org/10.1111/1365-2435.13585

Moore, S., Adu-Bredu, S., Duah-Gyamfi, A., Addo-Danso, S. D., Ibrahim, F., Mbou, A. T., Grandcourt, A., Valentini, R., Nicolini, G., Djagbletey, G., Owusu-Afriyie, K., Gvozdevaite, A., Oliveras, I., Ruiz-Jaen, M. C., & Malhi, Y. (2018). Forest biomass, productivity and carbon cycling along a rainfall gradient in West Africa. Global Change Biology, 24(2), e496–e510. https://doi.org/10.1111/gcb.13907

Mugasha, W. A., Eid, T., Bollandsås, O. M., Malimbwi, R. E., Chamshama, S. A. O., Zahabu, E., & Katani, J. Z. (2013). Allometric models for prediction of above- and belowground biomass of trees in

the miombo woodlands of Tanzania. Forest Ecology and Management, 310, 87–101. https://doi.org/10.1016/j.foreco.2013.08.003

Pan, Y., Birdsey, R. A., Phillips, O. L., & Jackson, R. B. (2013). The Structure, Distribution, and Biomass of the World's Forests. Annual Review of Ecology, Evolution, and Systematics, 44(1), 593–622. https://doi.org/10.1146/annurev-ecolsys-110512-135914

Potapov, P., Li, X., Hernandez-Serna, A., Tyukavina, A., Hansen, M. C., Kommareddy, A., Pickens, A., Turubanova, S., Tang, H., Silva, C. E., Armston, J., Dubayah, R., Blair, J. B., & Hofton, M. (2021). Mapping global forest canopy height through integration of GEDI and Landsat data. Remote Sensing of Environment, 253, 112165. https://doi.org/10.1016/j.rse.2020.112165

Ribeiro, N. S., Katerere, Y., Chirwa, P. W., & Grundy, I. M. (Eds). (2020). Miombo Woodlands in a Changing Environment: Securing the Resilience and Sustainability of People and Woodlands. Springer International Publishing. https://doi.org/10.1007/978-3-030-50104-4

Ribeiro, N. S., Shugart, H. H., & Washington-Allen, R. (2008). The effects of fire and elephants on species composition and structure of the Niassa Reserve, northern Mozambique. Forest Ecology and Management, 255(5–6), 1626–1636. https://doi.org/10.1016/j.foreco.2007.11.033

Ryan, C. M., Hill, T., Woollen, E., Ghee, C., Mitchard, E., Cassells, G., Grace, J., Woodhouse, I. H., & Williams, M. (2012). Quantifying small-scale deforestation and forest degradation in African woodlands using radar imagery. Global Change Biology, 18(1), 243–257. https://doi.org/10.1111/j.1365-2486.2011.02551.x

Ryan, C. M., Pritchard, R., McNicol, I., Owen, M., Fisher, J. A., & Lehmann, C. (2016). Ecosystem services from southern African woodlands and their future under global change. Philosophical Transactions of the Royal Society B: Biological Sciences, 371(1703), 20150312. https://doi.org/10.1098/rstb.2015.0312

Saliu, I. S., Satyanarayana, B., Bin Fisol, M. A., Wolswijk, G., Decannière, C., Lucas, R., Otero, V., & Dahdouh-Guebas, F. (2021). An accuracy analysis of mangrove tree height mensuration using forestry techniques, hypsometers and UAVs. Estuarine, Coastal and Shelf Science, 248, 106971. https://doi.org/10.1016/j.ecss.2020.106971

Sankaran, M., Hanan, N. P., Scholes, R. J., Ratnam, J., Augustine, D. J., Cade, B. S., Gignoux, J., Higgins, S. I., Le Roux, X., Ludwig, F., Ardo, J., Banyikwa, F., Bronn, A., Bucini, G., Caylor, K. K., Coughenour, M. B., Diouf, A., Ekaya, W., Feral, C. J., … Zambatis, N. (2005). Determinants of woody cover in African savannas. Nature, 438(7069), 846–849. https://doi.org/10.1038/nature04070

SEOSAW partnership. (2021). A network to understand the changing socio-ecology of the southern African woodlands (SEOSAW): Challenges, benefits, and methods. Plants, People, Planet, 3(3), 249–267. https://doi.org/10.1002/ppp3.10168

Sexton, J. O., Bax, T., Siqueira, P., Swenson, J. J., & Hensley, S. (2009). A comparison of lidar, radar, and field measurements of canopy height in pine and hardwood forests of southeastern North America. Forest Ecology and Management, 257(3), 1136–1147. https://doi.org/10.1016/j.foreco.2008.11.022

Shackleton, C. M., & Scholes, R. J. (2011). Above ground woody community attributes, biomass and carbon stocks along a rainfall gradient in the savannas of the central lowveld, South Africa. South African Journal of Botany, 77(1), 184–192. https://doi.org/10.1016/j.sajb.2010.07.014

Shugart, H. H., Saatchi, S., & Hall, F. G. (2010). Importance of structure and its measurement in quantifying function of forest ecosystems. Journal of Geophysical Research: Biogeosciences, 115(G2), 2009JG000993. https://doi.org/10.1029/2009JG000993

Slik, J. W. F., Paoli, G., McGuire, K., Amaral, I., Barroso, J., Bastian, M., Blanc, L., Bongers, F., Boundja, P., Clark, C., Collins, M., Dauby, G., Ding, Y., Doucet, J., Eler, E., Ferreira, L., Forshed, O., Fredriksson, G., Gillet, J., … Zweifel, N. (2013). Large trees drive forest aboveground biomass variation in moist lowland forests across the tropics. Global Ecology and Biogeography, 22(12), 1261–1271. https://doi.org/10.1111/geb.12092

Strohbach, B. J., & Petersen, A. (2007). Vegetation of the central Kavango woodlands in Namibia: An example from the Mile 46 Livestock Development Centre. South African Journal of Botany, 73(3), 391–401. https://doi.org/10.1016/j.sajb.2007.03.002

Timberlake, J., & Chidumayo, E. (2011). Miombo ecoregion vision report (Occasional Publications in Biodiversity). Occasional Publications in Biodiversity.

Van Wyk, B., & Van Wyk, P. (2013). Field Guide to Trees of Southern Africa (2nd rev. ed.). Struik Publishers.

Chapter 2: Rainfall shapes the dominance of large trees and forest biomass across tree-sizes in the Miombo ecoregion

Abstract

Understanding how biomass is regulated essential for predicting the role of African woodlands in the global carbon cycle. Using 2,749 forest inventory plots from the SEOSAW network across southern Africa, this study examined how rainfall, disturbance, and diameter-based structural attributes control structure and above-ground biomass (AGB) across the Miombo ecoregion. The contribution of large trees was quantified using three complementary metrics: (i) the proportion of biomass in trees ≥ 40 cm DBH, (ii) the biomass share of the largest 1% of stems, and (iii) the diameter threshold above which 50% of total AGB is stored (DBH_{50}). Generalised Additive Models (GAMs) and Linear Mixed-Effects Models (LMEs) were used to analyse patterns across a rainfall gradient (345–2000 mm yr^{-1}) and at the plot scale.

At the regional scale, AGB increased strongly and near-linearly with rainfall, from 17 Mg ha^{-1} in the driest woodlands to 133 Mg ha^{-1} in the wettest systems (R^2adj = 0.60). Stem density also increased with rainfall (R^2adj = 0.43). The contribution of large trees (≥ 40 cm DBH) rose from 14.9% to 38.6% of total AGB (R^2adj = 0.65), while DBH_{50} increased from 21.7 to 36.3 cm (R^2adj = 0.50), indicating that biomass accumulation is increasingly associated with larger stems. The biomass share of the top 1% of stems indicated a slight decreasing trend along the gradient (R^2adj = 0.48).At the plot scale, rainfall explained little of the variability in AGB, which was instead primarily controlled by stand structure. Total AGB was best explained by quadratic mean diameter, Gini coefficient, and DBH kurtosis, whereas large-tree dominance metrics were more strongly associated with DBH variability and distribution shape. These results reveal a hierarchical regulation of biomass in Miombo woodlands, where rainfall sets regional potential, while local stand structure governs its realisation.

Key words: rainfall gradient; above-ground biomass; large-diameter trees; carbon storage; fire disturbance

2.1 Introduction

Forests store a large part of terrestrial carbon and regulate ecosystem processes that sustain biodiversity and human well-being (Pan et al., 2011; Reichstein & Carvalhais, 2019). Much of this carbon is held in the woody biomass of trees, making above-ground biomass (AGB) a critical measure of both carbon storage and ecosystem productivity (Poorter et al., 2012). AGB is not an isolated trait; it reflects the combined influence of tree size distribution, wood density, and tree density, offering an integrated measure of vegetation structure and ecosystem functioning (Chave et al., 2014; Réjou-Méchain et al., 2017). Furthermore, AGB represents the cumulative outcome of growth and mortality processes and thus can partially serve as a proxy for long-term ecosystem productivity (Johnson et al., 2016). Spatial variation in AGB may therefore contribute to information on vegetation types, disturbance regimes and successional stages (Xu et al., 2025). Beyond its ecological significance, AGB is a key variable in global change research and climate policy because it directly links local ecosystem processes to global carbon budgets. Understanding the factors controlling AGB is essential for predicting the capacity of forests to mitigate climate change and improving the accuracy of the global carbon models.

Among the factors controlling AGB, vegetation structure plays a central role by determining how carbon is distributed among trees. It influences light interception, tree competition, regeneration, and overall ecosystem productivity (Bourdier et al., 2016; Coomes & Allen, 2007). Large-diameter trees, particularly, store a disproportionate share of total biomass and strongly affect microclimate and regeneration dynamics (Bastin et al., 2015; Lutz et al., 2018; Piponiot et al., 2022). Across tropical forests, the largest 1% of stems can contain more than half of the stand-level biomass, highlighting their dominant role in global carbon storage (Lutz et al., 2018).

Despite their importance, the role of large trees in shaping biomass and structure remains poorly quantified in tropical dry forests, especially in the Miombo ecoregion. Most research has focused on broad-scale relationships between AGB and climatic or edaphic gradients, such as rainfall, soil fertility, and disturbances (Godlee et al., 2021; Ryan & Williams, 2011; Shirima et al., 2011, 2015). For instance, Godlee et al. (2021) found that increased water availability and increased structural diversity both have a positive effect on AGB. However, the majority of studies analysing the contribution of large trees to biomass has been done in moist tropical forest (Bastin et al., 2015; Slik et al., 2013). Clarifying how the dominance of large trees varies at the regional scale and under local site conditions is therefore essential to understanding patterns of biomass and predicting how African woodlands may respond to future environmental change.

The Miombo ecoregion is the largest continuous expanse of tropical dry forest in Africa, spanning roughly 3.8 million km² across southern and eastern Africa (Byers, 2001; Mayaux et al., 2004). The Miombo woodland, *sensu stricto* is characterised by an open canopy with a continuous grass layer (Frost, 1996; Ryan et al., 2016). The region spans strong gradients in rainfall, soil fertility, and topography, which interact with disturbances such as fire and elephant activity to shape vegetation structure (Davies et al., 2023; Godlee et al., 2021; Halperin et al., 2016; Sankaran et al., 2005; Timberlake & Chidumayo, 2011). These interacting climatic and local factors may produce substantial spatial variation in canopy height, tree-size distribution, and AGB, making the relative contribution of large trees to total AGB and forest structure highly dependent on both rainfall and site conditions.

In this study, we investigate how climatic gradients and local ecological conditions influence vegetation structure and biomass distribution across the Miombo ecoregion. We specifically aim to:

- Describe how total biomass and structural attributes vary along the rainfall gradient,
- Assess how the contribution of large trees to stand biomass changes across the rainfall gradient, and
- Identify the environmental factor and structural metrics that explain variation in biomass.

By combining extensive field inventories with environmental data spanning diverse vegetation types, this study aims to provide new insights into the mechanisms by which regional climate, local site conditions, and stand organisation jointly shape carbon storage in the Miombo ecoregion.

2.2 Materials and methods

2.2.1 Study area

The study area is located within the Miombo ecoregion of eastern and southern Africa, one of the largest tropical woodland systems in the world. It spans a broad environmental gradient across several countries, encompassing a diversity of vegetation types and ecological conditions. The region includes seven major vegetation classes representing dominant physiognomic types, ranging from humid tropical lowlands to semi-arid drylands: Wetlands and Mangroves (WM), Coastal and Lowland forests (CL), Thickets and Bushlands (TB), Miombo woodlands (MW), Montane Forest and mosaics (MM), Mopane and dry Woodlands (MDW), and Grasslands and Savannas (GS) (Figure 2.1).The region covers a wide climatic range, with Mean Annual Precipitation (MAP) varying from 345 mm yr-1 in the arid region of Namibia to 1980 mm yr-1 in the more humid zones of Mozambique. Mean Annual Temperature (MAT) ranges between 17°C and 26°C (Zomer et al., 2022). Rainfall variability across the region is moderate, with coefficients of variation typically below 30% (Frost, 1996). The dry season occurs from May to October or November (Ribeiro et al., 2020). In most areas, over 95% of annual precipitation falls during a single wet season lasting approximately five to seven months (Frost, 1996), varying across the region (Ivory et al., 2012). This seasonal concentration of rainfall has a strong influence on vegetation phenology, soil moisture dynamics, and fire regimes throughout the Miombo and associated ecosystems.

2.2.2 Data collection

A total of 9478 forest inventory plots were obtained from the Socio-Ecological Observatory for Studying African Woodlands (SEOSAW) database (SEOSAW partnership, 2021), spanning seven countries (Figure 2.1). We only selected plots sampled between 2010 and 2023, and within each plot, only stems with a diameter at breast height (DBH; measured at 1.3 m) greater than 5 cm were included in the analysis. To reduce bias in estimating above-ground biomass (AGB) and stem density, plots were further filtered to retain those with an area greater than 0.1 ha and a minimum of stem density of 50 stems per hectare (Bordin et al., 2021; Godlee et al., 2021). After applying these criteria, a total of 2749 plots located in different vegetation types (table S1) and across the rainfall gradient were retained for analysis. For each stem, we extracted the following information: height, species name, and diameter at breast height (DBH).

Environmental variables were extracted using Google Earth Engine (GEE) at the plot level by applying a circular buffer of 100 m radius around each plot centroid. Mean values were computed within this

buffer to ensure consistency between plot-scale measurements and the spatial resolution of gridded datasets. Precipitation data were obtained from the ERA5-Land reanalysis, which provides physically consistent climate estimates through the integration of model simulations and observational data assimilation (Hersbach et al., 2020; Muñoz-Sabater et al., 2021). Data were extracted for the period 1960–2020 at ~9 km spatial resolution. Monthly aggregated precipitation totals were used, and mean annual precipitation (MAP) was subsequently derived through temporal aggregation.

Soil properties, including soil organic carbon (SOC), clay fraction, and cation exchange capacity (CEC), were obtained from the ISRIC SoilGrids v2 dataset at 250 m resolution (Hengl et al., 2017).

Fire frequency was calculated using the MODIS MCD64A1 monthly burned area product (500 m resolution). Each pixel in this dataset indicates the day of the year when a fire occurred. For each plot, fire occurrences were determined by counting all non-zero burn dates over a 10-year period preceding the year of plot measurement (e.g., for a plot measured in 2021, fire data from 2011–2020 were used).

Topographic variables, including elevation, slope, and aspect, were extracted from the Multi-Error-Removed Improved Terrain (MERIT) DEM v1.0.3. The dataset provides a spatial resolution of approximately 3 arc-seconds (~90 m at the equator).

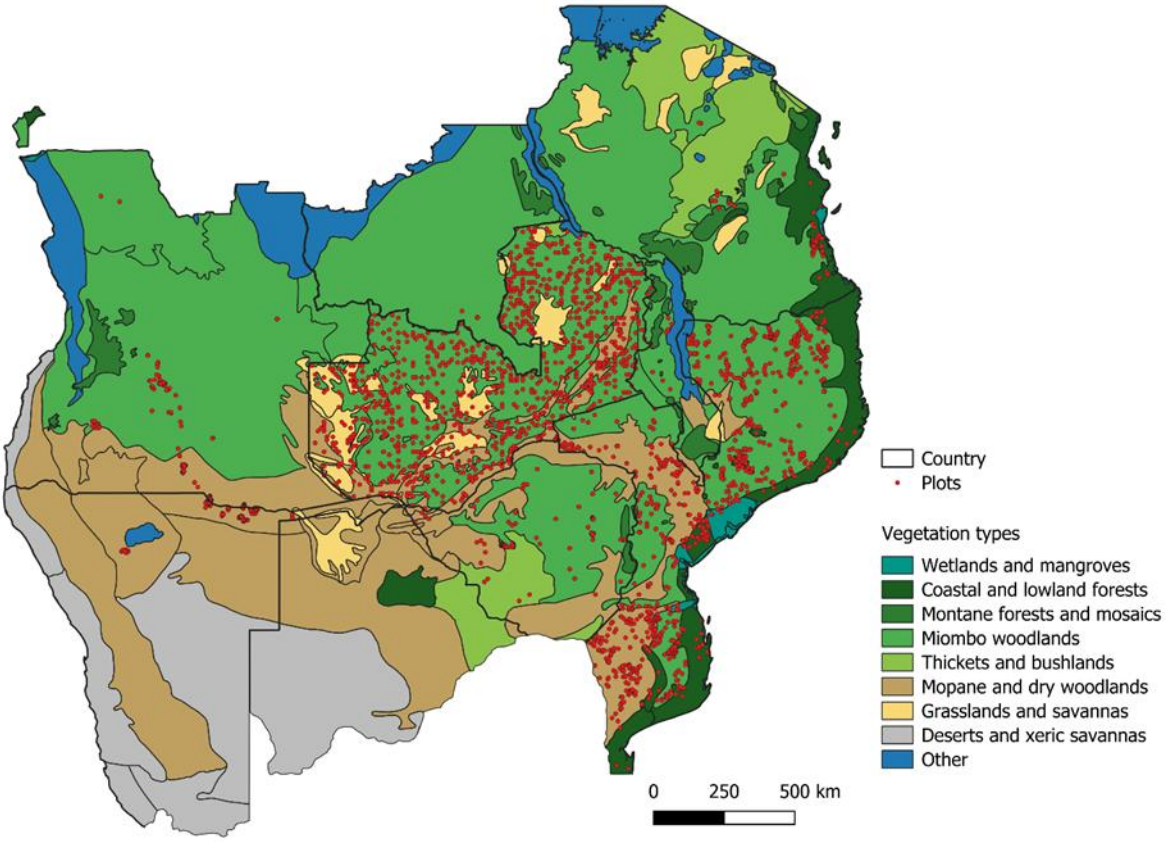


Figure 2.1. Location of the plots across the vegetation types in Miombo ecoregion. Classification of vegetation type is adapted from the WWF Global 200 Ecoregions

2.2.3 Data analysis

Definition of large-diameter trees

There is no universal criterion for defining what constitutes a large-diameter tree. In general, large trees are those that can reach the upper canopy layer and are larger than the majority of woody stems within a stand (Lutz et al., 2018). A large tree is defined based on either a diameter threshold or a cumulative percentage of biomass stored by a group of trees (Bastin et al., 2015; Bordin et al., 2021; Lutz et al., 2018; Piponiot et al., 2022). Diameter thresholds for defining large trees vary widely from 20 cm to 100 cm in DBH (Lutz et al., 2018; Piponiot et al., 2022; Slik et al., 2013), depending on vegetation type, vegetation structure, and study objectives.

Following Lutz et al. (2018), three complementary metrics were used to identify large-diameter trees in this study:

- The 99th percentile diameter represents the largest 1% of trees (≥ 5 cm DBH) in each plot.
- A fixed threshold of 40 cm DBH, commonly applied in African woodland studies.

- The diameter threshold (DBH_{50}%) above which trees cumulatively accounted for 50% of total plot AGB.

Diameter classes ([5-10); [10-15); [15-20); [20-25); [25-30); [30-35); [35-40); ≥40) were used to analyse how tree size structure and diameter-abundance relationships vary along the rainfall gradient. Rainfall was grouped in four broad classes to facilitate comparisons among contrasting climatic zones to derive representative mean values: R1 ≤ 800 mm yr^{-1} (1028 plots); R2 = 700 mm yr^{-1} – 1000 mm yr^{-1} (709 plots); R3 = 1000 mm yr^{-1} – 1200 mm yr^{-1} (577 plots); R4 = > 1200 mm yr^{-1} (435 plots) (table S2). This allowed assessment of stem density and biomass partitioning across DBH classes. To analyse continuous patterns along the rainfall gradient, we applied an adaptive classification scheme to ensure sufficient replication in each interval. Plots with MAP < 450 mm were grouped into a single class; from 450 to 1500 mm, rainfall was divided into 50 mm intervals; from 1500 to 1700 mm, 100 mm intervals were used; and all plots with MAP > 1700 mm were grouped together. Using this approach, a total of 25 finer rainfall classes (Table 1) were created, which avoids extremely small sample sizes in some intervals while preserving the ability to explore continuous patterns in total AGB and the contribution of large trees along the gradient.

Aboveground biomass (AGB)

AGB for each stem was estimated using the equations of Chave et al. (2014) Equation (4), which incorporates diameter, height, and wood density, was applied when height data were available, while Equation (7), which excludes height, was used otherwise.

Equation 4 from Chave et al. (2014):

$$AGB = 0.0673 \times (\rho\ D^2\ H)^{0.976} \times 1000 \quad (1)$$

Equation 7 from Chave et al. (2014):

$$AGB = exp[-1.803 - 0.976E + 0.976\ln(\rho) + 2.673\ln(D) - 0.0299(\ln(D))^{2}] \quad (2)$$

Where D is diameter (cm), H is height (m) and ρ is wood specific gravity ($g.cm^{-3}$). α and β are model coefficients (derived from least-squares regression), ε is an error term (Chave et al., (2014).

Wood density values were obtained from the Global Wood Density Database at the species level or at the genus level when species identification was not available (Zanne et al., 2009) using the R package BIOMASS (Réjou-Méchain et al., 2017). Plot-level AGB (Mg ha-1) was then computed as the sum of the individual stem AGB within each plot and converted to per unit area.

Basal area and stem density

The basal area of individual stems (gi) was calculated as:

$$gi = \pi \left(\frac{d_i}{2}\right)^2 \quad (3)$$

Where d_i is the stem diameter of the stem *i* recorded at 1.3 m. For multi-stemmed trees, the basal areas of all stems were summed to obtain the total basal area of the individual. The total basal area per hectare for each plot was then calculated by summing the basal areas of all stems in the plot and dividing by the plot area. Stem density (stems ha^{-1}) was calculated as the total number of stems in a plot divided by the plot area. For all plots and for each DBH class, we computed mean, standard deviation, and coefficient of variation (CV) for AGB, basal area, and stem density.

Structural variability metrics

To describe stand structural variability, the following metrics were computed for each plot:

- **Quadratic Mean Diameter (QMD):**

$$QMD = \sqrt{\left(\sum d_i^2\right)/n}\,; \quad (4)$$

Where d_i is the DBH of an individual stem, and *n* is the total number of stems. It represents the size-weighted mean DBH. QMD is size-weighted giving more weight to larger trees and is equal to or greater than the arithmetic mean depending on DBH variance. In stands of small mean DBH and narrow range in DBH, the differences are slight, while in stands with large mean DBH and a wide range of diameters or strongly skewed DBH distributions, the differences between the arithmetic mean of DBH and QMD can be substantial (Curtis & Marshall, 2000).

- **Gini coefficient of DBH (Gini_DBH)**

Gini_DBH was calculated using the ineq package (Zeileis, 2025). It is a common measure of the DBH inequality among values of a frequency distribution of DBH (Carrasco-Escobar et al., 2020). The Gini coefficient is easy to interpret as the values range from 0 to 1. It has a minimum value when all the trees are of equal size (Pach & Podlaski, 2015). A high Gini coefficient in DBH indicates pronounced inequality in tree sizes within the stand, typically resulting from high variance or skewness in the diameter distribution. The Gini coefficient is particularly sensitive to small changes in the mean DBH, especially when most trees are not small, as such variations modify the relative contribution of dominant versus subordinate trees to the overall vegetation structure (Lian et al., 2024).

- **Coefficient of Variation in DBH (DBH_CV):** expresses relative diameter variability:

  $DBH_{CV} = \left(\frac{SD\ (DBH)}{Mean\ (DBH)}\right) x\ 100$ (5) ; Where SD is the standard deviation.

- **Skewness (DBH_skew) and Kurtosis (DBH_kurt):**

Describe asymmetry and tail heaviness of the diameter distribution, computed using the e1071 package (Meyer et al., 2025).

These metrics provide a comprehensive characterization of stand structure and diameter heterogeneity, supporting analyses of biomass partitioning and large-tree dominance.

Table 2.1 . Structural dominance of large trees along rainfall gradient. Mean stand-level attributes are summarised for 25 rainfall classes (300 to above 1700)

Rainfall_class	Plots (n)	Stem density (stems ha^{-1})	Stem density SD	Stem density CV (%)	Total AGB (Mg ha^{-1})	AGB SD	AGB CV (%)	% AGB ≥40 cm	% AGB top 1%	Threshold DBH_{50}% (cm)
< 450	14	400.89	324.34	80.9	22.47	18.27	81.32	10.04	16.42	22.14
450-500	82	380.16	224.13	58.96	34.49	22.92	66.44	23.23	17.26	27.23
500-550	148	379.16	191.82	50.59	54.08	37.2	68.79	25.39	16.52	29.7
550-600	41	376.02	200.38	53.29	56.25	33.94	60.35	24.3	15.59	29.87
600-650	223	235.74	176.58	74.9	41.77	39.68	95.01	29.77	27.89	38.19
650-700	188	302.24	284.69	94.19	38.14	32.6	85.48	29.89	24.12	36.19
700-750	82	289.72	192.71	66.52	52.29	39.55	75.64	26.91	21.18	31.73
750-800	250	396.91	356.72	89.88	34.62	33.5	96.77	20.2	25.73	29.12
800-850	200	377.07	314.45	83.39	50.09	37.56	74.99	24.1	21.71	31.04
850-900	133	415.38	272.59	65.63	54.59	34.4	63.02	25.69	17.15	32.26
900-950	168	376.77	255.86	67.91	60.77	44.61	73.41	29.26	16.74	32.58
950-1000	208	399.83	266.05	66.54	67.99	59.19	87.05	26.72	19.24	33.23
1000-1050	203	369.29	246.08	66.64	60.24	46.32	76.89	25.15	17.99	31.72
1050-1100	144	421.93	271.12	64.26	50.15	32.1	63.99	20.1	16.1	29
1100-1150	122	391.56	218.81	55.88	52.25	39.11	74.85	21.09	16.92	28.96
1150-1200	108	368.16	218.6	59.38	50.38	37.94	75.31	20.88	15.05	28.61
1200-1250	103	407.26	273.13	67.07	56.66	39.23	69.24	19.55	16.99	29.07
1250-1300	89	432.45	238.38	55.12	61.82	39.13	63.3	22.68	17.13	29.35
1300-1350	129	573.12	393.62	68.68	67.3	46.3	68.79	19.15	21.91	27.54
1350-1400	27	379.57	208.03	54.81	52.17	32.73	62.75	20.5	18.33	27.99
1400-1450	38	391.83	181	46.19	63.3	49.69	78.5	18.43	16.93	26.62
1450-1500	14	484.94	330.2	68.09	85.36	43.92	51.45	23.37	17.59	33.81
1500-1600	14	452.61	264.99	58.55	63.66	29.32	46.06	27.46	18.49	30.39
1600-1700	10	534.63	238.81	44.67	85.68	33.47	39.06	24.08	12.47	28.69
>1700	11	496.86	167.12	33.64	78.14	47.63	60.96	28.22	12.94	32.21

2.2.4 Statistical analysis

Statistical analysis was performed using R software (R Core Team, 2023). We applied Generalized Additive Models (GAMs) using penalised cubic regression splines using the mgcv package (Wood, 2017) to assess non-linear relationships between mean annual precipitation (MAP) and structural attributes (total AGB, stem density, proportion of AGB ≥ 40 cm DBH, proportion in the top 1 % stems, and DBH_{50}%). Weighted GAMs (weights = number of plots per rainfall class) were used to correct for unequal sampling among rainfall intervals. For each model, we report the estimated degrees of freedom (edf) of the smoother, F-statistic, p-value, and adjusted R^2 (R^2adj). This approach allowed us to capture the functional form of rainfall–structure relationships and to identify potential ecological thresholds along the gradient.

To quantify the contribution of large-diameter trees to forest biomass structure, bivariate relationships were examined between total aboveground biomass (AGB) and three structural indicators: DBH_{50}%, the proportion of AGB in trees ≥ 40 cm DBH, and the proportion of biomass held by the top 1% of stems. For each relationship, ordinary least squares (OLS) regressions were fitted, and robust regression models (M-estimation; MASS package) were additionally used to evaluate the sensitivity of slope estimates to extreme values. To identify the local drivers of AGB and structural attributes, we fitted Linear Mixed-Effects Models (LMEs) using the lme4 package (Bates et al., 2015). LMEs account for the hierarchical structure of the dataset (plots nested within vegetation types) and allow separation of the effects of climate, environment, and vegetation structure while controlling for unmeasured biogeographic differences. Prior to model fitting, multicollinearity among predictors was assessed using variance inflation factors (VIF) and pairwise correlation matrices (Figure S1; Table S3). Environmental variables (MAP, elevation, slope, aspect, SOC, clay content, CEC, and fire frequency) showed low to moderate collinearity (VIF < 3). In contrast, structural metrics derived from DBH distributions (Gini coefficient, coefficient of variation, skewness, and kurtosis) exhibited moderate to high collinearity and were therefore not included simultaneously in the same model.

The general structure of the models was:

Response ~ Rainfall + Elevation + Slope + Aspect + SOC + Clay + CEC + Fire frequency + Structural metric(s) + (1|Vegetation type).

Here, vegetation type (seven categories) was included as a random intercept to account for unmeasured ecological and biogeographic variation (e.g., species composition, soil parent material). All continuous predictors were z-scores standardised (mean = 0, SD =1) prior to model fitting to place

variables on a common scale and allow direct comparison of effect sizes (Diesse et al., 2025). Four separate LMEs were developed: for total AGB, Proportion of AGB in large trees (DBH ≥ 40 cm), Proportion of AGB held by the top 1 % of stems, and DBH_{50}%. These models quantify how local conditions and vegetation structure mediate biomass partitioning and large-tree dominance.

Model selection and performance were assessed using Akaike Information Criterion (AIC) and coefficients of determination. AIC was used to compare alternative model formulations and identify the most parsimonious model for each response variable, while marginal (R^2m) and conditional (R^2c) coefficients of determination were used to evaluate explanatory power. R^2m represents the variance explained by fixed effects, whereas R^2c captures the total variance explained by both fixed and random effects. Small differences between R^2c and R^2m indicate that most of the variance arises from measured environmental and structural predictors rather than unaccounted differences in vegetation types. Standardised coefficients (β) and their 95% confidence intervals were extracted using the parameters and performance packages (Lüdecke et al., 2021) to visualise predictor importance. Predictors were deemed significant when their confidence intervals did not overlap zero. To separate the relative influence of vegetation-type identity and within-type heterogeneity, random-effect variances were decomposed using the performance package.

2.3 Results

2.3.1 Stem diameter and biomass distribution across the rainfall gradient

Across all four rainfall classes, the diameter class distribution of stems followed a typical inverse J-shaped pattern, characteristic of actively regenerating forests (Figure 2.2). Stem density was highest in the smallest diameter class (5–10 cm DBH) and progressively declined with increasing diameter, becoming rare above 30 cm. This pattern was consistent across the entire rainfall gradient. In contrast, above-ground biomass (AGB) increased steadily with stem diameter, showing that larger trees contribute disproportionately to total stand biomass.

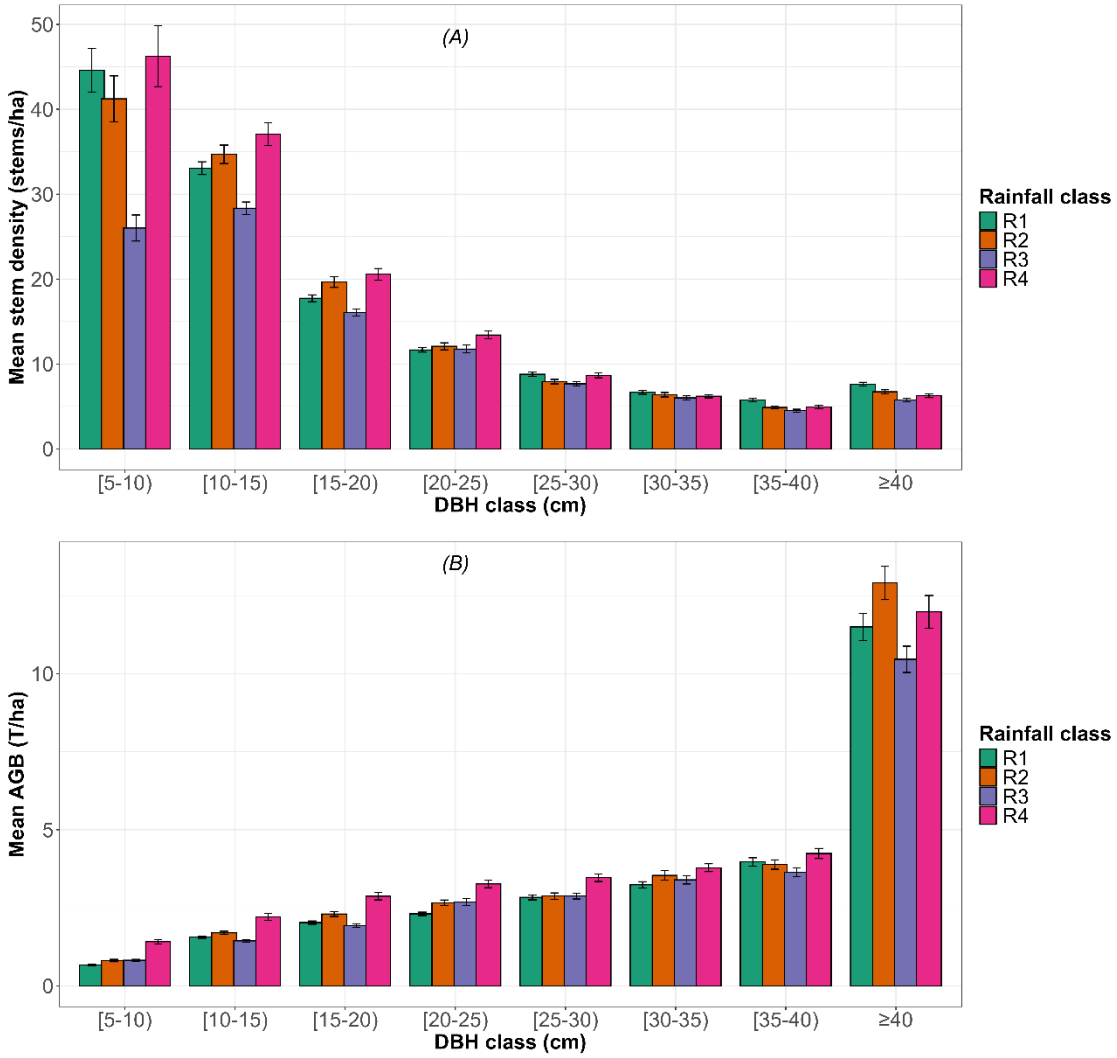


Figure 2.2. Variation in Stem density and Mean total AGB across four rainfall classes.

(a) Stem density and (b) Mean total AGB across four rainfall classes. R1 = rainfall between 345 MAP and 800 MAP, R2 = rainfall between 800 MAP – 1000 MAP, R3 = rainfall between 1000 – 1200 MAP and R4 = rainfall above 1200 MAP[

2.3.2 Contribution of Large-Diameter Trees to Forest Biomass Structure

Across the Miombo ecoregion, total above-ground biomass (AGB) was strongly linked to the dominance of large-diameter trees (Figure 2.3). The diameter threshold above which half of the stand's biomass is contained (DBH_{50}%) increased moderately with total AGB (R^2 = 0.16). In contrast, the proportion of AGB contributed by stems ≥ 40 cm DBH displayed a strong positive relationship with total biomass (R^2 = 0.63). A similarly strong association was found between total AGB and the proportion of biomass held by the top 1% of stems (R^2 = 0.56).

The relationships for DBH_{50}% and AGB ≥ 40 cm were consistent between ordinary least squares and robust regression models, with similar slope estimates (DBH_{50}%: 1.18 vs 1.11; AGB ≥ 40 cm: 1.30 vs 1.34). In contrast, the relationship involving the top 1% of stems showed a greater difference between the two approaches (2.74 vs 3.25), indicating a stronger influence of extreme values.

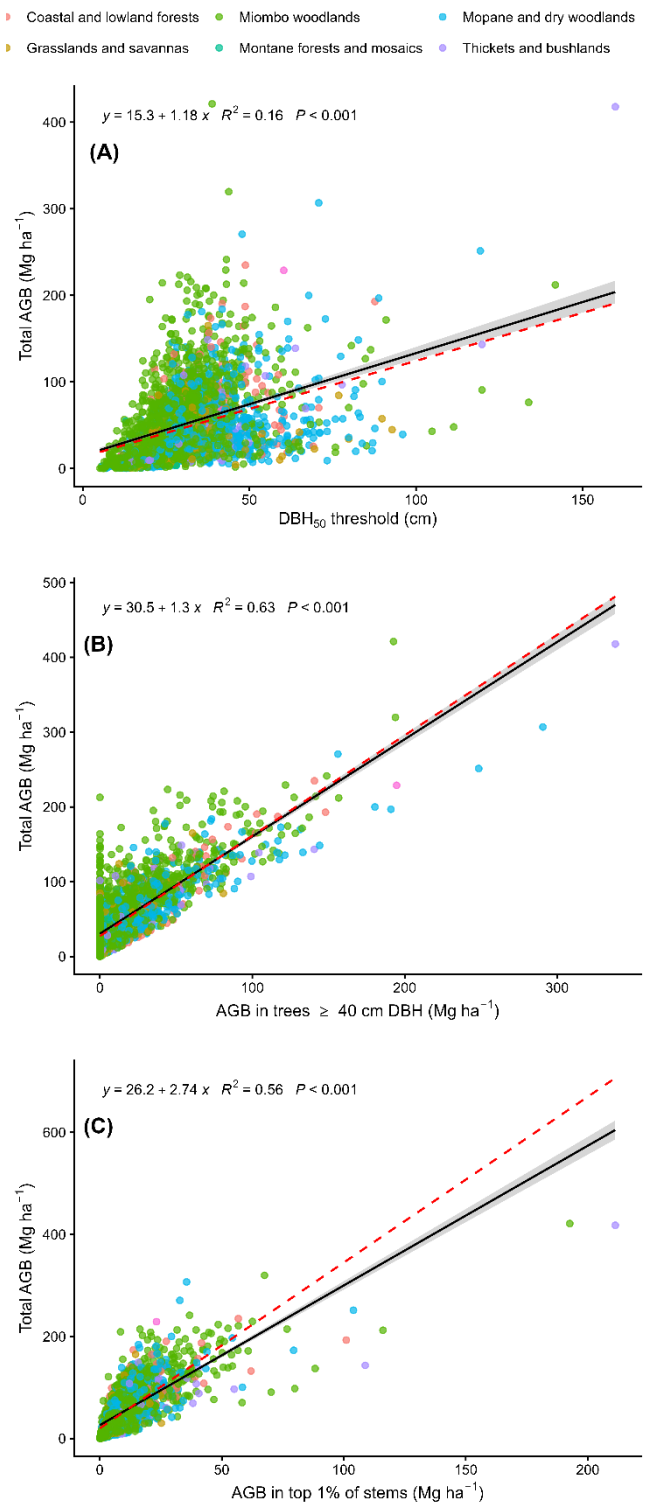


Figure 2.3. Relationships between total above-ground biomass (AGB) and structural indicators of large-diameter tree dominance across Miombo forest plots

(a) DBH_{50}, representing the diameter threshold above which 50% of stand biomass is contained; (b) proportion of AGB in trees ≥ 40 cm DBH; and (c) proportion of biomass in the top 1% of stems. Points are coloured by vegetation type. Black solid lines represent ordinary *least squares (OLS) regressions with 95% confidence*

intervals, while red dashed lines represent robust regression fits. Annotations show regression equations, coefficients of determination (R^2), and p-values.

2.3.3 Patterns of AGB and structure along the rainfall gradient

To analyse the impact of mean annual rainfall on AGB and vegetation structure, we created 25 rainfall classes (300–2000 mm yr^{-1}). The analysis revealed that the mean stand AGB increased almost linearly with rainfall (Figure 2.4; Table 1). A weighted Generalised Additive Model (GAM) fitted to class-mean values revealed a strong linear relationship between rainfall and total AGB (edf = 1.0, F = 36.67, p < 0.001), with rainfall explaining 62.1 % of the deviance in mean biomass (R^2adj = 0.60). Mean AGB rose from 17 ± 14 Mg ha^{-1} in the driest woodlands (< 400 mm yr^{-1}) to 133 ± 47 Mg ha^{-1} in the wettest woodlands (> 1800 mm yr^{-1}) highlighting a strong and continuous increase in biomass along the rainfall gradient. Stem density also increased with rainfall, following a non-linear pattern (edf = 8.5, F = 12.07, p <0.001), ranging from less than 250 to more than 500 stems ha^{-1} With rainfall explaining 47.1% of the deviance (R^2adj = 0.43) indicating a gradual increase in stand density toward wetter conditions.

The share of biomass stored in large trees (DBH ≥ 40 cm) exhibited a non-linear increase along the rainfall gradient (edf = 7.17, F = 5.95, p < 0.01), with rainfall explaining 75.8 % of the deviance (R^2adj = 0.65). In the driest sites, large trees accounted for 14.9 % of stand biomass, compared with 38.6 % in the wettest sites, indicating that higher precipitation favours a greater dominance of large stems. Similarly, the density of large trees (DBH ≥ 40 cm) increased strongly with rainfall and showed a highly non-linear pattern (edf = 8.53, F = 12.07, p < 0.001), with rainfall explaining 87.6% of the deviance (R^2adj = 0.81). Large stem density increased from fewer than 5 stems ha^{-1} in dry woodlands to more than 13 stems ha^{-1} in wetter systems.

The biomass share of the top 1% of stems also varied significantly with rainfall (edf = 5.22, F = 3.75, p < 0.05), explaining 59.8% of the deviance (R^2adj = 0.48), indicating moderate variation and a slight decreasing trend in the contribution of the largest individuals along the gradient.Finally, the diameter threshold above which trees collectively hold 50 % of plot biomass (DBH_{50}%) increased significantly with rainfall (edf = 5.53, F = 3.76, p < 0.05), from 20-22 cm in dry woodlands to 32-34 cm in wet Miombo (Figure 2.4), confirming that biomass accumulation in wetter sites is concentrated in fewer, larger stems.

These results demonstrate that rainfall is a dominant driver of vegetation structure, promoting greater size inequality and dominance of large individuals in wetter Miombo ecosystems.

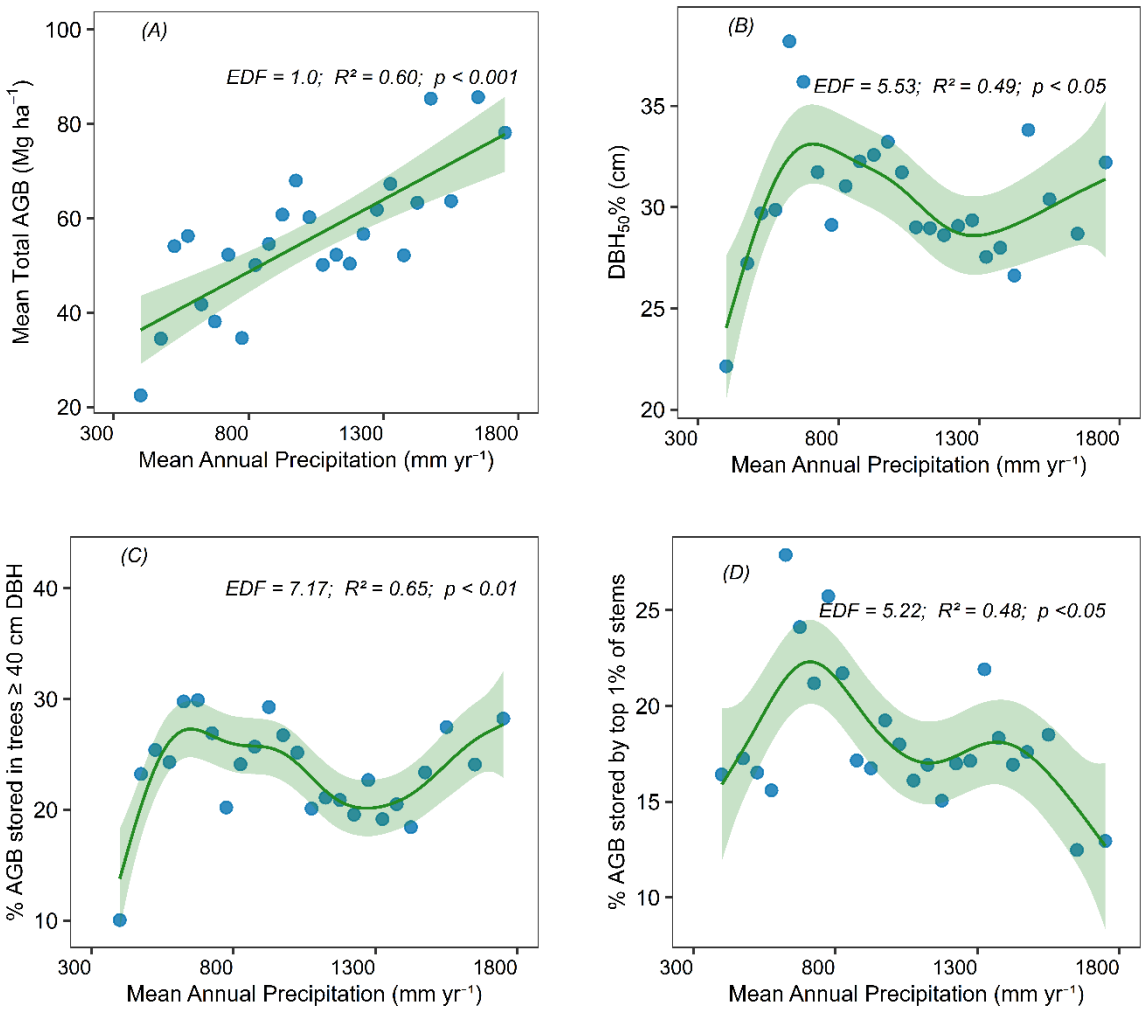


Figure 2.4.Relationships between mean annual precipitation and stand-level vegetation structure across the Miombo ecoregion.

(A)The upper left panel shows the increase in total above-ground biomass (AGB) with rainfall, while (B) the upper right panel illustrates the rise in the diameter threshold above which trees collectively store 50 % of plot biomass (DBH_{50}%). The lower left panel (C) displays the proportion of total AGB contributed by large trees (≥ 40 cm DBH), whereas the lower right panel (D) shows the proportion of AGB stored by the top 1 % along the rainfall gradient. Lines represent fitted generalized additive models (GAMs) with shaded 95 % confidence intervals; points correspond to mean values for each rainfall class (n = 25).

2.3.4 Local drivers of biomass and structure

At the plot level, however, the relationship between rainfall and biomass was much weaker. A GAM fitted to individual plots using rainfall as the sole predictor explained only 11.6% of the deviance in total AGB (edf = 8.40, F = 39.56, p < 0.001; R^2adj = 0.11), reflecting substantial local-scale heterogeneity. Similar weak relationships were observed for other structural attributes (Table S4).

To identify the factors underlying this variability, we applied linear mixed-effects models (LMEs) incorporating environmental, structural, and disturbance variables while accounting for differences

among vegetation types as a random effect. These models explained the AGB attributes better compared to the GAM model.

For total AGB, the best-supported model ($R^2m \approx 0.37$, $R^2c \approx 0.43$) included rainfall, elevation, slope, aspect, fire frequency, soil properties (SOC, clay, CEC), and stand structural variables (Gini coefficient, QMD, and DBH kurtosis). Among these, QMD was the strongest positive predictor of total biomass, followed by SOC, rainfall and Gini_DBH, while elevation and fire frequency had significant negative effects (Figure 2.5). DBH kurtosis also showed a positive effect. The difference between R^2c and R^2m (≈ 6%) indicates a modest contribution of the random effect, meaning that most of the explained variance originated from the fixed predictors.

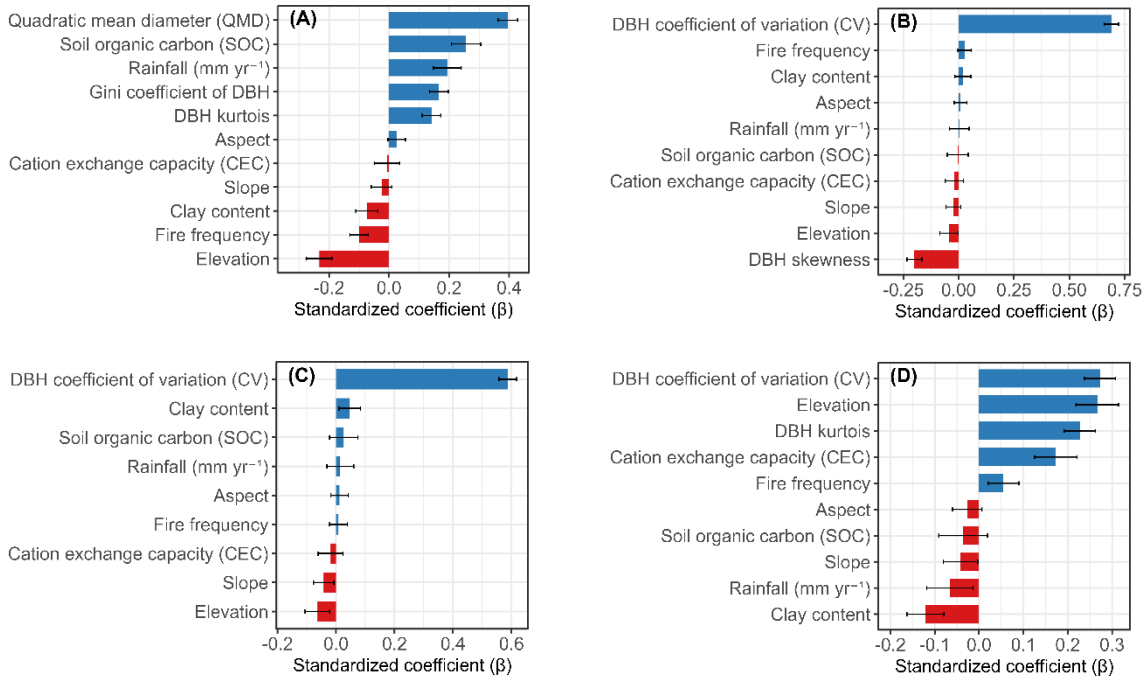


Figure 2.5. Standardised coefficients (β) and 95 % confidence intervals from linear mixed-effects models predicting forest structural and biomass attributes across Miombo ecoregion biomes.

. (a) Predictors of total AGB; (b) Predictors of $DBH_{50\%}$ threshold; (c) Predictors of % AGB stored in large trees (DBH ≥ 40 cm); (d) Predictors of % AGB stored in large trees (top 1%). Positive effects (blue) indicate predictors that increase the response variable, whereas negative effects (red) indicate variables associated with lower values.

For the proportion of AGB stored in large trees (DBH ≥ 40 cm), the best model ($R^2m \approx 0.37$, $R^2c \approx 0.39$) indicated that this attribute is primarily driven by structural variables, with DBH_CV exerting a strong positive effect and accounting for most of the explained variance (tables S5; S6; S7). Environmental variables, including rainfall, topography, and soil properties, had weak or non-significant effects. The very small difference between R^2c and R^2m (< 5%) indicates that the variance is almost entirely explained by fixed predictors, with negligible influence of vegetation type. The proportion of biomass

held by the largest 1% of stems ($R^2m \approx 0.20$, $R^2c \approx 0.29$) showed contributions from both structural and environmental variables. DBH_CV and elevation were the strongest predictors, followed by DBH kurtosis and soil properties (CEC positive, clay negative), while rainfall had a weak negative effect. The difference between R^2c and R^2m (≈ 9%) indicates a moderate contribution of the random effect, suggesting that part of the variability is associated with differences among vegetation types.

Similarly, the diameter threshold (DBH_{50}%), above which half of the stand's biomass is contained, was best explained ($R^2m \approx 0.40$, $R^2c \approx 0.43$) by DBH_CV (positive effect) and DBH skewness (negative effect), with smaller contributions from elevation and fire frequency. The small difference between R^2c and R^2m (≈ 3%) indicates that most of the explained variance is attributable to fixed predictors.

Across all models, structural variables consistently accounted for a large proportion of the explained variance, although their relative importance differed among response variables. DBH_CV was the dominant predictor for variables related to large trees (AGB ≥ 40 cm, top 1%, and DBH_{50}), while total AGB was additionally influenced by QMD, Gini_DBH and DBH kurtosis.As illustrated in Figure 2.6, the most variability in stand-level total or large tree biomass occurs within vegetation types rather than among them. These findings indicate that while rainfall defines the regional potential for biomass accumulation, local structural organisation, disturbance history, and soil properties determine how that potential is realised within stands. High-biomass plots are not simply influenced by rainfall; they are structurally more heterogeneous and less fire-affected, promoting the persistence and growth of large trees. Thus, Miombo ecoregion structure emerges from the interplay between broad climatic gradients and fine-scale ecological processes that shape tree size distributions and biomass allocation.

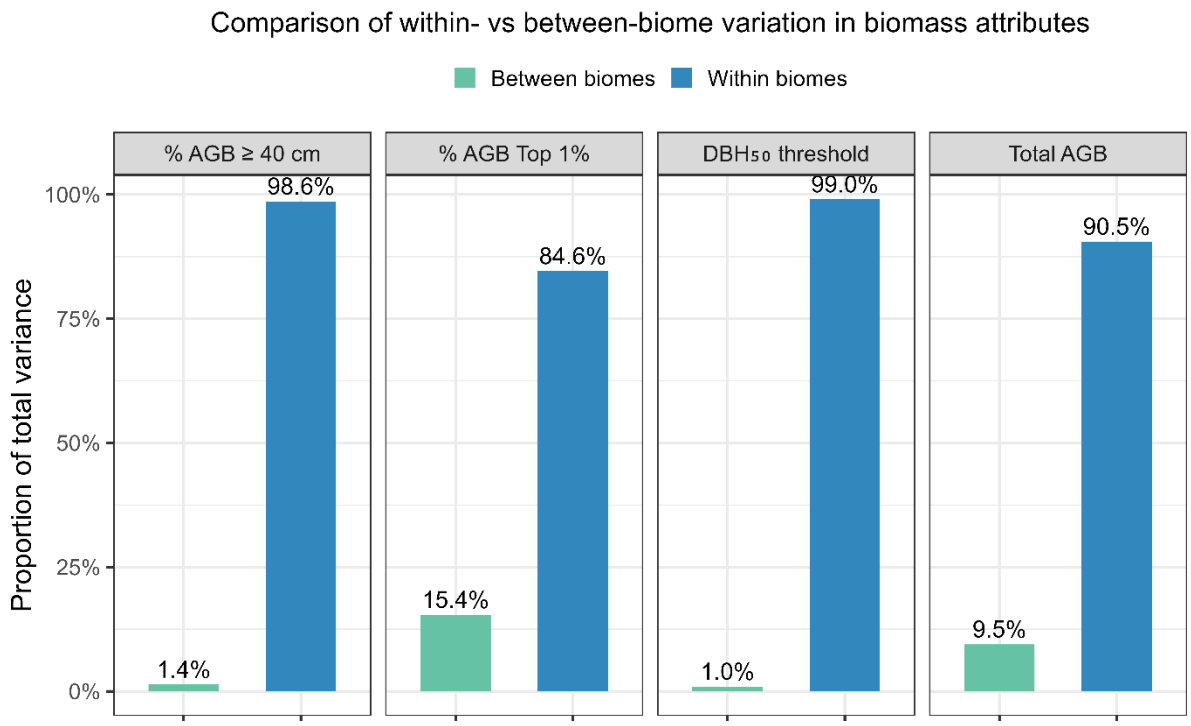


Figure 2.6. Partitioning of variance between and within Miombo vegetation types for each biomass-related attribute. Bars show the proportion of total variance explained by differences among vegetation types (green) and by within-vegetation types heterogeneity among plots (blue).

2.4 Discussion

2.4.1 Rainfall as a regional driver of forest biomass and structure

Our results shows that across the Miombo ecoregion, above-ground biomass (AGB) increased strongly and consistently with mean annual precipitation, confirming that water availability is the primary large-scale constraint on woody biomass in tropical dry forests. Mean stand AGB rose from 17 ± 14 Mg ha^{-1} in the driest woodlands (< 400 mm yr^{-1}) to 133 ± 47 Mg ha^{-1} in the wettest (> 1800 mm yr^{-1}). This result is aligns with previous researches showing that precipitation regulates total biomass through its control on tree growth and survival (February et al., 2013; Sankaran et al., 2005; Sterling & Orr, 2014; Xu et al., 2015). The near-linear increase observed here, with rainfall explaining more than 60% of the deviance in class-averaged AGB, highlights the dominant role of climate in setting the upper boundary of carbon storage across Miombo systems.

This increase in biomass was primarily associated with shifts in diameter structure rather than stem density. The strong increase in the contribution and density of large trees (≥ 40 cm DBH), together with the upward shift in DBH_{50}, indicates that biomass accumulation in wetter sites is driven by the development of larger stems rather than by higher recruitment. This pattern is consistent with studies showing that large trees account for a disproportionate share of forest carbon stocks (Slik et al., 2013; Bastin et al., 2018), and that their abundance increases under favourable moisture conditions. In contrast, the more moderate variation in the biomass share of the top 1% of stems suggests that biomass gains are not solely driven by a few extreme individuals, but by a broader shift in stand structure toward larger size classes. Together, these findings indicate that rainfall promotes biomass accumulation primarily through its effect on tree growth and size distribution.

2.4.2 Local modulation by soils, topography, and fire disturbance

At the plot scale, the explanatory power of rainfall declined sharply, while structural variables became the dominant predictors of biomass. The best-supported model for total AGB identified quadratic mean diameter (QMD), Gini coefficient, and DBH kurtosis as the key structural drivers, indicating that biomass is primarily controlled by the size and dominance of large stems. The strong positive effect of QMD reflects the central role of average stem size in biomass scaling, consistent with allometric theory, where biomass increases non-linearly with diameter (Chave et al., 2014). The positive effect of the Gini coefficient indicates that stands with greater size inequality store more carbon, as biomass becomes concentrated in

dominant individuals, a pattern also observed in tropical forests (Lutz et al., 2018). In addition, the positive effect of DBH kurtosis highlights the disproportionate contribution of extreme large trees, confirming that the presence of a small number of very large individuals strongly enhances stand-level biomass.

In contrast, attributes specifically related to large-tree dominance (AGB ≥ 40 cm, top 1%, and DBH_{50}) were best explained by DBH_CV and higher-order distribution metrics, indicating that different components of biomass are controlled by distinct aspects of diameter distribution. DBH_CV, which captures the overall spread of diameters, was the dominant predictor of these variables, suggesting that greater variability facilitates the emergence and persistence of large individuals within stands. This reflects the role of competitive differentiation and uneven growth in structuring tree populations. The additional influence of kurtosis and skewness further indicates that the shape of the diameter distribution, particularly the presence of extreme values and asymmetry controls how biomass is partitioned among trees. These results demonstrate that structural metrics are not interchangeable, but capture complementary ecological processes governing biomass organisation. Environmental variables had secondary but significant effects. Soil organic carbon (SOC) showed a positive relationship with total AGB, consistent with the role of soil fertility in enhancing productivity (Fayolle et al., 2012), while cation exchange capacity (CEC) was positively associated with the biomass share of the largest trees, suggesting that nutrient retention capacity may support long-term tree growth and survival. Elevation was negatively associated with total AGB, likely reflecting lower soil nutrient availability and cooler temperatures that constrain tree growth at higher altitudes (Ensslin et al., 2015; Moser et al., 2011; Ross et al., 2021). Similarly, fire frequency had negative effects on total AGB, reflecting environmental constraints and disturbance impacts on biomass accumulation. Fire is a key ecological process in Miombo woodlands, where frequent burning limits tree growth and maintains open stand structures (Saito et al., 2014). The weaker influence of these variables on large-tree metrics suggests that once trees reach large sizes, they become more resistant to disturbance, a pattern widely reported in savanna ecosystems.

2.4.3 Hierarchical regulation and ecological implications

The combined results reveal a clear hierarchical organisation of biomass controls across spatial scales. At the regional scale, rainfall defines the potential for biomass accumulation by regulating water availability and enabling the development of large trees. However, at the plot scale, this climatic control is largely overridden by local structural organisation and disturbance regimes. The relatively low explanatory power

of rainfall at the plot level, compared to the strong effects of structural variables, indicates that biomass variability is primarily driven by within-site processes rather than by broad environmental gradients.

Variance partitioning supports this interpretation, showing that most of the variation in biomass occurs within, rather than among, vegetation types. This suggests that stand-level processes such as disturbance history, competition, and size distribution play a more important role than biome classification in determining carbon storage.

These findings have important implications for carbon estimation and ecosystem modelling. They show that climatic variables alone are insufficient to explain biomass variability in Miombo systems, and that incorporating structural metrics, particularly those describing diameter distribution, can substantially improve predictions. Our results also align with Godlee et al. (2021) who showed that rainfall influences biomass indirectly by increasing species and structural diversity

2.4.4 Uncertainty related to ancillary datasets

The environmental variables used in this study are derived from gridded datasets and therefore represent averaged conditions at spatial resolutions coarser than individual plots. While this scale mismatch limits the ability to capture fine-scale variability, it is appropriate for analysing broad environmental gradients across large regions. In particular, soil variables such as SOC, clay content, and CEC are relatively stable properties that vary at broader spatial scales.

Fire frequency was derived from MODIS burned-area products, which are known to preferentially detect larger fires and under-represent small and low-intensity burns (Ramo et al., 2021; Sá et al., 2003). In Miombo ecoregion, where fire regimes are often patchy and dominated by small-scale events, this limitation likely leads to an underestimation of fire occurrence. As a result, the negative relationship between fire frequency and biomass observed here is likely stronger than what we detect, meaning that the true impact of fire may be stronger than estimated. Despite these limitations, the consistency of the observed relationships and the large spatial coverage of the dataset suggest that the main conclusions are robust.

2.5 Conclusion

This study demonstrates that above-ground biomass (AGB) across the Miombo ecoregion is governed by a hierarchical interaction between regional climatic gradients and local stand structure. Rainfall emerged as the dominant large-scale control, strongly increasing total biomass and promoting the development and persistence of large-diameter trees. However, this climatic effect weakened substantially at the plot scale, where biomass was primarily determined by diameter-based structural attributes. In particular, total AGB was best explained by quadratic mean diameter (QMD), Gini coefficient, and DBH kurtosis, indicating that biomass accumulation depends on average tree size, size inequality, and the presence of extreme large individuals. In contrast, metrics related to large-tree dominance (AGB ≥ 40 cm, top 1%, and DBH_{50}) were more strongly controlled by DBH_CV and distribution shape metrics, highlighting that different components of biomass are regulated by distinct aspects of stand structure.

These findings provide new empirical evidence that forest carbon storage in Miombo ecosystems is not only driven by rainfall, but also by how biomass is distributed among trees within stands. The strong contribution of large trees across the rainfall gradient confirms their disproportionate role in carbon storage, while the contrasting effects of structural metrics demonstrate that variability, inequality, and distribution shape capture complementary ecological processes. This multi-dimensional view of stand structure represents an important advance over approaches relying solely on mean size or density.

Overall, the results show that rainfall sets the upper limit of biomass accumulation, but local structural organisation and disturbance determine how this potential is realised. Consequently, accurate prediction of carbon stocks in tropical dry forests requires integrating structural metrics that describe diameter distributions in addition to climatic variables. Although this work spans a broad ecological gradient, it primarily focuses on structural and climatic determinants of biomass rather than productivity or turnover. Future research should combine long-term monitoring with functional trait approaches to capture the demographic and physiological mechanisms that sustain large trees and ensure long-term carbon stability across the Miombo landscape.

2.6 CRediT authorship contribution statement

Hermane Diesse: Writing – review & editing, Writing – original draft, Visualization, Methodology, Investigation, Formal analysis, Data curation, Conceptualization. **John L. Godlee**: Writing – review & editing, Supervision, Investigation, Conceptualization. **Nichola Knox:** Writing – review & editing, Conceptualization. **Vera De Cauwer:** Writing review & editing, Investigation, supervision, Conceptualization.

The following researchers have contributed to this chapter In providing their data through the SEOSAW network

Abel Siampale, Anderson Muchawona, Antje Ahrends, Aristides Muhate, Casey Ryan, Elifuraha Elisha Njoghomi, Emanuel Chidumayo, Francisco Maiato Pedro Gonçalves, Hemant Tripathi, Hermane Diesse, Iain McNicol, Joao Carreiras, Johannes Wallenfang, Rasmus Revermann, Jonathan Muledi, Manfred Finckh, Mathew Rees, Mathew Williams, Natasha Ribeiro, Pierre Proces, Rose Pritchard, Steve Makungwa, Tatenda Gotore, Thom Brade, Wilson Mugasha, Zimbabwe Forestry Commission, William Kindeketa, Canisius Kayombo, Soah Shabani, David Harris, Sérgio João, Emily Woollen, ACES, Sá Nogueira Lisboa, Penny Mograbi, Naftal Mahewa Lissu, Antonio Valter Chisingui, Jose João Tchamba, Kyle G. Dexter, Mylor Ngoy Shutcha, E. Mucau, M. Futuro, J. Da Conceicao, M. Kikongo, M. Panzo, M. Pedro, M. Monizi, N. Mampasi, E. Martins, Hermenegildo, Samuel Bowers, Joana Melo, Maria Vasconcelos, Isla Grundy, César Pérez-Cruzado, Cori Ham, Christoph Kleinn, Paul Magdon, J. Stoffels, Jolien de Ruytter, Miya Kabajani, Ninda Baptista and P. Graz.

2.7 References

Bastin, J.-F., Barbier, N., Réjou-Méchain, M., Fayolle, A., Gourlet-Fleury, S., Maniatis, D., De Haulleville, T., Baya, F., Beeckman, H., Beina, D., Couteron, P., Chuyong, G., Dauby, G., Doucet, J.-L., Droissart, V., Dufrêne, M., Ewango, C., Gillet, J. F., Gonmadje, C. H., … Bogaert, J. (2015). Seeing Central African forests through their largest trees. Scientific Reports, 5(1), 13156. https://doi.org/10.1038/srep13156

Bates, D., Mächler, M., Bolker, B., & Walker, S. (2015). Fitting Linear Mixed-Effects Models Using lme4. Journal of Statistical Software, 67(1). https://doi.org/10.18637/jss.v067.i01

Bordin, K. M., Esquivel-Muelbert, A., Bergamin, R. S., Klipel, J., Picolotto, R. C., Frangipani, M. A., Zanini, K. J., Cianciaruso, M. V., Jarenkow, J. A., Jurinitz, C. F., Molz, M., Higuchi, P., Silva, A. C. D., & Müller, S. C. (2021). Climate and large-sized trees, but not diversity, drive above-ground biomass in subtropical forests. Forest Ecology and Management, 490, 119126. https://doi.org/10.1016/j.foreco.2021.119126

Bourdier, T., Cordonnier, T., Kunstler, G., Piedallu, C., Lagarrigues, G., & Courbaud, B. (2016). Tree Size Inequality Reduces Forest Productivity: An Analysis Combining Inventory Data for Ten European Species and a Light Competition Model. plos one, 11(3), e0151852. https://doi.org/10.1371/journal.pone.0151852

Byers, B. (2001). Conserving the Miombo Ecoregion. WWF Southern Africa (p. 37).

Carrasco-Escobar, G., Schwalb, A., Tello-Lizarraga, K., Vega-Guerovich, P., & Ugarte-Gil, C. (2020). Spatio-temporal co-occurrence of hotspots of tuberculosis, poverty and air pollution in Lima, Peru. Infectious Diseases of Poverty, 9(1), 32. https://doi.org/10.1186/s40249-020-00647-w

Chave, J., Réjou-Méchain, M., Búrquez, A., Chidumayo, E. N., Colgan, M. S., Delitti, W. B. C., Duque, A., Eid, T., Fearnside, P. M., Goodman, R. C., Henry, M., Martínez-Yrízar, A., Mugasha, W. A., Muller-Landau, H. C., Mencuccini, M., Nelson, B. W., Ngomanda, A., Nogueira, E. M., Ortiz-Malavassi, E., … Vieilledent, G. (2014). Improved allometric models to estimate the aboveground biomass of tropical trees. Global Change Biology, 20(10), 3177–3190. https://doi.org/10.1111/gcb.12629

Coomes, D. A., & Allen, R. B. (2007). Mortality and tree-size distributions in natural mixed-age forests. Journal of Ecology, 95(1), 27–40. https://doi.org/10.1111/j.1365-2745.2006.01179.x

Curtis, R. O., & Marshall, D. D. (2000). Technical Note: Why Quadratic Mean Diameter? Western Journal of Applied Forestry, 15(3), 137–139. https://doi.org/10.1093/wjaf/15.3.137

Davies, R. W., Ryan, C. M., Harrison, R. D., Dexter, K. G., Ahrends, A., Te Beest, M., Benitez, L., Brade, T. K., Carreiras, J. M. B., Druce, D. J., Fayolle, A., Finckh, M., Godlee, J. L., Gonclaves, F. M., Grundy, I. M., Hoche, T., Holdo, R. M., Makungwa, S., McNicol, I. M., … Edwards, D. P. (2023). Precipitation gradients drive high

tree species turnover in the woodlands of eastern and southern Africa. Ecography, e06720. https://doi.org/10.1111/ecog.06720

Diesse, H., Godlee, J. L., Knox, N., Muledi, J., Naftal, L., Nkulu, D., Nkomba, B., Uusiku, G., Dexter, K., & De Cauwer, V. (2025). Quantifying unseen woody biomass and diversity in understorey trees and shrubs at the extremes of water availability in the Miombo ecoregion. Forest Ecosystems, 13, 100302. https://doi.org/10.1016/j.fecs.2025.100302

Ensslin, A., Rutten, G., Pommer, U., Zimmermann, R., Hemp, A., & Fischer, M. (2015). Effects of elevation and land use on the biomass of trees, shrubs and herbs at Mount Kilimanjaro. Ecosphere, 6(3), 1–15. https://doi.org/10.1890/ES14-00492.1

Fayolle, A., Engelbrecht, B., Freycon, V., Mortier, F., Swaine, M., Réjou-Méchain, M., Doucet, J.-L., Fauvet, N., Cornu, G., & Gourlet-Fleury, S. (2012). Geological Substrates Shape Tree Species and Trait Distributions in African Moist Forests. PLoS ONE, 7(8), e42381. https://doi.org/10.1371/journal.pone.0042381

February, E. C., Higgins, S. I., Bond, W. J., & Swemmer, L. (2013). Influence of competition and rainfall manipulation on the growth responses of savanna trees and grasses. Ecology, 94(5), 1155–1164. https://doi.org/10.1890/12-0540.1

Frost, P. (1996). The ecology of miombo woodlands. In The Miombo in transition: Woodlands and Welfare in Africa (B. Campbell, pp. 11–57). Centre for International Forestry Research.

Godlee, J. L., Ryan, C. M., Bauman, D., Bowers, S. J., Carreiras, J. M. B., Chisingui, A. V., Cromsigt, J. P. G. M., Druce, D. J., Finckh, M., Gonçalves, F. M., Holdo, R. M., Makungwa, S., McNicol, I. M., Mitchard, E. T. A., Muchawona, A., Revermann, R., Ribeiro, N. S., Siampale, A., Syampungani, S., … Dexter, K. G. (2021). Structural diversity and tree density drives variation in the biodiversity–ecosystem function relationship of woodlands and savannas. New Phytologist, 232(2), 579–594. https://doi.org/10.1111/nph.17639

Halperin, J., Lemay, V., Chidumayo, E., Verchot, L., & Marshall, P. (2016). Model-based estimation of above-ground biomass in the miombo ecoregion of Zambia. Forest Ecosystems, 1–17. https://doi.org/10.1186/s40663-016-0077-4

Hengl, T., Mendes De Jesus, J., Heuvelink, G. B. M., Ruiperez Gonzalez, M., Kilibarda, M., Blagotić, A., Shangguan, W., Wright, M. N., Geng, X., Bauer-Marschallinger, B., Guevara, M. A., Vargas, R., MacMillan, R. A., Batjes, N. H., Leenaars, J. G. B., Ribeiro, E., Wheeler, I., Mantel, S., & Kempen, B. (2017). SoilGrids250m: Global gridded soil information based on machine learning. PLOS ONE, 12(2), e0169748. https://doi.org/10.1371/journal.pone.0169748

Hersbach, H., Bell, B., Berrisford, P., Hirahara, S., Horányi, A., Muñoz-Sabater, J., Nicolas, J., Peubey, C., Radu, R., Schepers, D., Simmons, A., Soci, C., Abdalla, S., Abellan, X., Balsamo, G., Bechtold, P., Biavati, G., Bidlot, J., Bonavita, M., … Thépaut, J. (2020). The ERA5 global reanalysis. Quarterly Journal of the Royal Meteorological Society, 146(730), 1999-2049. https://doi.org/10.1002/qj.3803

Ivory, S. J., Lézine, A.-M., Vincens, A., & Cohen, A. S. (2012). Effect of aridity and rainfall seasonality on vegetation in the southern tropics of East Africa during the Pleistocene/Holocene transition. Quaternary Research, 77(1), 77–86. https://doi.org/10.1016/j.yqres.2011.11.005

Johnson, M. O., Galbraith, D., Gloor, M., De Deurwaerder, H., Guimberteau, M., Rammig, A., Thonicke, K., Verbeeck, H., Von Randow, C., Monteagudo, A., Phillips, O. L., Brienen, R. J. W., Feldpausch, T. R., Lopez Gonzalez, G., Fauset, S., Quesada, C. A., Christoffersen, B., Ciais, P., Sampaio, G., … Baker, T. R. (2016). Variation in stem mortality rates determines patterns of above-ground biomass in A mazonian forests: Implications for dynamic global vegetation models. Global Change Biology, 22(12), 3996–4013. https://doi.org/10.1111/gcb.13315

Lian, M., Chen, L., Hui, C., Zhu, F., & Shi, P. (2024). On the Relationship Between the Gini Coefficient and Skewness. Ecology and Evolution, 14(12), e70637. https://doi.org/10.1002/ece3.70637

Lüdecke, D., Ben-Shachar, M., Patil, I., Waggoner, P., & Makowski, D. (2021). performance: An R Package for Assessment, Comparison and Testing of Statistical Models. Journal of Open Source Software, 6(60), 3139. https://doi.org/10.21105/joss.03139

Lutz, J. A., Furniss, T. J., Johnson, D. J., Davies, S. J., Allen, D., Alonso, A., Anderson-Teixeira, K. J., Andrade, A., Baltzer, J., Becker, K. M. L., Blomdahl, E. M., Bourg, N. A., Bunyavejchewin, S., Burslem, D. F. R. P., Cansler, C. A., Cao, K., Cao, M., Cárdenas, D., Chang, L., … Zimmerman, J. K. (2018). Global importance of large-diameter trees. Global Ecology and Biogeography, 27(7), 849–864. https://doi.org/10.1111/geb.12747

Mayaux, P., Bartholomé, E., Fritz, S., & Belward, A. (2004). A new land-cover map of Africa for the year 2000. Journal of Biogeography, 31(6), 861–877. https://doi.org/10.1111/j.1365-2699.2004.01073.x

Meyer, D., Dimitriadou, E., Hornik, K., Weingessel, A., & Leisch, F. (2025). e1071: Misc Functions of the Department of Statistics, Probability Theory Group (Formerly: E1071), TU Wien (p. 1.7-16) [Data set]. https://doi.org/10.32614/CRAN.package.e1071

Moser, G., Leuschner, C., Hertel, D., Graefe, S., Soethe, N., & Iost, S. (2011). Elevation effects on the carbon budget of tropical mountain forests (S Ecuador): The role of the belowground compartment: elevation effects on forest carbon cycling. Global Change Biology, 17(6), 2211–2226. https://doi.org/10.1111/j.1365-2486.2010.02367.x

Muñoz-Sabater, J., Dutra, E., Agustí-Panareda, A., Albergel, C., Arduini, G., Balsamo, G., Boussetta, S., Choulga, M., Harrigan, S., Hersbach, H., Martens, B., Miralles, D. G., Piles, M., Rodríguez-Fernández, N. J., Zsoter, E., Buontempo, C., & Thépaut, J.-N. (2021). ERA5-Land : A state-of-the-art global reanalysis dataset for land applications. Earth System Science Data, 13(9), 4349-4383. https://doi.org/10.5194/essd-13-4349-2021

Pach, M., & Podlaski, R. (2015). Tree diameter structural diversity in Central European forests with Abies alba and Fagus sylvatica: Managed versus unmanaged forest stands. Ecological Research, 30(2), 367–384. https://doi.org/10.1007/s11284-014-1232-4

Pan, Y., Birdsey, R. A., Fang, J., Houghton, R., Kauppi, P. E., Kurz, W. A., Phillips, O. L., Shvidenko, A., Lewis, S. L., Canadell, J. G., Ciais, P., Jackson, R. B., Pacala, S. W., McGuire, A. D., Piao, S., Rautiainen, A., Sitch, S., & Hayes, D. (2011). A Large and Persistent Carbon Sink in the World's Forests. Science, 333(6045), 988–993. https://doi.org/10.1126/science.1201609

Piponiot, C., Anderson-Teixeira, K. J., Davies, S. J., Allen, D., Bourg, N. A., Burslem, D. F. R. P., Cárdenas, D., Chang-Yang, C., Chuyong, G., Cordell, S., Dattaraja, H. S., Duque, Á., Ediriweera, S., Ewango, C., Ezedin, Z., Filip, J., Giardina, C. P., Howe, R., Hsieh, C., … Muller-Landau, H. C. (2022). Distribution of biomass dynamics in relation to tree size in forests across the world. New Phytologist, 234(5), 1664–1677. https://doi.org/10.1111/nph.17995

Poorter, H., Niklas, K. J., Reich, P. B., Oleksyn, J., Poot, P., & Mommer, L. (2012). Biomass allocation to leaves, stems and roots: Meta-analyses of interspecific variation and environmental control. New Phytologist, 193(1), 30–50. https://doi.org/10.1111/j.1469-8137.2011.03952.x

Ramo, R., Roteta, E., Bistinas, I., Van Wees, D., Bastarrika, A., Chuvieco, E., & Van Der Werf, G. R. (2021). African burned area and fire carbon emissions are strongly impacted by small fires undetected by coarse resolution satellite data. *Proceedings of the National Academy of Sciences*, *118*(9), e2011160118. https://doi.org/10.1073/pnas.2011160118

R Core Team. (2023). R: A Language and Environment for Statistical Computing_. R Foundation for Statistical Computing, Vienna, Austria. <https://www.R-project.org/> [Computer software].

Reichstein, M., & Carvalhais, N. (2019). Aspects of Forest Biomass in the Earth System: Its Role and Major Unknowns. Surveys in Geophysics, 40(4), 693–707. https://doi.org/10.1007/s10712-019-09551-x

Réjou-Méchain, M., Tanguy, A., Piponiot, C., Chave, J., & Hérault, B. (2017). biomass: An r package for estimating above-ground biomass and its uncertainty in tropical forests. 8(9), 1163–1167. https://doi.org/10.1111/2041-210X.12753

Ribeiro, N. S., Katerere, Y., Chirwa, P. W., & Grundy, I. M. (Eds). (2020). Miombo Woodlands in a Changing Environment: Securing the Resilience and Sustainability of People and Woodlands. Springer International Publishing. https://doi.org/10.1007/978-3-030-50104-4

Ribeiro, N. S., Shugart, H. H., & Washington-Allen, R. (2008). The effects of fire and elephants on species composition and structure of the Niassa Reserve, northern Mozambique. Forest Ecology and Management, 255(5–6), 1626–1636. https://doi.org/10.1016/j.foreco.2007.11.033

Ross, C. W., Hanan, N. P., Prihodko, L., Anchang, J., Ji, W., & Yu, Q. (2021). Woody-biomass projections and drivers of change in sub-Saharan Africa. Nature Climate Change, 11(5), 449–455. https://doi.org/10.1038/s41558-021-01034-5

Ryan, C. M., Pritchard, R., McNicol, I., Owen, M., Fisher, J. A., & Lehmann, C. (2016). Ecosystem services from southern African woodlands and their future under global change. Philosophical Transactions of the Royal Society B: Biological Sciences, 371(1703), 20150312. https://doi.org/10.1098/rstb.2015.0312

Ryan, C. M., & Williams, M. (2011). How does fire intensity and frequency affect miombo woodland tree populations and biomass? Ecological Applications, 21(1).

Sá, A., Pereira, J., Vasconcelos, M.J., Silva, J.M., Ribeiro, N.S., & Awasse, A. (2003). Assessing the feasibility of sub-pixel burned area mapping in miombo woodlands of northern Mozambique using MODIS imagery. International Journal of Remote Sensing, 24, 1783 - 1796.

Saito, M., Luyssaert, S., Poulter, B., Williams, M., Ciais, P., Bellassen, V., Ryan, C. M., Yue, C., Cadule, P., & Peylin, P. (2014). Fire regimes and variability in aboveground woody biomass in miombo woodland. Journal of Geophysical Research: Biogeosciences, 119(5), 1014–1029. https://doi.org/10.1002/2013JG002505

Sankaran, M., Hanan, N. P., Scholes, R. J., Ratnam, J., Augustine, D. J., Cade, B. S., Gignoux, J., Higgins, S. I., Le Roux, X., Ludwig, F., Ardo, J., Banyikwa, F., Bronn, A., Bucini, G., Caylor, K. K., Coughenour, M. B., Diouf, A., Ekaya, W., Feral, C. J., … Zambatis, N. (2005). Determinants of woody cover in African savannas. Nature, 438(7069), 846–849. https://doi.org/10.1038/nature04070

SEOSAW partnership. (2021). A network to understand the changing socio-ecology of the southern African woodlands (SEOSAW): Challenges, benefits, and methods. plants, people, planet, 3(3), 249–267. https://doi.org/10.1002/ppp3.10168

Shirima, D. D., Munishi, P. K. T., Lewis, S. L., Burgess, N. D., Marshall, A. R., Balmford, A., Swetnam, R. D., & Zahabu, E. M. (2011). Carbon storage, structure and composition of miombo woodlands in Tanzania's Eastern Arc Mountains: Carbon storage in miombo woodlands. African Journal of Ecology, 49(3), 332–342. https://doi.org/10.1111/j.1365-2028.2011.01269.x

Shirima, D. D., Totland, Ø., Munishi, P. K. T., & Moe, S. R. (2015). Relationships between tree species richness, evenness and aboveground carbon storage in montane forests and miombo woodlands of Tanzania. Basic and Applied Ecology, 16(3), 239–249. https://doi.org/10.1016/j.baae.2014.11.008

Slik, J. W. F., Paoli, G., McGuire, K., Amaral, I., Barroso, J., Bastian, M., Blanc, L., Bongers, F., Boundja, P., Clark, C., Collins, M., Dauby, G., Ding, Y., Doucet, J., Eler, E., Ferreira, L., Forshed, O., Fredriksson, G., Gillet, J., … Zweifel, N. (2013). Large trees drive forest aboveground biomass variation in moist lowland forests across the tropics. Global Ecology and Biogeography, 22(12), 1261–1271. https://doi.org/10.1111/geb.12092

Sterling, S., & Orr, B. (2014). Patterns of Tree Distribution within Small Communities of the Sudanian Savanna-Sahel. Land, 3(4), 1284–1292. https://doi.org/10.3390/land3041284

Timberlake, J., & Chidumayo, E. (2011). Miombo ecoregion vision report (Occasional Publications in Biodiversity). Occasional Publications in Biodiversity.

Wood, S. N. (2017). Generalized Additive Models: An Introduction with R SECOND EDITION (2nd Edition). Chapman and Hall/CRC. https://doi.org/10.1201/9781315370279

Xu, X., Medvigy, D., & Rodriguez-Iturbe, I. (2015). Relation between rainfall intensity and savanna tree abundance explained by water use strategies. Proceedings of the National Academy of Sciences, 112(42), 12992–12996. https://doi.org/10.1073/pnas.1517382112

Xu, X., Yang, J., Qi, S., Ma, Y., Liu, W., Li, L., Lu, X., & Liu, Y. (2025). Estimation of Forest Aboveground Biomass Using Sentinel-1/2 Synergized with Extrapolated Parameters from LiDAR Data and Analysis of Its Ecological Driving Factors. Remote Sensing, 17(14), 2358. https://doi.org/10.3390/rs17142358

Zanne, A., Lopez-Gonzalez, G., Coomes, D. A., Ilic, J., Jansen, S., Lewis, S. L., Miller, R. B., Swenson, N. G., Wiemann, M. C., & Chave, J. (2009). Data from: Towards a worldwide wood economics spectrum. Dryad. https://doi.org/10.5061/dryad.234

Zeileis, A. (2025). ineq: Measuring Inequality, Concentration, and Poverty (p. 0.2-13) [Data set]. https://doi.org/10.32614/CRAN.package.ineq

Zomer, R. J., Xu, J., & Trabucco, A. (2022). Version 3 of the Global Aridity Index and Potential Evapotranspiration Database. Scientific Data, 9(1), 409. https://doi.org/10.1038/s41597-022-01493-1

Appendix 1

Figure S1. Heatmap of Pearson correlations between model predictors. Values are rounded to two decimals; darker colors indicate stronger correlations.

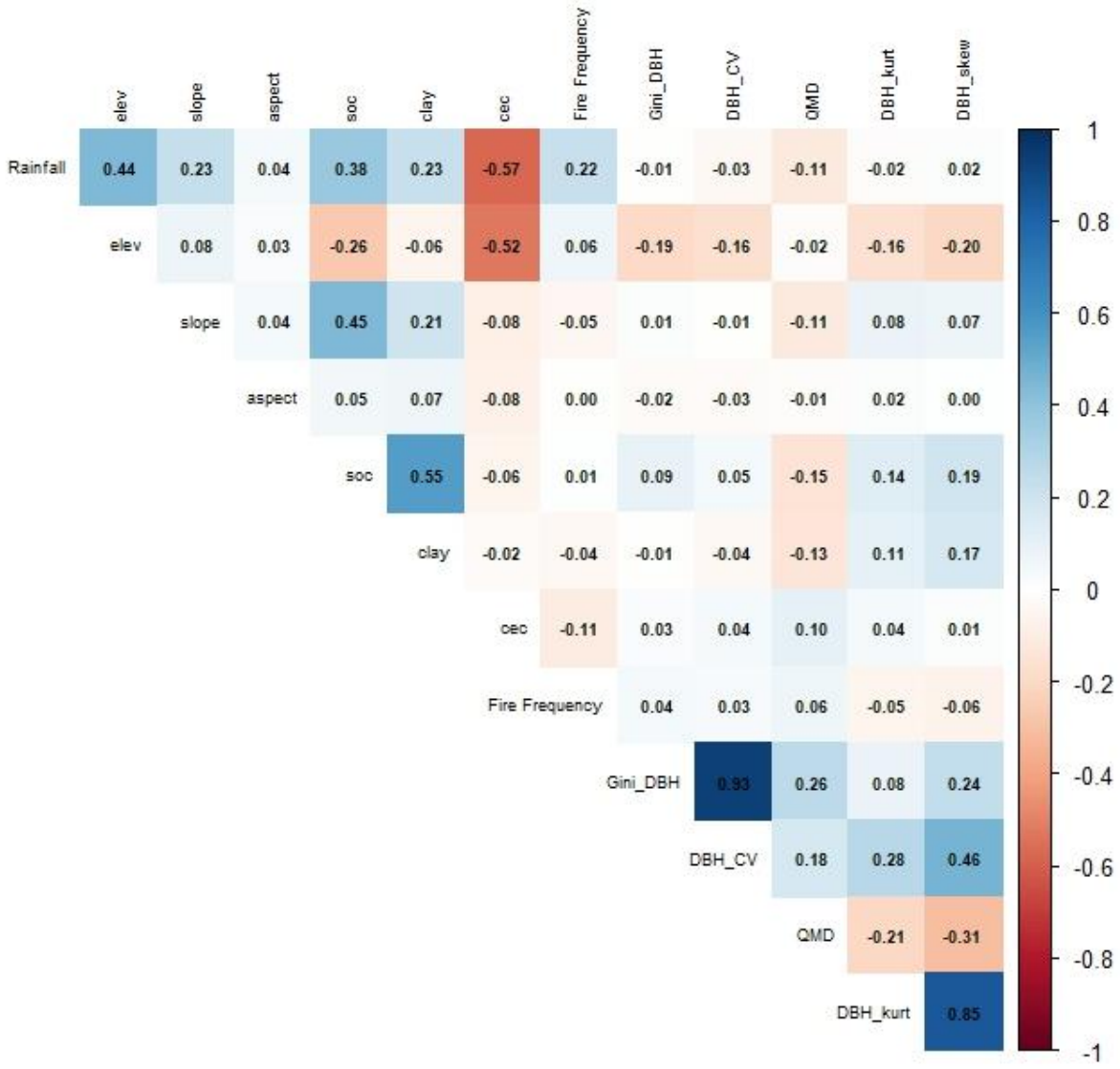


Table S1: The plot number per vegetation types

Vegetation types	Plot number
Coastal and lowland forests	127
Grasslands and savannas	103
Miombo woodlands	1586
Montane forests and mosaics	8

Mopane and dry woodlands	856
Thickets and bushlands	58
Wetlands and mangroves	11

Table S2: Distribution of plots by rainfall class

Rainfall Class (mm yr^{-1})	Number of Plots	% of total
R1: < 800	1028	37.3%
R2: 800–1000	709	25.7%
R3: 1000–1200	577	20.9%
R4: >1200	435	15.8%

Table S3. Collinearity assessment of explanatory variables included in the model predicting total aboveground biomass across study plots. The table reports VIF, adjusted VIF, tolerance, and their 95% confidence intervals. Gini_DBH and DBH_CV show high correlation, while other variables indicate low collinearity.

Term	VIF	VIF CI low	VIF_ CI high	SE_factor	Tolerance	Tolerance CI low	Tolerance CI high
MAP	1,79	1,7	1,89	1,34	0,56	0,53	0,59
Elev	2,04	1,93	2,16	1,43	0,49	0,46	0,52
Slope	1,3	1,25	1,37	1,14	0,77	0,73	0,8
Aspect	1,01	1	1,51	1	0,99	0,66	1
Soc	2,16	2,04	2,29	1,47	0,46	0,44	0,49
Clay	1,42	1,36	1,49	1,19	0,7	0,67	0,74
Cec	1,5	1,43	1,58	1,23	0,67	0,63	0,7
Fire frequency	1,08	1,04	1,13	1,04	0,93	0,88	0,96
Gini_DBH	13,15	12,24	14,14	3,63	0,08	0,07	0,08
DBH_CV	15,78	14,68	16,96	3,97	0,06	0,06	0,07
QMD	1,33	1,27	1,4	1,15	0,75	0,72	0,79
DBH_kurt	4,05	3,8	4,33	2,01	0,25	0,23	0,26
DBH_skew	6,45	6,03	6,92	2,54	0,15	0,14	0,17

Table S4. Summary of plot-level GAMs relating rainfall to biomass and structural attributes.

Response variable	edf	F	p-value	Deviance explained (%)	R^2adj
Total AGB	8,4	39,56	<0.001	11,6	0,11
Proportion of AGB ≥ 40 cm DBH	8,72	9,28	<0.001	3,1	0,03
Proportion of AGB in top 1% stems	8,28	8,71	<0.001	2,9	0,03
DBH_{50}	8,66	13,21	<0.001	4,3	0,04

Table S5. Relative importance of predictors in the final linear mixed-effects models for total aboveground biomass (AGB), proportion of AGB in large trees (DBH ≥ 40 cm), proportion of AGB in the largest 1% of stems, and DBH_{50}%.

Predictor	Total AGB	AGB ≥ 40 cm	AGB top 1%	DBH50
Aspect	0,02	0,01	0,02	0,00
Cation exchange capacity (CEC)	0,00	0,01	0,17	0,01
Clay content	0,07	0,04	0,12	0,01
DBH coefficient of variation (CV)		0,58	0,27	0,69
DBH kurtois	0,14		0,22	
DBH skewness				0,20
Elevation	0,23	0,06	0,26	0,04
Fire frequency	0,10	0,00	0,05	0,02
Gini coefficient of DBH	0,16			
Quadratic mean diameter (QMD)	0,39			
Rainfall (mm yr^{-1})	0,19	0,01	0,06	0,00
Slope	0,02	0,04	0,04	0,02
Soil organic carbon (SOC)	0,25	0,02	0,03	0,00

Table S6. Summary of the best-supported linear mixed-effects models for each response variable. Model performance is reported using marginal (R^2m) and conditional (R^2c) coefficients of determination. ΔR^2 ($R^2c - R^2m$) indicates the contribution of random effects and is interpreted as negligible (< 5%), modest (5–20%), or high (> 20%).

Response	Best_model	R2m	R2c	Delta_R2	Interpretation
Total AGB	Gini + QMD + kurtosis	0,37	0,43	0,064	Modest random effect
AGB ≥ 40 cm	DBH_CV	0,37	0,39	0,019	Negligible random effect
AGB top 1%	DBH_CV + kurtosis	0,2	0,29	0,083	Modest random effect
DBH_{50}	DBH_CV + skewness	0,4	0,43	0,036	Negligible random effect

Table S7. Comparison of alternative linear mixed-effects models tested for each response variable. Models differ in their representation of stand structural variables. The best-supported model for each response is identified based on the lowest AIC.

Response	Structural_variables	AIC	R2m	R2c	RMSE	Best_model
Total AGB	Gini	27296	0,25	0,34	35,36	
Total AGB	DBH_CV	27213	0,23	0,32	36,06	
Total AGB	Gini + QMD + kurt	26598	0,37	0,43	32,18	Yes
Total AGB	Gini + QMD + skew	26608	0,36	0,43	32,25	
AGB ≥ 40 cm	Gini	23990	0,29	0,32	19,31	
AGB ≥ 40 cm	DBH_CV	23494	0,37	0,39	18,16	Yes
AGB ≥ 40 cm	DBH_CV + kurt	23494	0,37	0,39	18,16	
AGB ≥ 40 cm	DBH_CV + skew	23495	0,37	0,39	18,16	
AGB top 1%	Gini + kurt	21162	0,15	0,24	11,78	
AGB top 1%	Gini + skew	21116	0,15	0,26	11,68	
AGB top 1%	DBH_CV + kurt	20961	0,2	0,29	11,36	Yes
AGB top 1%	DBH_CV + skew	20986	0,19	0,29	11,41	
DBH50	DBH_CV	20696	0,36	0,41	10,82	
DBH50	DBH_CV + kurt	20670	0,37	0,42	10,76	
DBH50	DBH_CV + skew	20566	0,4	0,43	10,56	Yes
DBH50	Gini + kurt	20809	0,33	0,39	11,04	
DBH50	Gini + skew	20819	0,33	0,39	11,06	

Chapter 3: Quantifying unseen woody biomass and diversity in understorey trees and shrubs at the extremes of rainfall in the Miombo ecoregion

Hermane Diesse [a,b,*], John L. Godlee [,c,b], Nichola Knox [d,g,i], Jonathan Muledi [b,e], Leena Naftal [a], David Nkulu [e], Ben Nkomba [e], Gabriel Uusiku [a], Kyle Dexter [b,c,f,h], Vera De Cauwer [a,b]

[a] Namibia University of Science and Technology, 13 Jackson Kaujeua Street, Windhoek, Namibia

[b] Socio-Ecological Observatory for Studying African Woodlands – SEOSAW network

[c] School of GeoSciences, University of Edinburgh, Edinburgh EH9 3FF, UK

[d] Downforce Technologies, 7 Albert Buildings, 49 Queen Victoria Street, London EC4N 4SA[e] Ecologie, Restauration Ecologique et Paysage, Faculté des Sciences Agronomiques, Route Kasapa BP 1825, Université de Lubumbashi, The Democratic Republic of the Congo

[f] Royal Botanic Garden Edinburgh, Edinburgh EH3 5LR, UK

[g] School of Earth and Space Exploration, Arizona State University, Phoenix, AZ 85287, USA

[h] Department of Life Sciences and Systems Biology, University of Torino, Torino, Italy

[i] College of Science and Engineering, Flinders University, Adelaide, SA, Australia

This chapter is adapted from the article published in Forest ecosystems:
https://doi.org/10.1016/j.fecs.2025.100302

Abstract

The Miombo ecoregion covers eastern and southern Africa, with variations in plant species composition, structure, and biomass across a broad precipitation gradient. Most studies of woody plant communities focus exclusively on larger overstorey trees (≥5 cm or ≥10 cm stem diameter), overlooking the contribution of small trees and shrubs in the understorey, which can comprise a significant portion of total biomass and diversity. Here, we evaluate the contribution of both large overstorey and small understorey woody plants to species diversity and above-ground biomass (AGB), with 17 plots (0.5–1 ha) across five sites representing both extremes of rainfall gradient spanning the Miombo ecoregion, in northeast Namibia (500–700 mm MAP) and southern Democratic Republic of Congo (>1200 mm MAP).

Mean AGB per site ranged from 21 to 119 Mg ha^{-1}, increasing with rainfall, while the proportional AGB contribution of small trees, saplings, and shrubs decreased. In dry Namibia, small trees, saplings, and shrubs (<5 cm DBH) contributed up to 28.2% of total AGB (mean ± standard deviation: 18.3% ± 3.4%), whereas in wet DRC, they contributed only up to 2.5% (2.3% ± 1.4%).

Namibian sites, on average, contained a large proportion of woody species diversity exclusively in small trees and shrubs (<5 cm DBH), with 55 species representing 59.4% of the total diversity. In contrast, DRC sites had higher overall small woody plant diversity (66 species) but fewer species found exclusively as small individuals (25.2%), with many saplings that grow to larger trees. Understorey composition also differed, with saplings of overstorey trees dominating in DRC, while shrubs dominated in Namibia.

Our findings show that woody biomass and diversity in dry woodlands are substantially underestimated when studies focus only on larger trees. This highlights the need to consider all woody vegetation to better understand woody plant diversity and biomass variation.

Keywords: Miombo woodlands, plant diversity, overstorey, understorey, biomass, shrubs, vegetation structure

3.1 Introduction

The Miombo ecoregion, spanning 11 countries in eastern and southern Africa, encompasses a variety of vegetation types, including the core Miombo woodlands dominated by the legume genera Brachystegia, Julbernardia and Isoberlinia, as well as other woodland types such as Mopane, Burkea-Terminalia, and Baikiaea woodlands (Timberlake and Chidumayo, 2011). These ecosystems provide numerous goods and services, including biodiversity conservation, carbon sequestration, and support for the livelihoods of millions of people (Ryan et al., 2016). Across the Miombo ecoregion, precipitation is a critical factor influencing ecosystem structure and function, resulting in highly heterogeneous vegetation patterns (Campbell, 1996; Godlee et al., 2021; Kuyah et al., 2016). Miombo woodlands sensu lato, found in regions with mean annual precipitation (MAP) between 600 and 1400 mm, are characterised by an open tree canopy overstorey, a discontinuous understorey of shrubs and small trees, and a grass-dominated ground layer (Frost, 1996; Mayaux et al., 2004; Ryan et al., 2012). Canopy cover in these woodlands ranges from 20% to almost 100%, leading to varied understorey light conditions (Timberlake and Chidumayo, 2011). The canopy cover and diversity of large canopy trees generally increase with water availability (Godlee et al., 2021; Sankaran et al., 2005), illustrating the important role of precipitation. However, these patterns may not reflect those of small woody plants in the understorey which may exhibit different or even contrasting responses to environmental gradients due to an overriding influence of large canopy trees. Exceptions also exist, particularly in wetter regions, where local disturbances such as tree mortality or selective logging can create canopy gaps, allowing more light to reach the ground, and supporting a diverse understorey layer. While most studies assessing woody diversity and biomass stocks focus only on large overstorey trees (diameter at breast height ≥ 5 or 10 cm), research integrating all structural layers and growth forms is essential for a more complete understanding of ecosystems.

Woodland ecosystems comprise distinct vertical structural layers and their balance is strongly influenced by environmental factors, including precipitation. The overstorey layer, composed of larger trees, plays a crucial role in vegetation structure, diversity, and functioning (Ali et al., 2019; Balandier et al., 2022; Godlee et al., 2024). Overstorey trees, with their large canopies and root systems, influence the establishment and growth of the understorey layer through competition for water, soil nutrients, space, and light (Ahmad et al., 2019; Balandier et al., 2022). In wetter regions, such as the Miombo woodlands of the Democratic Republic of the Congo (DRC), higher rainfall promotes overstorey tree growth, leading to denser canopies that limit light penetration and reduce the understorey layer contribution to the total AGB stocks (Frost, 1996; Munalula et al., 2020; Sankaran et al., 2005). This relationship, however, also

extends to understorey biodiversity. Increased canopy cover and tree density favour shade-tolerant species while restricting the establishment of light-demanding species (Baker et al., 2020; Dormann et al., 2020). In contrast, drier regions like Namibia's woodlands have more open canopies due to lower precipitation, allowing greater light availability for the understorey layer and potentially higher understorey biomass and woody plant species (Figure 3.1). Therefore, in dry woodlands, the understorey layer may constitute a major contribution to overall biomass stocks and woody plant diversity. Although some studies of wet forests have suggested that stand-level AGB can be predicted from a few large-sized trees (Ali et al., 2019; Slik et al., 2013), this view may overlook the significant roles of small trees and shrubs, especially in more open woodlands in lower rainfall areas, which can hold a substantial and diverse understorey component (Sagar et al. 2008).

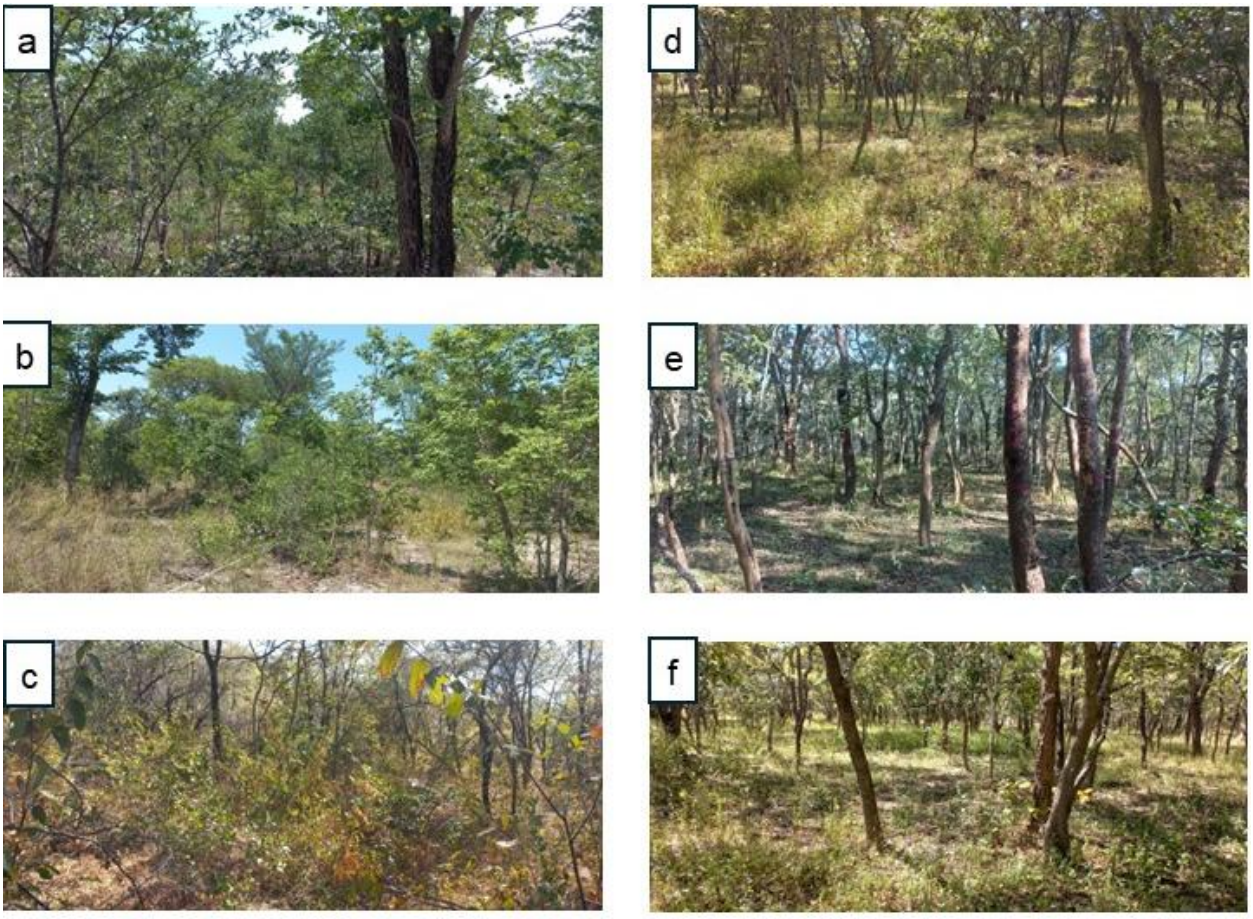


Figure 3.1. Typical representation of the understorey layer in dry and wet Miombo

Where 'a', 'b' and 'c' are respectively SK1 (plot 2 in Kanovlei state forest), H3 (plot 3 in Hamoye state forest) and Z1 (plot 1 in Sachinga Livestock). While 'd', 'e' and 'f' are respectively M2, M1 and M3. These pictures illustrate how dense is the understorey layer in dry Miombo compared to wet Miombo.

Smaller woody plants in the understorey layer are not frequently included in assessments of woody plant diversity and AGB monitoring (Huff et al., 2018). The minimum diameter at breast height (DBH) is commonly 10 cm in wet tropical forest biomass and diversity studies (Chave et al., 2014) and commonly 5 cm in dry tropical woodlands (Moonlight et al., 2020; SEOSAW partnership, 2021). Including smaller understorey woody plants in field inventories can be time-consuming due to their abundance and are perceived to contribute little to total AGB stocks and species diversity (Kindermann et al., 2022; Le et al., 2018). Yet, many studies have shown the critical role played by the understorey layer in determining fire behaviour, provision of non-timber products and firewood, soil protection, carbon sequestration, overstorey regeneration (Ferrara et al., 2023; Lombaerde et al., 2018; Suchar and Crookston, 2010), and biodiversity (Bricca et al., 2023). A high proportion of small trees in the understorey suggests good recruitment of tree species while a lack of small trees suggests potential future changes to vegetation structure and function (Muvengwi et al., 2020). Areas with dense and diversified understorey vegetation increase wildlife species presence by providing them with palatable forage and fruit which can help with the dispersal of trees and thus habitat stability (Lone et al., 2014; Nijland et al., 2014).

Investigating the diversity and contribution to the total biomass of smaller understorey woody plants in the Miombo ecoregion is imperative for understanding the full extent of forest functionality and guiding sustainable management efforts (Návar et al., 2004). Integrating understorey assessments can reveal their significant role in contributing to above-ground biomass (AGB) and enhance our understanding of ecosystem diversity (Le et al., 2018). This improved understanding would enable a reassessment of ecosystem service values and lead to more informed conservation priorities and targeted policies, such as the United Nations' Reducing Emissions from Deforestation and Forest Degradation Plus (REDD+). Despite its ecological importance, however, there remains a notable knowledge gap concerning the composition and biomass stocks of the understorey layer within the Miombo ecoregion.

This study describes covariation in woody species diversity and AGB in larger overstorey trees and understorey woody plants across the dry woodlands of Namibia and the wet Miombo woodlands of DRC, which represent the extremes of water availability in the Miombo ecoregion. Most previous research in the Miombo ecoregion on ecosystem structure has been carried out at single sites which precludes studying the role of variation in important environmental factors such as rainfall and water availability. Thus, there is a need to incorporate data on a large scale to better understand the composition, structure, and functioning of the Miombo ecoregion (Muvengwi et al., 2020). This study represents the first effort

to detail the contribution of overstorey and understorey trees and shrubs to species diversity, woodland structure, and woody biomass in five sites located in two areas within the savanna woodlands, representing an extreme contrast in rainfall and water availability. We hypothesise that the understorey in drier Namibian woodlands will make a substantial (> 10%) contribution to woody biomass stocks and plant species richness, while their contribution will be significant (> 2%) but more limited in wetter woodlands (in the DRC).

3.2 Materials and Methods

3.2.1 Study area

Data were collected in five sites located in two areas, representing extremes of the rainfall gradient observed across the broader Miombo ecoregion (Figure 3.2) (Burke, 2002; Timberlake and Chidumayo, 2011). The dry woodlands of Namibia, situated in the northeastern part of the country, are mainly composed of Mopane woodlands (dominated by Colophospermum mopane) and open Burkea, Pterocarpus, and Terminalia woodlands (De Cauwer, 2023; Strohbach and Petersen, 2007). The woodlands of the DRC receive higher and more evenly distributed precipitation, resulting in higher water availability throughout the year. The vegetation is typical Miombo woodland, dominated by trees belonging to the legume genera of *Brachystegia, Julbernardia*, and *Isoberlinia* (Campbell, 1996).

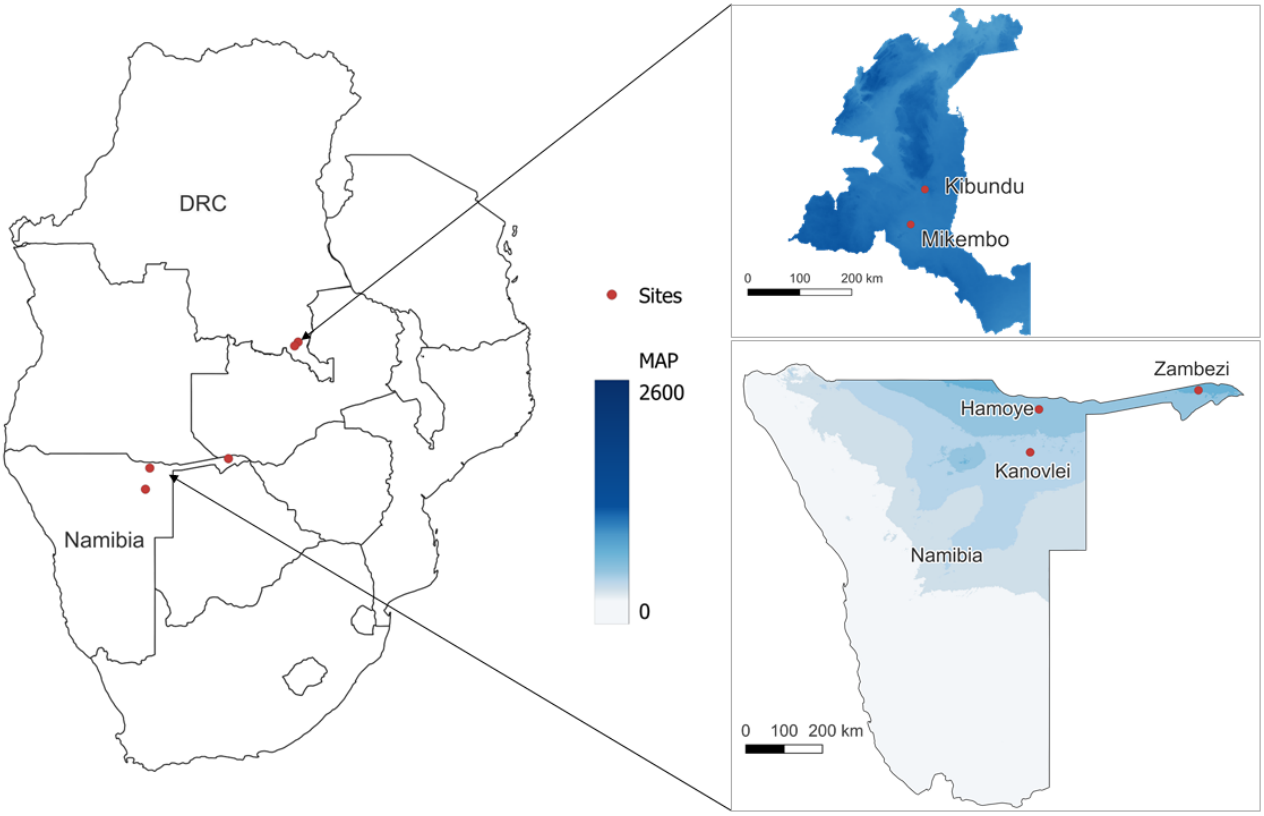


Figure 3.2. Location of study sites in Namibia and DRC.

(a) Upper Katanga Province in the Democratic Republic of Congo (DRC) (b), and Namibia (c). Panels b and c are shaded by Mean Annual Precipitation (MAP, mm). Kanovlei = 500 – 550 MAP; Hamoye = 560 MAP; Zambezi = 600 – 700 MAP; Kibundu = 1200 MAP; Mikembo = 1200 MAP.

The three Namibian study sites fall within the Kavango East Region (Hamoye State Forest), Otjozondjupa Region (Kanovlei State Forest) and Zambezi Region (Zambezi State Forest). Most of the soils in the northeastern part of Namibia are poor arenosols and have low water retention capacity (Hengl et al., 2014). The MAP in Hamoye is 560 mm whereas the MAP in Kanovlei is 500-550 mm (Atlas of Namibia Team, 2022; Cauwer et al., 2016; Mayr et al., 2018). The Zambezi region has the highest rainfall in Namibia with MAP between 600-700 mm (Mendelsohn et al., 2002), occurring mainly from November to March (Burke, 2006). The plots in the Zambezi State Forest were set up in the Sachinga Livestock Development Centre, a government farm under the Ministry of Agriculture Water and Land Reform. Wildfires impact the whole region, with limited controlled burning management implemented, the Sachinga site however has been actively protected from fire disturbance and fuelwood removal.

The two field sites in the DRC are in the Mikembo Reserve and Kibundu Village, both situated in the Upper Katanga Province in the southeastern part of the country. Mean annual temperature (MAT) is 20°C, and

MAP is 1200 mm, occurring mainly during the rainy season from November to April (Malaisse, 1997; Muledi et al., 2016). The soils of the Miombo woodlands in Upper Katanga are ferralsols, with a flat topography, but regularly punctuated (~3/ha) by large termite mounds up to 8 m in height (Muledi et al., 2016). Established in 2003, the Mikembo reserve is protected from fire disturbances and fuel-wood cutting (Muledi et al., 2016). In contrast, Kibundu Village, a community forest, has experienced disturbances from fire and fuel-wood harvesting. However, it was placed under protection in 2022, limiting any subsequent wood harvesting.

3.2.2 Data collection

All data were collected in 2023 during the period of peak vegetation cover. A total of 17 plots were established across the five sites, comprising seven plots of 1 ha and 10 plots of 0.5 ha. Variations in plot size accounted for differences in vegetation structure while balancing logistical constraints, ensuring a representative sample of biomass and species diversity across the study sites (Table S1 in the appendix). Overstorey vegetation was measured for the entire plot following the SEOSAW protocol v3.6 (https://seosaw.github.io/manuals.html).

Overstorey vegetation comprising large trees was defined as tree stems with a diameter at breast height (DBH, 1.3 m above ground) ≥ 5 cm. For each overstorey stem the following data were recorded: name of species, DBH at 1.3 m (or higher in case of possible deformities), crown diameter in two perpendicular directions, and stem height.

Understorey vegetation comprising small trees and shrubs was defined as woody individuals with stem diameter < 5 cm and with a plant height > 50 cm. Understorey vegetation was measured within nested plots of 25 m x 25 m within each 0.5/1 ha plot. A total of five subplots were established in each 1-ha plot while two subplots were established in each 0.5-ha plot (Figure 3.3). The following attributes were measured for the understorey woody vegetation: name of species, stem diameter measured with a Vernier calliper between 0.1 cm and 0.3 cm height above the ground, crown diameter in two perpendicular directions, height (measured by using a Vertex laser rangefinder or a measuring stick), and status, including dead and resprouting stems. All individuals were identified to the species level, except for two species comprising 42 individuals (3.6%) in the Zambezi State Forest, which were only identified by local names. Additionally, three species were assigned family-level morphospecies identities.

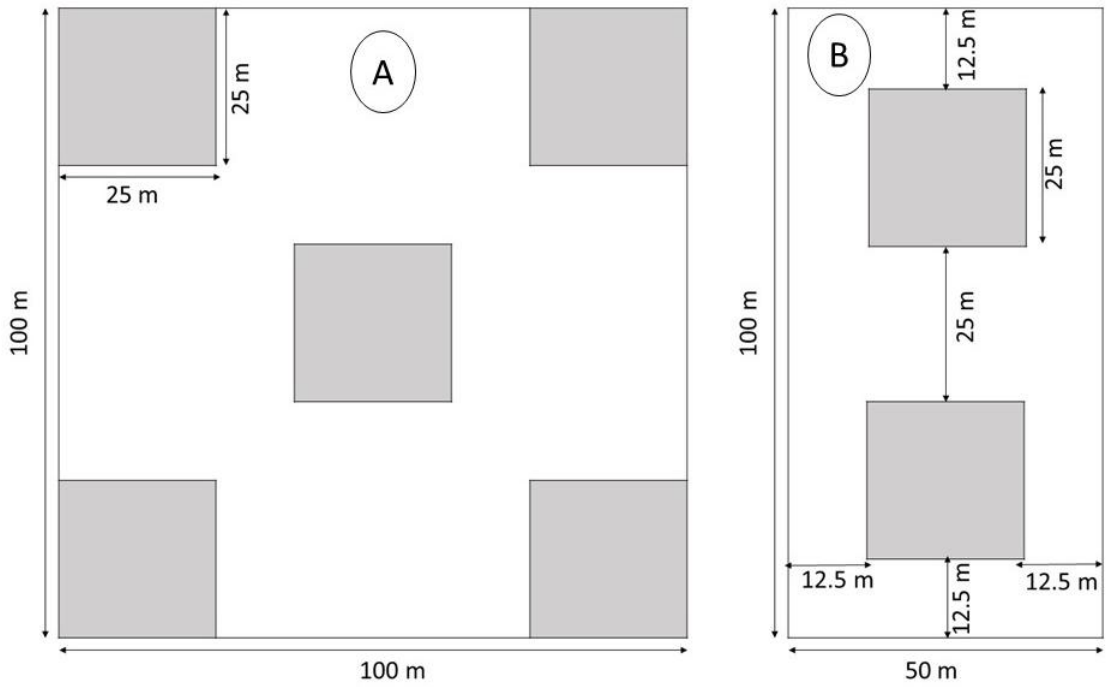


Figure 3.3. Plot design of the understorey subplots.
A = five nested plots within 1-ha or B = two nested plots within 0.5-ha

3.2.3 Data analysis

Woody plant density was calculated at the subplot level for all plots except for those in the Kibundu site, where the calculation was done at the plot level (0.5 ha) due to a lack of tree location data. To maintain consistency across sites, we extrapolated woody plant density to a 1-ha scale in all cases, regardless of whether measurements were taken at the subplot or plot level, ensuring comparability of woody plant density estimates across all sites.

To ensure consistency for diversity comparisons, 1-ha plots were divided into two halves, resulting in a 0.5-ha size for the overstorey diversity analysis. For understorey diversity analysis, two subplots per 0.5 ha were consolidated into one. In total, we analysed 24 plots of 0.5 ha for the overstorey diversity and 24 subplots of 0.125 ha total for the understorey diversity. All diversity metrics were calculated for both overstorey and understorey using the vegan package in R (Oksanen et al., 2015).

We calculated the Shannon-Wiener index (*H'*) using:

$$H' = -\sum_{i=1}^{s} p_i \ln p_i, \quad (1)$$

*w*here p_i is the proportion of individuals of species *i,* and *ln* is the natural logarithm. The value of *H'* ranges from 0 to *H'max* which depends on the species richness.

Secondly, we estimated species abundance evenness represented by the Shannon equitability index (*J*) (Smith and Wilson, 1996) using:

$$J = \frac{H'}{\ln s} \quad (2)$$

Where *s* is the species richness, calculated as the sum of species from each subplot. The evenness index measures how similar are the abundances of the different species within a community. A higher index value indicates a more balanced abundance of species, meaning that a few species do not dominate the community.

AGB of large trees in the overstorey layer was calculated using equation 4 from Chave et al. (2014) based on DBH, species woody density, and height.

$$AGB = 0.0673 \times (\rho\ D^2\ H)^{0.976} \times 1000 \quad (3)$$

Height measurements were collected for all trees at the Hamoye, Mikembo, and Kibundu sites, as well as the K1 and SK2 plots at the Kanovlei site. However, in the Zambezi site and the SK1 plot in Kanovlei, height measurements were limited to selected trees within the plots. For trees without height measurements, heights were predicted using the Regional Generalized Height Model developed by Mugasha et al. (2019)

$$H = 1.3 + (13.1646 \times BA^{0.1844}) \times (1 - \exp(-0.0537 \times D^{0.7896})) \quad (4)$$

Which has a percentage Root Mean Square Error of 31%, and uses mean annual precipitation, basal area (BA) per hectare and DBH (D) as explanatory variables.

To estimate understorey AGB, we used the models developed by Conti et al. (2019). These models have previously been applied to Miombo woodlands, including in the Zambezi State Forest by Kindermann et al. (2022). For multi-stemmed shrubs we used the canopy-based models, with two predictors including height (H) and mean crown diameter (CD) (Conti model equation 4):

$$AGB = \exp(-0.370 + 1.903 \ln(CD) + 0.652 \text{ Ln } (H)) \times 1.403 \quad (5)$$

For single-stemmed trees, we used equation 2 and equation 3, which incorporate basal diameter (BD) and either CD or H.

Equation 2 from Conti et al., (2019):

$$AGB = \exp(-2.057 + 1.741 \ln(BD) + 0.945 \ln(CD)) \quad (6)$$

Eqution 3 from Conti et al., (2019):

$$AGB = \exp(-2.869 + 2.584 \ln(BD)) \quad (7)$$

After calculating the AGB of individual woody plants, we determined each plot's total AGB per hectare by summing individual AGB values and dividing by the plot area. A diameter threshold of 10 cm DBH is sometimes used to define overstorey trees in tropical forest plots (e.g. RAINFOR, https://rainfor.org/). To assess the sensitivity of our findings to the DBH threshold, we recalculated the contribution of the understorey to total AGB by increasing the threshold to 10 cm DBH.

We calculated the basal area of each stem (g_i) for the overstorey layer using:

$$g_i = \pi (d_1/2 + d_2/2 + d_3/2, \ldots)^2.$$

Where d_i is the stem diameter of stem i recorded at 1.3 m. Each plot's basal area per hectare was calculated as the sum of overstorey tree stem basal areas divided by plot area (Table S1).

Understorey plants were categorized as either trees or shrubs based on field observations and descriptions from Mannheimer and Curtis (2018) and Van Wyk and Van Wyk (2013). Understorey trees were further differentiated into saplings or small trees according to their growth potential. Saplings are juvenile individuals of species that can eventually grow to large overstorey trees, while small trees are defined as individuals that remain confined to the understorey throughout their life cycle. A species was classified as a small tree if more than 90% of individuals were found in the understorey layer. This threshold was chosen based on empirical testing of various percentages (80%, 85%, 90%, and 95%). The 90% criterion effectively distinguishes species that are predominantly restricted to the understorey while minimizing misclassifications of saplings that may occasionally appear in the overstorey.

For diversity analyses, growth forms were grouped into ‘small trees and shrubs’, representing plants that remain in the understorey layer, and ‘saplings and large trees’, representing the plants that can reach the overstorey. For biomass stock analyses, growth forms were grouped into ‘small trees, shrubs and saplings’ i.e. the understorey, and ‘large trees’ i.e. the overstorey. These two different groupings both aimed to evaluate the diversity and biomass that may be respectively overlooked when focusing solely on trees with a diameter at breast height (DBH) ≥ 5 cm.

3.2.4 Statistical analysis

Statistical analysis was performed using R software (R Core Team, 2023). We checked the assumptions of parametric analysis for all data.

Linear Mixed effects models (LME) were employed to evaluate the relationships between overstorey and understorey characteristics, while accounting for potential variability across sites. The first set of LME assessed the influence of overstorey basal area on understorey species richness. Separate models were developed for understorey tree species richness and understorey shrub species richness with overstorey basal area included as a fixed effect and site as a random intercept term to account for unmeasured variability among sites.

The second set of LME assessed the influence of the overstorey basal area on the percentage of total AGB stored in the understorey layer. Overstorey basal area was included as a fixed effect and site again was treated as a random intercept term effect.

Prior to modelling, all continuous variables were centred and standardized using the scale function in R to make the model results reliable and easier to interpret. LME models were implemented using the lme4 package (Bates et al., 2015), and model diagnostics (e.g., linearity, homoscedasticity, and residual normality) were assessed using the performance package (Lüdecke et al., 2021) (Figure S1, Figure S2, Figure S3, Table S3 and Table S4).

A Kruskal-Wallis test, followed by a Dunn's test (using the Bonferroni method) was applied to compare the species richness, *J* and *H’* among sites because the assumptions required for parametric tests were not met.

A chi-squared test was performed to assess whether the different growth forms composing the understorey layer (small trees and saplings in one part and shrubs in another) have similar proportions of individuals at the study sites.

To analyse plant height structure, a total of eight classes were created (0.5 – 1 m, 1 – 2 m, 2 – 3 m, 3 – 4 m, 4 – 5 m, 5 – 7.5 m, 7.5 – 10 m and above 10 m).

A Mann-Whitney test was used to compare *H'* and the AGB stored in different understorey growth forms (shrubs, small trees, saplings).

3.3 Results

3.3.1 Floristic composition of the understorey and overstorey layers

Across all plots, 7,922 individuals were documented in the understorey layer and 5,118 individuals in the overstorey layer. Overall, the understorey layer in DRC sites had 67 species belonging to 50 genera and 27 families while the understorey layer in Namibian sites had 55 species belonging to 35 genera and 15 families. Overall, the overstorey layer in DRC sites had 79 species belonging to 54 genera and 27 families, whereas Namibian sites had 34 species belonging to 24 genera and 12 families. Examining family level composition, we found Fabaceae to be dominant across all layers in both the DRC and Namibia comprising 30 (40%) and 19 (28%) species respectively in the overstorey and understorey layers in DRC and 12 (38%) and 16 (30%) species in the overstorey and understorey in Namibia.

Analysis of plant growth forms in the understorey layer revealed significant differences across sites (χ^2 = 1630.7, df = 4, p-value < 0.001). In the DRC, small trees constituted 15.4% of plants sampled in the understorey, shrubs constituted 11.4%, and saplings of large trees constituted 74.5%. In contrast, in Namibia, small trees constituted 12%, shrubs constituted 47.3%, and saplings of large trees constituted 40.6%.

In Namibia, the understorey was dominated by *Ochna pulchra* (16%), *Psydrax livida* (11%), *Baphia massaiensis* (10%), while in the overstorey, *Burkea africana* (24%), *Combretum collinum* (12%), *Dialium engleranum* (12%) were the most abundant. In the DRC, the understorey was dominated by *Triumfetta dekindtiana* (15%), *Bridelia duvigneaudii* (13%), and *Julbernardia globiflora* (10%), while in the overstorey, *Julbernardia paniculata* (17%), *Brachystegia boehmii* (13%), and *Diplorhynchus condylocarpon* (9%) were the most dominant.

3.3.2 Distribution of species diversity and woody density across forest layers

Total woody plant species richness (including the understorey and overstorey) ranged from 18 to 53 species per 0.5 ha. In general, species diversity and woody plant density increase along the rainfall gradient. A post-hoc Dunn's test following the Kruskal-Wallis analysis revealed significant differences in the Shannon-Wiener index (*H'*) among sites (χ^2 = 17.072, df = 4, p-value < 0.01), with Kibundu having significantly higher *H'* than Hamoye and Kanovlei (Figure 3.4).

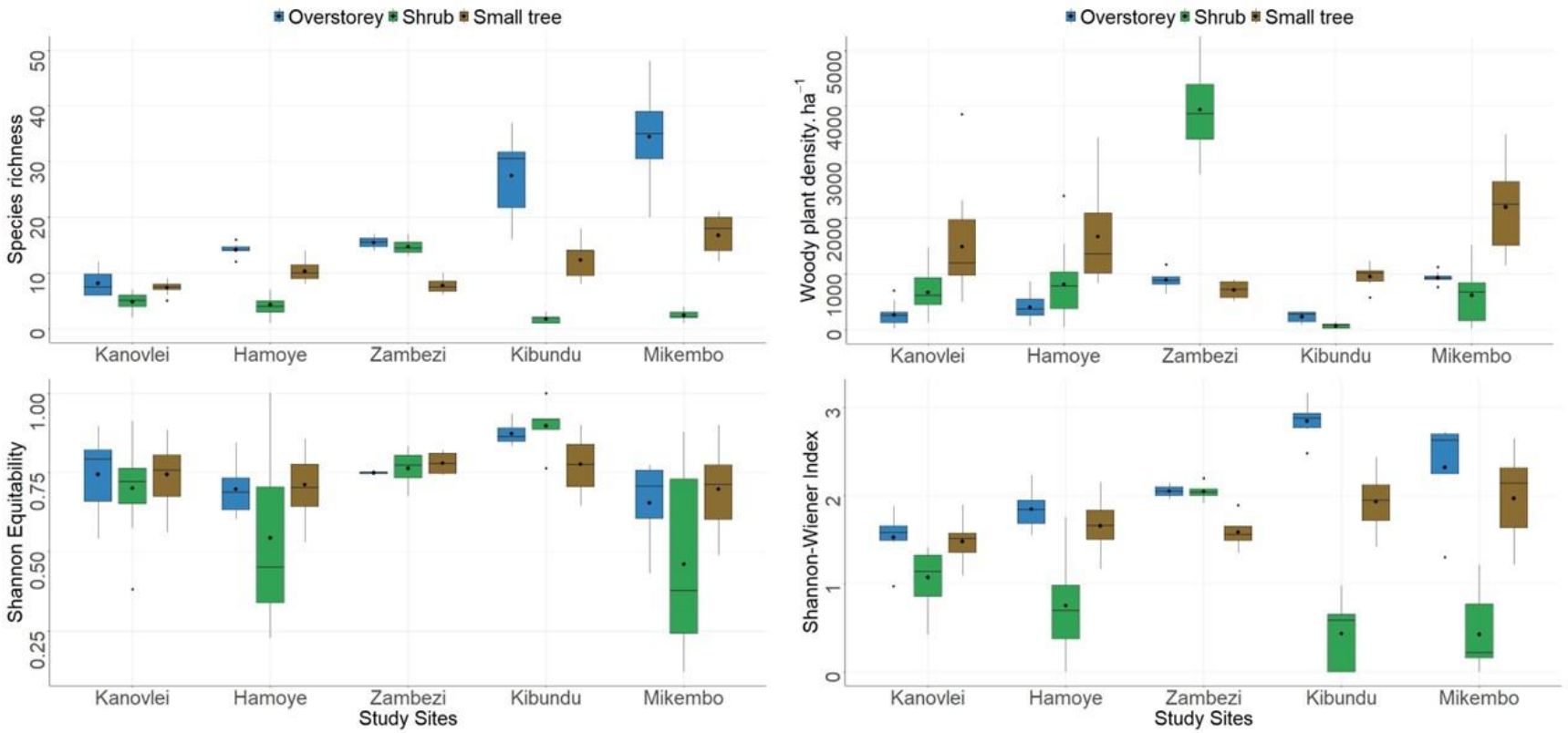


Figure 3.4. Variation in species richness, Shannon Equitability, woody plant density, and Shannon-Wiener index by site for understorey (small trees and shrubs) and overstorey (large trees and saplings) layers. Sites are ordered by mean annual precipitation: Kanovlei = 500 – 550 mm; Hamoye = 560 mm; Zambezi = 600 – 700 mm; Kibundu = 1200 mm; Mikembo = 1200 mm.

Additionally, a post hoc Dunn's test following the Kruskal-Wallis analysis revealed significant differences in Shannon equitability (*J*) across sites ($\chi^2 = 14.52$, df = 4, p-value < 0.01) with Kibundu having significantly higher *J* than Mikembo and Hamoye.

Focusing on the overstorey layer, species diversity was significantly ($\chi^2 = 12.638$, df = 1, p-value < 0.01) higher in the DRC sites compared to the Namibian sites (Figure 10). A post-hoc Dunn's test following the Kruskal-Wallis analysis revealed that overstorey species richness at Kanovlei was significantly lower than at Kibundu and Mikembo (Table 3.1). Additionally, the Shannon-Wiener index (*H'*) at Kanovlei was significantly lower than at Kibundu and Mikembo, while Kibundu had a higher *H'* than Hamoye (F = 11.52, p < 0.01). Shannon equitability (*J*) for the overstorey also varied significantly among sites, with Kibundu showing a higher *J* than Mikembo (F = 3.18, p < 0.05).

Table 3.1. Comparison of species richness, Shannon-Wiener index, Shannon equitability index, above-ground biomass (AGB), and woody plant density between overstorey and understorey layers. . Here the growth forms are combined. Values are presented as mean ± standard deviation. Letters indicate significant differences among sites for each metric within each layer (overstorey or understorey), with different letters (e.g., "a," "b," "c") denoting statistically distinct groups ($p < 0.05$).

Overstorey layer						
Country	Site	Species richness	Shannon-Wiener	Shannon equitability	AGB (Mg ha^{-1})	Woody plant density (ha^{-1})
Namibia	Kanovlei	8.1 ± 2.5 a	1.5 ± 0.3 a	0.74 ± 0.13 ab	15.4 ± 4.1 a	228 ± 145 a
Namibia	Hamoye	14.1 ± 1.3 ab	1.8 ± 0.2 ac	0.7 ± 0.09 ab	26.4 ± 9.4 a	364 ± 158 ac
Namibia	Zambezi	15.5 ± 2.1 ab	2.1 ± 0.1 ab	0.75 ± 0.01 ab	58.3 ± 0.0 ab	829 ± 168 ac
DRC	Kibundu	27.5 ± 8.1 b	2.8 ± 0.2 b	0.87 ± 0.04 b	51.0 ± 20.4 ab	233 ± 113 a
DRC	Mikembo	34.5 ± 11.4 b	2.3 ± 0.6 bc	0.66 ± 0.16 a	117.3 ± 43.2 b	901 ± 181 bc
Understorey layer						
Country	Site	Species richness	Shannon-Wiener	Shannon equitability	AGB (Mg ha^{-1})	Woody plant density (ha^{-1})
Namibia	Kanovlei	15.5 ± 0.8 a	2.0 ± 0.1 a	0.75 ± 0.04 a	5.9 ± 3.1 a	2078 ± 504 ab
Namibia	Hamoye	20.3 ± 1.9 ab	2.0 ± 0.2 a	0.68 ± 0.06 a	4.2 ± 1.2 ac	2339 ± 580 b
Namibia	Zambezi	29.0 ± 2.8 ab	2.6 ± 0.1 a	0.77 ± 0.04 a	8.7 ± 1.5 a	5048 ± 996 b
DRC	Kibundu	19.0 ± 3.5 ac	2.2 ± 0.3 a	0.76 ± 0.09 a	1.2 ± 1.4 b	1027 ± 238 ab
DRC	Mikembo	34.0 ± 7.1 bc	2.3 ± 0.6 a	0.67 ± 0.15 a	1.8 ± 0.4 bc	2671 ± 872 a

Similarly, in the understorey layer, species diversity indices were significantly higher in the DRC sites compared to the Namibian sites (Figure 3.5). A post-hoc Dunn's test following the Kruskal-Wallis analysis revealed that understorey species richness at Kanovlei was significantly lower than at Mikembo and Zambezi. In contrast, Kibundu's understorey species richness was significantly lower than that at Mikembo and Zambezi. However, no significant differences in *H*' and *J* were detected for the understorey layer across the sites.

Except in Zambezi, shrubs consistently exhibited the lowest *H'* and species richness, with values decreasing as rainfall increased. A Mann-Whitney test revealed a significant difference ($W = 278$, $p < 0.001$) in the *H'* between shrubs and trees within the understorey layer across the sites. Specifically, trees consistently exhibited a higher *H* than shrubs, except in Zambezi.

Comparing small trees and shrubs with saplings and large trees, a Mann-Whitney test revealed significant differences between them in both *H'* ($W = 43$, $p < 0.001$) and *J* ($W = 160$, $p < 0.01$) across all sites (Figure 3.6). Species richness, *H'*, and *J* for saplings and large trees increased with rainfall. In contrast, species richness and *H'* for small trees and shrubs decreased with rainfall on average. No significant differences in *J* were observed for small trees and shrubs across the sites.

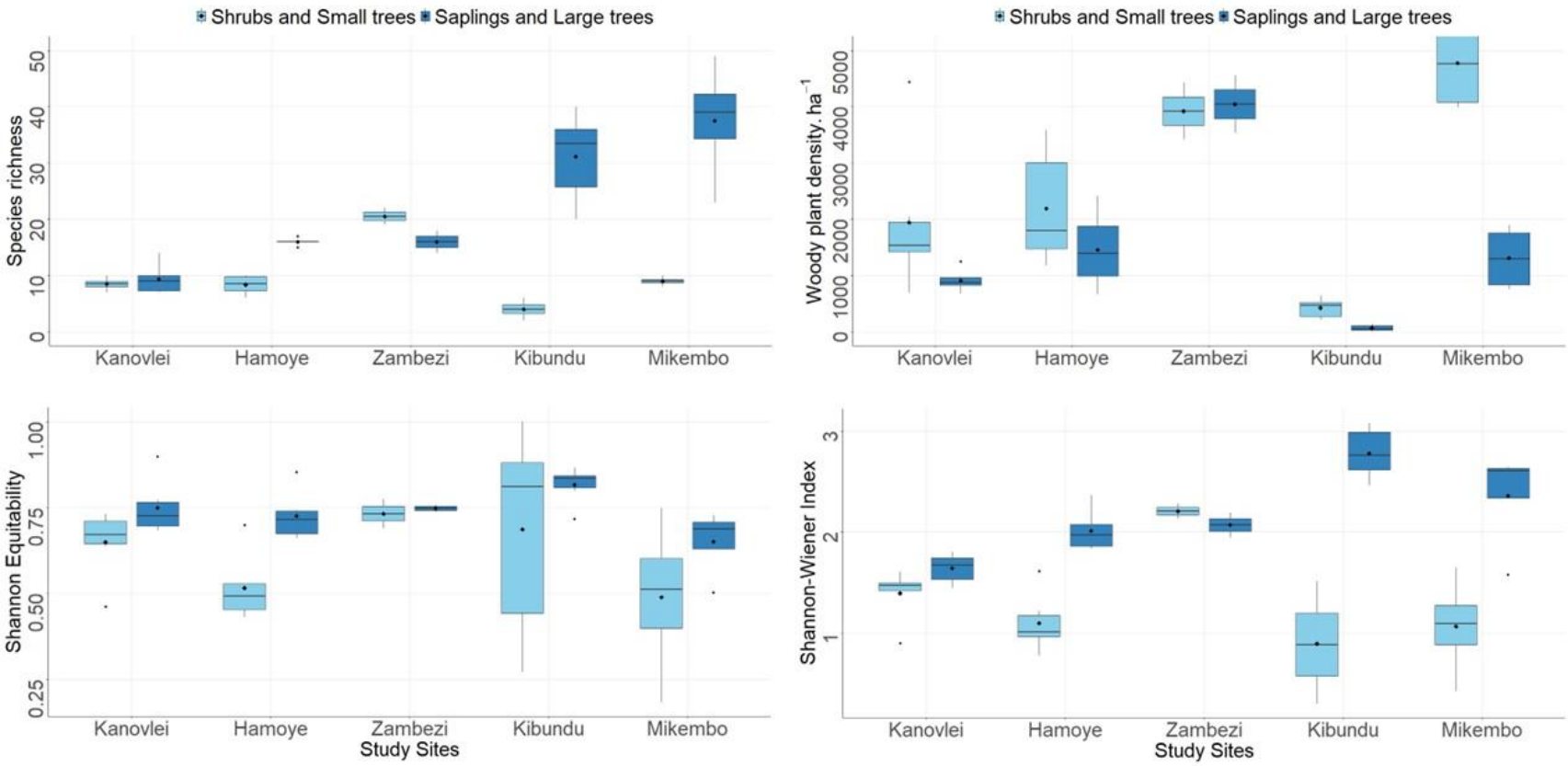


Figure 3.5. Changes in Diversity Indices and Woody Plant Density for Shrubs and Small Trees vs. Saplings and Large Trees.Sites are ordered by mean annual precipitation: Kanovlei = 500 – 550 mm; Hamoye = 560 mm; Zambezi = 600 – 700 mm; Kibundu = 1200 mm;Mikembo = 1200 mm.

Exploring the influence of overstorey conditions on understorey species richness, LME revealed a significant positive effect ($\rho = 0.57$, $p < 0.001$) of overstorey basal area on understorey tree species richness (small trees and saplings). This finding indicates that a higher overstorey basal area is associated with a greater richness of small trees in the understorey layer. The variance due to site was 0.45, suggesting a moderate proportion of the variation in understorey tree species richness is explained by the site-specific effects. In contrast, no significant effect of overstorey basal area was observed on understorey shrub species richness ($\rho = -0.07$, $p > 0.05$). (Figure 14). Although the relationship was not significant, the variance due to site was 1.82, suggesting that most of the variation in shrub species richness is explained by differences among sites. When excluding the Kibundu site, which is characterised by the highest levels of overstorey tree harvesting due to human activities, the relationship between understorey shrub species richness and overstorey basal area is more evident but remains statistically non-significant ($\rho = -0.42$, $p > 0.05$). An analysis of the proportion of species richness across structural layers and growth forms reveals distinct patterns influenced by rainfall gradients. In DRC, the percentage of saplings (juveniles of large trees) and large trees is higher (74.5%), with more species found exclusively in the overstorey, while in Namibia, the proportion of small trees and shrubs is higher (59.4%), decreasing with rainfall (Table 3.2).

The mean woody plant density of the plots located in Hamoye and Kanovlei followed a right-skewed distribution where the highest number of woody plant densities was found between 1 m and 2 m and decreased with the height classes (Figure 3.6). However, the plots located in Zambezi, Kibundu and Hamoye showed a second peak for trees between 5 m and 7.5 m height. Focusing only on the overstorey trees, the mean height per plot ranged from 4.7 m in the drier site to 11.56 m in the wetter site.

Table 3.2. Species richness and percentage contribution to total species richness of small trees, shrubs, and saplings and large trees across sites.

Country	Site	Small trees	Shrubs	Saplings and large trees
Namibia	Kanovlei	2.67 ± 0.58 (13.31 ± 2.35%)	8.67 ± 0.58 (43.75 ± 5.62%)	8.67 ± 2.08 (42.94 ± 4.53%)
Namibia	Hamoye	1.67 ± 0.58 (6.68 ± 2.58%)	8.67 ± 2.31 (34.01 ± 7.94%)	15 ± 1.73 (59.31 ± 7.34%)
Namibia	Zambezi	4 ± 0 (13.57 ± 2.56%)	16.5 ± 2.12 (55.31 ± 3.36%)	9.5 ± 3.54 (31.1 ± 5.92%)
DRC	Kibundu	2.5 ± 0.84 (8.1 ± 3.64%)	1.8 ± 0.84 (5.46 ± 1.39%)	28.67 ± 7.31 (87.35 ± 4.43%)
DRC	Mikembo	5.67 ± 1.15 (13.1 ± 3.39%)	4 ± 1 (9.85 ± 5.5%)	35.33 ± 12.5 (77.05 ± 8.17%)

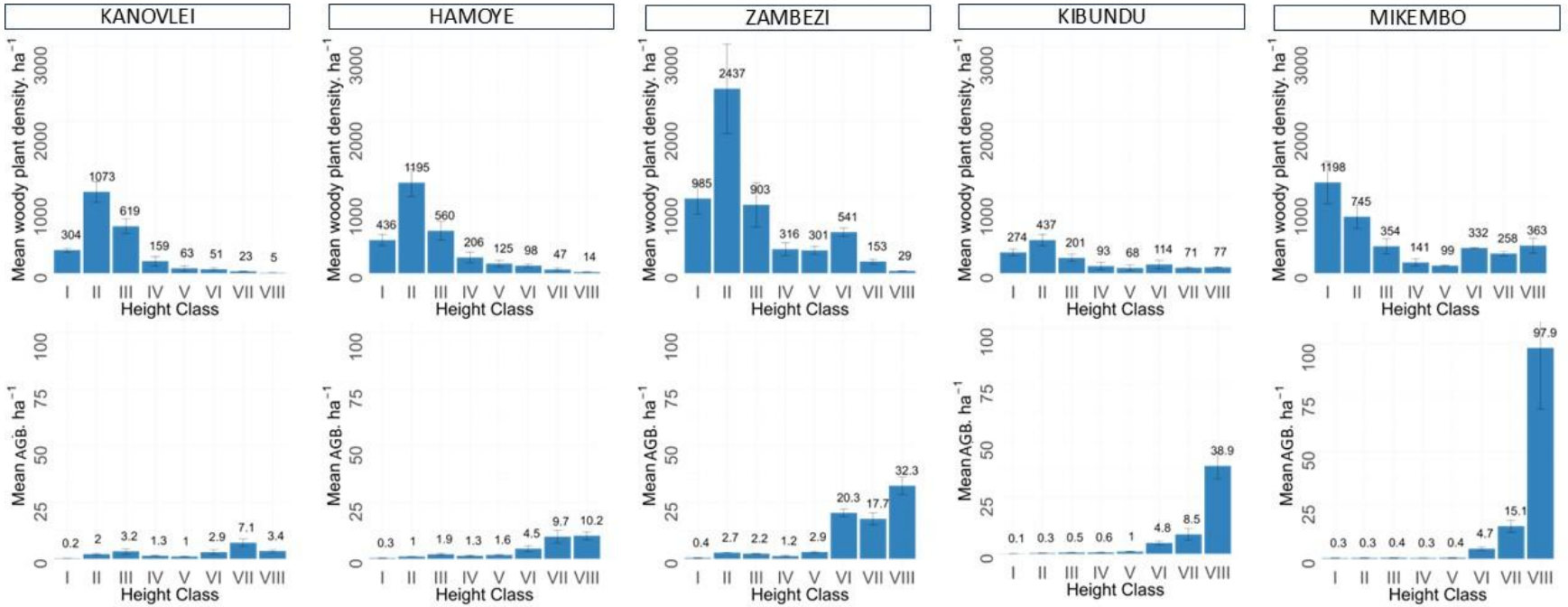


Figure 3.6. Distribution of Woody Plant Density tand AGB across height classes.

Woody Plant Density (top row) and AGB across height classes (bottom row). I = 0.5 – 1 m height, II = 1 – 2 m height, III = 2 – 3 m height, IV = 3 – 4 m height, V = 4 – 5 m height, VI = 5 – 7.5 m height, VII = 7.5 – 10 m height, VIII = > = 10 m height. Sites are ordered by mean annual precipitation: Kanovlei = 500 – 550 mm; Hamoye = 560 mm; Zambezi = 600 – 700 mm; Kibundu = 1200 mm; Mikembo = 1200 mm..

3.3.3 Contribution of each layer to the total biomass

The mean total AGB of each site ranged from 21 Mg.ha^{-1} in Kanovlei, Namibia to 119 Mg.ha^{-1} in Mikembo, DRC. AGB increased along the precipitation gradient. When analysing the distribution of AGB across height classes, we found that, more than 60% of AGB in Namibia was stored in plants taller than 5 m (Kanovlei = 63.5%; Hamoye = 78.9%; Zambezi = 85.7%). In contrast, in DRC, we found that more than 95% of AGB was stored in plants taller than 5 m (Kibundu = 95.1% and Mikembo = 98.1%) (Figure 3.6).

Analysing the contribution of each layer to the total AGB, Figure 3.7 shows that a large part of the AGB was stored by large trees in the overstorey (71.8% in Kanovlei, 85.1% in Hamoye, 87.8% in Zambezi, 97.5% in Kibundu and, 98.5% in Mikembo). The LME confirmed that an increase in overstorey basal area is associated with a significant reduction in the percentage of AGB stored in the understorey layer (Figure 3.9; $\rho = -0.59$, $p < 0.05$).

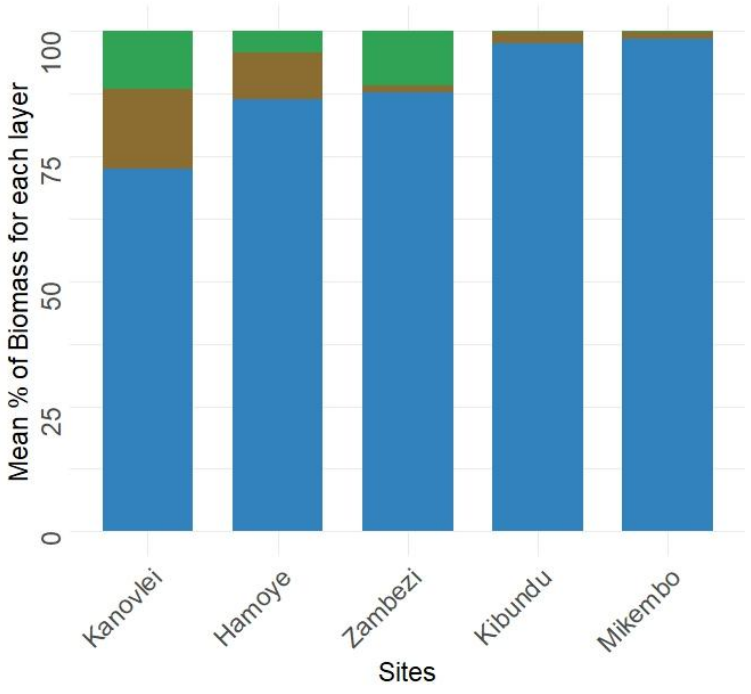


Figure 3.7. Above-ground biomass (AGB) stored by each layer within each site with a threshold of DBH ≥ 5 cm. The green colour is for the shrubs, the brown colour is for the small trees and saplings growth form and the blue colour is for the overstorey trees Sites are ordered by mean annual precipitation: Kanovlei = 500 – 550 mm; Hamoye = 560 mm; Zambezi = 600 – 700 mm; Kibundu = 1200 mm; Mikembo = 1200 mm.

When the DBH threshold for overstorey trees was increased to 10 cm, the contribution of the understorey layer to total AGB increased. Under this threshold, the overstorey contributed 67.5% in Kanovlei, 80.8%

in Hamoye, 76.4% in Zambezi, 93.1% in Mikembo, and 97.2% in Kibundu. These results illustrate that in drier woodlands, the understorey layer represents a considerable proportion of the total AGB, but its contribution decreases along the precipitation gradient.

We investigated the contribution of each species to the plot-level AGB (Table 3.4). We found that the top five species contributed to the plot-level overstorey AGB at 97% in Kanovlei, 91% in the Hamoye, 84% in Zambezi, 64% in Kibundu, and, 66% in the Mikembo. This trend reflects an increase in diversity along the rainfall gradient. For the understorey layer, the top five species contributed to the plot-level understorey AGB as follows: 80% in the Kanovlei, 64% in the Hamoye, 60% in the Zambezi, 65% in Kibundu, and, 67% in Mikembo.

Table 3.3 Top five species contributing to overstorey and understorey above-ground biomass (AGB) at each site.

Site	Overstorey			Understorey		
	Species	Mean AGB (Mg ha^{-1})	Mean woody plant density (ha^{-1})	Species	Mean AGB (Mg ha^{-1})	Mean woody plant density (ha^{-1})
Hamoye	*Baikiaea plurijuga*	6.71	17	*Dialium engleranum*	1.05	239
	Burkea Africana	6.68	105	*Psydrax livida*	0.44	596
	Dialium engleranum	5.61	105	*Bauhinia petersiana*	0.43	66
	Guibourtia coleosperma	2.97	6	*Burkea Africana*	0.39	229
	Pterocarpus angolensis	2.09	36	*Ochna pulchra*	0.38	612
Kanovlei	*Pterocarpus angolensis*	7.27	28	*Terminalia sericea*	1.60	478
	Burkea Africana	4.97	104	*Baphia massaiensis*	1.34	307
	Combretum collinum	1.13	31	*Bauhinia petersiana*	0.65	142
	Combretum psidioides	0.84	24	*Burkea Africana*	0.46	232
	Commiphora angolensis	0.45	7	*Ochna pulchra*	0.35	269
Zambezi	*Baikiaea plurijuga*	16.07	51	*Combretum elaeagnoides*	1.82	600
	Combretum collinum	16.07	214	*Combretum engleri*	1.10	120
	Terminalia sericea	9.14	137	*Bauhinia petersiana*	0.69	376
	Dichrostachys cinerea	5.65	121	*Baphia massaiensis*	0.67	1164
	Combretum psidioides	2.23	72	*Grewia retinervis*	0.59	300
Kibundu	*Brachystegia spiciformis*	13.7	24	*Julbernardia paniculata*	0.28	171
	Julbernardia paniculata	7.53	27	*Pterocarpus angolensis*	0.28	153

	Isoberlinia angolensis	5.71	18	*Terminalia brachystemma*	0.11	183
	Brachystegia boehmii	3.94	12	*Albizia antunesiana*	0.09	24
	Parinari curatellifolia	1.85	5	*Diplorhynchus condylocarpon*	0.09	61
Mikembo	*Julbernardia paniculata*	22.77	165	*Julbernardia globiflora*	0.29	240
	Brachystegia boehmii	18.9	186	*Triumfetta dekindtiana*	0.25	702
	Marquesia macroura	18.11	14	*Dalbergia boehmii*	0.23	192
	Pterocarpus tinctorius	9.77	52	*Diplorhynchus condylocarpon*	0.19	133
	Diplorhynchus condylocarpon	8.35	91	*Julbernardia paniculata*	0.12	106

3.4 Discussion

3.4.1 Variation in AGB across layers and rainfall gradient

Our findings demonstrate that biomass studies in dry woodlands that only consider woody biomass from large trees, defined by thresholds of ≥ 5 cm or ≥ 10 cm DBH, underestimate total woody biomass by an average of 18.3% and 24.1%, respectively. Understorey biomass contribution decreases with increasing rainfall. The estimated percentage of total AGB stored in the understorey layer in dry woodlands in the savanna woodlands aligns with the findings of a few previous studies on understorey biomass (Colgan et al., 2013; Frost, 1996; Kindermann et al., 2022). For instance, Kindermann et al. (2022), reported that the shrub layer contributes to stand-level AGB by an average of 19% and 27% respectively in the woodlands and savannas of Namibia. Our results highlight the substantial increase in total AGB when including trees and shrubs with a DBH < 5 cm or < 10 cm, especially in dry woodlands.

3.4.2 Variation in AGB across rainfall gradient

Our results show that overall AGB increases with MAP. Previous studies have shown the positive effect of rainfall on AGB in savanna woodlands (Godlee et al., 2021; Ngoma et al., 2018; Shackleton and Scholes, 2011). The AGB values reported in this study were generally within the range reported by other studies in the savanna woodlands. For instance, AGB in Tanzania ranged from 29.3 ± 6.5 Mg.ha-1 to 43.5 ± 7.0 Mg.ha-1 (Chamshama et al., 2004). The AGB in the Copperbelt region of Zambia was reported as 79.2 Mg.ha-1 by Kalaba et al. (2013). Ngoma et al. (2018) estimated 56 $Mg.ha^{-1}$ in Kabompo, 39 $Mg.ha^{-1}$ in Namwala, and 25 $Mg.ha^{-1}$ in Sesheke in Zambia. The AGB value in Mikembo was notably higher compared to other values reported in wet woodlands probably because the Mikembo reserve has been protected from fire since 2003.

Fire suppression and protection from harvesting at Mikembo have likely facilitated the accumulation of overstorey biomass. However, the long-term exclusion of fire has indirectly reduced understorey biomass by promoting a dense overstorey canopy, which limits light availability to the understorey. This demonstrates that fire management not only influences total above-ground biomass but also alters the balance of biomass between overstorey and understorey layers. These findings underscore the complex interactions between fire regimes, light availability, water availability and vegetation structure in shaping Miombo woodland dynamics.

3.4.3 Contribution of each layer to the total AGB

The contribution of the understorey to total AGB was higher in Namibia than in DRC and decreased with MAP. The understorey AGB (< 5 cm DBH) measured in this study ranged from 1.3 $Mg.ha^{-1}$ in Kibundu to 8.7 $Mg.ha^{-1}$ in Zambezi (Table 2). The percentage of AGB stored by the understorey layer ranged from 1.5% in Mikembo to 28.2% in Kanovlei (Figure 13). Kanovlei, the most arid site, receives MAP of ~550 mm and is prone to fire disturbance, which promotes a sparse, open canopy. Mayr et al. (2018) found that fire disturbance in this region affected vegetation structural parameters such as the height of woody species. In addition, fire also reduces the canopy tree density allowing more light to reach the soil and favouring the growth of the understorey layer. As indicated by Kindermann et al. (2022), the fraction of AGB stored by the small-size classes increases in more open and disturbed vegetation. Our LME results support this, showing a negative influence of the overstorey basal area on the percentage of AGB stored by the understorey layer (Figure 15). This aligns with previous studies suggesting that understorey AGB might not be responsive to stand age per se, but rather depends on overstorey biomass, overstorey basal area, forest management, anthropogenic disturbance, altitude, and soil conditions (Ahmad et al., 2019; Dar and Sundarapandian, 2015; Zhang et al., 2017).The accumulation of AGB in the overstorey layer indicates a concentration of resources and energy within the larger individuals. Notably, the number of shrubs and small trees does not decline with increasing rainfall, but the large trees get larger, increasing the overall AGB contribution of large trees.

3.4.4 Floristic composition, species diversity and woody density across forest layers and sites

To our knowledge, this is the first study addressing the co-variation of understorey and overstorey diversity, as well as the variation in the abundance and diversity of plant growth forms (shrubs and trees) across rainfall gradients in savanna woodlands.

The small size classes contain the most woody plant diversity, suggesting that the lower-height strata are crucial habitats for a diverse array of plant species and serve as a reservoir of plant diversity. Moreover, they indicate dynamic processes within the ecosystem, reflecting ongoing growth and regeneration. However, repeated harvesting may drastically reduce the population of large trees and favour the growth of small trees and shrubs (Muvengwi et al., 2020), as observed in Kibundu village in DRC.

3.4.5 Total species richness

The total species richness in this study ranged from 18 to 53 species within each plot. The species composition observed in this study matches previous findings in Miombo woodlands (Gonçalves et al., 2017; Muvengwi et al., 2020). The prevalence of Fabaceae species observed across Namibia and DRC woodlands aligns with earlier studies conducted in Zambezian woodlands and in Namibia (Frost, 1996; Godlee et al., 2020; Kazaba et al., 2020; Muledi et al., 2016).

3.4.6 Overstorey and Understorey species diversity

Our study reveals that woody plant diversity in dry woodlands can be significantly underestimated when the understorey is not included. Despite the larger plot size used for overstorey assessments, we found that the understorey species richness in dry woodlands was equal to or higher than that in the overstorey. This contrasts with the wet Miombo, where overstorey species richness was higher.

Understorey Shannon-Wiener index (*H'*) results for all sites were 2.0 or higher, indicating that the sites have medium to high diversity (Kalaba et al., 2013). However, no significant differences in H' and J were detected for the understorey layer across the sites. This lack of variation among sites suggests that understorey diversity remains relatively stable across environmental gradients. This stability underscores the importance of understorey vegetation as a key indicator of biodiversity and ecological resilience, regardless of site-specific conditions.

Overstorey tree species richness and overstorey Shannon-Wiener index results increased with rainfall. This result aligns well with the findings by Godlee et al. (2021) and Davies et al. (2023) across southern African savannas and woodlands, who observed that areas with greater rainfall contained more tree species. The energy-richness hypothesis (Currie et al., 2004) can be proposed to explain the positive relationships between rainfall and species richness in Miombo woodlands. Indeed, increased water availability enhances the resources and energy available to plants, leading to an increase in both the number of individuals and species. This is supported by our findings, where the overstorey woody plant density and species richness increased with rainfall. There may also be historical factors at play, with the ancestral angiosperm niche being located in wet tropical areas, accompanied by phylogenetic niche conservatism for these ancestral habitats (Augusto et al., 2014; Keil and Chase, 2019; Neves et al., 2020).

A significant difference in overstorey evenness was detected only between Kibundu (0.8) and Mikembo (0.6), despite both areas having the same range of MAP. The canopy in Kibundu is more open than in Mikembo because of historical disturbances (fire and wood harvesting). Many of the species present in the intermediate height classes and in the understorey layer in the Mikembo site may be shade tolerant. The more open canopy in Kibundu may favour the presence of various types of plants (shade-tolerant and shade-intolerant). This variety of species with different light and resource requirements can contribute to higher evenness in Kibundu, as no single species outcompete the others. In Mikembo, the competitive environment favours certain dominant species, reducing overall evenness. Additionally, the low number of trees in the intermediate height classes in Mikembo illustrates strong competition, causing trees to invest more in height growth to reach the canopy for better light capture, which is crucial for their survival and maintenance in the ecosystem.

3.4.7 Variation in shrub and small tree species diversity across rainfall gradient

The species diversity of small trees increases with MAP, while shrub species diversity decreases. Notably, except for the Zambezi site, shrubs had the lowest Shannon-Wiener index and species richness, with values decreasing as MAP increased. The unusually high shrub densities and species richness observed at the Zambezi site require further investigation, possibly linked to the dominance of *Combretum* and *Baphia* species, the exclusion of fire or high cattle abundance.

The decline in shrub diversity with increasing MAP aligns with findings from other continents, where high precipitation levels have been associated with a decline in shrub species richness (Martín-Queller et al., 2011). Although shrub richness is often negatively correlated with tree cover, as shrubs struggle to compete with larger trees and face limited light availability in the understorey (Moreno-Fernández et al., 2021). However, our results did not indicate a significant negative relationship between shrub species and tree cover (basal area) (Figure 3.8).

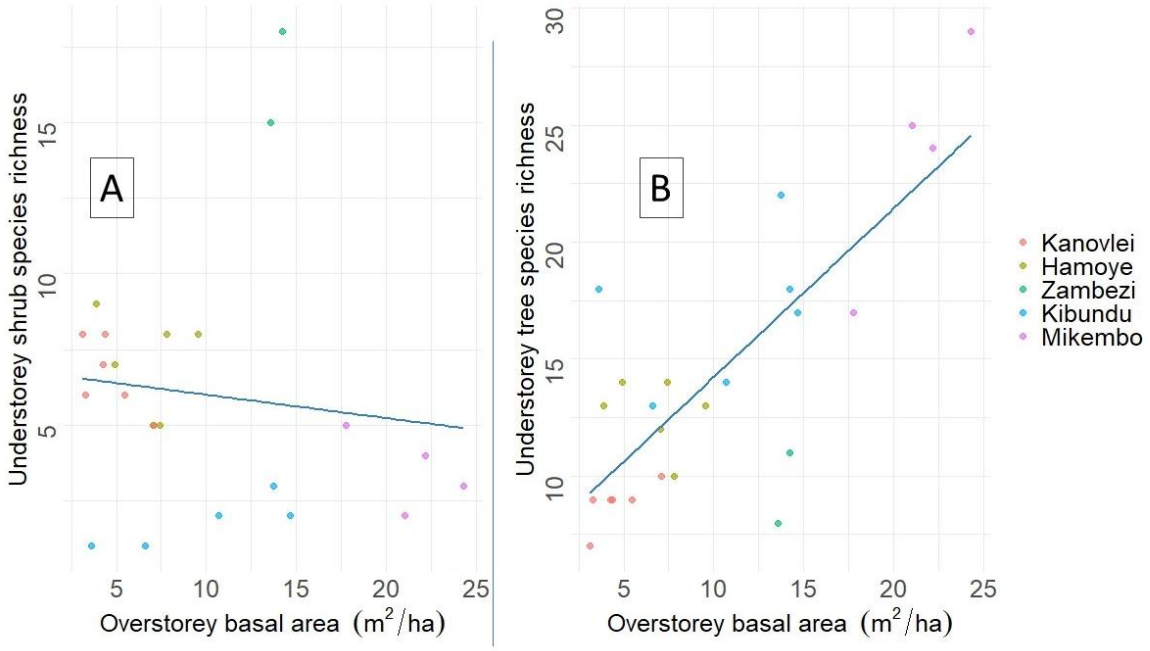


Figure 3.8. Variation of understorey species richness (understorey shrub species richness and understorey tree species richness) with overstorey basal area

A = understorey shrub species richness and B = understorey tree species richness with overstorey basal area. The blue lines represent the linear mixed model fit by REML. Sites vary in mean annual precipitation: Kanovlei = 500 – 550 mm; Hamoye = 560 mm; Zambezi = 600 – 700 mm; Kibundu = 1200 mm; Mikembo = 1200 mm.

In dry woodlands, shrubs are more numerous, generally do not reach the overstorey and are most abundant at lower DBH classes, with their number decreasing in higher DBH classes (Moreno-Fernández et al., 2021). In contrast, wet Miombo sites in the DRC, with a higher prevalence of small trees, exhibit more species that seem to be exclusive to the overstorey. The variation in shrub and tree species proportions across the rainfall gradient may explain these patterns. Hydric stress in dry woodlands likely limits tree growth more than shrub growth, contributing to the observed distribution of species across different layers (Martín-Queller et al., 2011; Moreno-Fernández et al., 2021). However, as most research on shrub species variation has been conducted in temperate forests, further studies are needed to better understand these dynamics in the context of African woodlands.

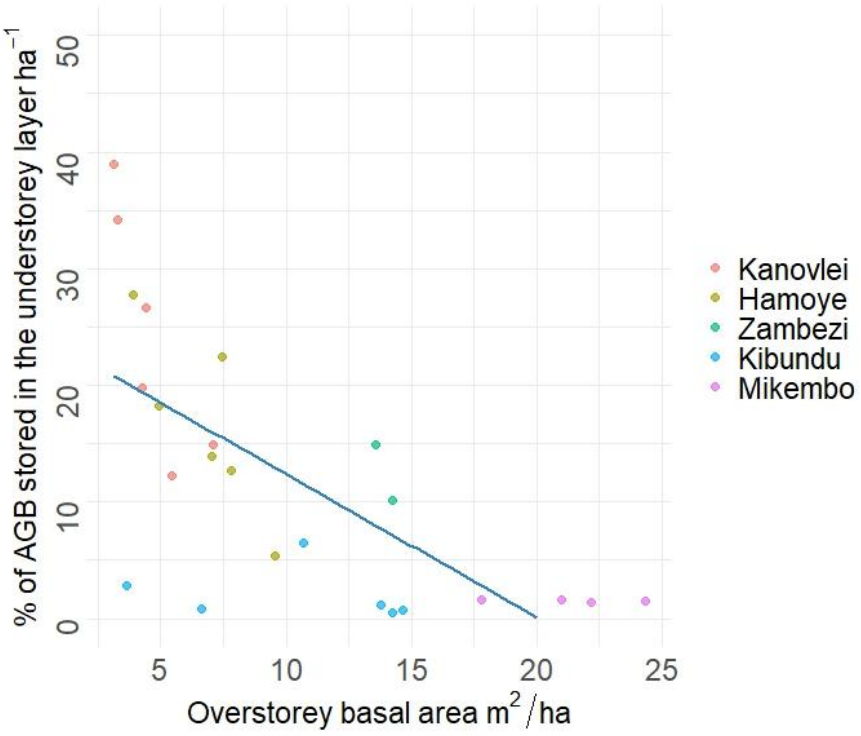


Figure 3.9. Variation of the percentage of the AGB stored in the understorey layer with the overstorey basal area The blue line represents the linear mixed model fit by REML. Sites vary in mean annual precipitation: Kanovlei = 500 – 550 mm; Hamoye = 560 mm; Zambezi = 600 – 700 mm; Kibundu = 1200 mm; Mikembo = 1200 mm.

3.4.8 Future research and possible implications

Our study was conducted at a limited number of sites within Namibia and DRC, which, while representing both extreme ends of the MAP gradient in the savanna woodlands, do not fully capture environmental variability across the whole ecoregion. Despite this, these sites provide valuable insights into what may prove to be general patterns and trends in biomass and species distribution. Future research should include sites with intermediate MAP values (between 700 mm and 1200 mm) to offer a more comprehensive understanding of biomass distribution across forest layers and lifeforms along the rainfall gradient. Additionally, there are multiple facets to rainfall patterns, such as rainfall intensity and seasonal distribution, which may also affect biomass and species diversity. Future studies could also consider the role of socioeconomic factors, fuelwood harvesting, and wildfire management in shaping vegetation structure. While the study did not explore soil fertility and microclimatic conditions, the results align with existing literature on the impact of rainfall and tree cover on biomass and diversity, reinforcing the validity of the findings.

3.5 Conclusion

This study aimed to describe the diversity and biomass distribution across the vertical structure of the savanna woodlands, including small trees and shrubs. A key contribution of this study is demonstrating that many biomass studies in African woodlands may underestimate total biomass by an average of 18.3% when trees and shrubs with a DBH < 5 cm are excluded, particularly in dry woodlands. The research highlights the importance of including different lifeforms to get more accurate biomass estimates. Furthermore, the study demonstrates how rainfall gradients impact species richness and biomass distribution, with significant implications for forest management and conservation strategies.

The findings from this study have several important applications and implications for forest management and conservation in savanna woodlands. By highlighting the significant contribution of the understorey to total AGB, particularly in dry woodlands, this research underscores the necessity of including smaller trees and shrubs in biomass assessments for more accurate biomass stock estimates. Additionally, it highlights the importance of understorey species in biodiversity assessments, particularly in dry woodlands where understorey species richness was equal to or greater than that of the overstorey.

3.6 CRediT authorship contribution statement

Hermane Diesse: Writing – review & editing, Writing – original draft, Visualization, Methodology, Investigation, Formal analysis, Data curation, Conceptualization. **John L. Godlee**: Writing – review & editing, Supervision, Investigation, Conceptualization. **Nichola Knox:** Writing – review & editing, Conceptualization. **Jonathan Muledi:** Writing – review & editing, Investigation. **Leena Naftal**: Writing – review & editing, Investigation. **David Nkulu:** Writing – review & editing, Investigation. **Ben Nkomba:** Writing – review & editing, Investigation. **Gabriel Uusiku**: Writing – review & editing, Investigation. Kyle Dexter: Writing – review & editing, Investigation. **Vera De Cauwer:** Writing review & editing, Investigation, supervision, Conceptualization.

3.7 References

Ahmad, B., Wang, Y., Hao, J., Liu, Y., Bohnett, E., Zhang, K., 2019. Optimizing stand structure for tradeoffs between overstory and understory vegetation biomass in a larch plantation of Liupan Mountains, Northwest China. Forest Ecology and Management 443, 43–50. https://doi.org/10.1016/j.foreco.2019.04.001

Ali, A., Lin, S., He, J., Kong, F., Yu, J., Jiang, H., 2019. Big-sized trees overrule remaining trees' attributes and species richness as determinants of aboveground biomass in tropical forests. Global Change Biology 25, 2810–2824. https://doi.org/10.1111/gcb.14707

Atlas of Namibia Team, 2022. Atlas of Namibia: its land, water and life. Namibia Nature Foundation, Windhoek.

Augusto, L., Davies, T.J., Delzon, S., De Schrijver, A., 2014. The enigma of the rise of angiosperms: can we untie the knot? Ecology Letters 17, 1326–1338. https://doi.org/10.1111/ele.12323

Baker, A.G., Catterall, C., Benkendorff, K., Fensham, R.J., 2020. Rainforest expansion reduces understorey plant diversity and density in open forest of eastern Australia. Austral Ecology 45, 557–571. https://doi.org/10.1111/aec.12871

Balandier, P., Mårell, A., Prévosto, B., Vincenot, L., 2022. Tamm review: Forest understorey and overstorey interactions: So much more than just light interception by trees. Forest Ecology and Management 526, 120584. https://doi.org/10.1016/j.foreco.2022.120584

Bates, D., Mächler, M., Bolker, B., Walker, S., 2015. Fitting Linear Mixed-Effects Models Using lme4. J. Stat. Soft. 67. https://doi.org/10.18637/jss.v067.i01

Bricca, A., Bonari, G., Padullés Cubino, J., Cutini, M., 2023. Effect of forest structure and management on the functional diversity and composition of understorey plant communities. Applied Vegetation Science 26, e12710. https://doi.org/10.1111/avsc.12710

Burke, A., 2006. Savanna trees in Namibia—Factors controlling their distribution at the arid end of the spectrum. Flora - Morphology, Distribution, Functional Ecology of Plants 201, 189–201. https://doi.org/10.1016/j.flora.2005.06.011

Burke, A., 2002. Present vegetation in the Kavango region 50, 133–145.

Campbell, B.M., 1996. The miombo in transition: woodlands and welfare in Africa. Center for International Forestry Research, Bogor, Indonesia.

Cauwer, V.D., Geldenhuys, C.J., Aerts, R., Kabajani, M., Muys, B., 2016. Patterns of forest composition and their long term environmental drivers in the tropical dry forest transition zone of southern Africa. Forest Ecosystems. https://doi.org/10.1186/s40663-016-0080-9

Chamshama, S.A.O., Mugasha, A.G., Zahabu, E., 2004. Stand biomass and volume estimation for Miombo woodlands at Kitulangalo, Morogoro, Tanzania. The Southern African Forestry Journal 200, 59–70. https://doi.org/10.1080/20702620.2004.10431761

Chave, J., Réjou-Méchain, M., Búrquez, A., Chidumayo, E., Colgan, M.S., Delitti, W.B.C., Duque, A., Eid, T., Fearnside, P.M., Goodman, R.C., Henry, M., Martínez-Yrízar, A., Mugasha, W.A., Muller-Landau, H.C., Mencuccini, M., Nelson, B.W., Ngomanda, A., Nogueira, E.M., Ortiz-Malavassi, E., Pélissier, R., Ploton, P., Ryan, C.M., Saldarriaga, J.G., Vieilledent, G., 2014. Improved allometric models to estimate the aboveground biomass of tropical trees. Glob Change Biol 20, 3177–3190. https://doi.org/10.1111/gcb.12629

Colgan, M.S., Asner, G.P., Swemmer, T., 2013. Harvesting tree biomass at the stand level to assess the accuracy of field and airborne biomass estimation in savannas. Ecological Applications 23, 1170–1184. https://doi.org/10.1890/12-0922.1

Conti, G., Gorné, L.D., Zeballos, S.R., Lipoma, M.L., Gatica, G., Kowaljow, E., Whitworth-Hulse, J.I., Cuchietti, A., Poca, M., Pestoni, S., Fernandes, P.M., 2019. Developing allometric models to predict the individual aboveground biomass of shrubs worldwide. Global Ecol Biogeogr 28, 961–975. https://doi.org/10.1111/geb.12907

Currie, D.J., Mittelbach, G.G., Cornell, H.V., Field, R., Guégan, J., Hawkins, B.A., Kaufman, D.M., Kerr, J.T., Oberdorff, T., O'Brien, E., Turner, J.R.G., 2004. Predictions and tests of climate-based hypotheses of broad-scale variation in taxonomic richness. Ecology Letters 7, 1121–1134. https://doi.org/10.1111/j.1461-0248.2004.00671.x

Dar, J.A., Sundarapandian, S., 2015. Variation of biomass and carbon pools with forest type in temperate forests of Kashmir Himalaya, India. Environ Monit Assess 187, 55. https://doi.org/10.1007/s10661-015-4299-7

Davies, R.W., Ryan, C.M., Harrison, R.D., Dexter, K.G., Ahrends, A., Te Beest, M., Benitez, L., Brade, T.K., Carreiras, J.M.B., Druce, D.J., Fayolle, A., Finckh, M., Godlee, J.L., Gonclaves, F.M., Grundy, I.M., Hoche, T., Holdo, R.M., Makungwa, S., McNicol, I.M., Mograbi, P.J., Muchawona, A., Muhate, A., Muledi, J., Pritchard, R., Revermann, R., Ribeiro, N.S., Siampale, A., Carla Staver, A., Syampungani, S., Williams, M., Swemmer, A.M., Edwards, D.P., 2023. Precipitation gradients

drive high tree species turnover in the woodlands of eastern and southern Africa. Ecography e06720. https://doi.org/10.1111/ecog.06720

De Cauwer, V., 2023. Status quo of sustainable forest management in Namibia. Hanns Seidel Foundation and Desert Research Foundation of Namibia (DRFN), Windhoek.

Dormann, C.F., Bagnara, M., Boch, S., Hinderling, J., Janeiro-Otero, A., Schäfer, D., Schall, P., Hartig, F., 2020. Plant species richness increases with light availability, but not variability, in temperate forests understorey. BMC Ecol 20, 43. https://doi.org/10.1186/s12898-020-00311-9

Ferrara, C., Puletti, N., Guasti, M., Scotti, R., 2023. Mapping Understory Vegetation Density in Mediterranean Forests: Insights from Airborne and Terrestrial Laser Scanning Integration. Sensors 23, 511. https://doi.org/10.3390/s23010511

Frost, P., 1996. The ecology of miombo woodlands, in: The Miombo in Transition: Woodlands and Welfare in Africa. Centre for International Forestry Research, Bogor, Indonesia, pp. 11–57.

Godlee, J.L., Gonçalves, F.M., Tchamba, J.J., Chisingui, A.V., Muledi, J.I., Shutcha, M.N., Ryan, C.M., Brade, T.K., Dexter, K.G., 2020. Diversity and Structure of an Arid Woodland in Southwest Angola, with Comparison to the Wider Miombo Ecoregion. Diversity 12, 140. https://doi.org/10.3390/d12040140

Godlee, J.L., Ryan, C.M., Bauman, D., Bowers, S.J., Carreiras, J.M.B., Chisingui, A.V., Cromsigt, J.P.G.M., Druce, D.J., Finckh, M., Gonçalves, F.M., Holdo, R.M., Makungwa, S., McNicol, I.M., Mitchard, E.T.A., Muchawona, A., Revermann, R., Ribeiro, N.S., Siampale, A., Syampungani, S., Tchamba, J.J., Tripathi, H.G., Wallenfang, J., te Beest, M., Williams, M., Dexter, K.G., 2021. Structural diversity and tree density drives variation in the biodiversity–ecosystem function relationship of woodlands and savannas. New Phytologist 232, 579–594. https://doi.org/10.1111/nph.17639

Godlee, J.L., Ryan, C.M., Siampale, A., Dexter, K.G., 2024. Tree species diversity drives the land surface phenology of seasonally dry tropical woodlands. Journal of Ecology 112, 1978–1991. https://doi.org/10.1111/1365-2745.14366

Gonçalves, F.M.P., Revermann, R., Gomes, A.L., Aidar, M.P.M., Finckh, M., Juergens, N., 2017. Tree Species Diversity and Composition of Miombo Woodlands in South-Central Angola: A Chronosequence of Forest Recovery after Shifting Cultivation. International Journal of Forestry Research 2017, 1–13. https://doi.org/10.1155/2017/6202093

Hengl, T., De Jesus, J.M., MacMillan, R.A., Batjes, N.H., Heuvelink, G.B.M., Ribeiro, E., Samuel-Rosa, A., Kempen, B., Leenaars, J.G.B., Walsh, M.G., Gonzalez, M.R., 2014. SoilGrids1km — Global Soil

Information Based on Automated Mapping. PLoS ONE 9, e105992. https://doi.org/10.1371/journal.pone.0105992

Huff, S., Poudel, K.P., Ritchie, M., Temesgen, H., 2018. Quantifying aboveground biomass for common shrubs in northeastern California using nonlinear mixed effect models. Forest Ecology and Management 424, 154–163. https://doi.org/10.1016/j.foreco.2018.04.043

Kalaba, F.K., Quinn, C.H., Dougill, A.J., Vinya, R., 2013. Floristic composition, species diversity and carbon storage in charcoal and agriculture fallows and management implications in Miombo woodlands of Zambia. Forest Ecology and Management 304, 99–109. https://doi.org/10.1016/j.foreco.2013.04.024

Kazaba, P.K., Numbi, D.M., Muledi, J.I., Shutcha, M.N., Tshikung, D.K., Sowunmi, A.A., Aweto, A.O., 2020. Human Impact on Diversity and Abundance of Baboon (Papio kindae)-edible Fleshy-fruited Trees in Miombo Forests of the Kundelungu National Park, D.R. Congo. Journal of Forest and Environmental Science 36, 175–186. https://doi.org/10.7747/JFES.2020.36.3.175

Keil, P., Chase, J.M., 2019. Global patterns and drivers of tree diversity integrated across a continuum of spatial grains. Nat Ecol Evol 3, 390–399. https://doi.org/10.1038/s41559-019-0799-0

Kindermann, L., Dobler, M., Niedeggen, D., Linstädter, A., 2022. A new protocol for estimation of woody aboveground biomass in disturbance-prone ecosystems. Ecological Indicators 135. https://doi.org/10.1016/j.ecolind.2021.108466

Kuyah, S., Sileshi, G., Rosenstock, T., 2016. Allometric Models Based on Bayesian Frameworks Give Better Estimates of Aboveground Biomass in the Miombo Woodlands. Forests 7, 13. https://doi.org/10.3390/f7020013

Le, A., Paull, D., Griffin, A., 2018. Exploring the Inclusion of Small Regenerating Trees to Improve Above-Ground Forest Biomass Estimation Using Geospatial Data. Remote Sensing 10, 1446. https://doi.org/10.3390/rs10091446

Lombaerde, E.D., Verheyen, K., Perring, M.P., Bernhardt-römermann, M., Calster, H.V., Brunet, J., Chudomelová, M., Decocq, G., Diekmann, M., Durak, T., Hédl, R., Heinken, T., Hommel, P., Lenoir, J., Macek, M., Mitchell, F.J.G., Naaf, T., Newman, M., Pet, P., Reczy, K., Schmidt, W., Swierkosz, K., 2018. Responses of competitive understorey species to spatial environmental gradients inaccurately explain temporal changes. https://doi.org/10.1016/j.baae.2018.05.013

Lone, K., Loe, L.E., Gobakken, T., Linnell, J.D.C., Odden, J., Remmen, J., Mysterud, A., 2014. Living and dying in a multi-predator landscape of fear: roe deer are squeezed by contrasting pattern of

predation risk imposed by lynx and humans. Oikos 123, 641–651. https://doi.org/10.1111/j.1600-0706.2013.00938.x

Lüdecke, D., Ben-Shachar, M., Patil, I., Waggoner, P., Makowski, D., 2021. performance: An R Package for Assessment, Comparison and Testing of Statistical Models. JOSS 6, 3139. https://doi.org/10.21105/joss.03139

Malaisse, F., 1997. Se nourrir en forêt claire africaine: Approche écologique et nutritionnelle. Les presses agronomiques de Gembloux.

Mannheimer, C.A., Curtis, B.A., 2018. Le Roux and Muller's Field Guide to the Trees and Shrubs of Namibia. Namibia Publishing House (Pty) Ltd, Windhoek.

Martín-Queller, E., Gil-Tena, A., Saura, S., 2011. Species richness of woody plants in the landscapes of Central Spain: the role of management disturbances, environment and non-stationarity: Landscape species richness: forest management and environmental factors. Journal of Vegetation Science 22, 238–250. https://doi.org/10.1111/j.1654-1103.2010.01242.x

Mayaux, P., Bartholomé, E., Fritz, S., Belward, A., 2004. A new land-cover map of Africa for the year 2000. Journal of Biogeography 31, 861–877. https://doi.org/10.1111/j.1365-2699.2004.01073.x

Mayr, M.J., Malß, S., Ofner, E., Samimi, C., 2018. Disturbance feedbacks on the height of woody vegetation in a savannah: a multi-plot assessment using an unmanned aerial vehicle (UAV). International Journal of Remote Sensing 39, 4761–4785. https://doi.org/10.1080/01431161.2017.1362132

Mendelsohn, J., Jarvis, A.M., Roberts, C., Robertson, T., 2002. Atlas of Namibia: A Portrait of the Land and Its People. David Philip, Cape Town.

Moonlight, P.W., Banda-R, K., Phillips, O.L., Dexter, K.G., Pennington, R.T., Baker, T.R., C. De Lima, H., Fajardo, L., González-M., R., Linares-Palomino, R., Lloyd, J., Nascimento, M., Prado, D., Quintana, C., Riina, R., Rodríguez M., G.M., Maria Villela, D., Aquino, A.C.M.M., Arroyo, L., Bezerra, C., Tadeu Brunello, A., Brienen, R.J.W., Cardoso, D., Chao, K., Cotta Coutinho, Í.A., Cunha, J., Domingues, T., Do Espírito Santo, M.M., Feldpausch, T.R., Ferreira Fernandes, M., Goodwin, Z.A., Jiménez, E.M., Levesley, A., Lopez-Toledo, L., Marimon, B., Miatto, R.C., Mizushima, M., Monteagudo, A., Soelma Beserra De Moura, M., Murakami, A., Neves, D., Nicora Chequín, R., César De Sousa Oliveira, T., Almeida De Oliveira, E., P. De Queiroz, L., Pilon, A., Marques Ramos, D., Reynel, C., Rodrigues, P.M.S., Santos, R., Särkinen, T., Fernando Da Silva, V., Souza, R.M.S., Vasquez, R., Veenendaal, E., 2020. Expanding tropical forest monitoring into Dry Forests: The

DRYFLOR protocol for permanent plots. Plants People Planet 3, 295–300. https://doi.org/10.1002/ppp3.10112

Moreno-Fernández, D., Canellas, I., Alberdi, I., 2021. Shrub richness is primarily driven by climate conditions in Southwestern European woodlands. Annals of Forest Science 78–98. https://doi.org/10.1007/s13595-021-01117-5

Mugasha, W.A., Mauya, E.W., Njana, A.M., Karlsson, K., Malimbwi, R.E., Ernest, S., 2019. Height-Diameter Allometry for Tree Species in Tanzania Mainland. International Journal of Forestry Research 2019, 1–17. https://doi.org/10.1155/2019/4832849

Muledi, J., Bauman, D., Drouet, T., Vleminckx, J., Jacobs, A., Lejoly, J., Meerts, P., Shutcha, M.N., 2016. Fine-scale habitats influence tree species assemblage in a miombo forest. JPECOL rtw104. https://doi.org/10.1093/jpe/rtw104

Munalula, F., Seifert, T., Meincken, M., 2020. Inter-annual growth response of three Miombo tree species to climatic effects. Southern Forests: a Journal of Forest Science 82, 135–147. https://doi.org/10.2989/20702620.2020.1814111

Muvengwi, J., Chisango, T., Mpakairi, K., Mbiba, M., Witkowski, E.T.F., 2020. Structure, composition and regeneration of miombo woodlands within harvested and unharvested areas. Forest Ecology and Management 458, 117792. https://doi.org/10.1016/j.foreco.2019.117792

Návar, J., Méndez, E., Nájera, A., Graciano, J., Dale, V., Parresol, B., 2004. Biomass equations for shrub species of Tamaulipan thornscrub of North-eastern Mexico. Journal of Arid Environments 59, 657–674. https://doi.org/10.1016/j.jaridenv.2004.02.010

Neves, D.M., Dexter, K.G., Baker, T.R., Coelho De Souza, F., Oliveira-Filho, A.T., Queiroz, L.P., Lima, H.C., Simon, M.F., Lewis, G.P., Segovia, R.A., Arroyo, L., Reynel, C., Marcelo-Peña, J.L., Huamantupa-Chuquimaco, I., Villarroel, D., Parada, G.A., Daza, A., Linares-Palomino, R., Ferreira, L.V., Salomão, R.P., Siqueira, G.S., Nascimento, M.T., Fraga, C.N., Pennington, R.T., 2020. Evolutionary diversity in tropical tree communities peaks at intermediate precipitation. Sci Rep 10, 1188. https://doi.org/10.1038/s41598-019-55621-w

Ngoma, J., Moors, E., Kruijt, B., Speer, J.H., Vinya, R., Chidumayo, E.N., Leemans, R., 2018. Acta Oecologica Below and above-ground carbon distribution along a rainfall gradient . A case of the Zambezi teak forests , Zambia. Acta Oecologica 87, 45–57. https://doi.org/10.1016/j.actao.2018.02.003

Nijland, W., Nielsen, S.E., Coops, N.C., Wulder, M.A., Stenhouse, G.B., 2014. Fine-spatial scale predictions of understory species using climate- and LiDAR-derived terrain and canopy metrics. J. Appl. Remote Sens 8, 083572. https://doi.org/10.1117/1.JRS.8.083572

Oksanen, J., Blanchet, F.G., Friendly, M., Kindt, R., Legendre, P., McGlinn, D., Minchin, P.R., O'Hara, R.B., Simpson, G.L., Solymos, P., Stevens, M.H.H., Szoecs, E., Wagner, H., 2015. "Community Ecology Package, R package version 2.3-1, R Foundation for Statistical Computing.

R Core Team, 2023. R: A Language and Environment for Statistical Computing_. R Foundation for Statistical Computing, Vienna, Austria. <https://www.R-project.org/>.

Ryan, C.M., Hill, T., Woollen, E., Ghee, C., Mitchard, E., Cassells, G., Grace, J., Woodhouse, I.H., Williams, M., 2012. Quantifying small-scale deforestation and forest degradation in African woodlands using radar imagery. Global Change Biology 18, 243–257. https://doi.org/10.1111/j.1365-2486.2011.02551.x

Ryan, C.M., Pritchard, R., McNicol, I., Owen, M., Fisher, J.A., Lehmann, C., 2016. Ecosystem services from southern African woodlands and their future under global change. Phil. Trans. R. Soc. B 371, 20150312. https://doi.org/10.1098/rstb.2015.0312

Sankaran, M., Hanan, N.P., Scholes, R.J., Ratnam, J., Augustine, D.J., Cade, B.S., Gignoux, J., Higgins, S.I., Le Roux, X., Ludwig, F., Ardo, J., Banyikwa, F., Bronn, A., Bucini, G., Caylor, K.K., Coughenour, M.B., Diouf, A., Ekaya, W., Feral, C.J., February, E.C., Frost, P.G.H., Hiernaux, P., Hrabar, H., Metzger, K.L., Prins, H.H.T., Ringrose, S., Sea, W., Tews, J., Worden, J., Zambatis, N., 2005. Determinants of woody cover in African savannas. Nature 438, 846–849. https://doi.org/10.1038/nature04070

SEOSAW partnership, 2021. A network to understand the changing socio-ecology of the southern African woodlands (SEOSAW): Challenges, benefits, and methods. Plants People Planet 3, 249–267. https://doi.org/10.1002/ppp3.10168

Shackleton, C.M., Scholes, R.J., 2011. Above ground woody community attributes, biomass and carbon stocks along a rainfall gradient in the savannas of the central lowveld, South Africa. South African Journal of Botany 77, 184–192. https://doi.org/10.1016/j.sajb.2010.07.014

Slik, J.W.F., Paoli, G., McGuire, K., Amaral, I., Barroso, J., Bastian, M., Blanc, L., Bongers, F., Boundja, P., Clark, C., Collins, M., Dauby, G., Ding, Y., Doucet, J., Eler, E., Ferreira, L., Forshed, O., Fredriksson, G., Gillet, J., Harris, D., Leal, M., Laumonier, Y., Malhi, Y., Mansor, A., Martin, E., Miyamoto, K., Araujo-Murakami, A., Nagamasu, H., Nilus, R., Nurtjahya, E., Oliveira, Á., Onrizal, O., Parada-Gutierrez, A., Permana, A., Poorter, L., Poulsen, J., Ramirez-Angulo, H., Reitsma, J., Rovero, F.,

Rozak, A., Sheil, D., Silva-Espejo, J., Silveira, M., Spironelo, W., Ter Steege, H., Stevart, T., Navarro-Aguilar, G.E., Sunderland, T., Suzuki, E., Tang, J., Theilade, I., Van Der Heijden, G., Van Valkenburg, J., Van Do, T., Vilanova, E., Vos, V., Wich, S., Wöll, H., Yoneda, T., Zang, R., Zhang, M., Zweifel, N., 2013. Large trees drive forest aboveground biomass variation in moist lowland forests across the tropics. Global Ecology and Biogeography 22, 1261–1271. https://doi.org/10.1111/geb.12092

Smith, B., Wilson, J.B., 1996. A Consumer's Guide to Evenness Indices. Oikos 76, 70. https://doi.org/10.2307/3545749

Strohbach, B.J., Petersen, A., 2007. Vegetation of the central Kavango woodlands in Namibia: An example from the Mile 46 Livestock Development Centre. South African Journal of Botany 73, 391–401. https://doi.org/10.1016/j.sajb.2007.03.002

Suchar, V.A., Crookston, N.L., 2010. Understory cover and biomass indices predictions for forest ecosystems of the Northwestern United States. Ecological Indicators 10, 602–609. https://doi.org/10.1016/j.ecolind.2009.10.004

Timberlake, J., Chidumayo, E., 2011. Miombo ecoregion vision report, Occasional Publications in Biodiversity. ed. Occasional Publications in Biodiversity.

Van Wyk, B., & Van Wyk, P. (2013). Field Guide to Trees of Southern Africa (2nd rev. ed.). Struik Publishers.Zhang, Y., Chen, H.Y.H., Taylor, A.R., 2017. Positive species diversity and above-ground biomass relationships are ubiquitous across forest strata despite interference from overstorey trees. Funct Ecol 31, 419–426. https://doi.org/10.1111/1365-2435.12699

Appendix 2

Table A1: List of plots at each field site. AGB = Above-Ground Biomass.

Country	Site	Plot name	Layer	AGB (Mg. ha^{-1})	Basal area (m^2.ha^{-1})	Tree density (ha^{-1})	Mean height (m)	Max height (m)
Namibia	Kanovlei	K1	Overstorey	11.06	3.21	92	5.85	12.50
Namibia	Kanovlei	K1	Understorey	9.47	0.12	2240	1.70	3.78
Namibia	Kanovlei	SK1	Overstorey	19.19	5.67	380	4.70	11.84
Namibia	Kanovlei	SK1	Understorey	4.05	0.96	2481	1.77	8.30
Namibia	Kanovlei	SK2	Overstorey	16.15	4.92	212	4.67	12.45
Namibia	Kanovlei	SK2	Understorey	4.18	0.19	1512	1.63	3.77
Namibia	Hamoye	H1	Overstorey	18.08	5.09	223	4.98	14.78
Namibia	Hamoye	H1	Understorey	3.27	0.54	1689	1.73	6.80
Namibia	Hamoye	H3	Overstorey	36.67	8.68	333	6.17	13.73
Namibia	Hamoye	H3	Understorey	3.70	0.72	2526	1.51	4.90
Namibia	Hamoye	H4	Overstorey	24.52	7.24	535	4.90	13.2
Namibia	Hamoye	H4	Understorey	5.68	1.40	2802	1.73	5
Namibia	Zambezi	Z1	Overstorey	58.34	14.23	948	6.42	14
Namibia	Zambezi	Z1	Understorey	7.60	0.67	4344	1.55	7
Namibia	Zambezi	Z2	Overstorey	58.28	13.56	710	6.27	13.6
Namibia	Zambezi	Z2	Understorey	9.77	0.99	5752	1.82	7
DRC	Kibundu	Kib1	Overstorey	65.76	14.23	278	8.05	16
DRC	Kibundu	Kib1	Understorey	0.42	0.20	632	1.35	3.50
DRC	Kibundu	Kib2	Overstorey	17.97	3.62	78	8.30	16
DRC	Kibundu	Kib2	Understorey	0.85	0.43	1096	1.47	3.10
DRC	Kibundu	Kib3	Overstorey	69.19	14.67	320	8.63	17.90
DRC	Kibundu	Kib3	Understorey	0.73	0.40	904	2.02	7.90
DRC	Kibundu	Kib4	Overstorey	67.88	13.77	286	8.58	20.50
DRC	Kibundu	Kib4	Understorey	1.04	0.4	1152	1.61	4.90
DRC	Kibundu	Kib5	Overstorey	46.7	10.7	332	7.19	16.40

DRC	Kibundu	Kib5	Understorey	4.29	1.04	1328	3.51	14
DRC	Kibundu	Kib6	Overstorey	39.05	6.62	102	11.56	16.50
DRC	Kibundu	Kib6	Understorey	0.43	0.3	1048	1.27	4.90
DRC	Mikembo	M1	Overstorey	158.64	22.67	772	10.17	26.50
DRC	Mikembo	M1	Understorey	2.33	0.82	3573	1.74	11.90
DRC	Mikembo	M2	Overstorey	72.4	17.78	824	7.89	14.89
DRC	Mikembo	M2	Understorey	1.56	0.45	2608	1.13	10.60
DRC	Mikembo	M3	Overstorey	121.01	22.19	1108	9.76	16
DRC	Mikembo	M3	Understorey	1.58	0.70	1832	1.84	10

1 Table A2: Species found in the understorey layer in DRC and Namibia. CPA is the canopy projected area. Values are means across all plots where
2 a given species was recorded. Species found in the plots of both countries are marked in bold text. NA = no data collected

DRC					**NAMIBIA**				
Species	Diam (cm)	Height (m)	CPA (m^2)	Individuals (ha^{-1})	Species	Diam (cm)	Height (m)	CPA (m^2)	Individuals (ha^{-1})
Albizia adianthifolia	1.6	3.1	0.8	2.7	*Acacia sp*	NA	1.9	2.8	1.5
Albizia antunesiana	3.3	3.5	2.7	34.1	*Baikiaea plurijuga*	3.1	2.1	NA	35.2
Albizia versicolor	2.9	1.8	1.2	19.6	*Baphia massaiensis*	1.4	1.4	1.2	406.5
Allophylus africanus	2.4	2.1	1.4	16.9	*Bauhinia petersiana*	2.1	1.8	NA	176.1
Anisophyllea boehmii	1.8	0.8	0.8	2.0	***Bobgunnia madagascariensis***	2.1	1.4	2.2	0.4
Annona senegalensis	4.5	2.5	NA	1.8	*Boscia albitrunca*	NA	0.9	0.4	3.0
Antidesma rufescens	1.8	1.1	1.0	1.1	*Burkea africana*	3.1	1.9	1.1	183.9
Bobgunnia madagascariensis	3.8	1.7	1.5	5.7	***Combretum collinum***	3.0	2.0	1.3	112.8
Brachystegia boehmii	2.7	1.9	1.5	33.8	*Combretum elaeagnoides*	2.4	2.4	1.6	150
Brachystegia gossweileri	2.1	1.4	0.9	4.4	*Combretum engleri*	3.5	2.6	2.1	31.6
Brachystegia spiciformis	2.0	1.7	1.0	48.9	*Combretum psidioides*	3.4	2.3	1.2	68.7
Brachystegia taxifolia	2.3	2.6	1.5	28.1	*Combretum sp*	2.2	2.7	2.1	3.2

Bridelia duvigneaudii	1.4	1.0	0.6	124.1	***Combretum zeyheri***	2.8	1.9	1.3	71.2
Cassia abbreviate	1.7	1.1	0.4	19.7	*Commiphora angolensis*	2.1	1.5	0.9	98.3
Combretum collinum	2.3	1.7	0.8	4.4	*Croton gratissimus*	2.3	1.6	1.1	74.0
Combretum molle	2.5	1.9	1.1	14.8	*Dialium engleranum*	3.3	2.3	NA	95.6
Combretum zeyheri	3.3	2.5	4.2	0.9	*Dichrostachys cinerea*	2.0	1.4	0.7	19.0
Dalbergia boehmii	2.4	1.7	1.1	123.9	***Diplorhynchus condylocarpon***	3.0	2.1	1.6	20.8
Dalbergia nitidula	2.5	2.1	0.8	1.8	*Entada arenaria*	NA	0.9	0.6	1.4
Diospyros mespiliformis	1.0	0.6	0.5	2.7	*Friesodielsia obovata*	1.6	2.1	1.3	2.0
Diospyros natalensis	1.4	0.8	0.7	3.6	*Grewia avellana*	1.5	1.4	1.3	71.4
Diplorhynchus condylocarpon	2.8	2.4	1.5	115.6	*Grewia bicolor*	NA	1.2	1.4	2.0
Erythrophleum africanum	3.7	2.4	5.2	7.1	*Grewia falcistipula*	1.5	1.1	1	12.1
Flacourtia indica	1.8	1.3	1.0	3.6	*Grewia flava*	2.5	2.9	2.8	2.0
Garcinia huillensis	NA	0.8	0.3	0.4	*Grewia flavescens*	1.3	1.9	1.6	56.6
Gymnosporia senegalensis	NA	0.8	0.2	0.9	*Grewia retinervis*	1.2	1.6	1.2	77.5
Haplocoelum foliolosum	1.3	1.4	0.4	7.5	*Grewia sp*	1.5	1.7	1.5	2.8
Harungana madagascariensis	1.9	0.8	0.5	11.4	*Guibourtia coleosperma*	3.5	2.1	2.0	5.6
Hexalobus monopetalus	2.4	1.3	1.1	3.6	*Katema vakuru*	NA	0.6	0.3	1.0

Hymenocardia acida	2.7	2.5	1.5	56.9	*Mpoko*	1.4	1.5	0.9	39
Isoberlinia angolensis	2.5	1.5	0.9	72.9	*Muvusa*	2.5	1.3	1.6	4.0
Julbernardia globiflora	2.3	2.5	1.4	93.5	*Ochna cinnabarina*	1.3	0.9	0.6	15
Julbernardia paniculata	2.6	2.6	1.6	192	*Ochna pulchra*	2.0	1.2	0.8	352
Lannea discolor	2.8	1.7	1.2	4.8	*Ozoroa longipes*	3.5	2.2	1.7	3.2
Markhamia obtusifolia	2.0	1.1	0.5	22.2	*Ozoroa paniculosa*	1.4	1.2	1.0	4.4
Marquesia macroura	3.5	1.6	NA	1.1	*Pavetta schumanniana*	1.0	1.3	1.2	1.2
Mimusops zeyheri	NA	0.5	0.4	0.9	*Pavetta sp*	1.3	1.5	1.2	45.2
Monotes katangensis	2.7	5.0	1.4	0.4	*Pavetta zeyheri*	NA	0.8	0.4	0.8
Multidentia crassa	1.6	0.5	0.6	0.9	*Philenoptera nelsii*	2.6	1.7	1.4	53.0
Ochna afzelii	2.5	2.4	1.6	51.6	*Psydrax livida*	1.8	1.4	0.8	238.4
Ochna puberula	1.5	1.3	0.9	13.2	***Pterocarpus angolensis***	3.8	2.2	1.2	14.7
Ochna schweinfurthiana	1.8	1.1	0.7	42.0	*Pterocarpus lucens*	1.0	1.5	1.0	4.0
Parinari curatellifolia	2.5	2.1	1.5	20.6	*Schinziophyton rautanenii*	3.7	1.8	NA	4.6
Pericopsis angolensis	1.9	0.9	0.6	1.8	*Searsia tenuinervis*	2.3	1.6	1.2	30.6
Philenoptera katangensis	2.2	1.3	0.5	2.7	***Securidaca longipedunculata***	2.9	1.7	0.9	2.0
Phyllanthus muellerianus	1.0	0.7	0.2	3.9	*Senegalia ataxacantha*	2.2	2.6	1.6	17.0
Phyllocosmus lemaireanus	2.8	2.4	1.2	14.6	***Strychnos cocculoides***	2.5	1.5	0.9	8.0

Pseudolachnostylis maprouneifolia	3.0	2.7	1.4	36.1	*Strychnos pungens*	2.5	1.9	1.2	57.6
Pterocarpus angolensis	2.7	2.1	1.7	188.8	*Terminalia sericea*	2.5	1.9	1.6	217.1
Pyrostria lobulate	3.5	2.0	1.9	0.9	*Vachellia erioloba*	3.6	2.3	2.0	1.2
Rothmannia engleriana	2.0	1.7	1.2	16.7	*Vachellia erubescens*	1.3	1.9	1.1	5.0
Rothmannia whitfieldii	2.4	1.1	0.7	2.7	*Vangueria cyanescens*	2.8	2.1	2.7	0.4
Schrebera trichoclada	1.0	1.3	0.6	1.1	*Vangueria infausta*	1.1	1.6	1.4	3.0
Securidaca longipedunculata	2.1	1.3	0.6	1.8	*Ximenia americana*	3.1	2.2	2.0	2.0
Strychnos cocculoides	2.1	1.7	NA	12.8	*Ximenia caffra*	2.1	1.3	1.4	1.2
Strychnos innocua	2.5	2.0	1.1	18.1					
Syzygium guineense	2.3	2.0	1.2	6.2					
Terminalia brachystemma	2.2	1.5	0.7	200.9					
Trema orientalis	1.3	1.1	0.9	3.6					
Triumfetta dekindtiana	1.7	0.9	0.6	236.3					
Uapaca kirkiana	NA	0.5	0.5	0.7					
Uapaca nitida	1.7	1.2	0.8	5.2					
Uapaca Pilosa	2.3	1.0	0.7	5.3					
Uvariastrum hexaloboides	2.5	1.9	1.3	26					
Vachellia amythethophylla	1.6	1.0	0.4	3.6					

Vitex madiensis	1.5	1.0	0.6	11.4	

3

Table A3: Summary of the Linear mixed model fit by REML analysing the influence of the overstorey basal area on the understorey tree or shrub species richness. t-tests use Satterthwaite's method ['lmerModLmerTest'].

Formula: Lifeform (understorey trees or shrub ~ Overstorey_Basal_area + (1 | site).

Small trees species				**Shrub species**			**Shrub species (without Kibundu site)**		
Predictors	*Estimates*	*CI*	*p*	*Estimates*	*CI*	*p*	*Estimates*	*CI*	*p*
(Intercept)	-0.09	-0.76 – 0.57	0.770	0.31	-0.96 –1.58	0.617	0.41	-1.21 –2.02	0.599
Overstorey Basal area	0.57	0.18 – 0.96	0.006	-0.07	-0.42 –0.27	0.659	-0.43	-1.11 –0.26	0.201
Random Effects									
σ2	0.19			0.11			0.13		
τ00	0.45 site			1.83 site			2.21 site		
ICC	0.71			0.94			0.94		
N	5 site			5 site			4 site		
Observations	24			24			18		
Marginal R2 / Conditional R^2	0.335 / 0.804			0.003 / 0.943			0.072 / 0.947		

Table A4: Summary of the Linear mixed model fit by REML analysing the influence of the overstorey basal area on the percentage of AGB stored in the understorey layer. t-tests use Satterthwaite's method ['lmerModLmerTest'].

Formula: percentage of AGB stored in the understorey layer~ overstorey basal area + (1 | site)

Predictors	*Estimates*	*CI*	*p*
(Intercept)	0.04	-0.52 – 0.60	0.883
Overstorey Basal Area	-0.59	-1.02 – -0.17	0.009
Random Effects			
σ2	0.32		
τ00 site	0.29		
ICC	0.47		
N site	5		
Observations	24		
Marginal R2 / Conditional R2	0.369 / 0.667		

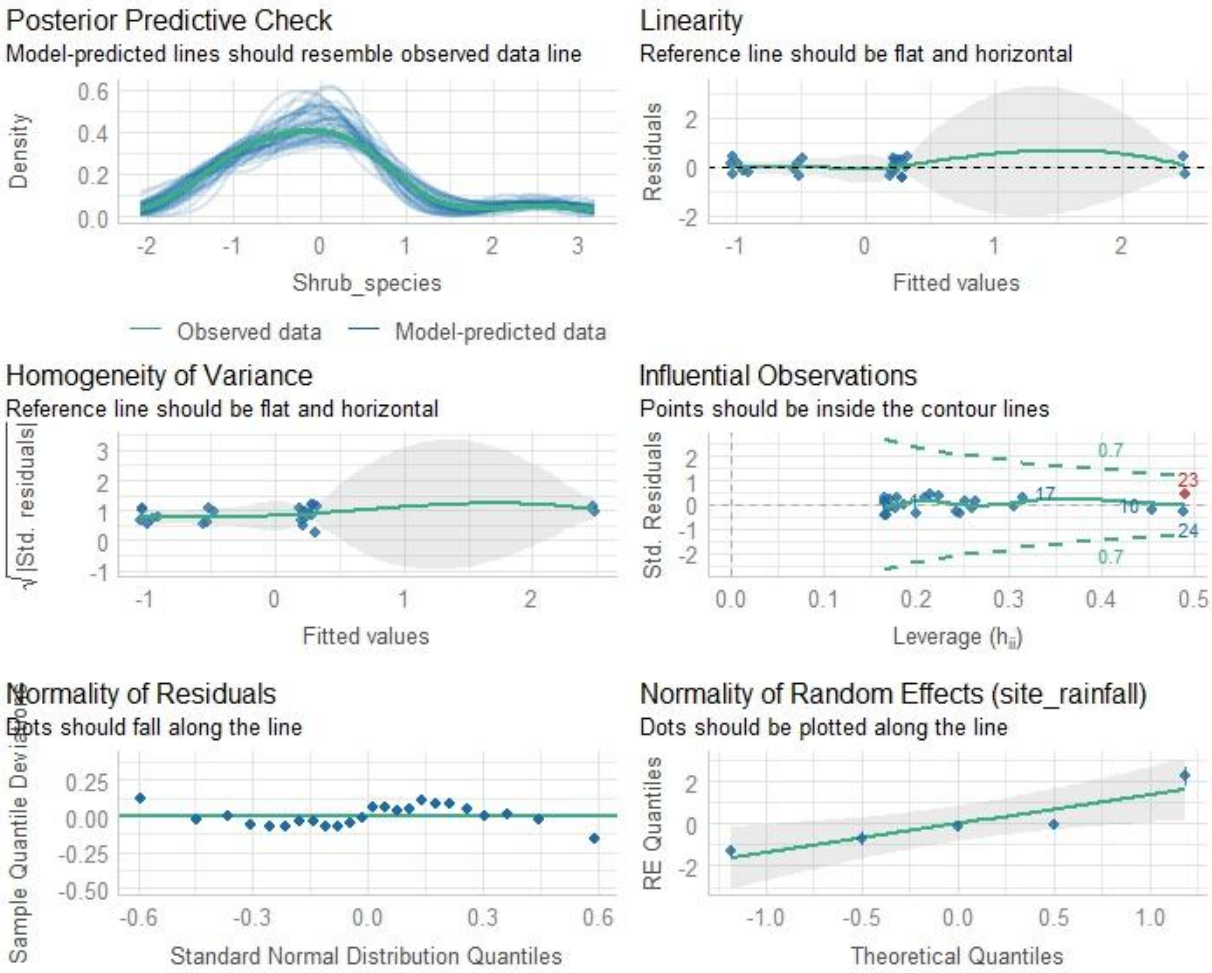


Fig. A1: Performance of the mixed effects model analysing the influence of overstorey basal area on understorey shrub species richness across sites.

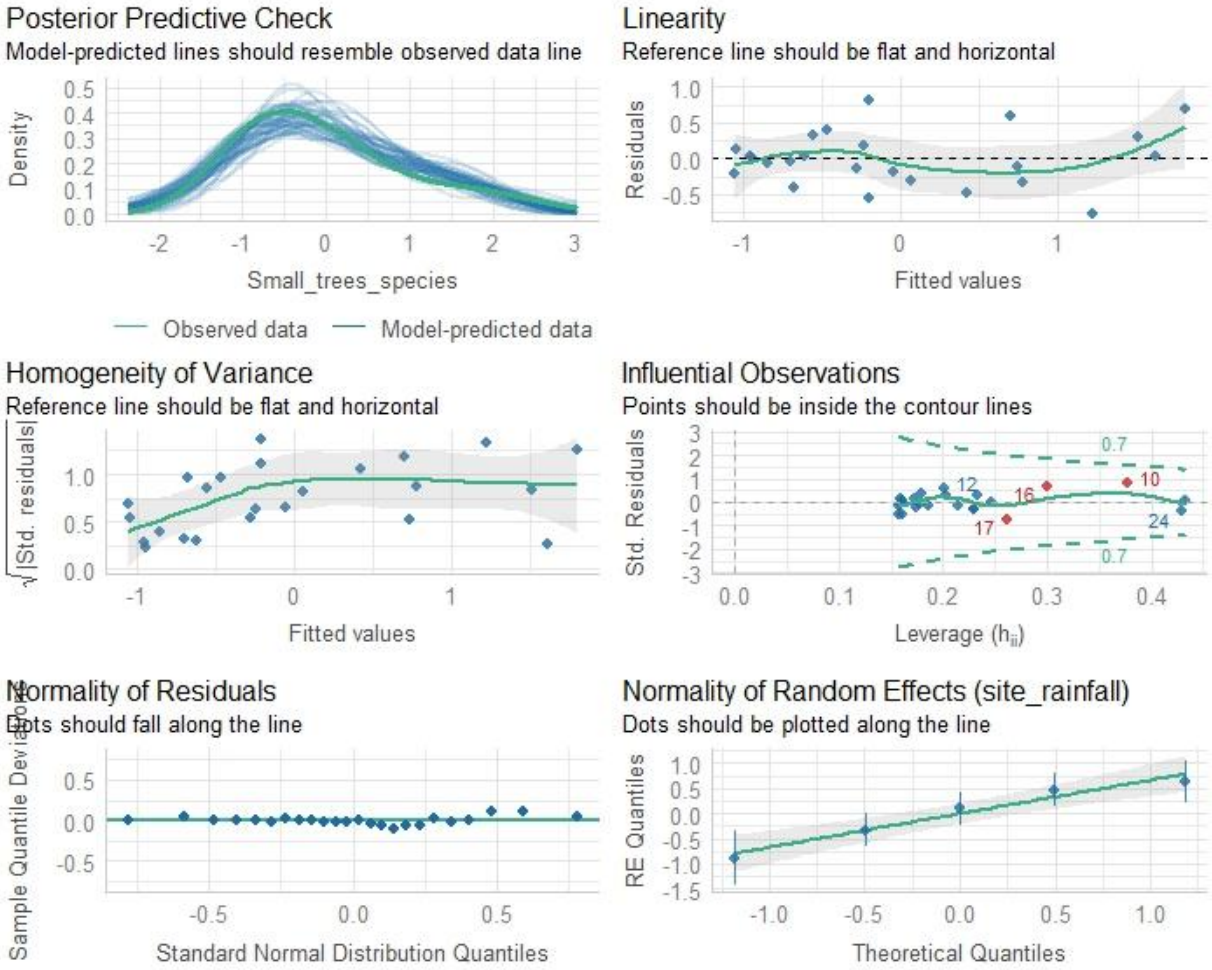


Fig. A2: Performance of the mixed effects model analysing the influence of overstorey basal area on understorey small tree species richness across sites.

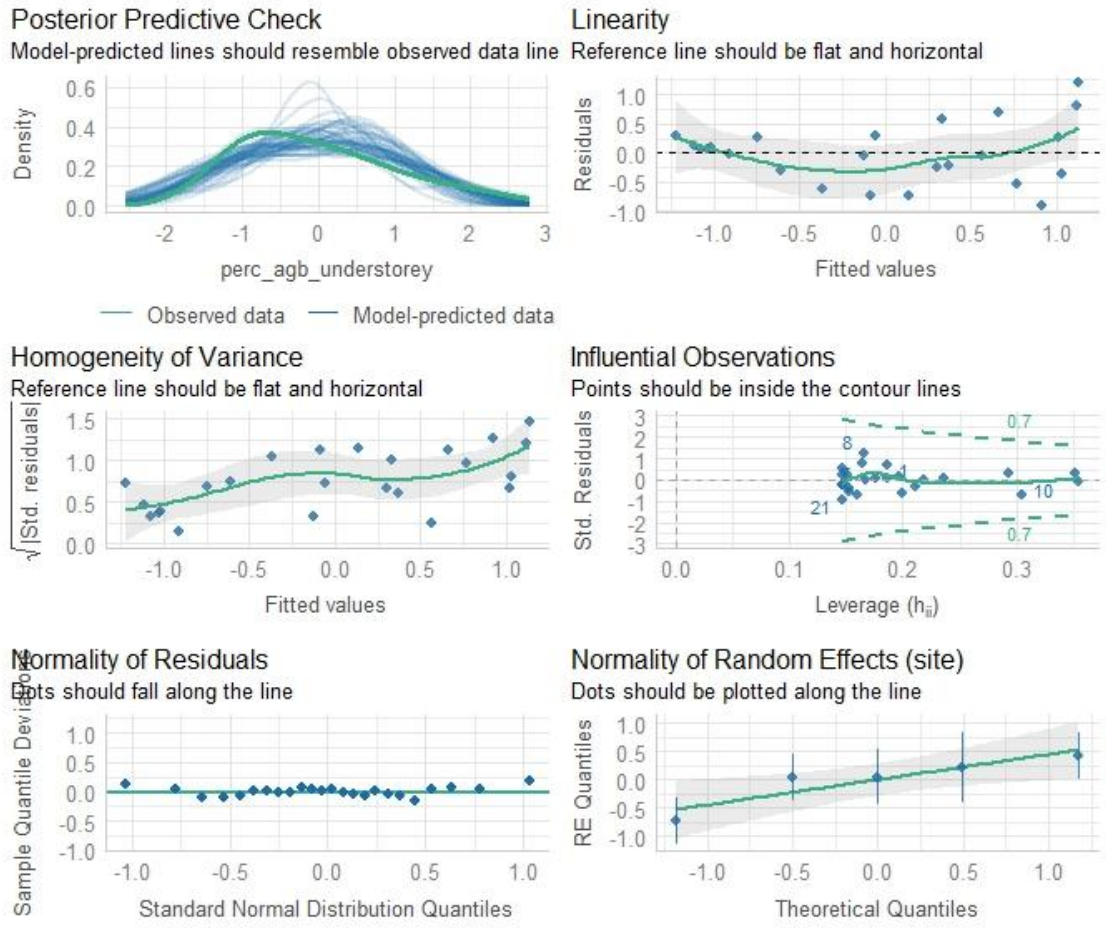


Fig. A3: Performance of the mixed effects model analysing the influence of overstorey basal area on the percentage of AGB stored in the understorey.

Chapter 4: Linking subcanopy vegetation to canopy structure and forest attributes in dry Namibian woodlands

Hermane Diesse [a,c,*], John L. Godlee [b,c,e], Kyle Dexter [c,fef,h], Nichola Knox [d,g,i], Leena Naftal [a], Olivia Haikali [a], Dav M. Ebengo [j,k], Vera De Cauwer [a,c]

a Namibia University of Science and Technology, 13 Jackson Kaujeua Street, Windhoek, Namibia

b Smithsonian National Museum of Natural History, Washington DC, USA

c Socio-Ecological Observatory for Studying African Woodlands – SEOSAW Network, UK

d Downforce Technologies, 7 Albert Buildings, 49 Queen Victoria Street, London, EC4N 4SA, UK

e School of GeoSciences, University of Edinburgh, Edinburgh, EH9 3FF, UK

f Royal Botanic Garden Edinburgh, Edinburgh, EH3 5LR, UK

g School of Earth and Space Exploration, Arizona State University, Phoenix, AZ, 85287, USA

h Department of Life Sciences and Systems Biology, University of Torino, Torino, Italy

i College of Science and Engineering, Flinders University, Adelaide, SA, Australia

j Institut One Health pour l'Afrique, Université de Kinshasa ; Democratic Republic of Congo

k Global Health Laboratory, INRB, Democratic Republic of Congo

Abstract

Understanding how canopy structure influences subcanopy vegetation and broader forest attributes is essential for advancing forest ecology and informing sustainable management, particularly in dry woodlands shaped by rainfall and disturbance. This study investigated the relationship between canopy architecture (≥ 3 m height) and subcanopy structure (< 3 m height) in dry Namibian woodlands using terrestrial laser scanning (TLS), a tool that captures fine-scale three-dimensional vegetation structure.

Data were collected from 24 subplots (25 x 25 m) across three plots in two forests (16 subplots in Hamoye State Forest and 8 in Kanovlei State Forest). A 5 x 5 m grid cells was applied to derive TLS-based metrics: Plant Density Index (PDI), vertical entropy, gap fraction profile, canopy height, canopy cover, and coefficient of variation (CV) in canopy cover. We examined how these attributes influence subcanopy PDI and ecological variables, including species richness, tree density, and above-ground biomass (AGB).

Canopy structure was organised along a dominant axis separating dense, vertically complex canopies (high canopy cover, PDI, and entropy) from open and heterogeneous canopies (high gap fraction and canopy variability). Subcanopy density increased with canopy density (PDI) and canopy openness, while horizontal heterogeneity (CV of canopy cover) and vertical complexity (entropy) had negative effects. Gap fraction also showed a context-dependent influence, being positive in the more open woodland but weak elsewhere, with evidence of saturation at high openness. Vertical complexity exhibited a non-linear effect on tree density, with intermediate levels supporting higher density. Species richness declined with increasing canopy heterogeneity, whereas above-ground biomass was positively associated with canopy density and showed a non-linear response to canopy openness, peaking at intermediate gap fraction.

These findings demonstrate that interactions among canopy density, openness, and vertical complexity regulate vegetation structure and ecological functioning in dry woodlands. TLS-derived metrics provide valuable insights for monitoring structurally complex and disturbance-prone ecosystems.

Key words: Terrestrial Laser Scanner, Vegetation structure, Namibian dry woodlands, Voxelisation, Canopy cover, Entropy, gap fraction profile

4.1 Introduction

Vegetation structure refers to the spatial arrangement of plant components in both vertical and horizontal dimensions within a forest stand (Zhang et al., 2017). It plays an important role in shaping ecological processes within forested ecosystems, influencing light penetration, microclimate conditions (Béland and Kobayashi, 2021), plant density, and species distribution. Vegetation structure directly affects plant development and habitat suitability for a wide range of organisms, including mammals, birds, and invertebrates (Ashcroft et al., 2014; James and Wamer, 1982; Vierling et al., 2013; Werner and Glennemeier, 1999). It not only reflects past demographic processes (e.g., growth, mortality, recruitment) but also influences future forest dynamics by determining resource availability and competition. In addition, the vertical and horizontal organisation of vegetation also affects fire behaviour and provides essential information for assessing forest carbon stocks (Donager et al., 2018). Many studies have highlighted that the heterogeneity of vegetation structure is driven by both forest management and natural processes, and is linked to biodiversity and forest productivity (Ehbrecht et al., 2016). As a result, understanding vegetation structure is essential for ecological research, forest management, and conservation, particularly in the natural dry woodlands in southern Africa, where vegetation is highly heterogeneous and prone to disturbances from fire and wildlife (Sankaran et al., 2005; Timberlake et al., 2010).

While many studies have documented relationships between canopy and subcanopy layers in tropical and temperate forests, there are no clear trends, and patterns depend on the region (Anderson et al., 2018; Bartels and Chen, 2013; Burton et al., 2011). In some cases, dense canopies suppress subcanopy development through light limitation, while in others, abundance in the upper layer promotes the development of the lower layers through facilitative processes such as nutrient cycling or microclimate buffering (Bartels and Chen, 2013; Weltzin and Coughenour, 1990). These contrasting findings highlight that canopy–subcanopy interactions are governed by multiple, potentially opposing mechanisms, whose relative importance may vary across ecosystems.

Dry woodlands in southern Africa, including those in Namibia, are ecologically and socioeconomically important. They play a crucial role in biodiversity (Chidumayo and Marunda, 2010), contribute to carbon storage (Marunda and Bouda, 2010), and provide essential resources for rural livelihoods (Ryan et al., 2016). Structurally, these ecosystems are complex, with an open vegetation organised into distinct vertical layers: a sparse canopy tree layer, a shrub and small tree subcanopy layer, and a ground layer composed of herbs, grasses, and low woody vegetation (Frost, 1996; Mayaux et al., 2004). In such environments, where water availability and disturbance regimes strongly influence

vegetation dynamics, canopy structure may exert both competitive and facilitative effects on subcanopy vegetation. However, despite their importance, southern African dry woodlands remain underrepresented in structural ecological studies, particularly with respect to fine-scale canopy–subcanopy interactions.

Recent studies suggest that subcanopy vegetation in dry woodlands can contribute substantially to above-ground biomass, particularly through shrubs and small trees (Diesse et al., 2025; Kindermann et al., 2022). One possible explanation is that open canopies facilitate greater light availability, favouring denser subcanopy vegetation. However, fine-scale structural data are needed to better understand the drivers of subcanopy variation. Fine-scale data allow for the detection of subtle spatial variations in canopy structure, such as small gaps, layering patterns, and localised foliage density that directly influence light distribution, resource competition, and microhabitat conditions (McIntosh et al., 2016; Tymen et al., 2017). These details are often obscured in coarser-scale measurements, potentially masking critical relationships between canopy structure and subcanopy dynamics.

Several metrics have been developed to characterise canopy structure. These include measures of canopy height, canopy cover (Decuyper et al., 2018), plant density index (Puletti et al., 2021), and vertical complexity index (Van Ewijk et al., 2011), among others. These attributes represent distinct but complementary dimensions of forest structure and are frequently used to infer ecological processes. However, their combined influence on subcanopy vegetation and broader ecological attributes in dry woodland ecosystems remains poorly understood.

Over the past decades, studies for quantifying canopy structure used traditional methods that often rely on visual estimates or single-point simplifications of three-dimensional structures into simple estimations of cover and height (Anderson et al., 2021). These methods risk overlooking fine-scale variability that could influence ecological processes (Lefsky et al., 2002). In contrast, Terrestrial Laser Scanning (TLS) is proposed as an alternative to characterise the canopy layer and to address the challenge associated with the traditional methods (Newnham et al., 2015). TLS offers a high-resolution, three-dimensional representation of the woodland structure, capturing detailed vertical and horizontal heterogeneity (Beyene, 2020). It has been successfully used to quantify vegetation layering (Ehbrecht et al., 2016; Robert T. Fahey et al., 2015), canopy gap fraction, leaf area density (Béland and Kobayashi, 2021), biomass (Knapp et al., 2020; Stovall et al., 2018), tree diameter (Koreň et al., 2017; Watt and Donoghue, 2005), and species richness (Anderson et al., 2021). However, its application in dry woodlands of southern Africa remains limited.

Therefore, this study uses TLS to characterise canopy structure in dry Namibian woodlands and to assess its ecological implications. Specifically, the study addresses the following questions:

(1) How can TLS derived forest structural metrics be used to describe and differentiate vegetation structure in dry woodland of Namibia?

(2) To what extent do canopy structural metrics influence the structure of the subcanopy layer?

(3) How are key ecological attributes such as species richness, tree density, and above-ground biomass related to canopy structure?

We hypothesise that canopy structure regulates subcanopy vegetation through interacting mechanisms of facilitation and competition, mediated by variations in vegetation density, canopy openness, and vertical structural complexity. In dry woodland ecosystems, where both light availability and water limitation influence vegetation dynamics, canopy structure is expected to exert both positive and negative effects on subcanopy development. Higher canopy density may promote subcanopy vegetation through microclimatic buffering and enhanced resource availability, whereas increased canopy openness may favour subcanopy growth by increasing light availability. In contrast, greater vertical structural complexity may constrain subcanopy development by intensifying competition for light and space across canopy layers.

We further hypothesise that these structural dimensions of the canopy influence key ecological attributes, including species richness, tree density, and above-ground biomass. Canopy density is expected to be associated with biomass accumulation, while structural heterogeneity and vertical complexity are expected to shape patterns of species coexistence and stand density through their influence on resource distribution and niche availability.

By integrating TLS data with detailed field inventories, this study provides novel insights into the multiscale interactions between canopy structure and forest ecological attributes in dry woodland systems.

4.2 Materials and methods

4.2.1 Study area

This study was conducted in two dry woodlands sites in northeastern Namibia: Kanovlei State Forest in the Otjozondjupa Region and Hamoye State Forest in the Kavango East Region (Figure 16). These areas are characterised by a semi-arid climate with a rainy season between October and April (Mendelsohn et al., 2002). According to WordClim, Kanovlei receives a mean annual precipitation (MAP) of less than 500 mm, while Hamoye receives about 560 mm (Fick and Hijmans, 2017).

Both forests exhibit an open woodland structure with semi-deciduous tree species, with an average canopy cover of 25 % and canopy heights of 10 to 15 m (De Cauwer et al., 2016; Mayr et al., 2018), with a large number of trees occupying the intermediate height class between 3m and 6 m (Diesse et al., 2025). The canopy layer in Kanovlei is primarily composed of Pterocarpus angolensis, Burkea africana, Combretum collinum, Combretum psidioides, and Commiphora angolensis. The subcanopy features Terminalia sericea, Baphia massaiensis, Bauhinia petersiana, Burkea africana, and Ochna pulchra (De Cauwer et al., 2016; Diesse et al., 2025; Graz, 2006). In contrast, the Hamoye canopy is dominated by Baikiaea plurijuga, Burkea africana, Dialium engleranum, Guibourtia coleosperma, and Pterocarpus angolensis, with the subcanopy comprised mostly of Dialium engleranum, Psydrax livida, Bauhinia africana, Burkea africana, and Ochna pulchra (Diesse et al., 2025).

In terms of floristic structure and biomass, Hamoye exhibits higher values compared to Kanovlei. Specifically, Hamoye supports a mean woody species richness of 14.1 species per hectare, an above-ground biomass (AGB) of 26.4 t/ha, and a woody plant density of 364 individuals/ha. In comparison, Kanovlei has 8.1 species/ha, 15.4 t/ha AGB, and 228 individuals/ha (Diesse et al., 2025). Notably, more than 50% of the species in Kanovlei's subcanopy layer do not occur in the overstorey, while this figure is about 40% in Hamoye.

The soils in both sites belong to the Kalahari formation, derived from unconsolidated aeolian sands. (Coetzee, 2001; Graz, 2006; Mayr et al., 2018).

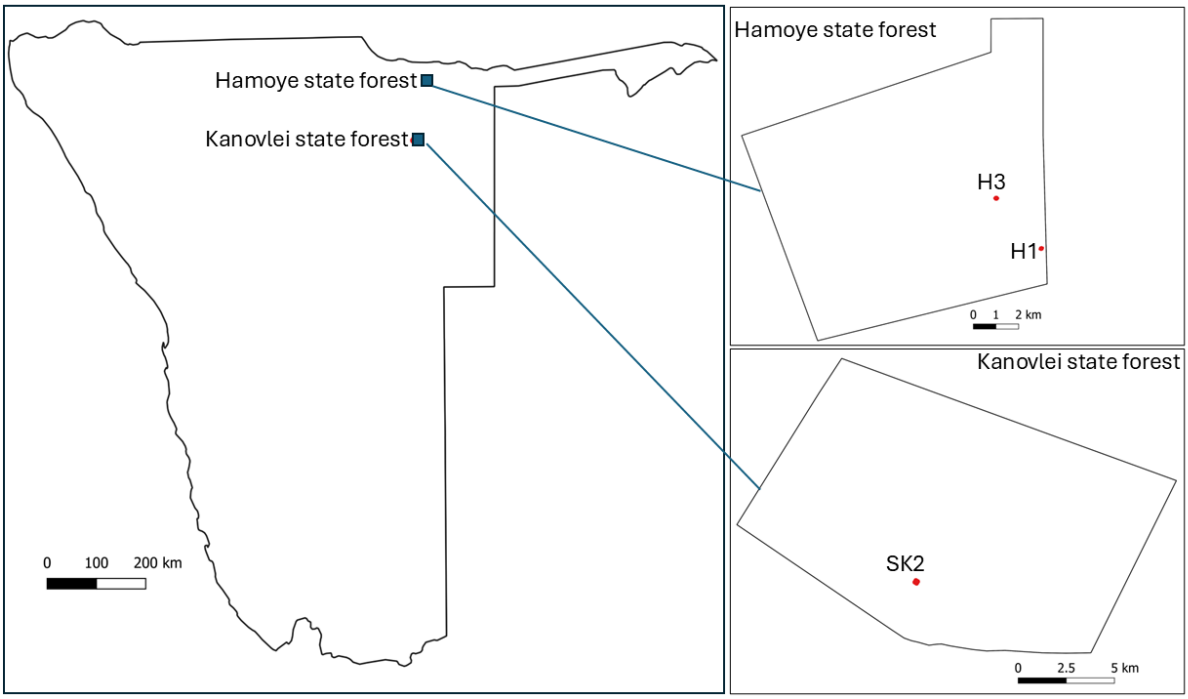


Figure 4.1 Study sites. Plots installed in Kanovlei and Hamoye State Forest are coloured in red.

4.2.2 Data collection

Data were collected in March and April 2023 during the leaf-on conditions in three plots of 0.5 ha (100 m by 50 m), with one plot located in Kanovlei and two plots in Hamoye. Each plot was divided into height subplots of 25 m x 25 m (625 m^2). Therefore, we have a total of 24 subplots.

4.2.3 Inventory data

The plots used for this study are part of the SEOSAW network (SEOSAW partnership, 2021) and thus they have been established following the SEOSAW protocols. Measurements were taken for all woody plants with a diameter at breast height (DBH, 1.3 m above ground) from 5cm. For each tree, the following parameters were recorded: species name, DBH using the diameter tape, tree height using a vertex laser rangefinder, and crown diameter in two perpendicular directions.

The inventory data were processed to estimate the woody above-ground biomass (AGB) using equation 4 from (Chave et al., 2014). Species-specific wood density values were extracted using the getWoodDensity() function from the BIOMASS R package (Réjou-Méchain et al., 2017), based on the global wood density database compiled by Zanne et al. (2009) The tree density was calculated as the number of trees recorded in each subplot.

4.2.4 TLS data

We used a Riegl VZ-1000 to scan the plots (Table 5). Four transects were set up for each plot, two inside the plot boundaries and two outside the plot boundaries.

Table 4.1 TLS acquisition parameters

Parameters	Value
Sensor	Riegl VZ-1000
Accuracy	8 mm
Precision	5 mm
Laser Class	1
Scan rate	Up to 122 000 points/sec
Field of view	360° horizontal, 100° vertical

Different spacing of the scan positions has been used according to the objectives of previous studies. For example, Brede et al. (2019) used a 20 m spacing but with a slightly wider spacing where visibility was good. Calders et al. (2015) used a 40 m spacing from the centre in each cardinal direction. For this study, we used a 25 m x 25 m sampling grid to minimise possible occlusion (Figure 4.2). This choice was motivated by the fact that the dry woodland subcanopy is more open as described in chapter 3, and as suggested by Wilkes et al. (2017).

At eight scanning position along Rows 2 and 3 (Figure 4.2), located inside each plot, the vegetation was scanned with the scanner in both horizontal and vertical orientations to capture the canopy structure. Horizontal orientation referred to the standard upright mounting of the scanner, in which the instrument rotates around a vertical axis to capture a horizontal 360° panorama, whereas vertical orientation involved tilting the scanner 90°, allowing the laser to sweep vertically across the vegetation structure.

In Rows 1 and 2, scanning was conducted only in the horizontal direction, with the purpose of minimising shadow effects and maximising spatial coverage of vegetation within the plot.

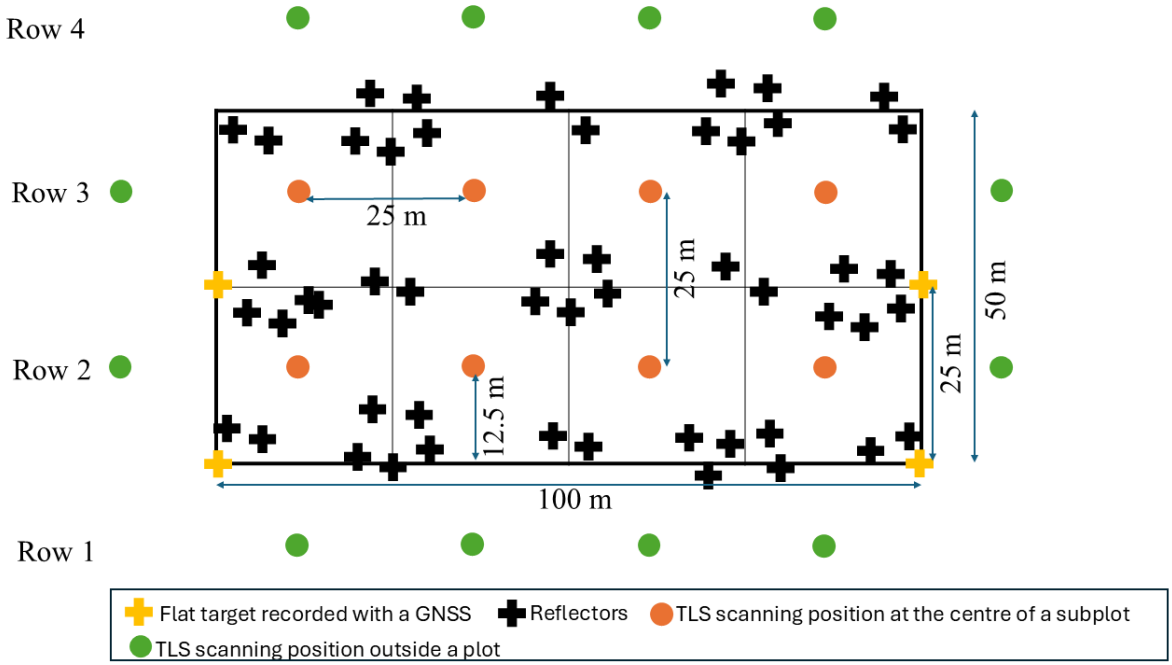


Figure 4.2. Layout of the reflectors and TLS scanning position.

. Each scan position was situated at the centre of a 25 m x 25 m subplot. The position of the reflectors is only representative. Reflectors were positioned opportunistically to maximise visibility.

Reflectors used as tie-points for aligning scans were placed at various locations within each transect, including the corners of the plots (Figure 4.3.A). Due to a limited number of reflectors, some were repositioned from the edges between Rows 3 and 4 before scanning commenced.



Figure 4.3. Reflectors used as tie points during the scanning.

: a flat reflector of 5 cm used in the corner of the plot. B: A white reflector of 10 cm length erected on a black pole. If the overstorey in the plot is dense, reflectors are put on high poles to ensure that it is seen over the bushes.

One scan position was located at the centre of each subplot. The distance between each scan position was approximately 25 m, though the exact distance varied based on vegetation density and the visibility of reflectors at each location. To ensure accurate georeferencing, a Global Navigation Satellite System (GNSS) base station was set up on a tripod in an open area near the southwestern corner of each plot. The GNSS rover, with its antenna mounted on tripods at the plot corners, was used to record precise plot corner locations. Corner locations were saved when the Geometric Dilution of Precision (GDOP) was below 2, with each corner taking approximately 5-10 minutes to record. The identification of targets as common anchor points served as ground control points and enabled the alignment of point clouds, three-dimensional datasets generated from individual scans within a subplot (Wilkes et al., 2017).

4.2.5 TLS processing

TLS data was initially processed using the RiSCAN Pro software v2.7. Scans per plot were co-registered and unified using the reflectors as common anchor points. The raw TLS data were converted to LAS format using the RiSCAN Pro v2.7 (Figure 19). LAS files were exported with georeferenced coordinates in UTM Zone 34s to ensure accurate spatial alignment with the GNSS-measured plot boundaries. To process TLS point clouds, we used R package lidR (Roussel et al., 2020) and CloudCompare software (CloudCompare (version 2.13.0.3), 2024). The TLS point clouds were first classified into ground points and non-ground points using the Cloth Simulation Function (CSF) (Zhang et al., 2016). After ground classification, point elevation was normalised using the normalize height function, which removes the influence of terrain using a Digital Terrain Model generated from the point cloud data (Roussel et al., 2020). The statistical outlier removal (SOR filter) algorithm was used in CloudCompare software to remove outliers. This algorithm assumes that the distribution of distances between each point and its nearest neighbour exhibits a Gaussian distribution. Points that deviated significantly from the mean distance were classified as outliers and removed (Duan et al., 2024). In this study, the SOR filter was configured using distances in the Z dimension (height) only. The formula of the SOR filter is as follows:

Max distance = $\mu + 1.96 * \sigma$ (1)

Where σ and μ are the standard deviation and mean of nearest neighbour distances, respectively.

Thereafter, the Statistical Outlier Suppression (SOS) filter removed the points that were farther than the average distance plus a number of times the SD (Abdelazeem et al., 2021). This included the removal of ‘ghost points’, which are artificial points generated by the scanner due to multiple reflections. These ghost points, along with other erroneous returns (e.g., laser interactions with airborne particles, reflective surfaces or gaps in foliage), did not represent actual vegetation structures and could bias subsequent structural analyses.

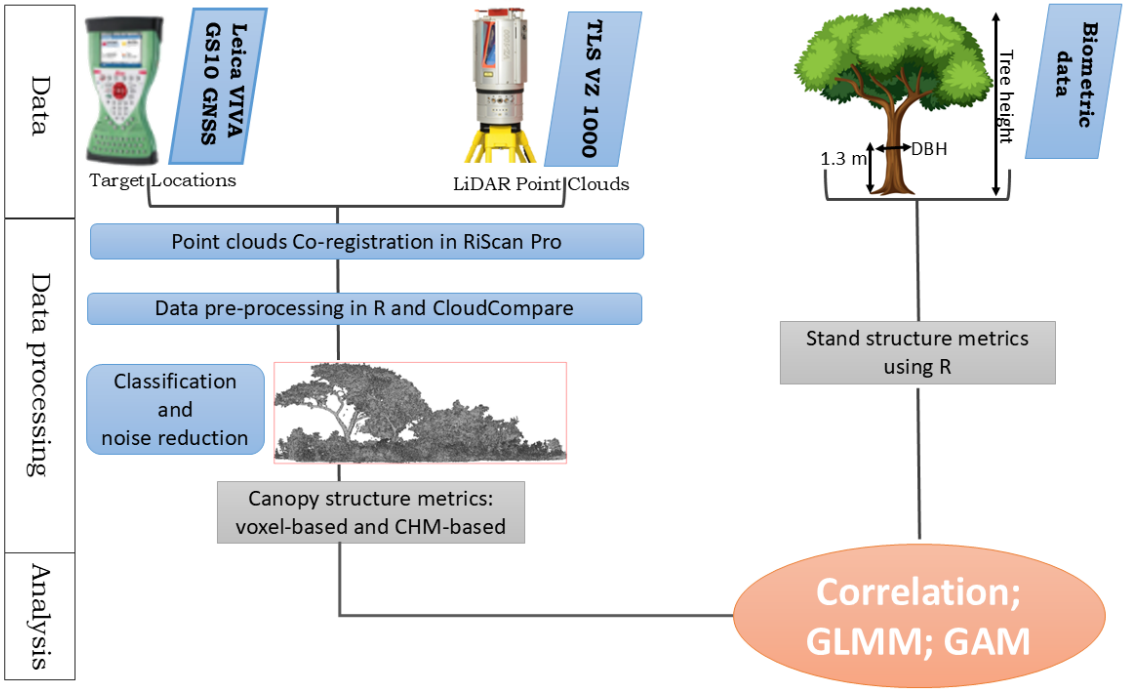


Figure 4.4. Schematic diagram summarising the data processing and analysis workflow for the TLS data. GAM is the generalised additive model and GLMM is generalised linear mixed-effects model.

4.2.6 TLS derived parameters

The point cloud was divided into two principal layers, including the canopy layer (height ≥ 3m) and the subcanopy layer (height < 3m), which included shrubs, small trees, and the ground layer. To further refine our understanding of vertical structure, the subcanopy layer was disaggregated into: a ground layer (< 0.5 m), which captured grasses, seedlings, and very low vegetation, and a shrub/small tree layer (0.5-3 m). This stratification reflected the ecological relevance of vertical layering in dry woodlands. By separating these layers, we aimed to explore the connectivity between layers.

To quantify the canopy structure across all plots, we employed both Canopy Height Model (CHM) and voxel-based model approaches. TLS-derived canopy metrics were used as relative indicators of vegetation structure rather than direct substitutes for field measurements.

- **CHM-based metrics**

A CHM was generated for each plot using the 'p2r' algorithm from the lidR package, which assigns the elevation of the highest point to each grid square, in our case with a spatial resolution of 30 cm x 30 cm area. This resolution allows for the capture of detailed variations in canopy surface elevation, enabling precise mapping of small canopy features. The resulting CHM was used to derive vertical structural metrics, including maximum canopy height, as well as variability (coefficient of variation).

Canopy cover was calculated as the proportion of CHM cells with height values greater than 3 m. To assess spatial variability in canopy cover, we computed the coefficient of variation (CV) of these CHM values above 3 m.

- **Voxel-based metrics**

To characterise vegetation stratification, we employed a voxelization approach. The three-dimensional space of each plot, with canopy top height determined by the largest tree, was subdivided into. a voxel of 25cm x 25cm x 25cm for further analysis (Puletti et al., 2021). This voxel dimension allowed for the generation of detailed vertical forest layers, assuring a fine resolution description of the vegetation (Figure 20). We used a threshold of 5 points to determine if a voxel is filled or not (Puletti et al., 2021). This allowed for the calculation of various canopy metrics. Table 6 summarises the metrics derived from the CHM-based and voxels-based models using the lidR package.

For fine-scale analysis, each 25 m × 25 m subplot was further divided into 5 m × 5 m grid cells. Canopy structural metrics were then computed at both the 25 m × 25 m and 5 m × 5 m scales.

.

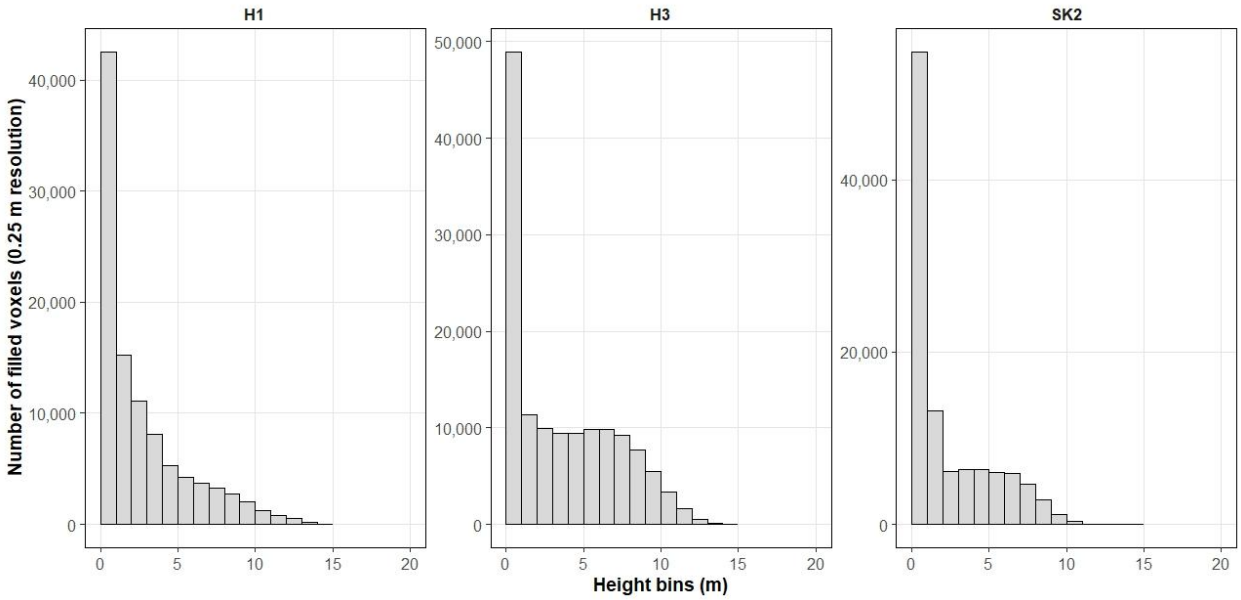


Figure 4.5. Vertical foliage structure derived from TLS data across forest plots.
The barplot shows the total number of filled voxels per height bin, illustrating the distribution of vegetation along the vertical axis.

Table 4.2 Description of canopy structure metrics derived from TLS data used in this study

Metric	Definition	Formula	Ecological Explanation
Plant Density Index (PDI) Per Layer	Ratio of filled to total voxels per layer	Filled Voxels / Total Voxels per layer	Indicates vegetation density within each layer. Higher PDI values reflect denser foliage or woody material, influencing habitat complexity and light attenuation
Vertical Entropy	Measure of vertical distribution evenness of lidar returns	VCI = $-\sum_{i=1}^{n} \rho i \log(\rho i)$ Where n is the total number of height bins, and ρ_i is the proportional abundance of lidar returns in height bin *i* (Van Ewijk et al., 2011)	Reflects vertical structural complexity of the canopy. Higher entropy values indicate more evenly distributed vegetation, supporting biodiversity and microhabitat differentiation.
Gap fraction profile	Proportion of laser pulses that passed through a given height interval	Computes the gap fraction profile using the method of Bouvier et al. (2015)	Measures vertical canopy openness. Higher values indicate more gaps or voids in the canopy, thus greater light penetration (Bouvier et al., 2015)
Canopy cover	Proportion of ground area covered by vegetation from a certain height upward	canopy cover derived from Canopy height model	Modulates light availability and microclimate by indicating how much of the ground is shaded by vegetation.

4.2.7 Statistical analysis

All statistical analyses were performed in R, version 4.3.3 (R Core Team, 2023). Before analysis, we checked the assumptions of parametric analysis for all data.

To assess how TLS-derived canopy structural metrics can be used to describe and differentiate vegetation structure among plots, we conducted both univariate and multivariate analyses.

Differences in canopy structural attributes (e.g., canopy height, canopy PDI, canopy cover, gap fraction, coefficient of variation of canopy height and cover, and vertical entropy) among plots were assessed using the Kruskal-Wallis test. Where significant differences were found, pairwise comparisons were performed using Dunn's test with Bonferroni correction. In addition, we used Spearman correlation analysis to assess co-variation among TLS-derived canopy metrics. Principal Component Analysis (PCA) was used to summarise multivariate patterns and visualise structural differentiation among plots. PCA was conducted using the FactoMineR (Lê et al., 2008) and factoextra (Kassambara and Mundt, 2016) packages. PCA was based on scaled variables, and 5 x 5 m grid cells were projected onto the first two principal components.

To evaluate how canopy structure influences the subcanopy layer, we evaluated relationships between canopy structural metrics and subcanopy plant density index (PDI, < 3 m). First we computed Spearman correlation coefficients separately for each plot. Canopy metrics included canopy cover, CV of canopy height and cover, gap fraction, and vertical entropy. Knowing that multiple parameters are not considered as independent values, but are causatively related, we used a generalised linear mixed-effects model (GLMM) to assess how canopy structural metrics influence subcanopy vegetation density, represented by PDI for vegetation below 3 m. The model was fitted using the glmmTMB package in R (McGillycuddy et al., 2025), with a beta distribution and logit link, since the subcanopy PDI is a proportion bounded between 0 and 1. All predictors were standardised and centred to facilitate model interpretation and comparability, and the performance package allowed for assessing the model diagnostics (Lüdecke et al., 2021). A random intercept accounts for the nested nature of the data, subplots inside plots.

To evaluate vertical interactions across forest layers, we first used the Spearman correlation between the canopy layer (> 3 m) and the overall subcanopy layer (0.1 – 3 m). To gain further resolution, the Spearman correlation analyses were subsequently conducted to examine (i) the relationship between the canopy layer (> 3 m) and shrub layer (0.5 – 3 m), and (ii) the relationship between the shrub layer (0.5 – 3 m) and ground layer (< 0.5 m). A pairwise comparison using Dunn's test (using Bonferroni method) following the Kruskal-Wallis analysis was used to compare the canopy metrics among plots.

To assess how canopy structure influences species richness, tree density, and biomass at the subplot level (25 x 25 m), we applied Generalised Additive Models (GAMs) using the mgcv package (Wood, 2017). TLS-derived predictor variables included canopy gap fraction, CV of canopy height and cover, canopy PDI, vertical entropy, and maximum canopy height. Response variables were derived from field inventories. For count data (species richness and tree density), models were fitted with a Poisson distribution. Predictors were standardised before modelling. Model outputs included adjusted R^2,

deviance explained, effective degrees of freedom (EDF), and smooth term significance. Model residuals were evaluated using the gam.check() function.

4.3 Result

4.3.1 Structural gradients of canopy metrics across plots

Several TLS-derived canopy metrics revealed distinct structural differences. Kruskal–Wallis tests followed by post hoc pairwise comparisons using Dunn's test with Bonferroni correction confirmed significant variations in key attributes.

TLS-derived canopy metrics revealed clear structural differences among plots (Figure S1). Overall, H3 was characterised by higher canopy density, height, and vertical complexity, whereas H1 and SK2 exhibited more open and heterogeneous canopy structures. These differences provide context for structural variability across plots. To better understand relationships among structural attributes, we examined the co-variation between TLS-derived canopy metrics. The correlation matrix revealed strong interrelationships among several TLS-derived structural metrics. Canopy cover, PDI, vertical entropy, and canopy height were all positively and strongly correlated ($r > 0.65$), suggesting that denser and taller canopies tend to be more vertically stratified and structurally complex. In contrast, gap fraction and the CV of canopy cover were negatively correlated with these structural metrics (r between -0.65 and -0.95), indicating that more open and discontinuous canopies are associated with reduced vertical complexity. CV of canopy height showed weaker and more intermediate correlations, suggesting it captures a different structural dimension (Figure 4.6).

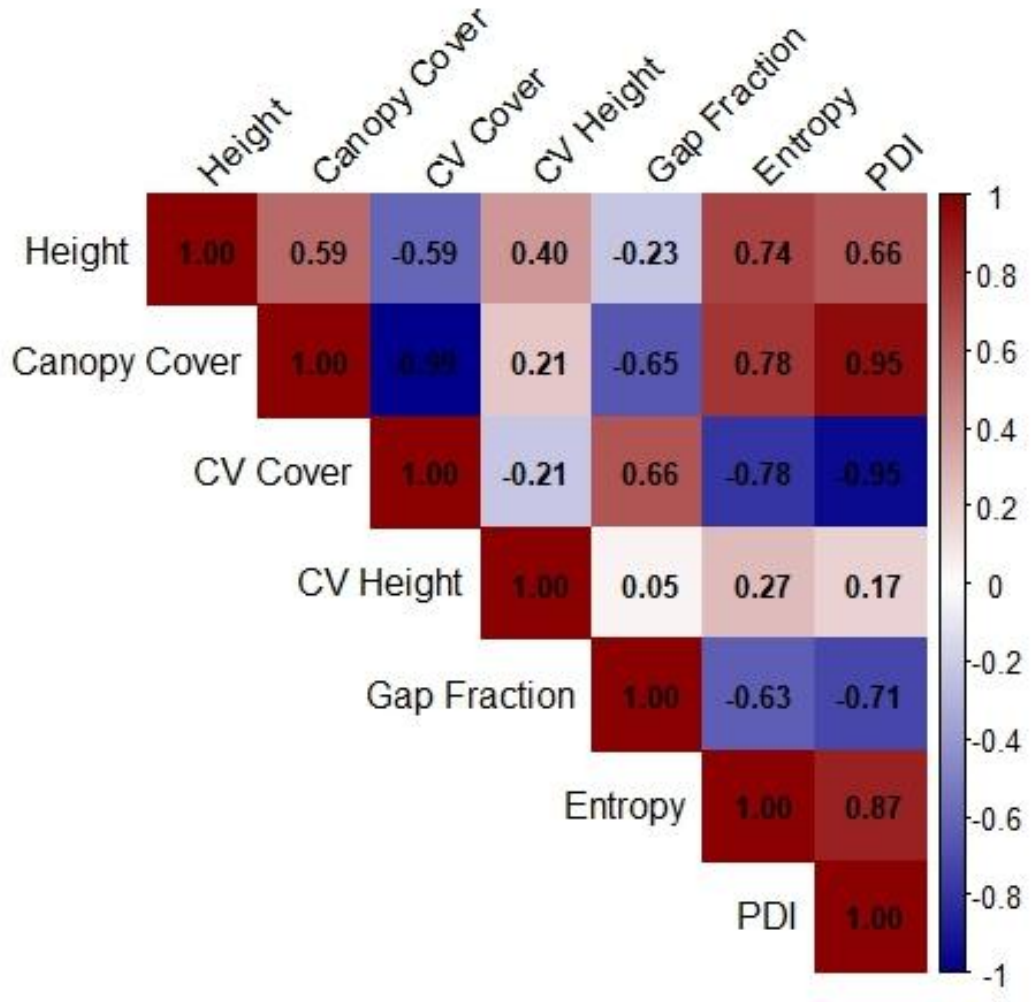


Figure 4.6. Correlation matrix showing pairwise Spearman correlation coefficients among TLS-derived canopy structural metrics.Positive correlations are shown in red and negative in blue. Colour intensity of the squares indicates the strength of the correlation

These multivariate relationships were further clarified by the Principal Component Analysis (PCA), which explained 82.2% of the total variance in the first two components (PC1 = 68.1%, PC2 = 14.0%) (Figure 4.7). The first principal component (PC1) represented a clear gradient of increasing canopy density and structural complexity, with strong positive contributions from canopy cover (0.93), canopy PDI (0.86), vertical entropy (0.90), and canopy height (0.72), and strong negative contributions from CV of canopy cover (–0.84) and gap fraction (–0.68). This axis reflects a transition from dense, vertically complex canopies to open and structurally heterogeneous ones.

The second principal component (PC2) was primarily associated with canopy height (0.62) and gap fraction (0.65), indicating a secondary gradient related to canopy elevation and openness. Together, these results demonstrate that canopy structure in dry woodlands is organised along a dominant gradient of vegetation density and vertical complexity, with secondary variation linked to canopy

openness and height distribution.

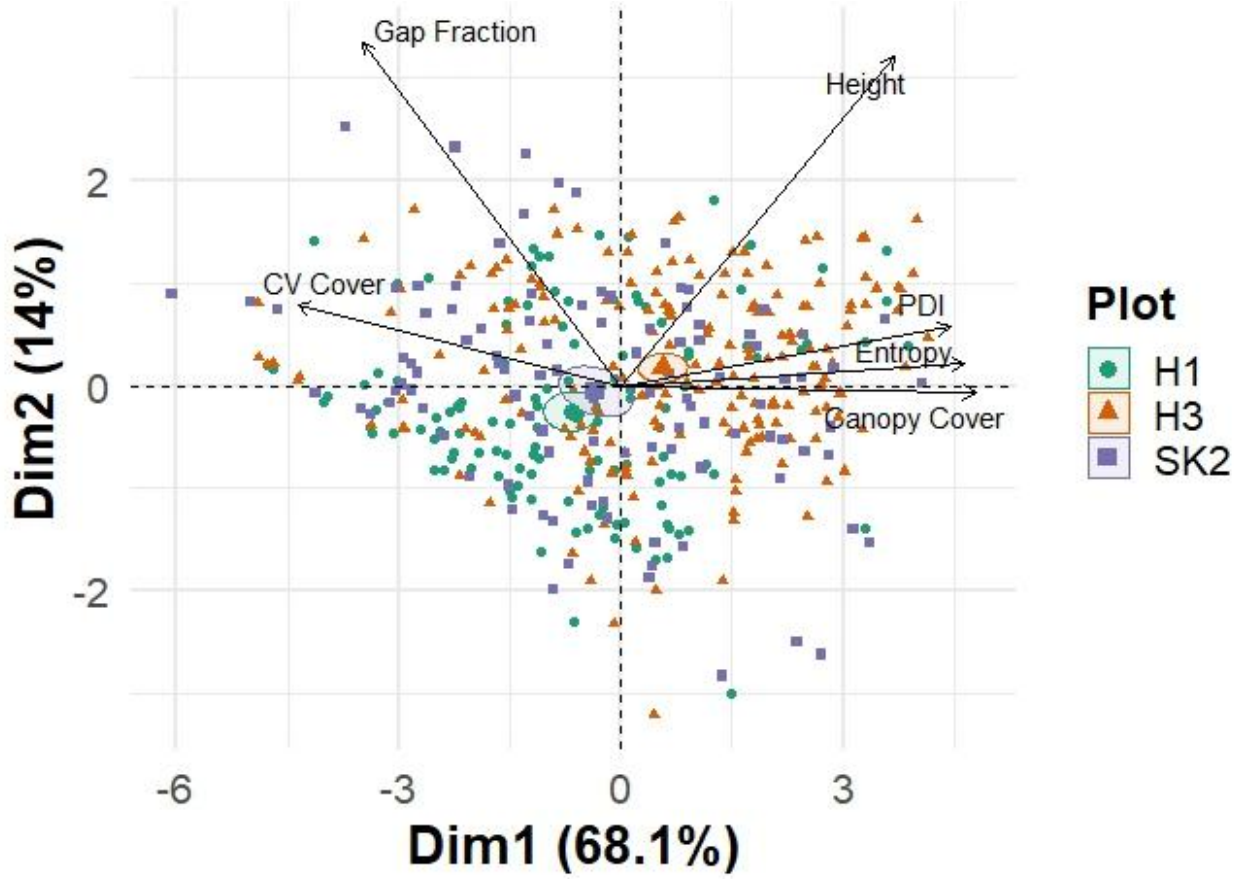


Figure 4.7. Principal Component Analysis (PCA) biplot of TLS-derived canopy structural metrics across 5 × 5 m grid cells within plots (H1, H3, SK2). .

Points represent individual grid cells, coloured by plot identity. Ellipses show the 95% confidence regions for each plot , and larger icons at the centre of ellipses represent the group centroids. Arrows represent the direction and contribution of each structural variable to the first two principal components (PC1 and PC2).

4.3.2 Influence of canopy structure on subcanopy vegetation

Pairwise Spearman correlations revealed that subcanopy density responded most strongly to canopy PDI and measures of canopy openness and heterogeneity (Figure 4.8).

A positive and significant relationship was found between canopy PDI and subcanopy PDI in both H1 (ρ = 0.53) and H3 (ρ = 0.34), highlighting the positive linkage between layers in these two plots, However, no significant correlation was observed in SK2, where the relationship was weak (ρ = 0.08). When the subcanopy layer was disaggregated into the ground layer (< 0.5 m) and the shrub layer (0.5–3 m), the correlation analysis showed a consistent vertical linkage between these two lower layers across all plots. The ground layer (0.1–0.5 m) was positively correlated with shrub layer density (0.5–3 m). In contrast, shrub layer density was positively correlated with the canopy (>3 m) only in H1 and H3, while no significant correlation was observed in SK2.

In H1 and H3, subcanopy PDI was negatively correlated with the coefficient of variation (CV) of canopy cover ($\rho = -0.52$ and -0.31, respectively; both $p < 0.001$), suggesting that greater horizontal variability limits the subcanopy development. SK2 showed no significant relationship. In contrast, gap fraction was positively related to subcanopy PDI in SK2 ($\rho = 0.20$, $p = 0.043$), implying that openness enhances understorey growth in this more open woodland. Although no significant relationships were observed in H1 and H3, Figure 24 shows that the relationship saturates at around 95% gap fraction. Variability in canopy height (CV) showed weak positive correlations with subcanopy PDI across all plots ($\rho = 0.15$–0.23). Entropy showed only a slight and significant effect in H3 ($\rho = 0.14$, $p = 0.036$), with no notable patterns elsewhere.

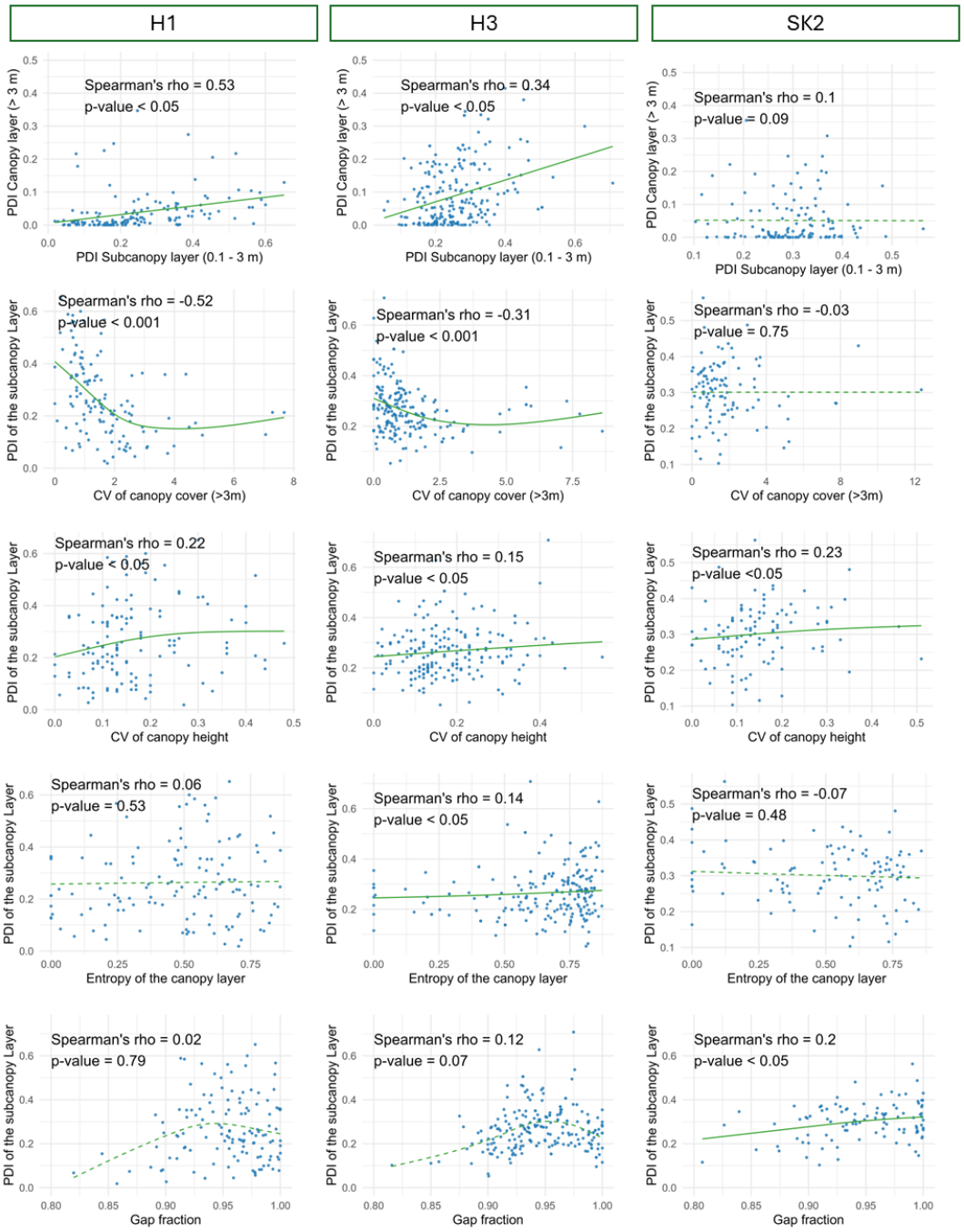


Figure 4.8. Relationships between the Plant Density Index (PDI) of the subcanopy layer (0.1–3 m) and canopy structural metrics across plots. Green lines represent fitted trends using Generalised Additive Models (GAMs), while blue points show individual 5 x 5 m subplot values. Solid green lines indicate statistically significant relationships ($p < 0.05$), while dashed lines represent non-significant trends. Spearman's rank correlation coefficient and corresponding p-value are reported within each scatterplot

These findings were corroborated by a generalised linear mixed model using a beta distribution (Table 7), which revealed that subcanopy PDI increased with canopy PDI ($\beta = 0.162$, $p < 0.001$) and gap fraction ($\beta = 0.260$, $p < 0.001$). In contrast, heterogeneity in canopy cover ($\beta = –0.328$, $p < 0.001$), and entropy of the canopy layer ($\beta = –0.148$, $p < 0.05$) were all negatively associated with canopy layer PDI.

Plot-level variance accounted for a small proportion of the model variance (σ^2 = 0.13). These results suggest that subcanopy layer density responds positively to open conditions in the canopy layer, while heterogeneity in vertical and horizontal direction may constrain its development.

Table 4.3. Summary of the generalised linear mixed model (GLMM) examining the influence of the canopy metrics on the subcanopy PDI.

Marginal R^2 indicates variance explained by fixed effects alone; conditional R^2 includes both fixed and random effects.

Predictors	**Estimates**	**P**
Intercept	-1.006	<0.001
PDI in the canopy	0.162	<0.001
Gap fraction profile	0.260	<0.001
CV of canopy cover	-0.328	<0.001
Entropy	-0.148	< 0.001
σ^2	0.13	
τ_{00} **Plot**	0.01	
ICC	0.09	
N plot	3	
Observations	448	
Marginal R^2 / Conditional R^2	0.38 / 0.44	

4.3.3 Influence of canopy metrics on key ecological attributes

For species richness, the coefficient of variation (CV) of canopy cover showed a significant and approximately linear relationship (EDF = 1.0, $p < 0.05$), explaining 25.3% of the deviance (Table 4.4; Figure 4.9). In contrast, neither canopy height variability (EDF = 2.41, p = 0.38), entropy (EDF = 3.51, p = 0.31), nor gap fraction (EDF = 1.0, p = 0.56) showed significant associations with species richness, despite entropy explaining 41.7% of deviance, suggesting some underlying complexity. Similarly, canopy height (EDF = 1.7, p = 0.24) and canopy PDI (EDF = 1.2, p = 0.28) were not significant predictors. As illustrated in Figure 25, greater variability in canopy cover tends to reduce species richness.

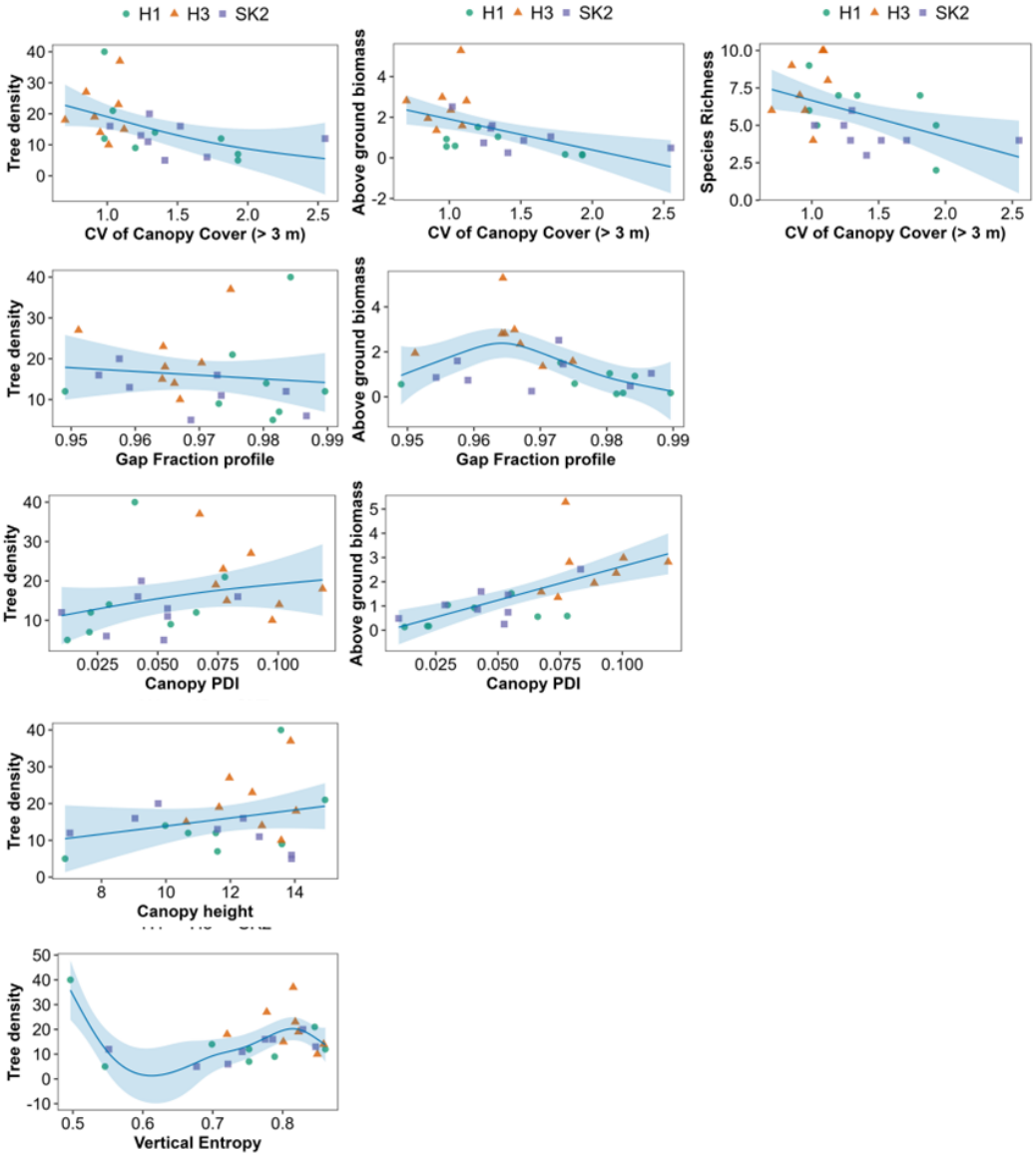


Figure 4.9. Relationships between TLS-[A1.1]derived canopy structure metrics and field-measured ecological attributes (species richness, tree density, and above-ground biomass) across plots.

Each panel shows a generalised additive model (GAM) fit (blue smooth line with 95% confidence band). CV means coefficient of variation. PDI means Plant Density Index. Points are coloured and shaped by 25 x 25 m subplot.

For tree density, all five canopy metrics demonstrated significant nonlinear relationships. The strongest predictor was the entropy of the canopy layer (EDF = 8.31, $p < 0.001$), which explained 66.1% of deviance. Both CV of canopy height (EDF = 6.70, $p < 0.001$) and CV of Canopy cover (EDF = 3.29, $p < 0.001$) also significantly influenced tree density, explaining 43.6% and 38.4% of deviance, respectively. The gap fraction was also significant (EDF = 8.28, $p < 0.001$), explaining 27.4% of the deviance. Additionally, canopy PDI (EDF = 8.31, $p < 0.001$) and canopy height (EDF = 1.00, $p = 0.0047$) were both significant, explaining 60.8% and 8.0% of deviance, respectively.

Figure 4.9 illustrates that variability in canopy cover and gap fraction negatively influenced the tree density, while tree density responded non-monotonically to canopy entropy. Specifically, moderate levels of vertical complexity were associated with higher tree density, whereas both low and high entropy values corresponded to reduced tree density. In addition, tree density increases with canopy PDI and canopy height.

For aboveground biomass, gap fraction was the strongest predictor (EDF = 7.62, p = 0.0095), explaining 70.9% of deviance. The relationship was non-linear, with biomass increasing with gap fraction up to a mid-range threshold and then declining thereafter, as illustrated by the inverted-V curve (Figure 4.9). Canopy PDI showed a significant positive linear relationship (EDF = 1.00, p = 0.0003), explaining 46.1% of deviance. The CV of Canopy cover also showed a significant negative linear relationship (EDF = 1.00, p = 0.0064), explaining 29.2% of deviance. Entropy showed a marginal effect (EDF = 1.00, p = 0.0692), while CV of canopy height (EDF = 3.57, p = 0.251) and canopy height (EDF = 5.47, p = 0.168) were not significant, although the latter still explained 44.2% of the deviance.

Table 4.4. Summary of Generalized Additive Models (GAMs) evaluating the influence of canopy structural metrics derived from TLS on field-measured ecological attributes. For each predictor, the deviance explained (%), estimated degrees of freedom (EDF), and p-value for the smooth term are reported. Models used a Poisson distribution for species richness and tree density, and a Gaussian distribution for biomass.

Ecological response from field data	GAM models	Deviance explained (%)	EDF	p-value
1. Species richness				
	CV of canopy cover (>3m)	25.3	1	<0.05
2. Tree density				
	CV of canopy cover (>3m)	38.4	3.29	<0.001
	Gap fraction profile	27.4	8.28	<0.01
	Entropy	66.1	8.3	<0.001
	Canopy PDI	60.8	8.31	<0.001
	Canopy height	7.9	1	<0.01
3. Biomass				
	CV of canopy cover (>3m)	29.2	1	<0.01
	Gap fraction profile	70.9	7.62	<0.01
	Canopy PDI	46.1	1	<0.001

4.4 Discussion

This study highlights three main findings. First, canopy structure in dry Namibian woodlands is organised along a dominant structural axis separating two contrasting canopy states: dense and vertically structured canopies characterised by high canopy cover, plant density index (PDI), vertical entropy, and canopy height, versus open and horizontally heterogeneous canopies characterised by high gap fraction and variability in canopy cover, as revealed by the PCA and correlation analyses. Second, canopy density, openness, and heterogeneity exert contrasting effects on subcanopy vegetation, with canopy density and openness generally promoting subcanopy development, while horizontal and vertical heterogeneity tend to constrain it. Third, canopy structural attributes differentially influence ecological responses, with canopy openness and density emerging as key drivers of above-ground biomass, while both canopy density and vertical complexity strongly influence tree density.

4.4.1 Influence of canopy structure on subcanopy vegetation

Across plots, greater CV in canopy cover was consistently and negatively associated with subcanopy PDI. A likely explanation is that heterogeneous canopy cover creates irregular horizontal light transmission, resulting in patchy or excessive shading, leading to the reduced subcanopy density.

In contrast, greater gap fraction, indicative of vertical canopy openness, was positively related to subcanopy density. This aligns with the expectation that increased vertical light penetration promotes subcanopy growth and supports earlier findings by Diesse et al. (2025) and Kindermann et al. (2022). This pattern also supports facilitation theory, where canopy gaps enhance understorey development through improved light and resource availability. The negative effect of entropy on subcanopy PDI suggests that increased vertical complexity may constrain subcanopy density by intensifying competition for light and space across layers. Canopy PDI was positively and consistently associated with subcanopy density. This vertical linkage is consistent with findings from Bartels and Chen (2013), who reported that increased canopy abundance promoted subcanopy development via soil nutrient cycling, and with Weltzin and Coughenour (1990), who observed facilitative effects of trees on herbaceous vegetation through niche partitioning in Kenyan savannas. This apparent contrast between canopy PDI and vertical entropy can be explained by the canopy architecture of dry woodlands in Namibia, dominated by short to medium trees. In these systems, a high canopy PDI may reflect vegetation concentrated within a relatively narrow vertical band, allowing sufficient light to reach the subcanopy. In contrast, high entropy reflects foliage distributed across multiple vertical layers, which may reduce light penetration and increase competition.

Therefore, in this context, high canopy PDI does not necessarily imply high entropy. A stand may be densely vegetated at a specific height range while still maintaining relatively low vertical complexity, a configuration that allows subcanopy growth. Conversely, when foliage is distributed across multiple layers, subcanopy development may be constrained due to shading and competition. These findings highlight the need to interpret structural density (PDI) and vertical complexity (entropy) as distinct but complementary dimensions of forest architecture. While PDI measures how much vegetation is present, entropy captures how that vegetation is vertically arranged. Both are essential for understanding how canopy structure influences ecological processes in dry woodland ecosystems.

4.4.2 Canopy metrics differentiation and vegetation structure characterisation

Our study demonstrated that TLS-derived metrics effectively captured and differentiated canopy structural variation across dry woodlands in Namibia. Plot H3 was characterised by higher canopy cover, PDI, vertical entropy, and canopy height, suggesting a more vertically complex and denser canopy structure. In contrast, H1 and SK2 showed greater horizontal heterogeneity, as indicated by higher coefficients of variation in canopy cover and greater gap fraction, reflecting more open and irregular canopy conditions.

Such patterns are commonly associated with drier conditions and repeated disturbances such as fire, herbivory, or anthropogenic activities. In particular, the low rainfall in Kanovlei (< 500 mm/year) and the prevalence of fire disturbance likely contribute to the sparse canopy observed in SK2, consistent with its reduced structural metrics (Mayr et al., 2018). Despite both H1 and H3 being located in Hamoye State Forest, H1 exhibits greater canopy openness due to past disturbances, including fire, livestock grazing, and tree cutting (Diesse et al., 2025). The lower canopy density and greater heterogeneity may therefore reflect degradation rather than natural variability.

The PCA and correlation analyses further support these distinctions. Structural complexity metrics such as PDI, entropy, and canopy cover were positively and strongly correlated, suggesting that these attributes co-occur in less disturbed stands such as H3. In contrast, CV of canopy cover and gap fraction were negatively correlated with these metrics, reinforcing their association with canopy openness and disturbance.

Ecologically, these findings indicate that dry woodland structure is shaped by the interaction between precipitation regimes, disturbance history, and possibly soil properties. TLS-derived metrics capture both vertical complexity and horizontal variability, providing complementary insights into stand structure.

4.4.3 Influence of canopy structure on field-measured ecological attributes

TLS-derived canopy metrics demonstrated varying degrees of association with field-measured ecological attributes. For species richness, only the CV of canopy cover showed a significant negative effect, indicating that fragmented or highly variable canopy structures may limit species diversity. These findings contrast with the habitat heterogeneity hypothesis (Tews et al., 2004), which predicts that structurally complex environments support higher biodiversity. One possible explanation is that, in dry woodlands, high variability in canopy cover reflects disturbance or dominance by a limited number of individuals, reducing recruitment opportunities and leading to competitive exclusion. Similar patterns have been reported by Anderson et al. (2021) and Fahey et al. (2015), where structurally complex or dense stands may suppress diversity through shading or dominance effects.

The non-significant relationship between canopy PDI and species richness also contrasts with expectations from our hypothesis and the theory of biodiversity-ecosystem functioning (BEF), which suggests that increased biomass should promote richness through niche diversification (Mittelbach et al., 2001; Tilman and Sowning, 1994). Indeed, the canopy PDI, which can be considered as the amount of vegetation present in the canopy, should have a positive relationship with diversity (Wang et al., 2024). Previous studies in dry woodlands (Godlee et al., 2021; Shirima et al., 2015), also found a positive association between biomass and diversity. However, as mentioned for canopy heterogeneity, the relationship between canopy PDI and species richness may also be regulated by tree density, as highlighted by Godlee et al. (2021).

For tree density, vertical complexity showed a strong non-linear relationship, where moderate levels of entropy supported higher density, while both low and high complexity reduced it. This pattern is consistent with niche partitioning theory, where intermediate structural complexity promotes coexistence by reducing direct competition, whereas excessive layering increases competition for resources. Ehbrecht et al. (2016) advanced that a decrease in vertical complexity with increasing tree density can be attributed to its relationship with mean diameter and basal area. Indeed, they found that tree density decreases with increasing mean diameter, either due to thinning, and harvesting or self-thinning.

Above-ground biomass was primarily influenced by canopy openness and density. Gap fraction showed a strong non-linear relationship with biomass, with peak values at intermediate levels of canopy openness. This suggests that biomass accumulation is maximised under conditions that balance light availability and canopy closure. Canopy PDI also showed a strong positive relationship with biomass, confirming that vegetation density is a key driver of carbon storage in these systems.

These results align with general principles of resource optimisation, where productivity is maximised under intermediate environmental constraints. Taken together, these findings highlight that canopy density and openness are key determinants of biomass and tree density, while vertical complexity plays a more nuanced role in shaping ecological patterns.

4.4.4 Methodological considerations and limitations

Beyond ecological interpretation, this study highlights several methodological considerations related to the use of TLS in dry woodland. In open and heterogeneous systems such as Namibian woodlands, TLS can effectively capture canopy and midstorey structure due to reduced occlusion compared to closed forests. However, the subcanopy layer is often dense, composed of shrubs, grasses, and multi-stemmed individuals, which can obscure the lower portions of larger trees. This occlusion can limit the accurate detection and reconstruction of individual stems, particularly at the base, which is critical for estimating structural attributes such as diameter and tree architecture. As a result, challenges arise for tree segmentation and the application of advanced approaches such as quantitative structure models (QSM), which rely on clear stem visibility.

In addition, the representation of vegetation structure depends on acquisition and processing choices, including voxel resolution, point density thresholds, and canopy height model derivation, which can influence the detection of smaller vegetation components. The spacing of scan positions is also a critical factor. In this study, a 25 m spacing was applied following recommendations from previous studies (e.g., Wilkes et al., 2017), which suggest adapting scan spacing to vegetation structure. However, in dense and multi-layered subcanopy conditions, closer scan spacing or multi-scan configurations may improve point cloud completeness and reduce occlusion effects. Future work should therefore evaluate the sensitivity of TLS-derived metrics to scan configuration in dry woodland environments.

TLS-derived structural metrics should therefore be interpreted as proxies of vegetation structure rather than complete representations. A further limitation is that these metrics were not explicitly calibrated against field-based measurements of canopy height or cover, which introduces some uncertainty in their absolute accuracy. Nevertheless, the consistency of observed ecological relationships supports their use as relative indicators of vegetation structure at fine spatial scales.

4.5 Conclusion

This study provides new insight into how fine-scale canopy structure influences subcanopy vegetation and broader ecological attributes in dry Namibian woodlands. By distinguishing between vegetation density (PDI) and vertical complexity (entropy), we offer a structural framework that helps explain the varying roles of canopy architecture in regulating forest dynamics.

Our findings demonstrate that canopy–subcanopy relationships are shaped by a balance between density and openness, with potential implications for how these woodlands respond to disturbance and climate variability. The observed patterns highlight that subcanopy density is not simply a function of openness or complexity alone, but emerges from their interaction.

The use of TLS in this context opens new opportunities for high-resolution forest monitoring, allowing for spatially explicit assessment of vegetation structure beyond traditional inventory methods. These insights are valuable for forest management aiming to support biodiversity, regeneration, and biomass under variable rainfall and disturbance regimes.

Future research should apply this approach across broader climatic gradients and forest types, compare fine- and coarse-scale interactions, and explore seasonal dynamics to refine our understanding of canopy–subcanopy coupling in dry ecosystems.

4.6 CRediT authorship contribution statement

Hermane Diesse: Writing – review & editing, Writing – original draft, Visualization, Methodology, Investigation, Formal analysis, Data curation, Conceptualization. **John L. Godlee**: Writing – review & editing, Supervision, Investigation, Conceptualization. **Kyle Dexter**: Writing – review & editing, Investigation. **Nichola Knox**: Writing – review & editing, Conceptualization. **Olivia Haikali**: Writing – review & editing, Investigation. **Leena Naftal**: Writing – review & editing, Investigation. **Dav Ebengo**: Writing – review & editing. **Gabriel Uusiku**: Writing – review & editing, Investigation. **Vera De Cauwer**: Writing review & editing, Supervision, Investigation, Conceptualization.

4.7 References

Abdelazeem, M., Elamin, A., Afifi, A., El-Rabbany, A., 2021. Multi-sensor point cloud data fusion for precise 3D mapping. Egypt. J. Remote Sens. Space Sci. 24, 835–844. https://doi.org/10.1016/j.ejrs.2021.06.002

Anderson, C.T., Dietz, S.L., Pokswinski, S.M., Jenkins, A.M., Kaeser, M.J., Hiers, J.K., Pelc, B.D., 2021. Traditional field metrics and terrestrial LiDAR predict plant richness in southern pine forests. For. Ecol. Manag. 491, 119118. https://doi.org/10.1016/j.foreco.2021.119118

Anderson, K.E., Glenn, N.F., Spaete, L.P., Shinneman, D.J., Pilliod, D.S., Arkle, R.S., McIlroy, S.K., Derryberry, D.R., 2018. Estimating vegetation biomass and cover across large plots in shrub and grass dominated drylands using terrestrial lidar and machine learning. Ecol. Indic. 84, 793–802. https://doi.org/10.1016/j.ecolind.2017.09.034

Ashcroft, M.B., Gollan, J.R., Ramp, D., 2014. Creating vegetation density profiles for a diverse range of ecological habitats using terrestrial laser scanning. Methods Ecol. Evol. 5, 263–272. https://doi.org/10.1111/2041-210X.12157

Bartels, S.F., Chen, H.Y.H., 2013. Interactions between overstorey and understorey vegetation along an overstorey compositional gradient. J. Veg. Sci. 24, 543–552. https://doi.org/10.1111/j.1654-1103.2012.01479.x

Béland, M., Kobayashi, H., 2021. Mapping forest leaf area density from multiview terrestrial lidar. Methods Ecol. Evol. 12, 619–633. https://doi.org/10.1111/2041-210X.13550

Beyene, S.M., 2020. Estimation of Forest Variable and Aboveground Biomass using Terrestrial Laser Scanning in the Tropical Rainforest. J. Indian Soc. Remote Sens. 48, 853–863. https://doi.org/10.1007/s12524-020-01119-2

Bouvier, M., Durrieu, S., Fournier, R.A., Renaud, J.-P., 2015. Generalizing predictive models of forest inventory attributes using an area-based approach with airborne LiDAR data. Remote Sens. Environ. 156, 322–334. https://doi.org/10.1016/j.rse.2014.10.004

Brede, B., Calders, K., Lau, A., Raumonen, P., Bartholomeus, H.M., Herold, M., Kooistra, L., 2019. Non-destructive tree volume estimation through quantitative structure modelling: Comparing UAV laser scanning with terrestrial LIDAR. Remote Sens. Environ. 233, 111355. https://doi.org/10.1016/j.rse.2019.111355

Burton, J.I., Mladenoff, D.J., Clayton, M.K., Forrester, J.A., 2011. The roles of environmental filtering and colonization in the fine-scale spatial patterning of ground-layer plant communities in north temperate deciduous forests. J. Ecol. 99, 764–776. https://doi.org/10.1111/j.1365-2745.2011.01807.x

Calders, K., Newnham, G., Burt, A., Murphy, S., Raumonen, P., Herold, M., Culvenor, D., Avitabile, V., Disney, M., Armston, J., Kaasalainen, M., 2015. Nondestructive estimates of above-ground biomass using terrestrial laser scanning. Methods Ecol. Evol. 6, 198–208. https://doi.org/10.1111/2041-210X.12301

Chave, J., Réjou-Méchain, M., Búrquez, A., Chidumayo, E.N., Colgan, M.S., Delitti, W.B.C., Duque, A., Eid, T., Fearnside, P.M., Goodman, R.C., Henry, M., Martínez-Yrízar, A., Mugasha, W.A., Muller-Landau, H.C., Mencuccini, M., Nelson, B.W., Ngomanda, A., Nogueira, E.M., Ortiz-Malavassi, E., Pélissier, R., Ploton, P., Ryan, C.M., Saldarriaga, J., Vieilledent, G., 2014. Improved allometric models to estimate the aboveground biomass of tropical trees. Glob. Change Biol. 20, 3177–3190. https://doi.org/10.1111/gcb.12629

Chidumayo, E., Marunda, C., 2010. Dry Forests and Woodlands in Sub-Saharan Africa: Context and Challenges, in: The Dry Forests and Woodlands of Africa, The Earthscan Forest Library.

CloudCompare (version 2.13.0.3), [GPL software], 2024. Retrieved from http://www.cloudcompare.org.

Coetzee, M.E., 2001. Agro-ecological Zoning Programme Directorate of Agricultural Research & Training Ministry of Agriculture, Water & Rural Development Private Bag 13184, Windhoek, Namibia 458.

De Cauwer, V., Geldenhuys, C.J., Aerts, R., Kabajani, M., Muys, B., 2016. Patterns of forest composition and their long term environmental drivers in the tropical dry forest transition zone of southern Africa. For. Ecosyst. 3, 23. https://doi.org/10.1186/s40663-016-0080-9

Decuyper, M., Mulatu, K.A., Brede, B., Calders, K., Armston, J., Rozendaal, D.M.A., Mora, B., Clevers, J.G.P.W., Kooistra, L., Herold, M., Bongers, F., 2018. Assessing the structural differences between tropical forest types using Terrestrial Laser Scanning. For. Ecol. Manag. 429, 327–335. https://doi.org/10.1016/j.foreco.2018.07.032

Diesse, H., Godlee, J.L., Knox, N., Muledi, J., Naftal, L., Nkulu, D., Nkomba, B., Uusiku, G., Dexter, K., De Cauwer, V., 2025. Quantifying unseen woody biomass and diversity in understorey trees and shrubs at the extremes of water availability in the Miombo ecoregion. For. Ecosyst. 100302. https://doi.org/10.1016/j.fecs.2025.100302

Donager, J.J., Sankey, T.Ts., Sankey, J.B., Sanchez Meador, A.J., Springer, A.E., Bailey, J.D., 2018. Examining Forest Structure With Terrestrial Lidar: Suggestions and Novel Techniques Based on Comparisons Between Scanners and Forest Treatments. Earth Space Sci. 5, 753–776. https://doi.org/10.1029/2018EA000417

Duan, D., Deng, Y., Zhang, J., Wang, J., Dong, P., 2024. Influence of VF and SOR-Filtering Methods on Tree Height Inversion Using Unmanned Aerial Vehicle LiDAR Data. Drones 8, 119. https://doi.org/10.3390/drones8040119

Ehbrecht, M., Schall, P., Juchheim, J., Ammer, C., Seidel, D., 2016. Forest Ecology and Management Effective number of layers : A new measure for quantifying three- dimensional stand structure based on sampling with terrestrial LiDAR. For. Ecol. Manag. 380, 212–223. https://doi.org/10.1016/j.foreco.2016.09.003

Fick, S.E., Hijmans, R.J., 2017. WorldClim 2: new 1-km spatial resolution climate surfaces for global land areas. Int J Clim.

Frost, P., 1996. The ecology of miombo woodlands, in: The Miombo in Transition: Woodlands and Welfare in Africa. Centre for International Forestry Research, Bogor, Indonesia, pp. 11–57.

Godlee, J.L., Ryan, C.M., Bauman, D., Bowers, S.J., Carreiras, J.M.B., Chisingui, A.V., Cromsigt, J.P.G.M., Druce, D.J., Finckh, M., Gonçalves, F.M., Holdo, R.M., Makungwa, S., McNicol, I.M., Mitchard, E.T.A., Muchawona, A., Revermann, R., Ribeiro, N.S., Siampale, A., Syampungani, S., Tchamba, J.J., Tripathi, H.G., Wallenfang, J., te Beest, M., Williams, M., Dexter, K.G., 2021. Structural diversity and tree density drives variation in the biodiversity–ecosystem function relationship of woodlands and savannas. New Phytol. 232, 579–594. https://doi.org/10.1111/nph.17639

Graz, F.P., 2006. Spatial Diversity of Dry Savanna Woodlands: Assessing the Spatial Diversity of a Dry Savanna Woodland Stand in Northern Namibia Using Neighbourhood-based Measures. Biodivers. Conserv. 15, 1143–1157. https://doi.org/10.1007/s10531-004-3105-6

James, F.C., Wamer, N.O., 1982. Relationships between Temperate Forest Bird Communities and Vegetation Structure. Ecology 63, 159–171. https://doi.org/10.2307/1937041

Kassambara, A., Mundt, F., 2016. factoextra: Extract and Visualize the Results of Multivariate Data Analyses. https://doi.org/10.32614/CRAN.package.factoextra

Kindermann, L., Dobler, M., Niedeggen, D., Linstädter, A., 2022. A new protocol for estimation of woody aboveground biomass in disturbance-prone ecosystems. Ecol. Indic. 135, 108466. https://doi.org/10.1016/j.ecolind.2021.108466

Knapp, N., Fischer, R., Cazcarra-Bes, V., Huth, A., 2020. Structure metrics to generalize biomass estimation from lidar across forest types from different continents. Remote Sens. Environ. 237, 111597. https://doi.org/10.1016/j.rse.2019.111597

Koreň, M., Mokroš, M., Bucha, T., 2017. Accuracy of tree diameter estimation from terrestrial laser scanning by circle-fitting methods. Int. J. Appl. Earth Obs. Geoinformation 63, 122–128. https://doi.org/10.1016/j.jag.2017.07.015

Lê, S., Josse, J., Husson, F., 2008. FactoMineR : An R Package for Multivariate Analysis. J. Stat. Softw. 25. https://doi.org/10.18637/jss.v025.i01

Lefsky, M.A., Cohen, W.B., Parker, G.G., Harding, D.J., 2002. Lidar Remote Sensing for Ecosystem Studies. BioScience 52, 19. https://doi.org/10.1641/0006-3568(2002)052[0019:LRSFES]2.0.CO;2

Lüdecke, D., Ben-Shachar, M., Patil, I., Waggoner, P., Makowski, D., 2021. performance: An R Package for Assessment, Comparison and Testing of Statistical Models. J. Open Source Softw. 6, 3139. https://doi.org/10.21105/joss.03139

Marunda, C., Bouda, H.-N., 2010. Environmental Services from the Dry Forests and Woodlands of Sub-Saharan Africa, in: The Dry Forests and Woodlands of Africa: Managing for Products and Services. Earthscan, London, p. 231.

Mayaux, P., Bartholomé, E., Fritz, S., Belward, A., 2004. A new land-cover map of Africa for the year 2000. J. Biogeogr. 31, 861–877. https://doi.org/10.1111/j.1365-2699.2004.01073.x

Mayr, M.J., Malß, S., Ofner, E., Samimi, C., 2018. Disturbance feedbacks on the height of woody vegetation in a savannah: a multi-plot assessment using an unmanned aerial vehicle (UAV). Int. J. Remote Sens. 39, 4761–4785. https://doi.org/10.1080/01431161.2017.1362132

McGillycuddy, M., Warton, D.I., Popovic, G., Bolker, B.M., 2025. Parsimoniously Fitting Large Multivariate Random Effects in glmmTMB. J. Stat. Softw. 112. https://doi.org/10.18637/jss.v112.i01

McIntosh, A.C.S., Macdonald, S.E., Quideau, S.A., 2016. Understory Plant Community Composition Is Associated with Fine-Scale Above- and Below-Ground Resource Heterogeneity in Mature Lodgepole Pine (Pinus contorta) Forests. PLOS ONE 11, e0151436. https://doi.org/10.1371/journal.pone.0151436

Mendelsohn, J., Jarvis, A.M., Roberts, C., Robertson, T., 2002. Atlas of Namibia: A Portrait of the Land and Its People. David Philip, Cape Town.

Mittelbach, G.G., Steiner, C.F., Scheiner, S.M., Gross, K.L., Reynolds, H.L., Waide, R.B., Willig, M.R., Dodson, S.I., Gough, L., 2001. What Is the Observed Relationship between Species Richness and Productivity? Ecology 82, 2381–2396.

Newnham, G. J., Armston, J. D., Calders, K., Disney, M. I., Lovell, J. L., Schaaf, C. B., Strahler, A. H., & Danson, F. M. (2015). Terrestrial Laser Scanning for Plot-Scale Forest Measurement. *Current Forestry Reports*, *1*(4), 239-251. https://doi.org/10.1007/s40725-015-0025-5

Puletti, N., Galluzzi, M., Grotti, M., Ferrara, C., 2021. Characterizing subcanopy structure of Mediterranean forests by terrestrial laser scanning data. Remote Sens. Appl. Soc. Environ. 24, 100620. https://doi.org/10.1016/j.rsase.2021.100620

R Core Team, 2023. R: A Language and Environment for Statistical Computing_. R Foundation for Statistical Computing, Vienna, Austria. <https://www.R-project.org/>.

Réjou-Méchain, M., Tanguy, A., Piponiot, C., Chave, J., Hérault, B., 2017. biomass: an r package for estimating above-ground biomass and its uncertainty in tropical forests 8, 1163–1167. https://doi.org/10.1111/2041-210X.12753

Robert T. Fahey, Fahey, R.T., Alexander T. Fotis, Fotis, A.T., K.D. Woods, Woods, K.D., 2015. Quantifying canopy complexity and effects on productivity and resilience in late-successional hemlock–hardwood forests. Ecol. Appl. 25, 834–847. https://doi.org/10.1890/14-1012.1

Roussel, J.-R., Auty, D., Coops, N.C., Tompalski, P., Goodbody, T.R.H., Meador, A.S., Bourdon, J.-F., De Boissieu, F., Achim, A., 2020. lidR: An R package for analysis of Airborne Laser Scanning (ALS) data. Remote Sens. Environ. 251, 112061. https://doi.org/10.1016/j.rse.2020.112061

Ryan, C.M., Pritchard, R., McNicol, I., Owen, M., Fisher, J.A., Lehmann, C., 2016. Ecosystem services from southern African woodlands and their future under global change. Philos. Trans. R. Soc. B Biol. Sci. 371, 20150312. https://doi.org/10.1098/rstb.2015.0312

Sankaran, M., Hanan, N.P., Scholes, R.J., Ratnam, J., Augustine, D.J., Cade, B.S., Gignoux, J., Higgins, S.I., Le Roux, X., Ludwig, F., Ardo, J., Banyikwa, F., Bronn, A., Bucini, G., Caylor, K.K., Coughenour, M.B., Diouf, A., Ekaya, W., Feral, C.J., February, E.C., Frost, P.G.H., Hiernaux, P., Hrabar, H., Metzger, K.L., Prins, H.H.T., Ringrose, S., Sea, W., Tews, J., Worden, J., Zambatis, N., 2005. Determinants of woody cover in African savannas. Nature 438, 846–849. https://doi.org/10.1038/nature04070

SEOSAW partnership, 2021. A network to understand the changing socio-ecology of the southern African woodlands (SEOSAW): Challenges, benefits, and methods. PLANTS PEOPLE PLANET 3, 249–267. https://doi.org/10.1002/ppp3.10168

Shirima, D.D., Totland, Ø., Munishi, P.K.T., Moe, S.R., 2015. Relationships between tree species richness, evenness and aboveground carbon storage in montane forests and miombo woodlands of Tanzania. Basic Appl. Ecol. 16, 239–249. https://doi.org/10.1016/j.baae.2014.11.008

Stovall, A.E.L., Anderson-Teixeira, K.J., Shugart, H.H., 2018. Assessing terrestrial laser scanning for developing non-destructive biomass allometry. For. Ecol. Manag. 427, 217–229. https://doi.org/10.1016/j.foreco.2018.06.004

Tews, J., Brose, U., Grimm, V., Tielbörger, K., Wichmann, M.C., Schwager, M., Jeltsch, F., 2004. Animal species diversity driven by habitat heterogeneity/diversity: the importance of keystone structures. J. Biogeogr. 31, 79–92. https://doi.org/10.1046/j.0305-0270.2003.00994.x

Tilman, D., Sowning, J.A., 1994. Biodiversity_and_stability_in_grasslands. Nature 367, 363–365.

Timberlake, J., Chidumayo, E.N., Sawadogo, L., 2010. Distribution and Characteristics of African Dry Forests and Woodlands, in: The Dry Forests and Woodlands of Africa: Managing for Products and Services, The Earthscan Forest Library. Earthscan, London, p. 11.

Tymen, B., Vincent, G., Courtois, E.A., Heurtebize, J., Dauzat, J., Marechaux, I., Chave, J., 2017. Quantifying micro-environmental variation in tropical rainforest understory at landscape scale by combining airborne LiDAR scanning and a sensor network. Ann. For. Sci. 74, 32. https://doi.org/10.1007/s13595-017-0628-z

Van Ewijk, K.Y., Treitz, P.M., Scott, N.A., 2011. Characterizing Forest Succession in Central Ontario using Lidar-derived Indices. Photogramm. Eng. Remote Sens. 77, 261–269. https://doi.org/10.14358/PERS.77.3.261

Vierling, L.A., Xu, Y., Eitel, J.U.H., Oldow, J.S., 2013. Shrub characterization using terrestrial laser scanning and implications for airborne LiDAR assessment. Can. J. Remote Sens. 38, 709–722. https://doi.org/10.5589/m12-057

Wang, M., Calders, K., Verbeeck, H., Verheyen, K., Baeten, L., Blondeel, H., Muys, B., Ponette, Q., Armston, J., Van Coillie, F., 2024. Exploring the influence of tree species richness on vertical structure variability in young plantations using terrestrial laser scanning. For. Ecol. Manag. 554, 121662. https://doi.org/10.1016/j.foreco.2023.121662

Watt, P.J., Donoghue, D.N.M., 2005. Measuring forest structure with terrestrial laser scanning. Int. J. Remote Sens. 26, 1437–1446. https://doi.org/10.1080/01431160512331337961

Weltzin, J.F., Coughenour, M.B., 1990. Savanna tree influence on understory vegetation and soil nutrients in northwestern Kenya. J. Veg. Sci. 1, 325–334. https://doi.org/10.2307/3235707

Werner, E.E., Glennemeier, K.S., 1999. Influence of Forest Canopy Cover on the Breeding Pond Distributions of Several Amphibian Species. Copeia 1999, 1. https://doi.org/10.2307/1447379

Wilkes, P., Lau, A., Disney, M., Calders, K., Burt, A., Gonzalez de Tanago, J., Bartholomeus, H., Brede, B., Herold, M., 2017. Data acquisition considerations for Terrestrial Laser Scanning of forest plots. Remote Sens. Environ. 196, 140–153. https://doi.org/10.1016/j.rse.2017.04.030

Wood, S.N., 2017. Generalized Additive Models: An Introduction with R SECOND EDITION, 2nd Edition. ed. Chapman and Hall/CRC, New York, NY.

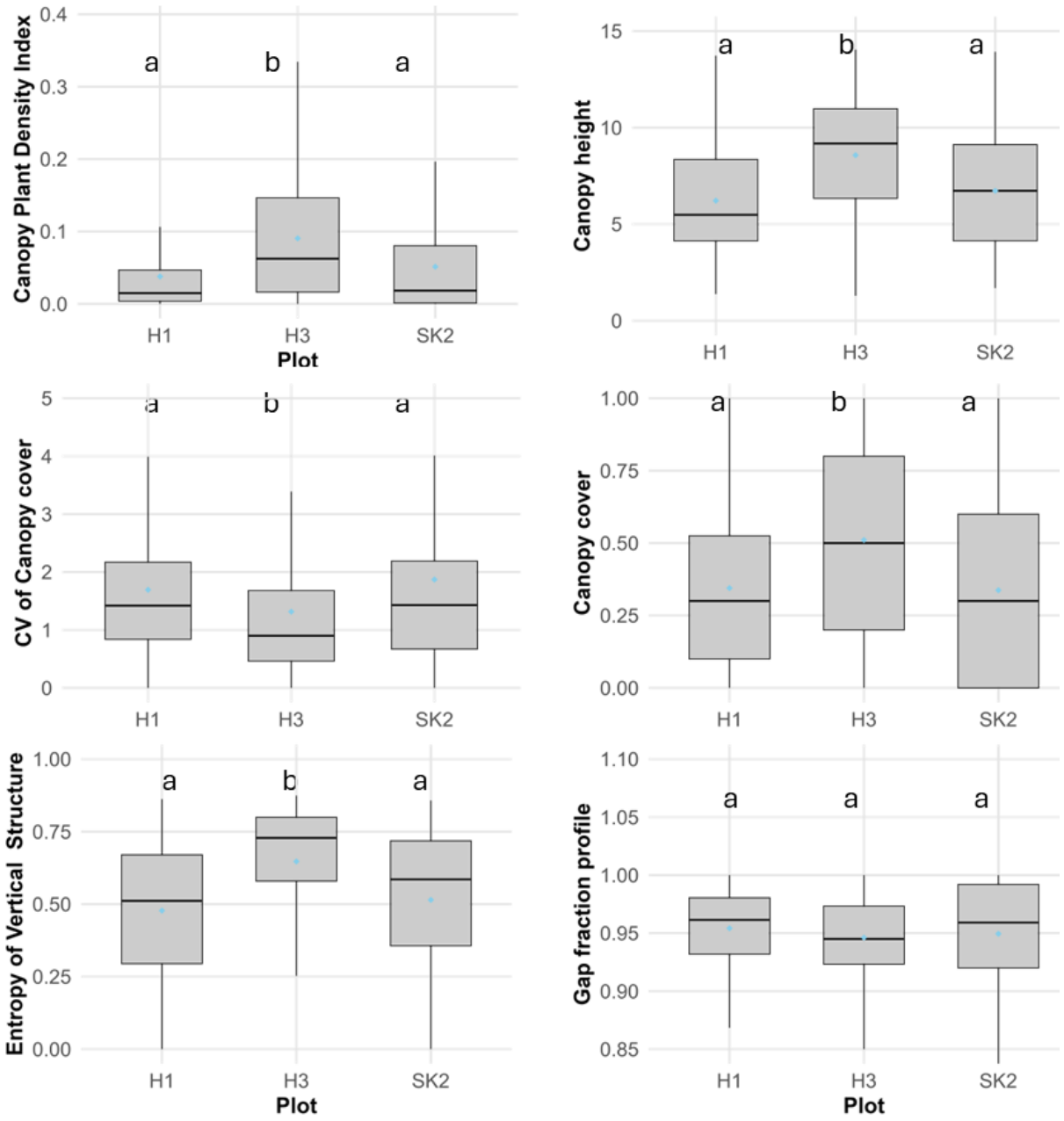
Zanne, A., Lopez-Gonzalez, G., Coomes, D.A., Ilic, J., Jansen, S., Lewis, S.L., Miller, R.B., Swenson, N.G., Wiemann, M.C., Chave, J., 2009. Data from: Towards a worldwide wood economics spectrum. Dryad. https://doi.org/10.5061/dryad.234

Zhang, W., Qi, J., Wan, P., Wang, H., Xie, D., Wang, X., Yan, G., 2016. An Easy-to-Use Airborne LiDAR Data Filtering Method Based on Cloth Simulation. Remote Sens. 8, 501. https://doi.org/10.3390/rs8060501

Zhang, Z., Cao, L., She, G., 2017. Estimating Forest Structural Parameters Using Canopy Metrics Derived from Airborne LiDAR Data in Subtropical Forests. Remote Sens. 9, 940. https://doi.org/10.3390/rs9090940

Appendix 3

Figure S.1. Boxplots showing the variation in canopy structural metrics among plots. Each box represents the interquartile range (IQR), with the horizontal line indicating the median and whiskers extending to 1.5 × IQR. Letters above boxplots indicate significant differences among plots based on Dunn's test comparison ($p < 0.05$).



Chapter 5: Evaluating GEDI Canopy Height Accuracy Across Forest Structural Gradients in the Miombo Ecoregion

Abstract

Accurate estimates of forest canopy height are essential for understanding ecosystem functioning, carbon dynamics, and biodiversity conservation. However, tropical dry woodlands remain under-represented in global canopy monitoring, leading to uncertainties in carbon accounting and conservation planning. The Global Ecosystem Dynamics Investigation (GEDI), launched by NASA in 2018, provides high-resolution LiDAR measurements of forest vertical structure, but its accuracy in African dry woodlands remains poorly understood.

We assessed GEDI canopy height accuracy using SEOSAW plots distributed across the Miombo ecoregion of southern Africa using extensive plot-based field measurements. GEDI underestimated canopy height (mean bias = –2.79 m; MAE = 3.88 m; RMSE = 4.99 m), with increasing underestimation for taller canopies, from about of -1.85 m at 10 m canopy height, to -4.33 m at 20 m. Errors were influenced by terrain slope and water availability, with strong underestimation on steep slopes (>10°) and drier sites, whereas overestimation occurred in wetter areas (mean annual precipitation > 1000 mm).

We developed Random Forest models combining canopy structural metrics derived from GEDI with climatic, topographic, and spectral predictors to refine canopy height estimates. The model including GEDI metrics alone explained 39% (MAE = 2.70 m) of field height variance, whereas the integrated model explained 64% (MAE = 1.95 m). Compared to the global canopy height map (GFCH) of Potapov et al. (2021), which largely underestimated canopy height in Miombo (bias = -7.67), and the Lang et al. 2023 (bias = -1.47 m) product, our regionally calibrated GEDI-based models achieved comparable accuracy to Lang et al. (2023) (-1.01 m for RF1 and -0.27 m for RF2).

This first regional-scale assessment of the performance of GEDI for predicting canopy height in dry African woodlands highlights the potential of fusing GEDI with ancillary datasets, improving canopy monitoring in structurally complex ecosystems and providing critical insights for biodiversity conservation and climate policy.

Key words: LiDAR, savannas, southern Africa, Random Forest, Validation

5.1 Introduction

Forest canopy height is a fundamental attribute of vegetation structure, reflecting the vertical arrangement of plant material and serving as a key determinant of ecosystem functioning (Lang et al., 2023; Tao et al., 2016). It regulates light penetration, microclimate, and resource availability, thereby shaping biodiversity patterns (Jucker et al., 2018; Smith-Tripp et al., 2022). Height heterogeneity has been linked to species diversity through the height variation hypothesis, emphasising the role of canopy height in maintaining forest complexity (Gatti et al., 2017; Torresani et al., 2023). In addition, canopy height is widely used as a structural proxy for modelling above-ground biomass, particularly with airborne and satellite LiDAR observations (Knapp et al., 2020). It has also been associated with the capacity of forests to withstand environmental stressors such as drought, underscoring its importance as an indicator of ecosystem resilience (Li et al., 2023; Xu et al., 2018).

Climatic and disturbance gradients strongly influence patterns of canopy height. Maximum tree height generally increases with precipitation and competition for sunlight, reflecting the role of water availability in sustaining taller canopies (Scholes et al., 2002; C. Xu et al., 2016). Conversely, canopy height is an effective indicator of disturbance, in particular fire, where increased frequency and intensity are associated with reductions in tree height and size (Mayr et al., 2018; Ryan et al., 2011; Saito et al., 2014; Smit et al., 2010). Monitoring canopy height across these gradients provides crucial insights into forest dynamics, informing land-use planning, carbon accounting, and fire management strategies.

These precipitation-disturbance interactions are especially relevant in the Miombo ecoregion, the most extensive tropical dry woodland on the African continent (Campbell, 1996; Frost, 1996). The Miombo ecoregion forms a mosaic of vegetation types, ranging from dense, closed canopy stands to open woodlands interspersed with shrubs and grasslands. Its structure is shaped by gradients in mean annual precipitation and recurrent disturbances such as fire, shifting cultivation, herbivory, and selective harvesting (Campbell, 1996; Sankaran et al., 2005; Smit et al., 2010). Despite its relatively lower stature compared to humid tropical forests, the Miombo stores large amounts of carbon and supports millions of people (Demol et al., 2024; Ryan et al., 2016). Yet, its structural heterogeneity, like other savannas and open woodlands, may pose challenges for accurate canopy monitoring, particularly with remote sensing tools (Gwenzi & Lefsky, 2016).

Several methods exist for measuring canopy height, ranging from field instruments to airborne and satellite remote sensing. However, sensitivity to vegetation structure and scale means that different methods can yield divergent estimates even for the same stands (Sexton et al., 2009). Among recent

advances, the Global Ecosystem Dynamics Investigation (GEDI) mission, launched in 2018 aboard the International Space Station, represents a major step in spaceborne LiDAR remote sensing (Dubayah et al., 2020). GEDI was primarily designed to capture vertical canopy profiles in tall, dense tropical and temperate forests (Dubayah et al., 2020, 2022). It fits Gaussian models to identify the centre of energy in the waveform (Hancock et al., 2019; Hofton & Blair, 2019), causing difficulties in distinguishing ground and canopy signals. GEDI uses a short pulse length (15.6 ns), which can facilitate the separation of canopy and ground returns in relatively open vegetation such as the Miombo ecoregion (Cardenas-Martinez et al., 2025; Dubayah et al., 2022; Li et al., 2023). However, this does not eliminate limitations in low or sparse canopies, where weak or discontinuous returns from both low vegetation and isolated tall trees may reduce the ability of the waveform to accurately capture vertical structure and maximum canopy height.. Nevertheless, its accuracy varies across vegetation types and ecological gradients, with studies showing sensitivity to slope, elevation, water availability, and canopy cover (Adam et al., 2020; Adrah et al., 2022; Liu et al., 2021; Liu et al., 2025).

In southern Africa, evaluations of GEDI remain scarce and site-specific, often focusing on plots in Mozambique (Liang et al., 2021, 2023), Namibia (Atmani et al., 2022), Tanzania or South Africa (X. Li et al., 2023, 2024). These site-level studies suggest that while GEDI captures canopy height reasonably well in medium-stature systems, it struggles in open or seasonal vegetation and tends to underestimate biomass in savanna ecosystems (Atmani et al., 2022; X. Li et al., 2024). To date, no study has assessed GEDI canopy height accuracy across the a wide range of structural and environmental gradients using plot-based data distributed across the Miombo ecoregion. By integrating field data from Namibia, Angola, Zambia, the Democratic Republic of Congo, Mozambique, and Zimbabwe, this study provides the first regional-scale evaluation of GEDI accuracy in African dry woodlands.

Therefore, this study aims to evaluate the performance of GEDI-derived canopy height estimates across different regions of the Miombo ecoregion and to identify the key factors that influence estimation accuracy. Specifically, we assess the correlation between GEDI height and field-measured canopy height and examine whether GEDI errors are systematically associated with terrain slope, aridity, vegetation indices, and structural complexity. By identifying the drivers of GEDI error, we seek to improve understanding of where and why GEDI tends to over- or underestimate canopy height.

In addition, the study explores whether field-measured canopy height can be more accurately predicted by integrating GEDI-derived metrics with other remote sensing data. We apply machine learning models to test the predictive power of these combined datasets, intending to develop a robust, scalable approach to estimate canopy height where field data are unavailable. Finally, we

compare the accuracy of the global canopy height maps of Potapov et al. (2021) and Lang et al. (2023) with field-measured height and our predictive machine learning models.

By addressing these questions, this study contributes to improving the accuracy of forest structural assessments in the Miombo ecoregion and informs future applications of GEDI and other spaceborne sensors for large-scale ecological monitoring and carbon accounting.

5.2 Materials and methods

5.2.1 Study area

Our study covers the Miombo ecoregion, which spans diverse climatic and ecological gradients in eastern and southern Africa (Figure 26). Mean Annual Precipitation (MAP) ranges from as low as 345 mm yr^{-1} in the arid region of Namibia to 1980 mm yr-1 in the more humid zones of Mozambique (Figure 1). Mean Annual Temperature (MAT) varies between 17°C and 26°C (Zomer et al., 2022), and elevation ranged from 13 m to 1653 m above sea level.

The region includes a wide variety of vegetation types, including wet and dry Miombo woodlands, Mopane woodland, Montane forests, dry deciduous forests, and East African coastal mosaic biomes (Dinerstein et al., 2017).

These ecosystems extending, extend over approximately 2.7 million km^2, where tree cover and structure are controlled by the combined effects of rainfall, fire, and herbivory (Archibald et al., 2019). Fire frequency and grazing limit the recruitment and maintain a heterogeneous mosaic of woody and grassy patches (Frost, 1996). Tree cover generally increases from arid to humid regions, leading to a decline in lower vegetation layers. Within the lower vegetation strata, shrub species dominate in the drier areas, whereas small trees become more prevalent in wetter zones (Diesse et al., 2025).

5.2.2 Data

Plot selection

This study used 963 plots from the SEOSAW (Socio-Ecological Observatory for Studying African Woodlands) database (SEOSAW partnership, 2021), located across six countries in southern Africa, including Angola, Democratic Republic of Congo (DRC), Mozambique, Namibia, Zambia, and Zimbabwe (Figure 5.1). We selected forest plots surveyed after 2015 and up to 2023 to minimise the temporal gap with the GEDI acquisitions (2019 – 2024). To ensure data quality and consistency, only plots with an area greater than 0.1 hectares and a minimum stem density of 50 stems per hectare were included in the analysis. The minimum plot size threshold was chosen to reduce sampling error in canopy height estimates, as smaller plots are more prone to edge effects where tree crowns extend into or out of the plot area while stems fall outside the boundary. The stem density threshold excluded sparsely vegetated sites that do not meet typical woodland definitions.

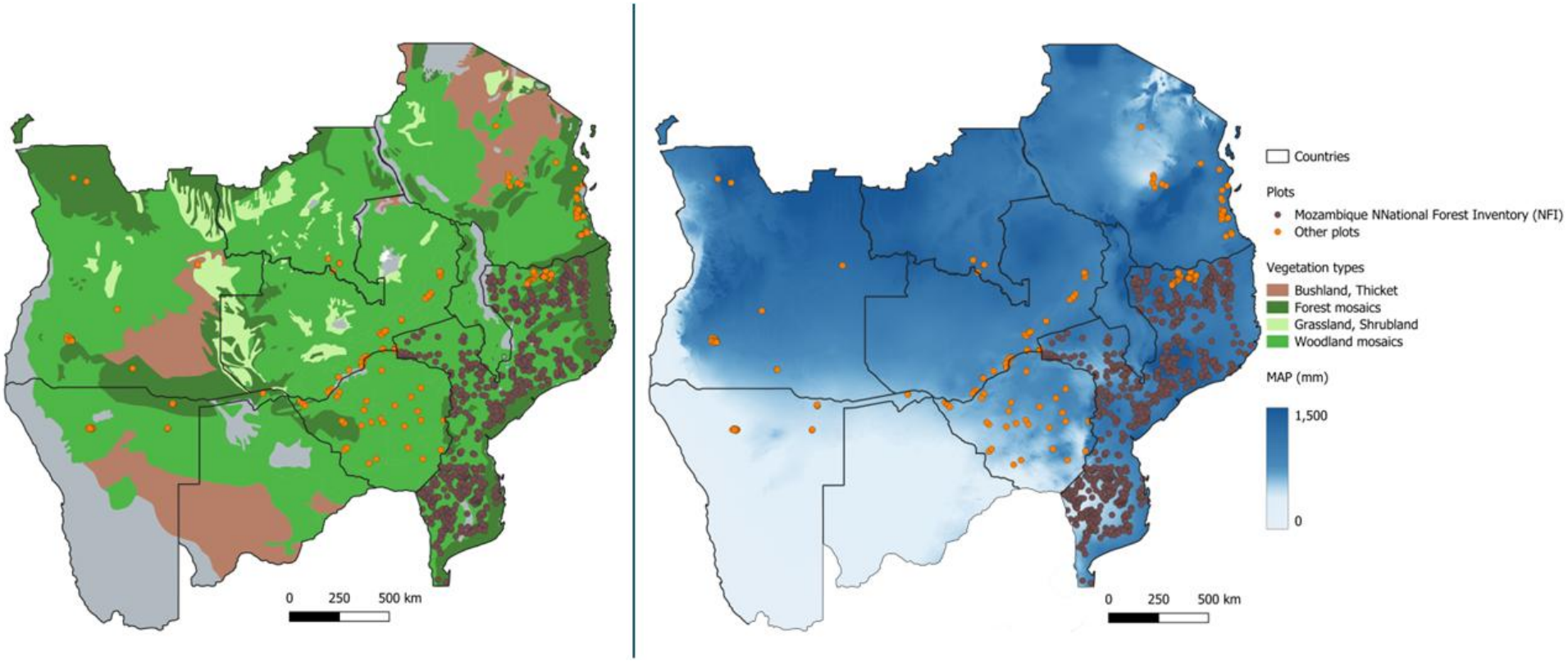


Figure 5.1 Left: Major savanna vegetation types within southern Africa. Right: Plot locations within southern Africa across the gradient of mean annual precipitation (MAP, mm)

Field data

Only living stems with a diameter at breast height (DBH) greater than 5 cm were included in the analysis. For each tree, we extracted the following information: tree height, tree species name, and DBH. Tree height was measured using a range of instruments, including rangefinders, hypsometers, clinometers, and measuring poles. As noted by Schwartz et al. (2024), the accuracy of field height measurements depends on both the surveyor's skill, the aim of the survey, and the measurement methods used. Our dataset was compiled from multiple teams and programmes, including the National Forest Inventory (NFI) in Mozambique (Dataset: MNI) (Table 5.1).

We generated various metrics of plot-level canopy height against which to validate GEDI canopy height estimates. Previous studies have employed many metrics to describe field-measured plot-level canopy height. We tested several of these metrics, including maximum tree height, mean tree height, the mean height of the two largest DBH trees (Fayad et al., 2021; Schwartz et al., 2024), and upper percentiles from the 90th through the 98th of the tree height. Following the accuracy comparisons with GEDI canopy height (Table S1 in the appendix), we defined the field canopy height as the 98th percentile of the tree height measurements from field inventories.

Table 5.1 Details of sampling sites used in this study, including sample sizes, dataset codes, principal investigators, associated projects, and whether the data originated from national forest inventories.

Country	Number of plots	Dataset code	Principal Investigator	National Forest Inventories
Angola	22	ABG	John L. Godlee; Francisco Maiato Gonçalves; Antonio Valter Chisingui; José João Tchamba; Kyle G. Dexter	No
		AUR	Mathew Rees; M. Pedro; M. Futuro; Hermenegildo	
		VAS	Manfred Finckh	No
DRC	2	DMD	Hermane Diesse; Jonathan Ilunga Muledi; Vera De Cauwer; John L. Godlee	No
Mozambique	22	MNR	Natasha Ribeiro	No
	356	MNI	Aristides Muhate; Sérgio João	Yes
Namibia	13	NOC	Vera De Cauwer; John L. Godlee; Kyle G. Dexter	No

		NKA	Vera De Cauwer; Leena Naftal; Hermane Diesse; John L. Godlee; Gabriel Uusiku; Kyle G. Dexter	No
		NHA	Vera De Cauwer; Leena Naftal; Hermane Diesse; John L. Godlee; Gabriel Uusiku; Kyle G. Dexter	No
		NZD	Vera De Cauwer; Hermane Diesse; Leena Naftal; John L. Godlee; Gabriel Uusiku; Kyle G. Dexter	No
Tanzania	2	TKM	Wilson Mugasha	No
	3	TKX	Helena Wood	No
Zambia	21	ZLT	Hemant Tripathi	No
Zimbabwe	23	ZNF	Anderson Muchawona	No

GEDI data and download

GEDI was launched to acquire data sets on canopy height, canopy cover, vertical vegetation profile, canopy leaf area index and topography over a large area of +/- 51.6 degrees latitude (Dubayah et al., 2020). GEDI acquires data using three lasers that produce eight ground tracks spaced 600 m apart (Padalia et al., 2023). Two of the lasers operate at full power, while one functions as a coverage laser. Within the eight tracks, each footprint is approximately 25 m in diameter and spaced at 60 m intervals (Boucher et al., 2020; Chen et al., 2021).

The study used GEDI Level 1B, Level 2A, and Level 2B products. GEDI footprints were downloaded across the study region for the period 2019 to 2024 from NASA's Earth Science Data Systems (https://search.earthdata.nasa.gov/search?q=gedi%20v002).

In Python version 3.11 (Rossum & Drake, 2009), a GEDI finder script was adapted to create a list of download links for GEDI products intersecting the study plots within a buffer of 500 m around each plot. All the GEDI products were downloaded in R software version 4.3.3 (R Core Team, 2023) using the list of links created. The R script for downloading the GEDI data was adapted from the DAACDataDownload.R script developed by LP DAAC (git.earthdata.nasa.gov/projects/LPDUR/repos/daac_data_download_r/browse). GEDI L2A, L1B and L2B files were merged and georeferenced using the gedixr package in Python (Wolsza, 2024). Only full-power laser beams were extracted using default parameters (Padalia et al., 2023). From GEDI L2A, we extracted the 98th percentile relative height (RH98). From L2B we extracted Total Canopy Cover (TCC), Foliage Height Diversity (FHD), and Total Plant Area Index (PAI). GEDI RH98 was considered the

primary canopy height metric, consistent with previous studies, as it is less affected by noise caused by isolated leaves, branches, or other small particles producing weak signals compared to RH100 (Yang et al., 2025). However, it may underestimate true maximum canopy height, particularly in structurally heterogeneous or open-canopy systems where the highest vegetation elements contribute weakly to the waveform signal.

To ensure data quality, GEDI footprints were filtered (Figure 5.2), following the criteria from Dubayah et al. (2021). Specifically, we kept records with a quality flag of 1, sensitivity between 0.9 and 1 (a sensitivity above 0.9 indicates that the laser beam can detect the ground through the canopy 90% of the time), a degraded flag of 0, and more than one detected mode (i.e., distinct waveform peaks corresponding to canopy and ground surfaces).

To address GEDI geolocation errors and to select plots with GEDI footprints within them, we created several buffer sizes ranging from 50 m to 250 m radius around the centre of each plot and identified GEDI footprints that fell within these buffers. Buffer size plays a critical role in balancing spatial accuracy and sample size. Crockett et al. (2023) recommended using different buffer sizes to ensure sufficient GEDI coverage: a 50 m buffer if at least one footprint is present, a 100 m buffer if at least three footprints are present, and a 200 m buffer if at least three footprints are required for larger plots. In this study, we systematically evaluated different combinations of buffer sizes and minimum numbers of intersecting footprints by comparing field-measured canopy height with GEDI-derived canopy height. The final selection (100 m buffer with at least two footprints) was chosen as it provided the best compromise between spatial accuracy and footprint availability, while maintaining sufficient statistical robustness across plots. This approach allowed us to maximise the number of usable plots while minimising geolocation mismatch between GEDI observations and field measurements. Applying these criteria, we retained 464 plots for analysis (Table 5.1).

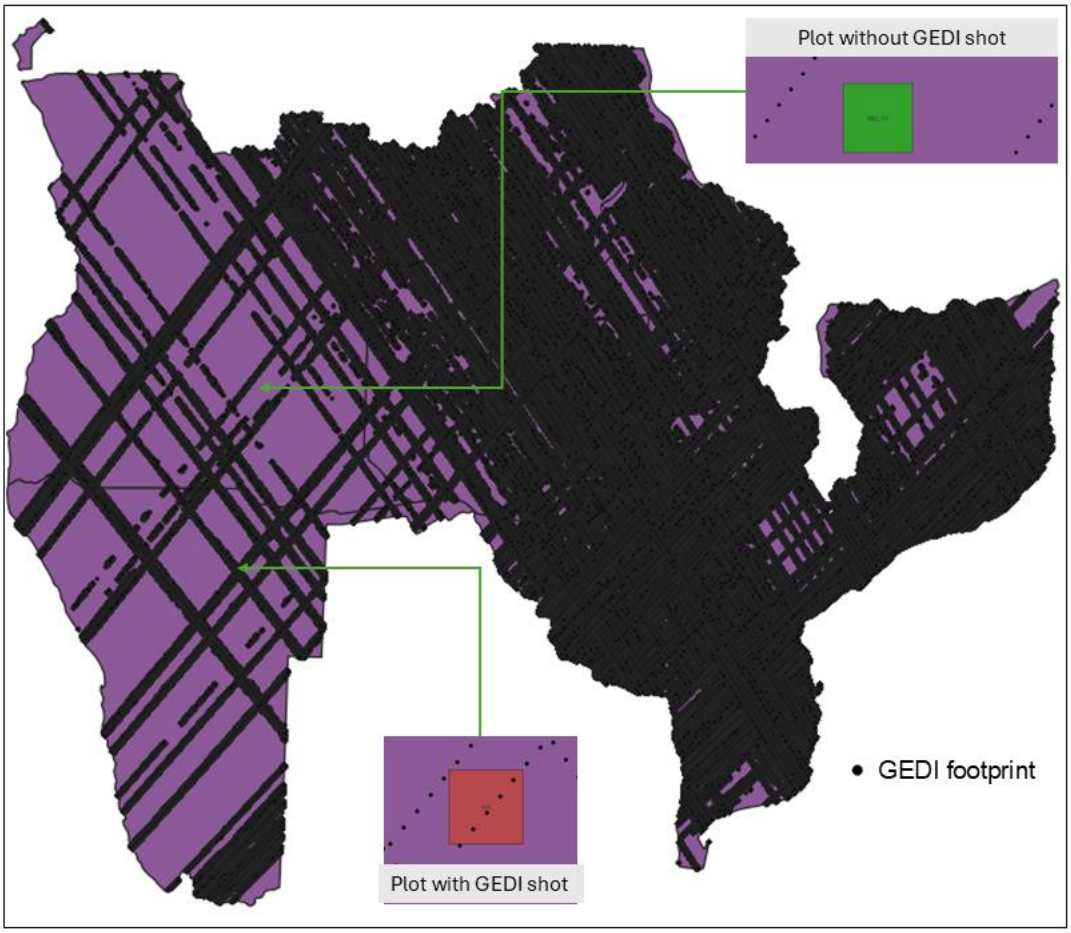


Figure 5.2 Visual example of filtered GEDI footprints for the study countries from 2019 to 2024. Zoomed insets show examples of plots with and without intersecting GEDI footprints.

Ancillary data

In addition to GEDI and field measurements, several ancillary satellite datasets were compiled to provide spectral, radar, climatic, topographic, and disturbance predictors for the models predicting field-measured canopy height. All datasets were accessed and processed within Google Earth Engine (GEE). To ensure comparability across data sources, all variables were harmonised within a fixed 100 m radius buffer centred on each plot. For each plot, all pixels intersecting the buffer were aggregated to derive summary statistics, including the mean, standard deviation, and percentiles (10th, 25th, 50th, 75th, and 90th) (Adrah et al., 2022). These summary statistics were applied to satellite-derived variables to capture both central tendency and spatial variability, whereas coarse-resolution datasets (e.g. climate variables) were extracted without additional spatial aggregation. This aggregation reduced mismatches in pixel size and footprint geometry and mitigates sub-pixel heterogeneity. All ancillary remote sensing products were obtained as time series for the period that matched the GEDI

acquisition period (2019 – 2023), and aggregated using mean values to represent average conditions, except for fire frequency, which was computed over a 10-year period preceding field data collection.

- **Sentinel-2 optical indices**

Sentinel-2A data with 10 m spatial resolution were acquired in Google Earth Engine (GEE). Level-2A surface reflectance products were used, which include atmospheric correction. Images were selected based on cloud cover <5% and aggregated over the study period (2019–2023) using mean to reduce noise and represent average conditions. Surface reflectance bands (B2, B3, B4, B8, B11, and B12) were used to derive vegetation and moisture indices, including the Normalised Difference Moisture Index (NDMI), Normalised Difference Water Index (NDWI), Enhanced Vegetation Index (EVI), Normalised Difference Vegetation Index (NDVI), and Soil-Adjusted Vegetation Index (SAVI) (Table 5.2). These indices capture canopy greenness, vigour, and water content, which are directly related to canopy density and height development (Tsao et al., 2023).

- **Sentinel-1 C-band radar**

Sentinel-1A C-band radar data with 10 m spatial resolution were acquired from GEE using the Ground Range Detected (GRD) product (COPERNICUS/S1_GRD). We extracted vertical transmit/vertical receive (VV) and vertical transmit/horizontal receive (VH) backscatter coefficients under the Interferometric Wide (IW) swath mode. The data provided in GEE are preprocessed (radiometric calibration and terrain correction). From these bands, four additional radar metrics were derived: VH+VV, VV/VH ratio, Normalised Difference Radar Index (NDRI), and Radar Vegetation Index (RVI) (see Table 11). These indices provide sensitivity to canopy volume and structural roughness. Radar penetrates cloud cover and can capture information on woody components. Backscatter values were temporally aggregated to reduce speckle noise and improve signal stability.

- **ALOS-2 L band SAR data**

The PALSAR sensor (Phased Array type L-band Synthetic Aperture Radar), launched in 2014 by the Japan Aerospace Exploration Agency (JAXA), provides data in single, dual, and quad polarimetric modes with a 14-day revisit interval. ALOS-2 PALSAR data at 25 m spatial resolution were accessed via GEE (JAXA/ALOS/PALSAR/YEARLY/SAR_EPOCH). In addition to the HH and HV bands, we derived the following indices: HH+HV, HV/HH ratio, and the Normalised Difference Index (NDI). L-band SAR penetrates deeper into the canopy than C-band and is therefore sensitive to larger woody components such as trunks and branches. These properties make L-band particularly suited for characterising woody biomass and canopy structure in heterogeneous woodlands.

- **Climate**

Bioclimatic variables were retrieved from multiple sources. From WorldClim, we extracted Mean Annual Precipitation (MAP), Mean Annual Temperature (MAT), and Precipitation Seasonality calculated as the coefficient of variation (CV) of the monthly precipitation totals. Monthly Potential Evapotranspiration (PET) and Global Aridity Index were sourced from the CGIAR-Consortium for Spatial Information (CGIAR-CSI) (Zomer et al., 2022). Climatic water deficit (CWD) and Environmental stress (E) were downloaded at 2.5 arc-minute (~ 4.2 -4.6 km across the plots, depending on latitude) spatial resolution from the Pantropical Allometry Database (Chave et al., 2014 ; http://chave.ups-tlse.fr/pantropical_allometry.htm). These metrics were included to represent long-term water and energy availability, which strongly constrain maximum canopy height and growth potential in Miombo woodlands. Due to their coarse spatial resolution, these variables were directly extracted at plot locations without computing additional spatial summary statistics.

- **Topography**

Elevation and slope were derived from the Multi-Error-Removed Improved-Terrain Digital Elevation Model (MERIT DEM v1.0.3) in GEE. MERIT DEM has a spatial resolution of 3-arc-sec (~90 m at the equator). These metrics were used because topography shapes hydrology, soil properties, and disturbance regimes, while also affecting GEDI ground detection accuracy.

- **Disturbance**

Fire disturbance was quantified using the MODIS Monthly Burned Area Product (MCD64A1) at 500 m spatial resolution, accessed through GEE. Each pixel in this product records the day of the year on which a fire event occurred. To account for temporal variation in plot sampling, we calculated fire frequency over a 10-year period preceding the field data collection for each plot. For example, if a plot was surveyed in 2021, fire frequencies were counted from 2010 to 2020. Second, we derived the Normalized Burn Ratio (NBR) from Sentinel-2 surface reflectance data (10 m resolution) as a spectral indicator of fire disturbance in the period 2019 - 2024. NBR is sensitive to burned versus unburned vegetation and captures fire severity and recent burn scars at finer spatial scales, complementing the MODIS-based fire frequency data.

Table 5.2 Variables used in the random forest to model canopy height.

Data set	Variables
SEOSAW plots	: 98th percentile of tree heights in the plot
GEDI L2A/L2B (from 2019-2023)	Canopy height (rh98) Canopy Cover (CC) Foliage Height Diversity (FHD) Plant Area Index (PAI)
Ancillary data	
Climate (1970 – 2000)	Mean Annual Precipitation (MAP) Mean Annual Temperature (MAT) Precipitation seasonality Monthly Potential Evapotranspiration (PET) Environmental stress (E) Aridity Climatic water deficit (CWD)
Topography MERIT DEM	Slope Elevation
Disturbance MODIS Burned Area Monthly Global 500m (10 years before the field inventory)	Fire frequency (ten years before plot data collection)
Sentinel-2 (from 2019-2023)	B2; B3; B4; B5; B6; B7; B8; B11, B12 NDMI = (B8 -B11) / (B8 + B11) NDWI = (B3 _ B8) / (B3 + B8) EVI = 2.5 * (B8 – B4) / (B8 + 6 * B4 – 7.5 * B2 + 1)) NDVI = (B8 – B4) / (B8 + B4) NBR = (B8 – B12) / (B8 + B12) SAVI = 1.5 * ((NIR – RED)) / (NIR = RED = 0.5))
Sentinel-1 (from 2019-2023)	Polarization VH Polarization VV VHplus VV = VH+VV VVVH ratio = VH /VV NDRI = (VV – VH) / (VV + VH) Radar Vegetation Index (RVI) = 4 * VH / (VV + VH)

ALOS PALSAR (2019 – 2023)	Polarization HH Polarization HV HHplusHV = HH+HV HVHH ratio = HV / HH NDI = (HH – HV) / (HH + HV)

5.2.3 Statistical analysis

All statistical analyses were conducted using R software (R Core Team, 2023).

The initial dataset consisted of 450 plots for which GEDI and field measurements met the quality and spatial matching criteria. However, the accuracy and precision of field-measured tree heights can vary among datasets due to differences in measurement instruments, field team experience, and canopy structural complexity. To assess data consistency, we evaluated the relationship between field-measured and GEDI-derived canopy heights across countries (Table S2). The R^2 for Mozambique was lower than for other countries, indicating greater variability in height measurements. To assess whether this variability affected model performance, we tested alternative models excluding the MNI dataset, the MNR dataset, and both simultaneously. Based on these tests, the MNI dataset was excluded from subsequent modelling to maintain consistency and ensure robust model calibration. As a result, two datasets were used in this study: (i) the full dataset (n = 450 plots) and (ii) a reduced dataset (n = 94 plots).

To assess spatial variation in GEDI canopy height, GEDI-derived RH98 values were grouped by environmental and topographic classes, including aridity, MAP, NDVI, elevation, and slope. Boxplots were used to visualise variations in GEDI canopy height across these gradients using the full dataset (n = 450 plots).

To validate GEDI estimates of canopy height, GEDI RH98 values were compared with field-measured canopy height using Root Mean Square Error (RMSE), Mean Absolute Error (MAE), and bias for the full dataset (n = 450 plots). We further assessed GEDI canopy height accuracy across forest structural and environmental gradients to identify conditions under which the agreement with field height was stronger or weaker. We tested significant differences in GEDI error across categorical variables (height class, tree density class, MAP class, Seasonality MAP class, slope class, elevation class, aridity index class, and NDVI class) using Kruskal–Wallis tests followed by Dunn's post hoc tests with Bonferroni correction using both the full dataset (n = 450 plots) and the reduced dataset (n = 94 plots), in order to examine the influence of excluding the MNI dataset.

We then developed three types of Random Forest (RF) models to predict canopy height using the reduced dataset (n = 94 plots):

- RF1 used only GEDI-derived metrics, including RH98, canopy cover, FHD, and PAI;
- RF2 incorporated GEDI-derived metrics with climate, disturbance, optical satellite, and radar data (Table 2);
- RF3 excluded GEDI-derived metrics.

RF is a non-parametric machine learning method widely applied in canopy height modelling (Dorado-Roda et al., 2021; Potapov et al., 2021; Yang et al., 2025). We examined multicollinearity using a Pearson correlation matrix and retained only predictors with $|r| < 0.6$ (Aponte et al., 2020). In total, 65 predictor variables were initially considered. Based on this filtered set, we generated multiple combinations of predictor variables that satisfied the collinearity criterion, resulting in 980 Random Forest models, each based on a different predictor set.

RF modelling was done using caret (Kuhn et al., 2025) and randomForest (Breiman et al., 2024) packages in R. For each model, the dataset was randomly split into training (80%) and testing (20%) subsets, and models were fitted using 500 trees (ntree = 500). Model performance was evaluated on the independent test dataset using R^2, RMSE, and MAE. Final models were selected based on predictive performance across these metrics.

Residuals (field-measured height minus predicted field height) were analysed to assess systematic prediction bias across height classes and environmental gradients using the reduced dataset (n = 94 plots). Variable importance was extracted from the final RF models to identify key predictors of canopy height.

Finally, we compared the performance of GEDI and RF-predicted heights against the global canopy height product (GFCH) developed by Potapov et al. (2021) and Lang et al. (2023) using 14 independent validation plots, which were not used in model training. There are limited plots in southern Africa with recent canopy height data with which the GEDI footprint overlaps.

The Potapov map provides global forest canopy height for 2019 at 30 m resolution. It was generated using an ensemble of regression tree models trained on GEDI LiDAR footprints as reference data, combined with multi-temporal Landsat imagery (spectral bands and vegetation indices) and ancillary topographic variables (elevation, slope).

The Lang map represents a newer generation of global maps at 10 m spatial resolution. It was produced by integrating GEDI-derived canopy height metrics with Sentinel-1 radar and Sentinel-2 optical imagery using a hybrid machine learning framework that combines RF regression with spatio-temporal ensemble modelling.

The agreement was assessed using R^2, RMSE, and MAE. Pairwise model comparisons were also conducted to evaluate how well each prediction approach captured field-observed structural variation in the Miombo ecoregion.

5.3 Results

5.3.1 Variation in GEDI Canopy Height Across Environmental Gradients

Analysis of the selected GEDI canopy heights distributed across southern Africa showed that GEDI-derived canopy height increases with water availability (Figure 28a–e). Canopies were taller in humid and high-MAP zones compared to arid and low-MAP areas, suggesting a structural transition in vegetation along moisture availability gradients. NDVI classes (Figure 28e) also exhibit a positive association, with greener areas showing greater canopy height. Regarding slope, canopy height increased with steeper slopes (Figure 3c). In contrast, for elevation (Figure 28d), no consistent trend was evident; however, plots located below 200 m and above 1000 m tended to exhibit lower canopy heights.

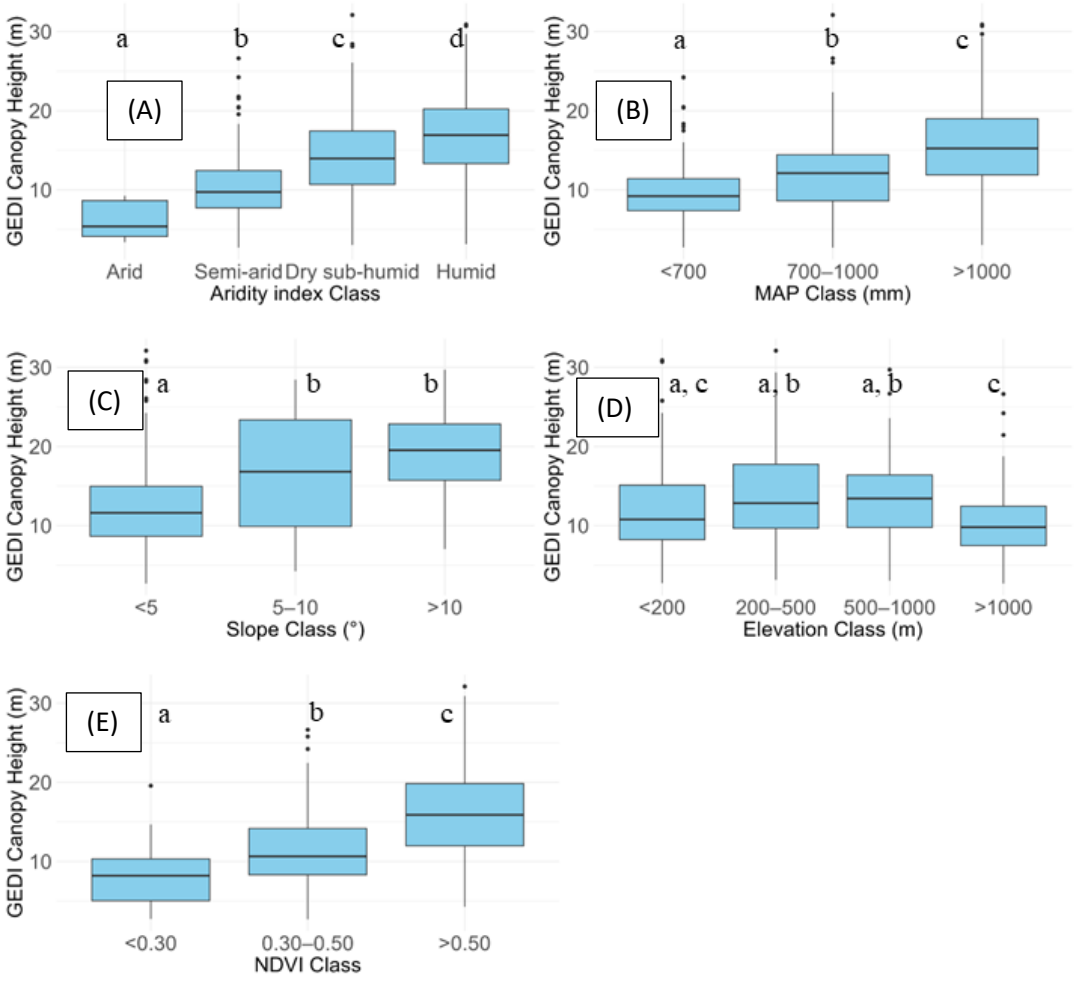


Figure 5.3. Variation in GEDI-derived canopy height across environmental gradients in Miombo ecoregion. A) aridity classes: Arid (0.05 – 0.2), Semi-arid (0.2 – 0.5), Dry sub-humid (0.5 – 0.65), and Humid (>0.65), (B) mean annual precipitation (MAP) classes, (C) slope classes, (D) elevation classes, (E) NDVI classes. Each boxplot represents the distribution of RH 98 canopy height estimates for GEDI footprints grouped by the specific

environmental class. Different letters above the boxes denote significant differences between classes (Kruskal–Wallis with Dunn's post hoc test, $p < 0.05$).

5.3.2 Accuracy of GEDI Canopy Height vs. Field-Measured Height

GEDI-derived canopy height showed moderate deviations from field-measured values. MAE was 4.38 m, indicating that GEDI estimates differed from field measurements by about 4 m on average. RMSE was 5.53 m, reflecting the influence of larger discrepancies. Bias was -1.37 m, reflecting a general tendency for GEDI to underestimate canopy height (Figure 5.4).

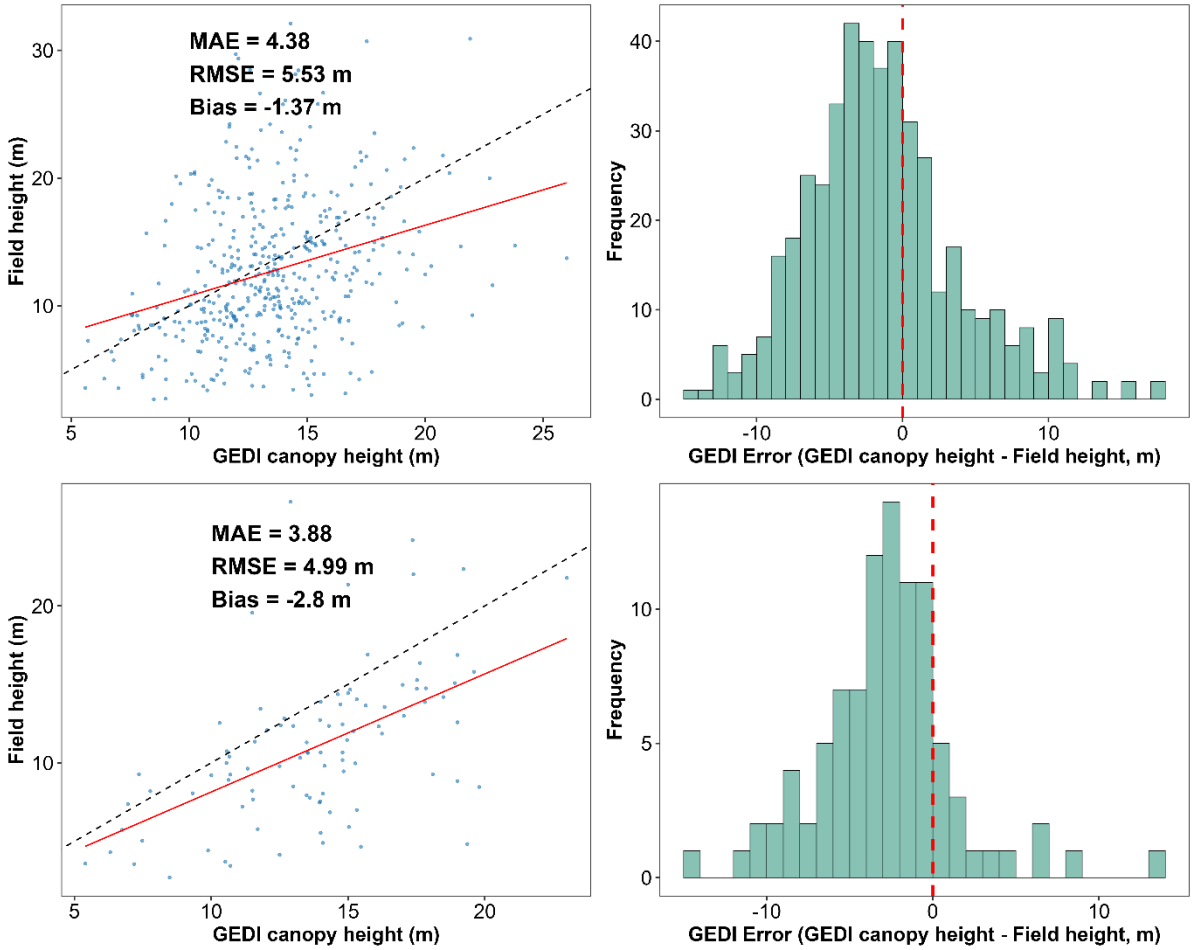


Figure 5.4. Comparison between GEDI-derived canopy height and field-measured canopy height. Across forest plots for all the data (top, n = 450) and after excluding the MNI National Forest Inventory dataset (bottom, n = 94). The left side presents the relationship between GEDI maximum canopy height (RH98) and field-based maximum canopy height, with a 1:1 reference line (dashed black), linear regression fit (red line), and key accuracy statistics: root mean square error (RMSE), mean absolute error (MAE), and bias. The right side presents a histogram of GEDI height error (GEDI – Field). Positive (negative) values indicate where GEDI over- (under-) estimates canopy height compared to estimates derived from field measurements of tree height. The dashed red line indicates zero error (perfect agreement).

This underestimation was also evident from the error distribution. The median error was -1.93 m, and half of the GEDI errors lay between -4.82 m and +1.35 m. The histogram of GEDI errors (Figure 5.5)

showed a clear skew toward negative values, indicating that underestimation occurred more frequently than overestimation.

When the MNI dataset was excluded, the model showed improved accuracy compared to the full model: the MAE decreased to 3.88 m and the RMSE to 4.99 m. However, the overall bias increased to -2.79 m. As illustrated in Figure 5, the bias was lower for smaller trees but progressively increased for taller trees, ranging from an average underestimation of –1.86 m at 10 m canopy height to –4.33 m at 20 m.

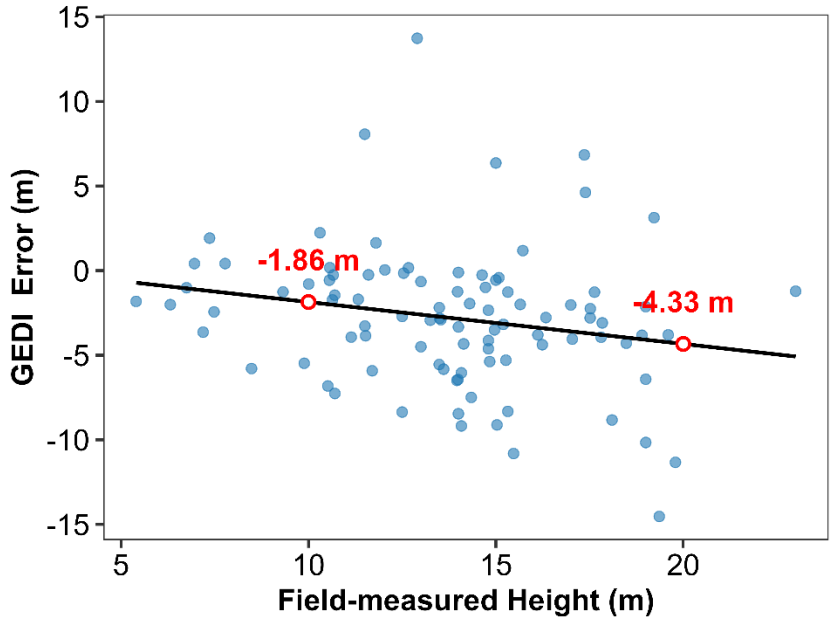


Figure 5.5 Distribution of GEDI error across field-measured height (n = 94). The annotation in red color represents the average underestimation at 10m and 20m canopy height.

5.3.3 Environmental and Structural Drivers of GEDI Canopy Height Error

We analysed the GEDI errors for the reduced dataset (excluding the MNI dataset). Terrain slope influenced GEDI accuracy ($\chi^2 = 5.33$, $p = 0.07$). Although not statistically significant at the 5% level, Dunn's post hoc test indicated that plots with steep slopes (>10°) tended to show more positive bias (overestimation) compared to flat plots (<5°) that exhibited minimal or slightly negative errors, suggesting potential terrain effects on laser returns (Figure 5.7).

Elevation had no significant influence on GEDI error ($p = 0.54$), and all pairwise comparisons were non-significant, indicating that elevation per se was not a major driver once low-quality and high-variability data were removed (Figure 5.8).

In contrast, precipitation and aridity showed more consistent patterns. GEDI errors varied significantly across MAP classes ($\chi^2 = 6.52$, $p = 0.038$), with a significant post hoc difference between intermediate (700–1000 mm) and high MAP areas (>1000 mm). Similarly, aridity index classes showed a significant overall effect ($\chi^2 = 10.35$, $p = 0.016$). However, post hoc comparisons revealed no statistically significant pairwise contrasts after Bonferroni correction, though some trends approached significance (e.g. arid and semi-arid tended to underestimate canopy height). This suggests that aridity may influence GEDI error, though the effect may be more gradual or interact with other factors.

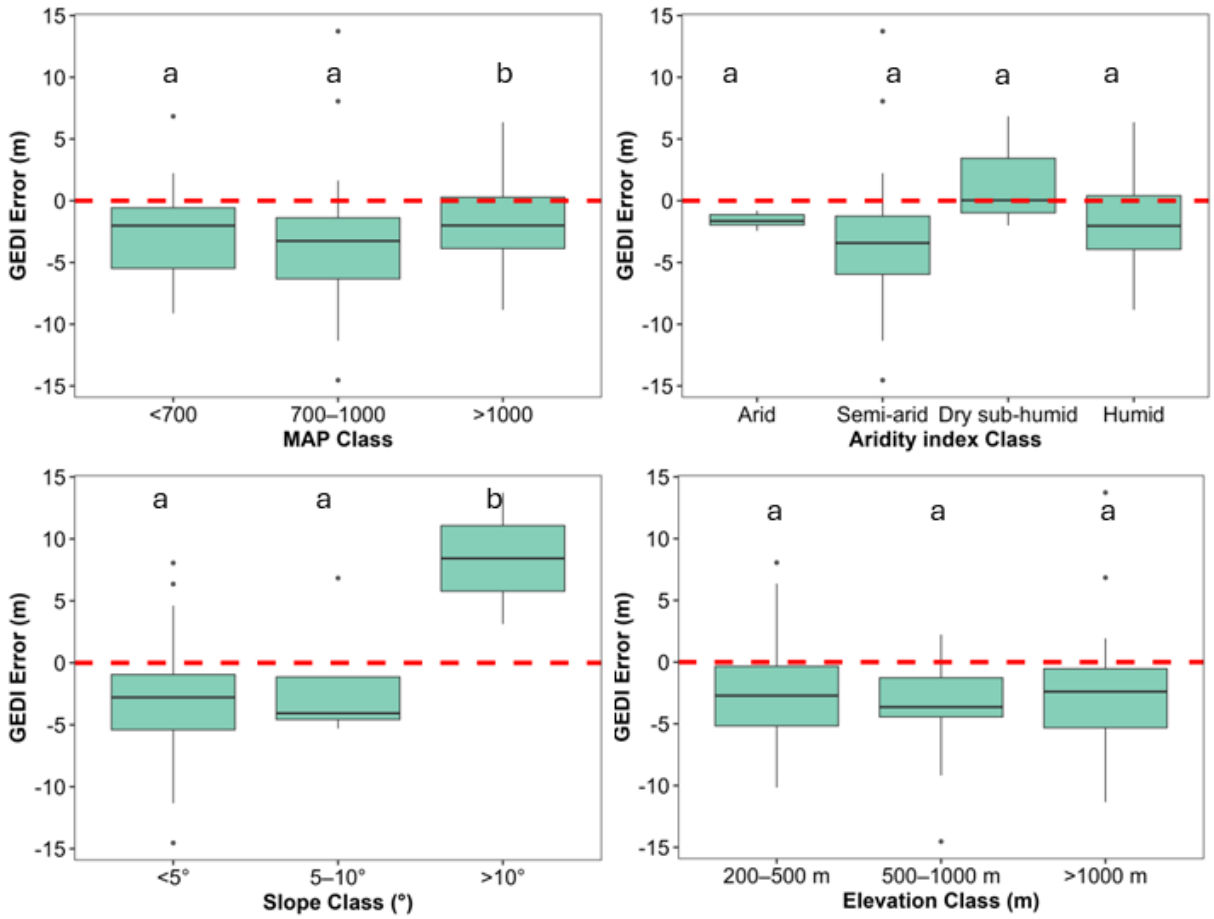


Figure 5.6. Variation in GEDI canopy height error across vegetation structure and environmental gradients. (n = 94). Boxplots show the distribution of GEDI canopy height error (GEDI RH98 – field maximum height) across various environmental classes. The horizontal line within each box represents the median error, boxes span the interquartile range (IQR), and whiskers extend to 1.5×IQR. Red dashed lines indicate zero error (perfect agreement between GEDI and field canopy height). Different letters above the boxes denote significant differences between classes (Kruskal–Wallis with Dunn's post hoc test, $p < 0.05$).

5.3.4 Modelling Field-Measured Tree Height using Random Forest

Three models were developed to test the contribution of GEDI-derived metrics relative to ancillary predictors: (i) RF1, which included only GEDI-derived structural metrics; (ii) RF2, which combined GEDI

metrics with climatic, topographic, and spectral predictors; and (iii) RF3, which excluded GEDI metrics entirely.

The final RF 1 model included GEDI height, FHD and PAI. The final RF 2 model included GEDI height, FHD, EVI, RVI, VV, HVHHratio, standard deviation (SD) of NNDI, SD of HHplusHV, SD of HV, elevation, slope, aridity, MAP, and fire frequency. The final RF 3 model included EVI, RVI, Fire, slope, Aridity, elevation, MAP, VV, SD of HHplusHV, HVHHratio, SD of NDI, SD of HV.

Performance results in Figure 32 indicated clear differences among models. RF1 captured a modest proportion of the variance in field-measured canopy height (R^2 = 0.39; RMSE = 3.54 m; MAE = 2.70 m). RF2 substantially improved predictive power (R^2 = 0.64; RMSE = 2.69 m; MAE = 1.95 m), underscoring the added value of integrating environmental and spectral covariates with GEDI-derived structure (Figure 5.7). RF3, which excluded GEDI metrics, still performed better than RF1 and only slightly below RF2 (R^2 = 0.55; RMSE = 2.89 m; MAE = 2.11 m). This comparison highlights that while GEDI metrics provide useful information, the integration of spectral, radar, climatic, and topographic predictors greatly enhances canopy height modelling in Miombo woodlands.

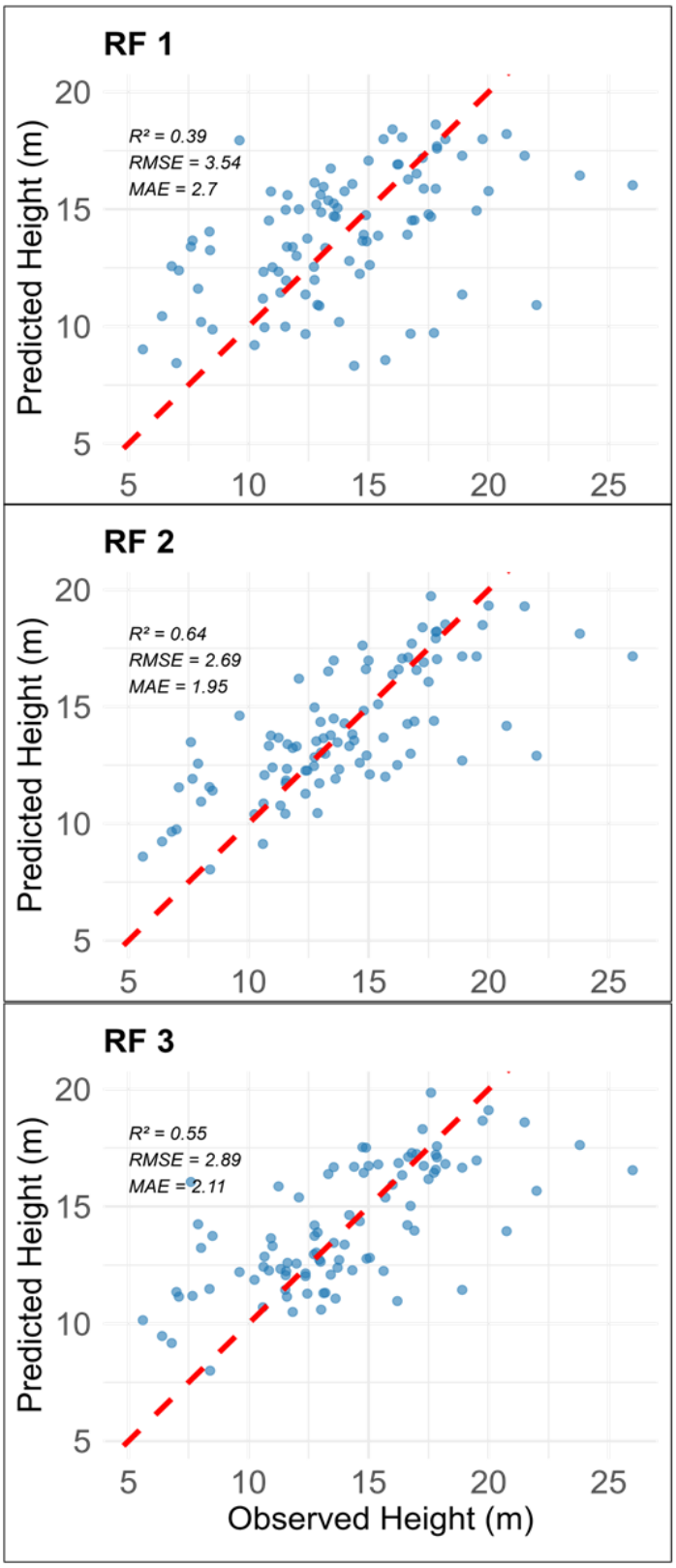


Figure 5.7. Observed versus predicted field-measured canopy height using Random Forest models.

RF 1 is the model used with the GEDI metrics only. RF 2 is the model used GEDI metrics with environmental and spectral variables. The RF 3 is the model excluding GEDI metrics. The dashed red line represents the 1:1 line.

We conducted a residual analysis of each model to further explore the performance of the RF models. The residual analysis reveals systematic biases in canopy height predictions (Figure 5.8). The models tend to underestimate taller canopies, as indicated by increasingly negative residuals in higher field height classes, suggesting limited capacity to capture structural complexity in taller canopies. Conversely, overestimation is observed for lower canopies, highlighting a nonlinear pattern in prediction accuracy across height gradients.

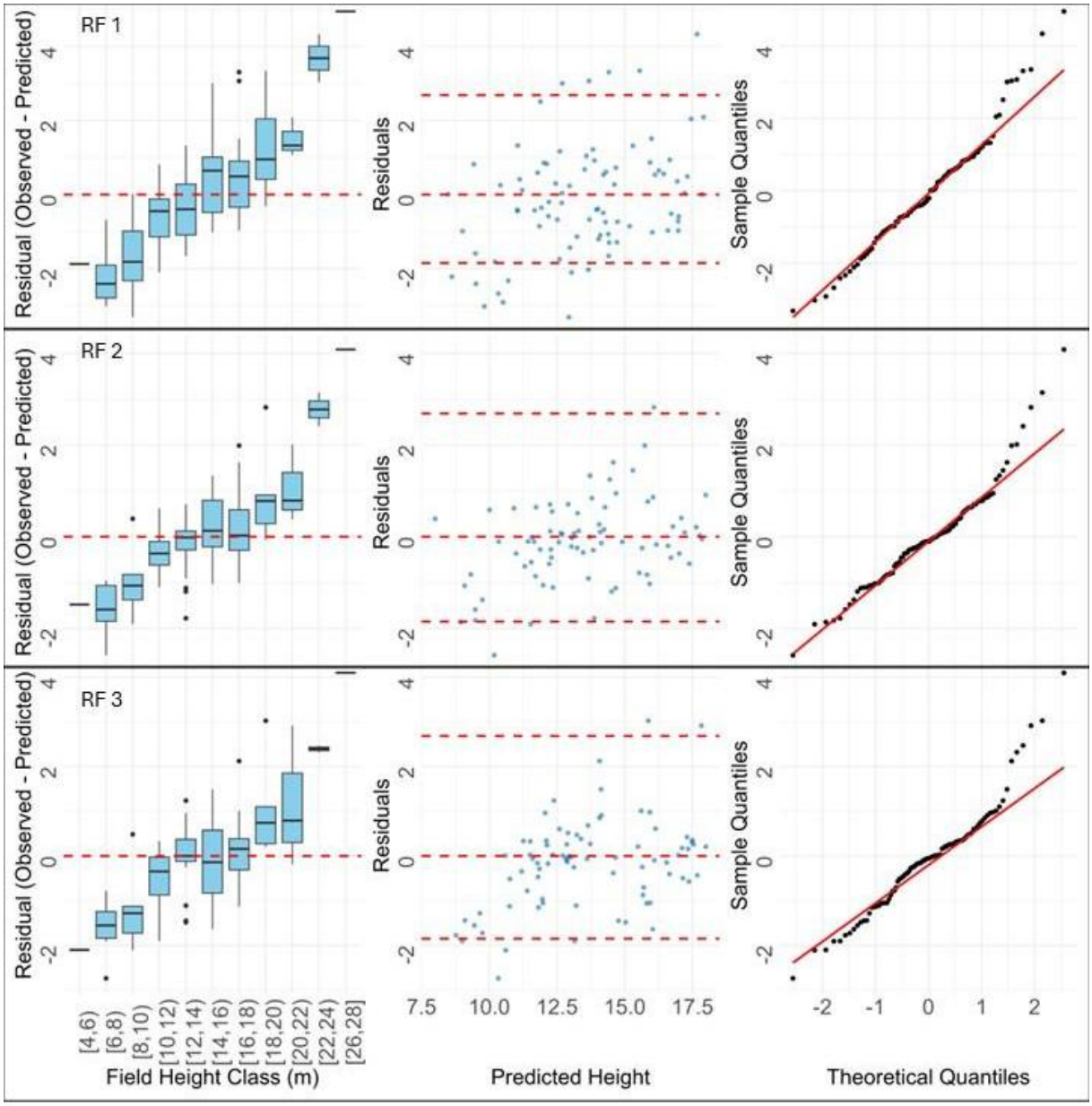


Figure 5.8. Diagnostic plots for the Random Forest model predicting field canopy height (Model RF 1, RF 2, and RF 3).

(A) Boxplots showing the distribution of residuals (observed – predicted) across 2-meter field height classes. (B) Residuals plotted against predicted values, with red dashed lines indicating the 0 and 95% confidence bands. (C) QQ plot of residuals assessing normality.

Exploration of residual analysis for the RF 2 across environmental drivers revealed no significant differences among classes. Nevertheless, RF 2 tends to overestimate field-measured canopy height clearly in arid and humid regions of the Miombo ecoregion (Figure 5.9). This suggests reduced model accuracy at the climatic extremes of the gradient. However, the average of residuals for all other classes were very small (less than 0.5m), showing that the model performed well in general.

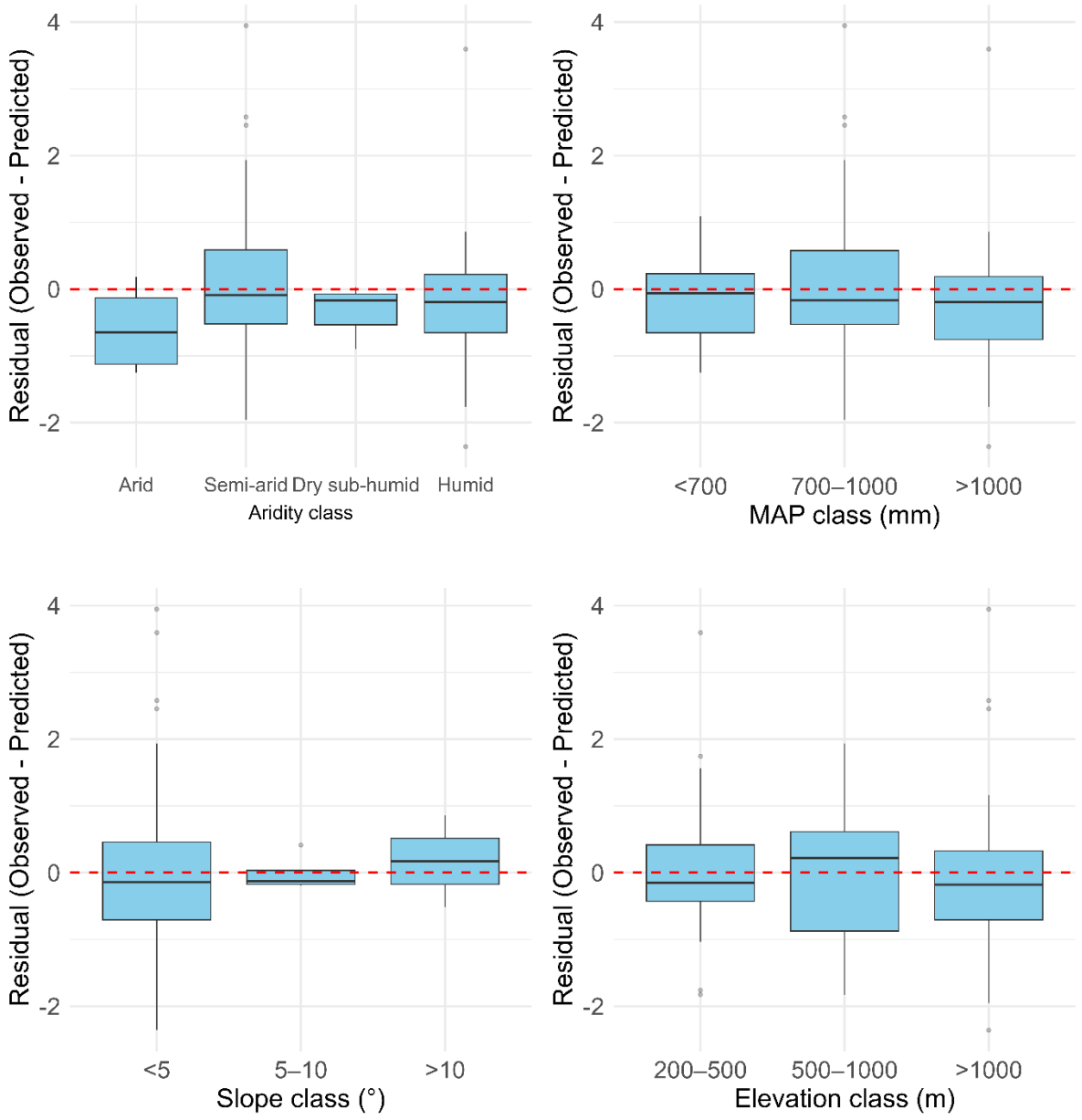


Figure 5.9. Boxplots showing the distribution of prediction residuals in meter (Field Height − Predicted Height) . from the RF 2 model across key environmental gradients: aridity class, mean annual precipitation (MAP) class, slope class, and elevation class. The red dashed line represents perfect prediction (residual = 0).

5.3.5 Variable Importance analysis

In Model RF 1, GEDI height and GEDI Max FHD were the most influential predictors, with similar importance scores (17.47 and 17.20, respectively). In contrast, GEDI Max PAI had minimal influence (Figure 5.10).

In Model RF 2, MAP emerged as the most significant variable, indicating that regional climatic gradients have a substantial impact on canopy height variation. Other key predictors included GEDI Max FHD, slope, GEDI height, and aridity, reflecting the combined role of vegetation structure, topography, and moisture availability. Sentinel-derived indices (e.g., EVI, Sentinel_1_RVI) and PALSAR metrics also contributed, albeit with lower importance (Figure 35). The RF 3 model that excluded the GEDI metrics confirmed the importance of MAP, slope, aridity, and EVI.

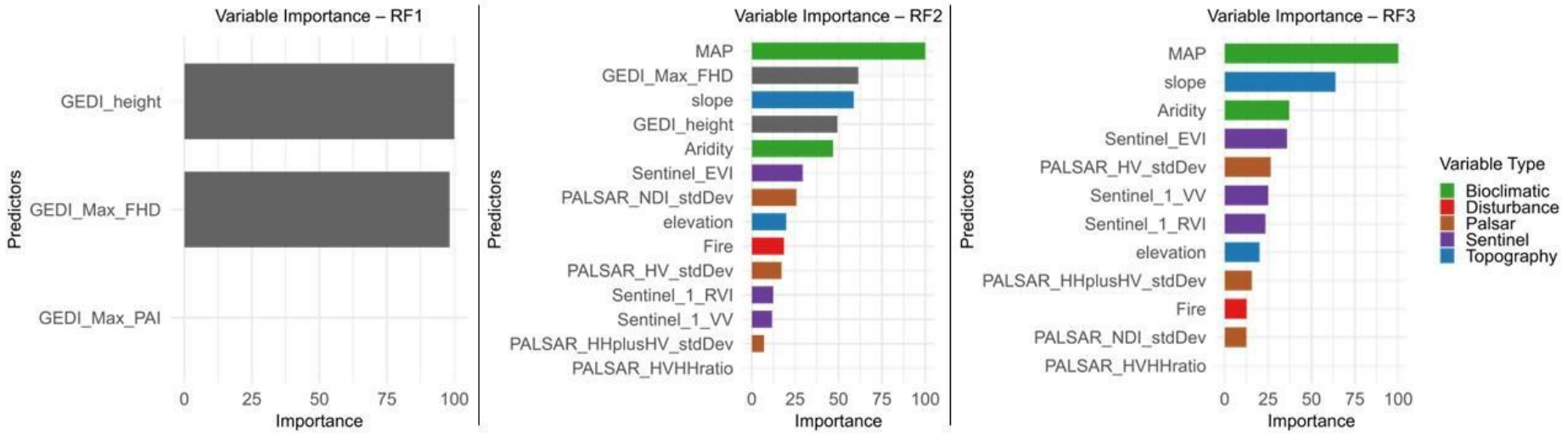


Figure 5.10. Variable importance.

(measured as % increase in MSE) for the three Random Forest models (RF 1, RF 2, and RF 3). Bar colors represent the type of predictor: grey (GEDI), blue (Topography), green (Bioclimatic), red (Disturbance), and purple (Sentinel spectral indices).

5.3.6 Comparison with Global Canopy Height Product

Model performance varied among the global forest canopy height products (GFCH) and Random Forest models (Table 5.3). The GFCH from Potapov et al. (2021) showed the highest overall error (RMSE = 8.17 m; MAE = 7.67 m) and a strong negative bias (–7.67 m), indicating consistent underestimation of field canopy height. The GFCH from Lang et al. (2023) performed considerably better, with lower errors (RMSE = 3.55 m; MAE = 3.02 m) and a smaller bias (–1.47 m).

Among the Random Forest models, accuracy was comparable to or slightly better than Lang et al. (2023)? product in terms of bias reduction. The RF1 model (GEDI only) achieved RMSE = 3.52 m, MAE = 2.76 m, and Bias = –1.01 m, while adding environmental variables in RF2 further reduced bias to –0.27 m (RMSE = 3.79 m; MAE = 2.61 m). The RF3 model, based solely on environmental predictors, had the largest errors among the Random Forest models (RMSE = 4.38 m; MAE = 2.76 m) and showed negligible bias (+0.09 m)..

Table 5.3 Performance of global canopy height products and Random Forest models compared to field-measured canopy height (n = 14)

Model	N	RMSE	MAE	BIAS
Canopy height from Potapov et al. (2021)	14	8.17	7.67	-7.67
Canopy height from Lang et al. (2023)	14	3.55	3.02	-1.47
Model RF1	14	3.52	2.76	-1.01
Model RF 2	14	3.79	2.61	-0.27
Model RF3	14	4.38	2.76	0.09

5.4 Discussion

5.4.1 Accuracy of GEDI height compared to the field height

Our results show that GEDI underestimates canopy height across the Miombo ecoregion, with biases of -1.37 m (all data) and -2.79 m (reduced dataset), and average deviations of 4–5 m (MAE). While moderate in magnitude, the results align with other studies that also found that GEDI tends to underestimate the canopy height at global level (A. Liu et al., 2021; J. Liu et al., 2014; Vatandaslar et al., 2023). This underestimation has clear implications for ecological applications because tree height is used in several models that estimate biomass (Chave et al., 2014; Gwenzi & Lefsky, 2016). Moreover, it is challenging to compare the GEDI height accuracy reported in this paper with other studies, as some, like ours, have used field-measured height as a reference value (Crockett et al., 2023; Gupta & Sharma, 2022) while others have compared GEDI canopy height with airborne laser scanning (A. Liu et al., 2021; Wang et al., 2022; Yang et al., 2025).

Analysis by canopy height showed minimal bias in small trees but a progressive underestimation for taller trees above 20 m. This pattern is consistent with earlier reports that GEDI accuracy declines with increasing canopy height (Adam et al., 2020; A. Liu et al., 2021; Yu et al., 2024). Together, these findings highlight that vegetation structure, including canopy height itself, strongly affects canopy height estimates (Jucker et al., 2018).

Several factors explain the observed underestimation of canopy height. A key issue is the structural complexity of Miombo woodlands, which are characterised by scattered tall trees, dense understorey vegetation, and frequent canopy gaps. This heterogeneity results in weak and uneven energy returns, especially in dry, open woodlands where signals may originate from shrubs, grasses, or bare ground rather than from the canopy (X. Li et al., 2023). Because GEDI uses Gaussian models to identify the centre of energy in the waveform (Hancock et al., 2019; Hofton & Blair, 2019), the limited contribution of sparse tall trees to the cumulative waveform energy can result in systematic underestimation. This effect is further reinforced by the use of RH98 as a canopy height metric, which may not fully capture the tallest canopy elements when their contribution to the waveform energy is weak, particularly in open and structurally heterogeneous woodlands. Additionally, the GEDI footprint, approximately 25 m in radius, may not fully capture narrow or isolated canopy trees, which can further lower RH98 relative to field-measured height due to geometric sampling effects.

5.4.2 Factors influencing GEDI error

Our results show that GEDI error is influenced by both structural and environmental gradients. Slope emerged as one of the strongest drivers. GEDI tended to overestimate canopy height on steep slopes (>10°). The tendency of canopy height to increase with slope in our analysis may reflect the difficulty GEDI faces in detecting the ground when slope increases, as ground and vegetation signals become increasingly mixed (Wang et al., 2022). Previous studies have also shown that slope reduces terrain detection accuracy and increases residual variability. Yang et al. (2025) found that GEDI sensitivity to slope was reflected in declining R^2 values as slope increased, while H. Li et al. (2024) demonstrated that GEDI canopy height shifted from underestimation on gentle terrain to overestimation on steeper terrain. Similarly, A. Liu et al. (2021) noted that slope consistently acted as an error driver, with residuals shifting upward with increasing slope. However, Adrah et al. (2022) observed the opposite, with taller trees on flat land and shorter trees on steeper slopes, likely because their study was conducted at a coarser scale (1 km × 1 km), smoothing out local variability.

Precipitation also played a central role in explaining GEDI error. GEDI underestimated canopy height in dry areas with less than 1000 mm MAP and overestimated in humid sites above 1000 mm, patterns that were also reflected in the aridity class. Such behaviour is consistent with waveform attenuation and ground signal occlusion in humid, closed-canopy sites. Elevation effects were weaker and not statistically significant, although shorter canopies at both low (<200 m) and high (>1000 m) elevations suggest edaphic constraints. Adrah et al. (2022) reported similar nonlinear responses in tropical montane forests, where canopy height–environment relationships weakened or reversed at high elevations. These findings reinforce the idea that environmental gradients interact with structural complexity to drive GEDI error patterns in heterogeneous landscapes such as the Miombo.

5.4.3 Effects of National Forest Inventory Data

Excluding the Mozambique National Forest Inventory (MNI dataset) led to improved GEDI validation accuracy, suggesting that differences among field datasets can influence remote sensing validation. This is not necessarily due to flaws in the dataset itself, but likely reflects variations in measurement protocols, plot design, instrumentation, or team expertise (Schwartz et al., 2024). National inventories often operate under different objectives and constraints compared to research-oriented surveys, which may affect the precision of tree height measurements. In our study, some environmental classes, such as rainfall or

aridity zones, were unevenly represented across datasets. This uneven sampling complicates the interpretation of GEDI error along ecological gradients, as part of the signal may reflect dataset-specific characteristics rather than environmental effects.

Moreover, uncertainty in field measurements is rarely quantified but can affect validation outcomes. Variability in observer technique, tree architecture, or measurement conditions may introduce error that propagates into accuracy assessments. Future work should examine how the inclusion of heterogeneous inventory sources affects GEDI validation outcomes, as resolving these biases is essential for producing reliable large-scale assessments.

5.4.4 GEDI Canopy Height Across Environmental Gradients

Beyond accuracy assessments, GEDI canopy height itself reflected ecological patterns. Taller canopies were consistently observed in wetter and higher-MAP zones, confirming the central role of water availability in shaping woodland structure and this confirms the results found in chapter 2 and 3. These findings reinforce the ecological theory that links tree height to resource availability (Scholes et al., 2002). No clear monotonic trend emerged with elevation, although plots at very low (<200 m) and very high (>1000 m) altitudes tended to support shorter canopies, possibly reflecting human disturbance at lowland sites and edaphic constraints and climatic limitations at higher elevations.

5.4.5 Modelling Field Canopy Height

Our modelling framework highlighted the limitations of GEDI metrics when used in isolation. GEDI canopy height (RH98), foliage height diversity (FHD), and plant area index (PAI) explained only 39% of the variation in field-measured canopy height, underscoring the difficulty of capturing structural complexity in open-canopy, heterogeneous woodlands. Model performance improved substantially ($R^2 = 0.64$) when ancillary predictors were included, particularly mean annual precipitation, aridity, slope, and spectral indices such as EVI and RVI. Moreover, a model using only ancillary variables outperformed the GEDI-only model ($R^2 = 0.55$; RMSE = 2.89 m; MAE = 2.11 m). These results highlight the value of multi-sensor integration for canopy height estimation. Optical indices contribute information on canopy greenness and density, radar backscatter captures canopy volume and vertical complexity, and climate variables contextualise structural development through long-term water availability and seasonality. Moreover, the many predictors needed to explain 64% of the variation in canopy height also highlights the need for good ground-data representing a wide range of ecological conditions

This finding is consistent with work in tropical montane forests of Ethiopia, where combining GEDI with optical and SAR predictors significantly improved extrapolation of canopy height beyond GEDI footprints (Geremew et al., 2023). Similar results have been reported in studies that fused GEDI with ancillary datasets to produce spatially continuous canopy structure estimates at regional scales (Lang et al., 2022, 2023; Potapov et al., 2021). Collectively, these findings demonstrate that GEDI is most powerful when used as part of an integrated modelling framework rather than as a stand-alone source of canopy height.

5.4.6 Residual Patterns of the Model

Residual diagnostics revealed systematic biases in the Random Forest model. Taller trees were consistently underestimated, while shorter trees were overestimated. This non-linear pattern indicates that model predictions saturate at canopy height extremes, a limitation also reported in other GEDI studies (Adam et al., 2020). The result highlights the difficulty of representing very tall emergent trees within a 25 m footprint, particularly in open-canopy woodlands where such trees are sparse and may be missed or only partially captured by the waveform.

Environmental extremes also amplified prediction errors. The model tended to overestimate canopy height in both the driest and wettest regions of the Miombo ecoregion. A similar pattern was observed across elevation, where overestimation occurred at low and high altitudes. Biases were also linked to slope, with canopy height overestimated in flat terrain and underestimated in steeper plots. These results underscore the fact that terrain and climate context can introduce systematic errors in canopy height prediction. The patterns observed suggest that further improvements could be achieved by adopting slope correction.

5.4.7 Comparison with Global Canopy Height Products

The GFCH map of Potapov et al. (2021) showed the largest errors and strongest underestimation (RMSE = 8.17 m; MAE = 7.67 m; Bias = –7.67 m), whereas Lang et al. (2023) achieved substantially lower errors and a smaller negative bias (RMSE = 3.55 m; MAE = 3.02 m; Bias = –1.47 m). Other evaluations also reported that the Potapov product exhibited higher RMSE/MAE than the newer high-resolution product from Lang et al. (2023) (Moudrý et al., 2024; Pascual et al., 2022).

Lang et al. (2023) demonstrated that their model reduces mean bias from about -7.1 m (in Potapov) to -1.7 m and lowers RMSE/MAE across biomes. Their biome-level evaluation showed minimal bias (< 1 m) in

tropical dry broadleaf and tropical/temperate grasslands, ecosystems structurally similar to Miombo ecoregion. This agrees with our smaller observed bias for Lang (-1.47 m). Furthermore, our GEDI-based RF models performed comparably to Lang, achieving near-zero bias (RF1: −1.01 m; RF2: −0.27 m), confirming the robustness and regional reliability of our models.

5.4.8 Limitations and future directions

This study highlights both the potential and the limitations of GEDI in African dry woodlands. Geolocation uncertainty, footprint averaging, and the structural heterogeneity of Miombo remain persistent sources of error. It should also be noted that the analysis is based on SEOSAW plots, which are designed to sample tree-dominated systems and therefore do not fully represent the entire range of vegetation types within the Miombo ecoregion, such as shrublands and grasslands. This introduces a structural bias that should be considered when interpreting the regional applicability of the results. In addition, uncertainty in field-measured tree height, particularly for taller trees and where model-based estimates are used, may contribute to the observed discrepancies with GEDI. Consequently, part of the mismatch may reflect limitations in the reference data rather than GEDI alone. The variability of field datasets, especially NFIs, further complicates accuracy assessments. Harmonising field measurements, increasing sampling in tall-canopy sites, and stratifying models across climatic zones may improve accuracy. Future research should also integrate GEDI with complementary spaceborne LiDAR and radar missions such as ICESat-2 and ESA's BIOMASS. Because canopy height is a critical input to biomass and carbon models, the underestimation of tall trees has direct consequences for regional and global carbon accounting. Our findings thus reinforce the need for regionally calibrated, multi-sensor approaches to canopy monitoring, particularly in structurally complex and underrepresented ecosystems such as the Miombo woodlands.

5.5 Conclusion

This study represents the first regional-scale evaluation of GEDI canopy height accuracy in the Miombo ecoregion of southern Africa using field-measured heights. We show that GEDI systematically underestimates canopy height, particularly in taller stands, and that errors are shaped by water availability and slope. These findings highlight the sensitivity of waveform LiDAR to both structural and environmental gradients in open-canopy tropical woodlands. Our Random Forest analysis demonstrates that integrating GEDI with climatic, spectral, and topographic predictors markedly improves predictions of canopy height, capturing 64% of the variance compared to less than 40% when using GEDI metrics alone.

At a global scale, our findings contribute new evidence that dry tropical woodlands pose unique challenges for spaceborne LiDAR, as global canopy height maps perform poorly in these ecosystems. By providing regionally calibrated models, this research advances the understanding of how GEDI performs in heterogeneous and underrepresented forests and underscores the need for multi-sensor approaches to reduce uncertainty in biomass and carbon assessments.

Because canopy height is a critical input to above-ground biomass estimation, these results directly inform carbon accounting efforts and highlight the risks of relying on uncalibrated global products in carbon markets and REDD+ initiatives. By improving the accuracy of canopy structure monitoring in dry Miombo woodlands, this research strengthens the foundations for more reliable climate mitigation policies, enhancing the role of African forests in global climate strategies.

5.6 CRediT authorship contribution statement

Hermane Diesse: Writing – review & editing, Writing – original draft, Visualization, Methodology, Investigation, Formal analysis, Data curation, Conceptualization. **John L. Godlee**: Writing – review & editing, Supervision, Investigation, Conceptualization. **Nichola Knox:** Writing – review & editing, Conceptualization. **Vera De Cauwer:** Writing review & editing, Investigation, supervision, Conceptualization.

The following researchers have contributed to this chapter In providing their data through the SEOSAW network

John Godlee, Francisco Maiato Pedro Gonçalves, Antonio Valter Chisingui, Jose Joao Tchamba, Kyle G. Dexter, Nichola Knox, Manfred Finckh, Jonathan Muledi, Vera De Cauwer, Natasha Ribeiro, Aristides Muhate, Sérgio João, Leena Naftal, Gabriel Uusiku, Hemant Tripathi and Anderson Muchawona.

References

Adam, M., Urbazaev, M., Dubois, C., & Schmullius, C. (2020). Accuracy Assessment of GEDI Terrain Elevation and Canopy Height Estimates in European Temperate Forests: Influence of Environmental and Acquisition Parameters. Remote Sensing, 12(23), 3948. https://doi.org/10.3390/rs12233948

Adrah, E., Wan Mohd Jaafar, W. S., Omar, H., Bajaj, S., Leite, R. V., Mazlan, S. M., Silva, C. A., Chel Gee Ooi, M., Mohd Said, M. N., Abdul Maulud, K. N., Cardil, A., & Mohan, M. (2022). Analyzing Canopy Height Patterns and Environmental Landscape Drivers in Tropical Forests Using NASA's GEDI Spaceborne LiDAR. Remote Sensing, 14(13), 3172. https://doi.org/10.3390/rs14133172

Aponte, C., Kasel, S., Nitschke, C. R., Tanase, M. A., Vickers, H., Parker, L., Fedrigo, M., Kohout, M., Ruiz-Benito, P., Zavala, M. A., & Bennett, L. T. (2020). Structural diversity underpins carbon storage in Australian temperate forests. Global Ecology and Biogeography, 29(5), 789–802. https://doi.org/10.1111/geb.13038

Archibald, S., Hempson, G. P., & Lehmann, C. (2019). A unified framework for plant life-history strategies shaped by fire and herbivory. New Phytologist, 224(4), 1490–1503. https://doi.org/10.1111/nph.15986

Atmani, F., Bookhagen, B., & Smith, T. (2022). Measuring Vegetation Heights and Their Seasonal Changes in the Western Namibian Savanna Using Spaceborne Lidars. Remote Sensing, 14(12), 2928. https://doi.org/10.3390/rs14122928

Boucher, P., Hancock, S., Orwig, D., Duncanson, L., Armston, J., Tang, H., Krause, K., Cook, B., Paynter, I., Li, Z., Elmes, A., & Schaaf, C. (2020). Detecting Change in Forest Structure with Simulated GEDI Lidar Waveforms: A Case Study of the Hemlock Woolly Adelgid (HWA; Adelges tsugae) Infestation. Remote Sensing, 12(8), 1304. https://doi.org/10.3390/rs12081304

Breiman, L., Cutler, A., Liaw, A., & Wiener, M. (2024). Random Forests for Classification and Regression (p. 4.7-1.2) [Data set]. https://doi.org/10.32614/CRAN.package.randomForest

Campbell, B. M. (1996). The miombo in transition: Woodlands and welfare in Africa (Center for International Forestry Research, Ed.). Center for International Forestry Research.

Cardenas-Martinez, A., Pascual, A., Guisado-Pintado, E., & Rodriguez-Galiano, V. (2025). Using airborne LiDAR and enhanced-geolocated GEDI metrics to map structural traits over a Mediterranean forest. Science of Remote Sensing, 11, 100195. https://doi.org/10.1016/j.srs.2025.100195

Chave, J., Réjou-Méchain, M., Búrquez, A., Chidumayo, E. N., Colgan, M. S., Delitti, W. B. C., Duque, A., Eid, T., Fearnside, P. M., Goodman, R. C., Henry, M., Martínez-Yrízar, A., Mugasha, W. A., Muller-Landau, H. C., Mencuccini, M., Nelson, B. W., Ngomanda, A., Nogueira, E. M., Ortiz-Malavassi, E., … Vieilledent, G.

(2014). Improved allometric models to estimate the aboveground biomass of tropical trees. Global Change Biology, 20(10), 3177–3190. https://doi.org/10.1111/gcb.12629

Chen, H., Cloude, S. R., & White, J. C. (2021). Using GEDI Waveforms for Improved TanDEM-X Forest Height Mapping: A Combined SINC + Legendre Approach. Remote Sensing, 13(15), 2882. https://doi.org/10.3390/rs13152882

Crockett, E. T. H., Atkins, J. W., Guo, Q., Sun, G., Potter, K. M., Ollinger, S., Silva, C. A., Tang, H., Woodall, C. W., Holgerson, J., & Xiao, J. (2023). Structural and species diversity explain aboveground carbon storage in forests across the United States: Evidence from GEDI and forest inventory data. Remote Sensing of Environment, 295, 113703. https://doi.org/10.1016/j.rse.2023.113703

Demol, M., Aguilar-Amuchastegui, N., Bernotaite, G., Disney, M., Duncanson, L., Elmendorp, E., Espejo, A., Furey, A., Hancock, S., Hansen, J., Horsley, H., Langa, S., Liang, M., Locke, A., Manjate, V., Mapanga, F., Omidvar, H., Parsons, A., Peneva-Reed, E., … Burt, A. (2024). Multi-scale lidar measurements suggest miombo woodlands contain substantially more carbon than thought. Communications Earth & Environment, 5(1), 366. https://doi.org/10.1038/s43247-024-01448-x

Diesse, H., Godlee, J. L., Knox, N., Muledi, J., Naftal, L., Nkulu, D., Nkomba, B., Uusiku, G., Dexter, K., & De Cauwer, V. (2025). Quantifying unseen woody biomass and diversity in understorey trees and shrubs at the extremes of water availability in the Miombo ecoregion. Forest Ecosystems, 13, 100302. https://doi.org/10.1016/j.fecs.2025.100302

Dinerstein, E., Olson, D., Joshi, A., Vynne, C., Burgess, N. D., Wikramanayake, E., Hahn, N., Palminteri, S., Hedao, P., Noss, R., Hansen, M., Locke, H., Ellis, E. C., Jones, B., Barber, C. V., Hayes, R., Kormos, C., Martin, V., Crist, E., … Saleem, M. (2017). An Ecoregion-Based Approach to Protecting Half the Terrestrial Realm. BioScience, 67(6), 534–545. https://doi.org/10.1093/biosci/bix014

Dorado-Roda, I., Pascual, A., Godinho, S., Silva, C., Botequim, B., Rodríguez-Gonzálvez, P., González-Ferreiro, E., & Guerra-Hernández, J. (2021). Assessing the Accuracy of GEDI Data for Canopy Height and Aboveground Biomass Estimates in Mediterranean Forests. Remote Sensing, 13(12), 2279. https://doi.org/10.3390/rs13122279

Dubayah, R., Armston, J., Healey, S., Bruening, J. M., Patterson, P., Kellner, J., Duncanson, L., Saarela, S., Ståhl, G., Yang, Z., Tang, H., Blair, J., Fatoyinbo, L., Goetz, S., Hancock, S., Hansen, M., Hofton, M., Hurtt, G., & Luthcke, S. (2022). GEDI launches a new era of biomass inference from space. Environmental Research Letters. https://doi.org/10.1088/1748-9326/ac8694

Dubayah, R., Blair, J. B., Goetz, S., Fatoyinbo, L., Hansen, M., Healey, S., Hofton, M., Hurtt, G., Kellner, J., Luthcke, S., Armston, J., Tang, H., Duncanson, L., Hancock, S., Jantz, P., Marselis, S., Patterson, P. L., Qi, W., &

Silva, C. (2020). The Global Ecosystem Dynamics Investigation: High-resolution laser ranging of the Earth's forests and topography. Science of Remote Sensing, 1, 100002. https://doi.org/10.1016/j.srs.2020.100002

Dubayah, R., Tang, H., Armston, J., Luthcke, S., Hofton, M., & Blair, J. B. (2021). GLOBAL Ecosystem Dynamics Investigation (GEDI) Level 2 User Guide.

Fayad, I., Baghdadi, N. N., Alvares, C. A., Stape, J. L., Bailly, J. S., Scolforo, H. F., Zribi, M., & Maire, G. L. (2021). Assessment of GEDI's LiDAR Data for the Estimation of Canopy Heights and Wood Volume of Eucalyptus Plantations in Brazil. IEEE Journal of Selected Topics in Applied Earth Observations and Remote Sensing, 14, 7095–7110. https://doi.org/10.1109/JSTARS.2021.3092836

Frost, P. (1996). The ecology of miombo woodlands. In The Miombo in transition: Woodlands and Welfare in Africa (B. Campbell, pp. 11–57). Centre for International Forestry Research.

Gatti, R. C., Di Paola, A., Bombelli, A., Noce, S., & Valentini, R. (2017). Exploring the relationship between canopy height and terrestrial plant diversity. Plant Ecology, 218(7), 899–908. https://doi.org/10.1007/s11258-017-0738-6

Geremew, T., Gonsamo, A., Zewdie, W., & Pellikka, P. (2023). Extrapolation of canopy height and cover metrics of GEDI LiDAR in tropical montane forest ecosystem. African Geographical Review, 1–17. https://doi.org/10.1080/19376812.2023.2164865

Gupta, R., & Sharma, L. K. (2022). Mixed tropical forests canopy height mapping from spaceborne LiDAR GEDI and multisensor imagery using machine learning models. Remote Sensing Applications: Society and Environment, 27, 100817. https://doi.org/10.1016/j.rsase.2022.100817

Gwenzi, D., & Lefsky, M. A. (2016). Plot-level aboveground woody biomass modeling using canopy height and auxiliary remote sensing data in a heterogeneous savanna. Journal of Applied Remote Sensing, 10(1), 016001. https://doi.org/10.1117/1.JRS.10.016001

Hancock, S., Armston, J., Hofton, M., Sun, X., Tang, H., Duncanson, L. I., Kellner, J. R., & Dubayah, R. (2019). The GEDI Simulator: A Large-Footprint Waveform Lidar Simulator for Calibration and Validation of Spaceborne Missions. Earth and Space Science, 6(2), 294–310. https://doi.org/10.1029/2018EA000506

Hofton, M., & Blair, J. B. (2019). Algorithm Theoretical Basis Document (ATBD) for GEDI Transmit and Receive Waveform Processing for L1 and L2 Products. https://lpdaac.usgs.gov/documents/581/GEDI_WF_ATBD_v1.0.pdf

Jucker, T., Bongalov, B., Burslem, D. F. R. P., Nilus, R., Dalponte, M., Lewis, S. L., Phillips, O. L., Qie, L., & Coomes, D. A. (2018). Topography shapes the structure, composition and function of tropical forest landscapes. Ecology Letters, 21(7), 989–1000. https://doi.org/10.1111/ele.12964

Knapp, N., Fischer, R., Cazcarra-Bes, V., & Huth, A. (2020). Structure metrics to generalize biomass estimation from lidar across forest types from different continents. Remote Sensing of Environment, 237, 111597. https://doi.org/10.1016/j.rse.2019.111597

Kuhn, M., Wing, J., Williams, A., Keefer, C., Engelhardt, A., Cooper, T., Mayer, Z., Kenkel, B., R Core Team, & Benesty, M. (2025). caret: Classification and Regression Training (p. 7.0-1) [Data set]. https://doi.org/10.32614/CRAN.package.caret

Lang, N., Jetz, W., Schindler, K., & Wegner, J. D. (2023). A high-resolution canopy height model of the Earth. Nature Ecology & Evolution, 7(11), 1778–1789. https://doi.org/10.1038/s41559-023-02206-6

Lang, N., Kalischek, N., Armston, J., Schindler, K., Dubayah, R., & Wegner, J. D. (2022). Global canopy height regression and uncertainty estimation from GEDI LIDAR waveforms with deep ensembles. Remote Sensing of Environment, 268, 112760. https://doi.org/10.1016/j.rse.2021.112760

Li, H., Li, X., Kato, T., Hayashi, M., Fu, J., & Hiroshima, T. (2024). Accuracy assessment of GEDI terrain elevation, canopy height, and aboveground biomass density estimates in Japanese artificial forests. Science of Remote Sensing, 10, 100144. https://doi.org/10.1016/j.srs.2024.100144

Li, T., Guo, L., He, B., Liu, L., Yuan, W., Chen, X., Hao, X., Liu, X., Zheng, H., Zheng, H., & Wang, R. (2023). The Forest Resistance to Droughts Differentiated by Tree Height in Central Europe. Journal of Geophysical Research: Biogeosciences, 128(4), e2021JG006668. https://doi.org/10.1029/2021JG006668

Li, X., Wessels, K., Armston, J., Duncanson, L., Urbazaev, M., Naidoo, L., Mathieu, R., & Main, R. (2024). Evaluation of GEDI Footprint Level Biomass Models in Southern African Savannas using Airborne LiDAR and Field Measurements. Science of Remote Sensing. https://doi.org/10.1016/j.srs.2024.100161

Li, X., Wessels, K., Armston, J., Hancock, S., Mathieu, R., Main, R., Naidoo, L., Erasmus, B., & Scholes, R. (2023). First validation of GEDI canopy heights in African savannas. Remote Sensing of Environment, 285, 113402. https://doi.org/10.1016/j.rse.2022.113402

Liang, M., Duncanson, L., Duncanson, L., & Sedano, F. (2021). Quantifying Local-scale Forest Degradation Intensity from Charcoal Production Using a Fusion of GEDI and Landsat Data. https://doi.org/10.5194/egusphere-egu21-3147

Liang, M., Duncanson, L., Silva, J. A., & Sedano, F. (2023). Quantifying aboveground biomass dynamics from charcoal degradation in Mozambique using GEDI Lidar and Landsat. Remote Sensing of Environment, 284, 113367. https://doi.org/10.1016/j.rse.2022.113367

Liu, A., Cheng, X., & Chen, Z. (2021). Performance evaluation of GEDI and ICESat-2 laser altimeter data for terrain and canopy height retrievals. Remote Sensing of Environment, 264, 112571. https://doi.org/10.1016/j.rse.2021.112571

Liu, J., Liu, D., & Alsdorf, D. (2014). Extracting Ground-Level DEM From SRTM DEM in Forest Environments Based on Mathematical Morphology. IEEE Transactions on Geoscience and Remote Sensing, 52(10), 6333–6340. https://doi.org/10.1109/tgrs.2013.2296232

Liu, S., Csillik, O., Ordway, E. M., Chang, L.-L., Longo, M., Keller, M., & Moorcroft, P. R. (2025). Environmental drivers of spatial variation in tropical forest canopy height: Insights from NASA's GEDI spaceborne LiDAR. Proceedings of the National Academy of Sciences, 122(10), e2401755122. https://doi.org/10.1073/pnas.2401755122

Mayr, M. J., Vanselow, K. A., & Samimi, C. (2018). Fire regimes at the arid fringe: A 16-year remote sensing perspective (2000–2016) on the controls of fire activity in Namibia from spatial predictive models. Ecological Indicators, 91, 324–337. https://doi.org/10.1016/j.ecolind.2018.04.022

Moudrý, V., Gábor, L., Marselis, S., Pracná, P., Barták, V., Prošek, J., Navrátilová, B., Novotný, J., Potůčková, M., Gdulová, K., Crespo-Peremarch, P., Komárek, J., Malavasi, M., Rocchini, D., Ruiz, L. A., Torralba, J., Torresani, M., Cazzolla Gatti, R., & Wild, J. (2024). Comparison of three global canopy height maps and their applicability to biodiversity modeling: Accuracy issues revealed. Ecosphere, 15(10), e70026. https://doi.org/10.1002/ecs2.70026

Padalia, H., Prakash, A., & Watham, T. (2023). Modelling aboveground biomass of a multistage managed forest through synergistic use of Landsat-OLI, ALOS-2 L-band SAR and GEDI metrics. Ecological Informatics, 77, 102234. https://doi.org/10.1016/j.ecoinf.2023.102234

Pascual, A., Tupinambá-Simões, F., & De Conto, T. (2022). Using multi-temporal tree inventory data in eucalypt forestry to benchmark global high-resolution canopy height models. A showcase in Mato Grosso, Brazil. Ecological Informatics, 70, 101748. https://doi.org/10.1016/j.ecoinf.2022.101748

Potapov, P., Li, X., Hernandez-Serna, A., Tyukavina, A., Hansen, M. C., Kommareddy, A., Pickens, A., Turubanova, S., Tang, H., Silva, C. E., Armston, J., Dubayah, R., Blair, J. B., & Hofton, M. (2021). Mapping global forest canopy height through integration of GEDI and Landsat data. Remote Sensing of Environment, 253, 112165. https://doi.org/10.1016/j.rse.2020.112165

R Core Team. (2023). R: A Language and Environment for Statistical Computing_. R Foundation for Statistical Computing, Vienna, Austria. <https://www.R-project.org/> [Computer software].

Ryan, C. M., Pritchard, R., McNicol, I., Owen, M., Fisher, J. A., & Lehmann, C. (2016). Ecosystem services from southern African woodlands and their future under global change. Philosophical Transactions of the Royal Society B: Biological Sciences, 371(1703), 20150312. https://doi.org/10.1098/rstb.2015.0312

Ryan, C. M., Williams, M., & Grace, J. (2011). Above- and Belowground Carbon Stocks in a Miombo Woodland Landscape of Mozambique: Carbon Stocks in a Miombo Woodland. Biotropica, 43(4), 423–432. https://doi.org/10.1111/j.1744-7429.2010.00713.x

Saito, M., Luyssaert, S., Poulter, B., Williams, M., Ciais, P., Bellassen, V., Ryan, C. M., Yue, C., Cadule, P., & Peylin, P. (2014). Fire regimes and variability in aboveground woody biomass in miombo woodland. Journal of Geophysical Research: Biogeosciences, 119(5), 1014–1029. https://doi.org/10.1002/2013JG002505

Sankaran, M., Hanan, N. P., Scholes, R. J., Ratnam, J., Augustine, D. J., Cade, B. S., Gignoux, J., Higgins, S. I., Le Roux, X., Ludwig, F., Ardo, J., Banyikwa, F., Bronn, A., Bucini, G., Caylor, K. K., Coughenour, M. B., Diouf, A., Ekaya, W., Feral, C. J., … Zambatis, N. (2005). Determinants of woody cover in African savannas. Nature, 438(7069), 846–849. https://doi.org/10.1038/nature04070

Scholes, R. J., Dowty, P. R., Caylor, K., Parsons, D. A. B., Frost, P. G. H., & Shugart, H. H. (2002). Trends in savanna structure and composition along an aridity gradient in the Kalahari. Journal of Vegetation Science, 13(3), 419–428. https://doi.org/10.1111/j.1654-1103.2002.tb02066.x

Schwartz, M., Ciais, P., Ottlé, C., De Truchis, A., Vega, C., Fayad, I., Brandt, M., Fensholt, R., Baghdadi, N., Morneau, F., Morin, D., Guyon, D., Dayau, S., & Wigneron, J.-P. (2024). High-resolution canopy height map in the Landes forest (France) based on GEDI, Sentinel-1, and Sentinel-2 data with a deep learning approach. International Journal of Applied Earth Observation and Geoinformation, 128, 103711. https://doi.org/10.1016/j.jag.2024.103711

SEOSAW partnership. (2021). A network to understand the changing socio-ecology of the southern African woodlands (SEOSAW): Challenges, benefits, and methods. PLANTS, PEOPLE, PLANET, 3(3), 249–267. https://doi.org/10.1002/ppp3.10168

Sexton, J. O., Bax, T., Siqueira, P., Swenson, J. J., & Hensley, S. (2009). A comparison of lidar, radar, and field measurements of canopy height in pine and hardwood forests of southeastern North America. Forest Ecology and Management, 257(3), 1136–1147. https://doi.org/10.1016/j.foreco.2008.11.022

Smit, I. P. J., Asner, G. P., Govender, N., Kennedy-Bowdoin, T., Knapp, D. E., & Jacobson, J. (2010). Effects of fire on woody vegetation structure in African savanna. Ecological Applications, 20(7).

Smith-Tripp, S. M., Eskelson, B. N. I., Coops, N. C., & Schwartz, Naomi B. (2022). Canopy height impacts on the growing season and monthly microclimate in a burned forest of British Columbia, Canada. Agricultural and Forest Meteorology, 323. https://doi.org/10.1016/j.agrformet.2022.109067

Tao, S., Guo, Q., Li, C., Wang, Z., & Fang, J. (2016). Global patterns and determinants of forest canopy height. Ecology, 97(12), 3265–3270. https://doi.org/10.1002/ecy.1580

Torresani, M., Rocchini, D., Alberti, A., Moudrý, V., Heym, M., Thouverai, E., Kacic, P., & Tomelleri, E. (2023). LiDAR GEDI derived tree canopy height heterogeneity reveals patterns of biodiversity in forest ecosystems. Ecological Informatics, 76, 102082. https://doi.org/10.1016/j.ecoinf.2023.102082

Tsao, A., Nzewi, I., Jayeoba, A., Ayogu, U., & Lobell, D. B. (2023). Canopy Height Mapping for Plantations in Nigeria Using GEDI, Landsat, and Sentinel-2. Remote Sensing, 15(21), 5162. https://doi.org/10.3390/rs15215162

Vatandaslar, C., Narin, O. G., & Abdikan, S. (2023). Retrieval of forest height information using spaceborne LiDAR data: A comparison of GEDI and ICESat-2 missions for Crimean pine (Pinus nigra) stands. Trees, 37(3), 717–731. https://doi.org/10.1007/s00468-022-02378-x

Wang, C., Elmore, A. J., Numata, I., Cochrane, M. A., Shaogang, L., Huang, J., Zhao, Y., & Li, Y. (2022). Factors affecting relative height and ground elevation estimations of GEDI among forest types across the conterminous USA. GIScience & Remote Sensing, 59(1), 975–999. https://doi.org/10.1080/15481603.2022.2085354

Wolsza, M. (2024). Gedixr [Computer software]. https://github.com/maawoo/gedixr

Xu, C., Hantson, S., Holmgren, M., Van Nes, E. H., Staal, A., & Scheffer, M. (2016). Remotely sensed canopy height reveals three pantropical ecosystem states. Ecology, 97(9), 2518–2521. https://doi.org/10.1002/ecy.1470

Xu, P., Zhou, T., Yi, C., Fang, W., Hendrey, G., & Zhao, X. (2018). Forest drought resistance distinguished by canopy height. Environmental Research Letters, 13(7), 075003. https://doi.org/10.1088/1748-9326/aacadd

Yang, C., Peng, D., Zhang, N., Chen, M., Zeng, W., Sun, X., Li, L., & Li, W. (2025). Performance evaluation and improvement of ICESat-2 and GEDI forest canopy height retrievals in Northeast China. GIScience & Remote Sensing, 62(1), 2497603. https://doi.org/10.1080/15481603.2025.2497603

Yu, Q., Ryan, M. G., Ji, W., Prihodko, L., Anchang, J. Y., Kahiu, N., Nazir, A., Dai, J., & Hanan, N. P. (2024). Assessing canopy height measurements from ICESat-2 and GEDI orbiting LiDAR across six different biomes with G-LiHT LiDAR. Environmental Research: Ecology, 3(2), 025001. https://doi.org/10.1088/2752-664X/ad39f2

Zomer, R. J., Xu, J., & Trabucco, A. (2022). Version 3 of the Global Aridity Index and Potential Evapotranspiration Database. Scientific Data, 9(1), 409. https://doi.org/10.1038/s41597-022-01493-1

Appendix 4

Table S1: Comparison between GEDI height metrics (max RH98 and mean RH98) with various field height metrics. Various field height metrics have been tested, including the percentile height from 90th to 98th, maximum field height, mean field height, and the mean height of the two largest diameter breast height (DBH). The field height metrics are sorted by R^2 for each GEDI height metrics.
The best GEDI height metric was the maximum RH98. Concerning the field-measured height, the 95th percentile to 98th percentile gave the best agreement. For our research, we selected the 98th percentile, as we also used the 98th percentile for GEDI height.

Field height metrics	**GEDI height metrics**	**R^2**	**RMSE**	**MAE**
96th	max RH98	0.31	4.54	3.38
95th	max_rh_98	0.31	4.41	3.24
94th	max_rh_98	0.30	4.34	3.20
97th	max_rh_98	0.30	4.73	3.58
98th	max_rh_98	0.30	4.99	3.88
92th	max_rh_98	0.30	4.23	3.16
93th	max_rh_98	0.29	4.30	3.18
91th	max_rh_98	0.29	4.20	3.16
90th	max_rh_98	0.28	4.20	3.16
Mean height of the two largest DBH	max_rh_98	0.27	4.79	3.63
Mean height	max_rh_98	0.23	5.06	3.86
Max height	max_rh_98	0.23	6.16	5.08
95th	mean_rh_98	0.33	5.15	4.22
94th	mean_rh_98	0.33	4.98	4.03
96th	mean_rh_98	0.33	5.40	4.51
97th	mean_rh_98	0.32	5.67	4.83
93th	mean_rh_98	0.32	4.86	3.88
98th	mean_rh_98	0.32	6.03	5.22
92th	mean_rh_98	0.31	4.72	3.71

Mean height of the two largest DBH	mean_rh_98	0.31	5.57	4.61
91th	mean_rh_98	0.31	4.60	3.60
90^{th}	mean_rh_98	0.30	4.52	3.54
Mean height	mean_rh_98	0.26	3.52	2.64
Max height	mean_rh_98	0.24	7.41	6.50

Table S2: Accuracy of GEDI Canopy Height vs. Field-Measured Height at the country level

Country	**R2**	**RMSE**	**MAE**
Angola	0.53	3.77	3.02
DRC	0.57	0.62	0.54
Mozambique	0.07	2.66	2.09
Namibia	0.93	0.87	0.68
Zambia	0.31	2.84	2.18
Zimbabwe	0.19	2.13	1.63

Chapter 6: Synthesis and conclusion

6.1 Integrative Overview and Conceptual Foundations

Understanding the mechanisms that shape vegetation structure and biomass distribution in tropical dry woodlands remains a central challenge in ecology, particularly in regions such as the Miombo ecoregion, where climate and disturbance interact in complex ways.

This PhD thesis aimed to investigate the interactions between environmental gradients, vegetation structure, and biomass partitioning, and how these interactions influence LiDAR-based canopy height estimation across the Miombo ecoregion, using integrated field and remotely sensed data.

To respond to this aim, this research uses an integrated multiscale approach that combines:

- Regional-scale Forest inventory data from the A Socio-Ecological Observatory for Studying African Woodlands (SEOSAW),
- Plot inventories established during this PhD research, spanning the extremes of the Miombo rainfall gradient,
- Terrestrial laser scanning (TLS) to capture fine-scale structural organisation, and
- Global Ecosystem Dynamics Investigation (GEDI) spaceborne LiDAR to assess remote-sensing performance across structurally heterogeneous woodland systems.

Four research questions guided the thesis:

- How do rainfall, disturbance, topography, and soil characteristics influence vegetation structure and biomass distribution across tree size classes, and how do these factors affect the contribution of large trees in the Miombo ecoregion? (chapter 2).
- To what extent does understorey vegetation (DBH < 5 cm) contribute to total woody biomass and species diversity across contrasting rainfall conditions in the Miombo ecoregion? (Chapters 3)
- How do canopy structural attributes influence the subcanopy layer (tree height < 3 m) and associated ecological attributes, including species richness, tree density, and above-ground biomass? (chapter 4)

- How do structural and environmental gradients impact the accuracy of spaceborne LiDAR canopy height estimates across the Miombo ecoregion, and under which conditions does GEDI performance improve or decline? (chapter 5)

These questions were addressed through four empirical chapters whose interconnections form an explicit causal chain from environmental drivers → forest structural attributes → biomass distribution → observation through remote sensing.

This perspective shifts the interpretation from isolated empirical findings toward a process-based understanding of how dry tropical woodlands function and how they are observed through remote sensing.

6.2 Conceptual Framework

Understanding Miombo ecoregion requires engaging with the fundamental ecological principle that vegetation structure is both a product and a regulator of environmental processes (Li et al., 2024; J. Liu et al., 2018). In the Miombo ecoregion, rainfall sets fundamental physiological constraints that control tree growth and recruitment (Sankaran et al., 2005; Scholes et al., 2002). Fire frequency, itself conditioned by rainfall seasonality and human activity (Archibald et al., 2013; Frost, 1996; Ryan & Williams, 2011), acts as an additional filter influencing the vegetation structure. Elevation and slope further modulate edaphic conditions, drainage, and soil depth, thereby producing finely resolved gradients in resource availability and tree performance (Colgan et al., 2012; Franz et al., 2011; Shetie et al., 2017).

The thesis conceptualises this environmental matrix as the determinant of forest structural attributes, including canopy height, vertical stratification, gap fraction, and the distribution of stems across diameter and height classes. These structural attributes, in turn, determine how biomass is allocated across the vertical profile, whether concentrated in large emergent stems, distributed through intermediate-sized trees, or stored disproportionately in small-diameter shrubs and saplings.

The framework explicitly distinguishes between two interacting domains:

- the ecological system that governs vegetation structure and biomass distribution, and
- the observation system through which this structure is measured

Remote sensing operates as an observational layer that interacts with, but does not modify, the ecological system. Spaceborne LiDAR measurements are therefore conditioned by vegetation structure rather than independent of it. Canopy height retrieval depends on waveform interactions with vegetation layers, foliage density, and ground visibility

(Dubayah et al., 2020, 2022). Thus, any attempt to assess GEDI performance must be grounded in an understanding of the environmental and structural conditions that shape the forest canopy.

This distinction is fundamental: ecological processes generate structure, and structure conditions measurement

Accordingly, remote-sensing performance must be interpreted as a function of ecological organisation. Within this framework, GEDI is positioned not as a driver of ecosystem processes, but as a tool whose accuracy depends on the structural context it samples.

6.3 Synthesis of Results Across the Four Research Questions

6.3.1 Climatic Control of Vegetation structure and Biomass Allocation Across Tree Size Classes

Rainfall emerged as the dominant driver shaping forest structural and biomass distribution across the Miombo ecoregion. My regional analysis (Chapter 2) revealed a pronounced increase in total above-ground biomass (AGB), from dry regions receiving <400 mm yr^{-1} to wet Miombo sites receiving >1800 mm yr^{-1}. This trend underscores the fundamental role of rainfall in regulating AGB in these woodlands, consistent with long-standing findings in the Miombo ecoregion (Godlee et al., 2021; Sankaran et al., 2005; Scholes et al., 2002).

Yet, beyond total AGB, the more revealing pattern concerned how biomass was distributed across tree size classes (chapters 2 and 3). Contrary to the dominance patterns observed in humid tropical forests, where a small fraction of extremely large stems often accounts for a disproportionate share of biomass (Bastin et al., 2015; Lutz et al., 2018; Slik et al., 2013), my results show that in the Miombo, the biomass share of the top 1% of stems indicated a slight decreasing trend along the gradient (chapter 2). Although wet sites contained more large stems (≥40 cm DBH) than dry sites, the most extreme large individuals did not disproportionately dominate biomass. This finding indicates that wet Miombo supports a broader

cohort of large stems rather than a few individual large trees. This is also confirmed by the increase in the mean diameter threshold above which trees cumulatively account for 50% of the total AGB. The ecological implication is profound: in contrast to humid tropical forests, where biomass can often be predicted from a few dominant large trees (Bastin et al., 2015), Miombo biomass is not concentrated solely in the largest individuals. Instead, biomass is more evenly distributed across stem sizes.

This regional pattern is complemented by plot-level evidence from Chapter 2, where total AGB is best explained by structural metrics describing tree size distribution, particularly the Gini coefficient and quadratic mean diameter (QMD). These variables capture complementary aspects of stand structure: QMD reflects the overall size of trees contributing to biomass, while the Gini coefficient describes the inequality in size distribution within the stand. However, the determinants of large-tree dominance differ from those of total biomass. Chapter 2 shows that metrics such as DBH coefficient of variation (DBH_CV) are more strongly associated with the contribution of large trees, indicating that variability in diameter distribution, rather than central tendency alone, plays a key role in structuring the upper tail of the size distribution.

These patterns are further reinforced by Chapter 3, which demonstrates that small-diameter vegetation (DBH < 5 cm) contributes substantially to total biomass in dry Miombo systems. This highlights an additional structural dimension: biomass is not only redistributed among large trees but also extends into lower strata under water-limited conditions. Together, Chapters 2 and 3 show that rainfall controls biomass through a multi-layered structural pathway, influencing both the upper and lower bounds of the size distribution.Consequently, standard forest inventory protocols that exclude stems <5 cm (Chave et al., 2014; SEOSAW partnership, 2021) systematically underestimate AGB in dry Miombo, highlighting a critical mismatch between measurement conventions and ecological reality, with implications for carbon accounting.

Tree height exhibits a parallel rainfall-driven pattern. Across the gradient (chapters 3 and 5), canopy height increased with precipitation, and the distribution of height classes differed sharply between dry and wet woodlands. These results align with theoretical expectations that water availability promotes vertical canopy development (Tao et al., 2016). Yet my findings refine this understanding by showing that in the Miombo, increased rainfall enhances large-stem biomass and canopy height without producing the hyper-dominant emergent stems typical of closed tropical forests.

These results demonstrate that rainfall governs not only the magnitude of AGB but also its structural organisation of Miombo vegetation. It influences stem size distributions, height profiles, and the layering of biomass across vegetation strata, underpinning the ecological distinctiveness of Miombo woodlands relative to humid tropical forests.

6.3.2 Disturbance and Environmental Controls on Vegetation structure and Biomass Partitioning

While rainfall defines the regional potential for biomass accumulation, Chapters 2–4 collectively demonstrate that disturbance and local environmental conditions determine how this potential is realised within stands. Fire, in particular, emerges as a key process regulating vegetation structure across scales, consistent with its central role in Miombo dynamics (Archibald et al., 2013; Ryan & Williams, 2011; Bond & Midgley, 2012).

In chapter 2, I found that fire frequency exerted a strongly negative effect on total AGB, consistent with numerous studies showing that repeated fire reduces carbon stocks and suppresses recruitment into larger size classes (Ribeiro et al., 2008; Ryan & Williams, 2011). However, my results also revealed a critical nuance: fire had a negligible influence on large trees, which retained their share biomass across the gradient. Instead, fire disproportionately impacted the lower and intermediate layers, inhibiting the growth of subcanopy individuals and reducing the number of plants that ultimately reach canopy height. This finding is consistent with the ecological theory of “fire filtering”, where repeated disturbances restrict individuals to a “fire-trap” zone, preventing them from surpassing the height threshold required to escape flame exposure (Bond & Midgley, 2012).

This interpretation is directly supported by the field-based analysis in Chapter 3, which shows that dry, fire-prone systems are characterised by shrub-dominated understorey layers and a reduced presence of saplings capable of reaching canopy height. In contrast, wetter and less disturbed systems favour the recruitment of canopy-forming species. This shift in life-form composition reflects the combined influence of disturbance and environmental limitation on regeneration pathways (Martín-Queller et al., 2011; Clarke et al., 2013).

Fine-scale structural metrics derived from terrestrial laser scanning in chapter 4 further clarify how disturbance and environmental conditions shape vegetation structure in dry Namibian woodlands. Fire-disturbed plots exhibited high gap fraction and strong horizontal heterogeneity in canopy cover, reflecting

structurally open and irregular stands (Mayr et al., 2018). These gaps increased light penetration and were associated with a higher subcanopy plant density index (PDI), consistent with theoretical expectations for dry woodlands (Kindermann et al., 2022). Conversely, high vertical complexity (entropy) reduced subcanopy PDI, demonstrating that layers of foliage distributed through the canopy restrict resource availability for the lower strata.

Furthermore, canopy PDI was positively associated with subcanopy PDI. In dry Miombo, “canopy” vegetation often falls between 3 and 5 m rather than forming a fully developed upper canopy. Consequently, dense foliage within this intermediate layer does not necessarily suppress the subcanopy because shading is partial and ephemeral. This structural configuration matches the height-distribution patterns described in Chapter 3, where most stems in dry Namibian plots were between 1 and 4 m tall in dry sites.

Environmental controls other than fire also contributed to structural variation. In Chapter 2, elevation exhibited a significant negative effect on total AGB, likely reflecting soil depth, nutrient availability, or temperature constraints on growth in high- and low-elevation extremes. Furthermore, canopy cover, shaped by both rainfall and disturbance, modulated light availability and understorey responses across all study sites. These environmental constraints reinforce that vegetation structure in the Miombo emerges from a multi-factor interaction between water availability, disturbance, canopy architecture, and local habitat conditions.

Together, chapters 2 and 3reveal a coherent ecological gradient: dry and open woodlands support structurally simple, multi-stemmed stands with high understorey and intermediate biomass, while wet, closed-canopy Miombo allocates biomass predominantly to tall, overstorey trees. Disturbance and environmental constraints do not simply influence biomass stocks but fundamentally determine the vertical and horizontal architecture of Miombo, shaping recruitment pathways, competitive dynamics, and ecosystem functioning.

6.3.3 GEDI Performance Across Structural Gradients and Calibration of Regional Canopy Height Models

Having established how environmental gradients and disturbance shape vegetation structure, and how structure governs biomass distribution, Chapter 5 examines how this structure is captured by spaceborne LiDAR. In this study, the GEDI analysis should be understood as a methodological extension of the

ecological framework rather than a core ecological component. While Chapters 2–4 characterise the structure of Miombo woodlands, Chapter 5 evaluates how well this structure can be observed using remote sensing.

The results demonstrate that GEDI systematically underestimates canopy height across the Miombo ecoregion, with bias increasing in structurally complex environments (A. Liu et al., 2021; Vatandaslar et al., 2023). This pattern is not random but reflects the structural characteristics identified in earlier chapters.

In dry woodlands, open canopies, vertically compressed vegetation, and strong contributions from intermediate layers reduce the likelihood that waveform energy captures the true canopy top (Hancock et al., 2019; Hofton & Blair, 2019). Because GEDI relies on Gaussian decomposition to estimate the centre of energy in the waveform (Hancock et al., 2019; Hofton & Blair, 2019), the sparse contribution of emergent trees, particularly in dry sites, combined with strong intermediate and understorey returns, results in a downward bias in height.

TLS-derived metrics (Chapter 4) provide direct evidence for this mechanism, showing dry woodlands of Namibia concentrated vegetation between 1 and 4 m and high spatial heterogeneity within GEDI footprints.

Environmental factors such as slope further influence GEDI performance by altering waveform-ground interactions, particularly in complex terrain (Yang et al., 2025).

The Random Forest models developed in Chapter 5 demonstrate that GEDI performance improves when structural and environmental variables are incorporated. However, these models do not overcome the fundamental limitations of footprint-based LiDAR sampling.

Therefore, the GEDI analysis should be interpreted as a first step toward integrating ecological structure with large-scale observation systems, rather than a complete solution for wall-to-wall ecosystem characterisation. While it provides valuable insights into the structural drivers of remote-sensing bias, achieving continuous spatial representation of Miombo vegetation will require multi-sensor integration and advanced modelling approaches.

Comparisons with existing global canopy height products reveal that my regionally calibrated approach performs favourably. Potapov et al. (2021) showed the largest errors and strongest underestimation,

whereas Lang et al. (2023) reduced these errors substantially. My GEDI-based Random Forest models produced biases comparable to or smaller than those of Lang product, achieving strong performance across all Miombo subregions. These results underscore the necessity of regional calibration for structurally complex and underrepresented ecosystems, and they demonstrate that integrating GEDI with local environmental predictors yields substantial accuracy gains.

From above, the findings from Chapter 5 reveal that GEDI accuracy is intimately linked to the structural and environmental gradients characterised in Chapters 2–4. The canopy height biases detected are not random measurement errors but predictable outcomes of Miombo structure: open canopies and dense subcanopies in dry areas, tall and dense canopies in wet areas, and variable topography across the region. By quantifying these interactions and incorporating them into regional modelling, this thesis provides a pathway toward improved canopy-height mapping and, by extension, more reliable biomass estimation for Miombo ecoregion.

6.4 Implications for Ecology, Remote Sensing, and Forest Monitoring in the Miombo Ecoregion

The collective findings of this thesis have several important implications for ecological theory, forest monitoring practices, and the interpretation of remote-sensing products in savanna-woodland systems.

6.4.1 Ecological Implications: Rethinking Biomass Allocation and Large-Tree Dominance

A major ecological contribution of this thesis is the demonstration that biomass in the Miombo ecoregion is not dominated by a few exceptionally large stems. Even in wet Miombo, where tall trees contribute strongly to biomass, the share of biomass stored by the largest 1% of stems slightly decreased across the rainfall gradient. This contrasts sharply with humid tropical forests, where a small cohort of emergent giants often accounts for a disproportionate share of AGB.

By showing that biomass in wet Miombo is distributed across many medium and large stems rather than a few hyper-dominant individuals, this thesis refines prevailing assumptions about biomass–structure relationships in tropical woodlands. Biomass accumulation along the rainfall gradient reflects broad demographic progression into higher size classes, not the emergence of rare, extremely large trees.

In dry Miombo, small trees, shrubs, and saplings contribute substantially to total AGB, up to 30% in Namibian sites. These components are invisible to traditional inventory protocols that exclude stems <5

cm DBH, resulting in substantial underestimation of carbon storage. This finding underscores the need to revise forest monitoring standards and adopt multilayer biomass accounting in dry woodland systems.

6.4.2 Implications for Forest Dynamics: Fire as a Structural Filter

Chapters 2–4 collectively show that fire shapes the structural trajectory of Miombo woodlands by constraining vertical development. Frequent burning reduces total AGB by limiting sapling survival and preventing individuals from transitioning into medium and tall size classes, while leaving biomass stored in the largest trees largely intact. In dry regions, this interaction between fire and water limitation reinforces a shrub-dominated understorey and a compressed vertical profile.

TLS analyses reveal the mechanism: recurrent burning, less moisture availability, and drough can creates open, heterogeneous canopies with high gap fraction, promoting subcanopy proliferation but restricting recruitment into the upper canopy. These results provide empirical support for the fire-trap mechanism and demonstrate that understanding the vertical and horizontal distribution of vegetation is essential for explaining productivity, recruitment, and resilience in Miombo woodlands.

6.4.3 Implications for Remote Sensing: Structural Controls on Spaceborne LiDAR Performance

Chapter 5 shows that GEDI canopy height errors are not random but rather reflect the structural conditions documented in Chapters 2–4. Underestimation in dry and open woodlands is driven by sparse tall trees, vertically compressed foliage, and discontinuous canopies that reduce the contribution of true canopy tops to waveform energy. Overestimation in wet, dense forests arises from ground-signal occlusion under closed canopies.

This demonstrates a direct, causal link between ecological gradients and remote-sensing error patterns. GEDI signals “inherit” the complexity of the Miombo ecoregion. As a result, canopy height products must be calibrated against regional conditions rather than applied globally without adjustment. My Random Forest models (Chapter 5) confirm this, showing that incorporating environmental and structural covariates dramatically improves predictions of canopy height. This finding has major implications for biomass mapping, national forest monitoring systems, and REDD+ baselines, all of which increasingly rely on LiDAR-derived canopy height.

6.4.4 Implications for Management, Conservation, and Carbon Accounting

The findings have significant consequences for Miombo forest management and carbon accounting. In dry Miombo, nearly one-third of total AGB is stored in small stems, saplings, and shrubs, components excluded from most national inventory protocols. Their omission leads to systematic and substantial underestimation of carbon stocks, undervaluing dry woodlands in climate reporting and carbon-credit schemes. Revising inventory approaches to include these components is therefore essential for accurate carbon assessment.

The thesis also shows that fire management has an influence on the long-term capacity of woodlands to accumulate biomass. Frequent burning reduces the number of individuals that can grow beyond small and intermediate size classes, thereby constraining the development of taller strata. This reduces future carbon gains even when current carbon stocks appear stable. Fire management strategies that reduce burn frequency or create refuge for sapling growth will therefore have a long-term impact on carbon sequestration, structural complexity, and woodland persistence.

A further implication concerns the reliability of remote-sensing products. The analyses show that GEDI systematically underestimates canopy height in dry, open woodlands and overestimates it under closed, wet canopies. These errors are structural and predictable, reflecting the influence of canopy openness, vegetation layering, and terrain. For this reason, regional calibration of LiDAR-based height models is essential. Without such calibration, national carbon maps and biomass models will inherit systematic biases that compromise MRV (Monitoring, Reporting, Verification) systems under REDD+ and other global frameworks.

6.5 Limitations and Directions for Future Research

Although this thesis provides new insight into the climatic controls, disturbance dynamics, structural complexity, and remote-sensing detectability of Miombo ecoregion, several limitations offer avenues for further research. These are summarised below:

- Spatial coverage of field data can be expanded.

Regional analyses in Chapters 2 and 5 relied on extensive SEOSAW data, but certain vegetation types remain underrepresented. Increasing plot coverage in these areas would improve estimates of rainfall-

structure-biomass relationships. In the same direction, it is also important to add plots, especially in the intermediate rainfall gradient (700 – 1000 MAP) to better clarify whether the shrub-to-sapling shift documented here represents a universal Miombo pattern or localised dynamics driven by site history and management.

The TLS analyses in Chapter 4 provide unprecedented insight into foliage distribution and canopy-subcanopy interactions but were restricted to Namibian sites. Applying similar voxel- and CHM-based analyses across the rainfall gradient would test whether the relationships identified here, such as the opposing effects of gap fraction and entropy on subcanopy density, hold across the wider ecoregion.

- Growth pathways and recruitment bottlenecks deserve longer-term monitoring.

Chapters 2 and 4 suggest that many Miombo trees remain confined in the 1–4 m height band due to repeated fire and water limitation. Long-term demographic studies, using permanent plots or repeated TLS scans, are necessary to quantify transition rates between size classes and to determine the conditions that allow individuals to escape the lower strata.

- Tree allometry and wood-density variation need refinement.

Wood density and height-diameter relationships influence AGB estimates, particularly in systems dominated by multi-stemmed species. Collecting species-specific woody density and allometry for shrubs, small trees, and fire-resprouting species would reduce uncertainty in biomass estimation, especially in dry Miombo, where these forms dominate.

- GEDI calibration should incorporate multi-sensor fusion.

While Chapter 5 demonstrates that combining GEDI with ancillary variables improves canopy height predictions, future work should explore fusion with ICESat-2 photon-counting LiDAR and Sentinel-1 radar to capture canopy top, vertical structure, and ground signals simultaneously. This would be particularly valuable in open woodlands with strong gap dynamics.

- Slope and topographic complexity require targeted evaluation.

The strong influence of slope on GEDI error indicates that elevation-driven biases may influence canopy maps in hilly Miombo landscapes. Dedicated studies should assess how terrain correction, footprint orientation, and multi-angle acquisitions could reduce these errors.

- Protocols for forest inventory should be revised to include stems <5 cm DBH.

Chapter 3 demonstrates that excluding small stems leads to severe underestimation of biomass in dry Miombo. Future research should design and test revised inventory protocols that balance accuracy with field efficiency, especially for national forest monitoring systems under REDD+.

- Climate change impacts on Miombo structure remain poorly understood.

Given projected increases in aridity and fire frequency across southern Africa, modelling studies are needed to assess how changing rainfall and disturbance regimes will affect biomass allocation, recruitment pathways, and canopy height. Future research should also investigate feedback mechanisms, whereby changes in biomass, canopy height, and vegetation structure influence local climate conditions and disturbance regimes, particularly fire behaviour and microclimate dynamics.

6.6 Concluding remarks

This thesis examined how climatic gradients, disturbance regimes, and vegetation structure shape biomass distribution and canopy height in the Miombo ecoregion. By combining regional plot networks, detailed field inventories, TLS measurements, and spaceborne LiDAR, it provides an integrated view of woodland structure across scales.

The findings show that biomass patterns in Miombo ecoregion arise from broad demographic contributions rather than exceptionally large trees, and that frequent fire and low rainfall constrain vertical development. These structural conditions also influence the performance of spaceborne LiDAR, with GEDI accuracy improving substantially once environmental and structural context is accounted for.

Overall, this work clarifies the ecological drivers of Miombo ecoregion structure and demonstrates the value of combining ground-based and remote-sensing data for carbon and forest monitoring. Continued integration of fine-scale field measurements with emerging satellite technologies will be essential for capturing the complexity of these dry tropical woodlands.

6.7 References

Adam, M., Urbazaev, M., Dubois, C., & Schmullius, C. (2020). Accuracy Assessment of GEDI Terrain Elevation and Canopy Height Estimates in European Temperate Forests: Influence of Environmental and Acquisition Parameters. Remote Sensing, 12(23), 3948. https://doi.org/10.3390/rs12233948

Archibald, S., Lehmann, C. E. R., Gómez-Dans, J. L., & Bradstock, R. A. (2013). Defining pyromes and global syndromes of fire regimes. Proceedings of the National Academy of Sciences, 110(16), 6442–6447. https://doi.org/10.1073/pnas.1211466110

Archibald, S., Roy, D. P., Van Wilgen, B. W., & Scholes, R. J. (2009). What limits fire? An examination of drivers of burnt area in Southern Africa. Global Change Biology, 15(3), 613–630. https://doi.org/10.1111/j.1365-2486.2008.01754.x

Bastin, J.-F., Barbier, N., Réjou-Méchain, M., Fayolle, A., Gourlet-Fleury, S., Maniatis, D., De Haulleville, T., Baya, F., Beeckman, H., Beina, D., Couteron, P., Chuyong, G., Dauby, G., Doucet, J.-L., Droissart, V., Dufrêne, M., Ewango, C., Gillet, J. F., Gonmadje, C. H., … Bogaert, J. (2015). Seeing Central African forests through their largest trees. Scientific Reports, 5(1), 13156. https://doi.org/10.1038/srep13156

Bond, W. J., & Midgley, G. F. (2012). Carbon dioxide and the uneasy interactions of trees and savannah grasses. Philosophical Transactions of the Royal Society B: Biological Sciences, 367(1588), 601–612. https://doi.org/10.1098/rstb.2011.0182

Chave, J., Réjou-Méchain, M., Búrquez, A., Chidumayo, E. N., Colgan, M. S., Delitti, W. B. C., Duque, A., Eid, T., Fearnside, P. M., Goodman, R. C., Henry, M., Martínez-Yrízar, A., Mugasha, W. A., Muller-Landau, H. C., Mencuccini, M., Nelson, B. W., Ngomanda, A., Nogueira, E. M., Ortiz-Malavassi, E., … Vieilledent, G. (2014). Improved allometric models to estimate the aboveground biomass of tropical trees. Global Change Biology, 20(10), 3177–3190. https://doi.org/10.1111/gcb.12629

Clarke, P. J., Lawes, M. J., Midgley, J. J., Lamont, B. B., Ojeda, F., Burrows, G. E., Enright, N. J., & Knox, K. J. E. (2013). Resprouting as a key functional trait: How buds, protection and resources drive persistence after fire. New Phytologist, 197(1), 19–35. https://doi.org/10.1111/nph.12001

Colgan, M. S., Asner, G. P., Levick, S. R., Martin, R. E., & Chadwick, O. A. (2012). Topo-edaphic controls over woody plant biomass in South African savannas. Biogeosciences, 9(5), 1809–1821. https://doi.org/10.5194/bg-9-1809-2012

Dubayah, R., Armston, J., Healey, S., Bruening, J. M., Patterson, P., Kellner, J., Duncanson, L., Saarela, S., Ståhl, G., Yang, Z., Tang, H., Blair, J., Fatoyinbo, L., Goetz, S., Hancock, S., Hansen, M., Hofton, M., Hurtt, G., & Luthcke, S. (2022). GEDI launches a new era of biomass inference from space. Environmental Research Letters. https://doi.org/10.1088/1748-9326/ac8694

Dubayah, R., Blair, J. B., Goetz, S., Fatoyinbo, L., Hansen, M., Healey, S., Hofton, M., Hurtt, G., Kellner, J., Luthcke, S., Armston, J., Tang, H., Duncanson, L., Hancock, S., Jantz, P., Marselis, S., Patterson, P. L., Qi, W., & Silva, C. (2020). The Global Ecosystem Dynamics Investigation: High-resolution laser ranging of the Earth's forests and topography. Science of Remote Sensing, 1, 100002. https://doi.org/10.1016/j.srs.2020.100002

Franz, T. E., King, E. G., Caylor, K. K., & Robinson, D. A. (2011). Coupling vegetation organization patterns to soil resource heterogeneity in a central Kenyan dryland using geophysical imagery. Water Resources Research, 47(7), 2010WR010127. https://doi.org/10.1029/2010WR010127

Frost, P. (1996). The ecology of miombo woodlands. In The Miombo in transition: Woodlands and Welfare in Africa (B. Campbell, pp. 11–57). Centre for International Forestry Research.

Godlee, J. L., Ryan, C. M., Bauman, D., Bowers, S. J., Carreiras, J. M. B., Chisingui, A. V., Cromsigt, J. P. G. M., Druce, D. J., Finckh, M., Gonçalves, F. M., Holdo, R. M., Makungwa, S., McNicol, I. M., Mitchard, E. T. A., Muchawona, A., Revermann, R., Ribeiro, N. S., Siampale, A., Syampungani, S., … Dexter, K. G. (2021). Structural diversity and tree density drives variation in the biodiversity–ecosystem function relationship of woodlands and savannas. New Phytologist, 232(2), 579–594. https://doi.org/10.1111/nph.17639

Hancock, S., Armston, J., Hofton, M., Sun, X., Tang, H., Duncanson, L. I., Kellner, J. R., & Dubayah, R. (2019). The GEDI Simulator: A Large-Footprint Waveform Lidar Simulator for Calibration and Validation of Spaceborne Missions. Earth and Space Science, 6(2), 294–310. https://doi.org/10.1029/2018EA000506

Hofton, M., & Blair, J. B. (2019). Algorithm Theoretical Basis Document (ATBD) for GEDI Transmit and Receive Waveform Processing for L1 and L2 Products. https://lpdaac.usgs.gov/documents/581/GEDI_WF_ATBD_v1.0.pdf

Kindermann, L., Dobler, M., Niedeggen, D., & Linstädter, A. (2022). A new protocol for estimation of woody aboveground biomass in disturbance-prone ecosystems. Ecological Indicators, 135, 108466. https://doi.org/10.1016/j.ecolind.2021.108466

Lang, N., Jetz, W., Schindler, K., & Wegner, J. D. (2023). A high-resolution canopy height model of the Earth. Nature Ecology & Evolution, 7(11), 1778–1789. https://doi.org/10.1038/s41559-023-02206-6

Li, W., Duveiller, G., Wieneke, S., Forkel, M., Gentine, P., Reichstein, M., Niu, S., Migliavacca, M., & Orth, R. (2024). Regulation of the global carbon and water cycles through vegetation structural and physiological dynamics. Environmental Research Letters, 19(7), 073008. https://doi.org/10.1088/1748-9326/ad5858

Liu, A., Cheng, X., & Chen, Z. (2021). Performance evaluation of GEDI and ICESat-2 laser altimeter data for terrain and canopy height retrievals. Remote Sensing of Environment, 264, 112571. https://doi.org/10.1016/j.rse.2021.112571

Liu, J., Gao, G., Wang, S., Jiao, L., Wu, X., & Fu, B. (2018). The effects of vegetation on runoff and soil loss: Multidimensional structure analysis and scale characteristics. Journal of Geographical Sciences, 28(1), 59–78. https://doi.org/10.1007/s11442-018-1459-z

Lutz, J. A., Furniss, T. J., Johnson, D. J., Davies, S. J., Allen, D., Alonso, A., Anderson-Teixeira, K. J., Andrade, A., Baltzer, J., Becker, K. M. L., Blomdahl, E. M., Bourg, N. A., Bunyavejchewin, S., Burslem, D. F. R. P., Cansler, C. A., Cao, K., Cao, M., Cárdenas, D., Chang, L., … Zimmerman, J. K. (2018). Global importance of large-diameter trees. Global Ecology and Biogeography, 27(7), 849–864. https://doi.org/10.1111/geb.12747

Martín-Queller, E., Gil-Tena, A., & Saura, S. (2011). Species richness of woody plants in the landscapes of Central Spain: The role of management disturbances, environment and non-stationarity: Landscape species richness: forest management and environmental factors. Journal of Vegetation Science, 22(2), 238–250. https://doi.org/10.1111/j.1654-1103.2010.01242.x

Mayr, M. J., Malß, S., Ofner, E., & Samimi, C. (2018). Disturbance feedbacks on the height of woody vegetation in a savannah: A multi-plot assessment using an unmanned aerial vehicle (UAV). International Journal of Remote Sensing, 39(14), 4761–4785. https://doi.org/10.1080/01431161.2017.1362132

Mugasha, W. A., Eid, T., Bollandsås, O. M., Malimbwi, R. E., Chamshama, S. A. O., Zahabu, E., & Katani, J. Z. (2013). Allometric models for prediction of above- and belowground biomass of trees in the

miombo woodlands of Tanzania. Forest Ecology and Management, 310, 87–101. https://doi.org/10.1016/j.foreco.2013.08.003

Potapov, P., Li, X., Hernandez-Serna, A., Tyukavina, A., Hansen, M. C., Kommareddy, A., Pickens, A., Turubanova, S., Tang, H., Silva, C. E., Armston, J., Dubayah, R., Blair, J. B., & Hofton, M. (2021). Mapping global forest canopy height through integration of GEDI and Landsat data. Remote Sensing of Environment, 253, 112165. https://doi.org/10.1016/j.rse.2020.112165

Ribeiro, N. S., Shugart, H. H., & Washington-Allen, R. (2008). The effects of fire and elephants on species composition and structure of the Niassa Reserve, northern Mozambique. Forest Ecology and Management, 255(5–6), 1626–1636. https://doi.org/10.1016/j.foreco.2007.11.033

Ryan, C. M., & Williams, M. (2011). How does fire intensity and frequency affect miombo woodland tree populations and biomass? Ecological Applications, 21(1).

Sankaran, M., Hanan, N. P., Scholes, R. J., Ratnam, J., Augustine, D. J., Cade, B. S., Gignoux, J., Higgins, S. I., Le Roux, X., Ludwig, F., Ardo, J., Banyikwa, F., Bronn, A., Bucini, G., Caylor, K. K., Coughenour, M. B., Diouf, A., Ekaya, W., Feral, C. J., … Zambatis, N. (2005). Determinants of woody cover in African savannas. Nature, 438(7069), 846–849. https://doi.org/10.1038/nature04070

Scholes, R. J., Dowty, P. R., Caylor, K., Parsons, D. A. B., Frost, P. G. H., & Shugart, H. H. (2002). Trends in savanna structure and composition along an aridity gradient in the Kalahari. Journal of Vegetation Science, 13(3), 419–428. https://doi.org/10.1111/j.1654-1103.2002.tb02066.x

SEOSAW partnership. (2021). A network to understand the changing socio-ecology of the southern African woodlands (SEOSAW): Challenges, benefits, and methods. PLANTS, PEOPLE, PLANET, 3(3), 249–267. https://doi.org/10.1002/ppp3.10168

Shetie, G. M., Dondeyne, S., Nyssen, J., Vancampenhout, K., & Deckers, J. (2017). Elucidating woody vegetation patterns in relation to soil and topography in tropical Africa: The case of Nech Sar National Park (Ethiopia). Plant Ecology and Evolution, 150(1), 45–58. https://doi.org/10.5091/plecevo.2017.1162

Slik, J. W. F., Paoli, G., McGuire, K., Amaral, I., Barroso, J., Bastian, M., Blanc, L., Bongers, F., Boundja, P., Clark, C., Collins, M., Dauby, G., Ding, Y., Doucet, J., Eler, E., Ferreira, L., Forshed, O., Fredriksson, G., Gillet, J., … Zweifel, N. (2013). Large trees drive forest aboveground biomass variation in moist lowland forests across the tropics. Global Ecology and Biogeography, 22(12), 1261–1271. https://doi.org/10.1111/geb.12092

Tao, S., Guo, Q., Li, C., Wang, Z., & Fang, J. (2016). Global patterns and determinants of forest canopy height. Ecology, 97(12), 3265–3270. https://doi.org/10.1002/ecy.1580

Vatandaslar, C., Narin, O. G., & Abdikan, S. (2023). Retrieval of forest height information using spaceborne LiDAR data: A comparison of GEDI and ICESat-2 missions for Crimean pine (Pinus nigra) stands. Trees, 37(3), 717–731. https://doi.org/10.1007/s00468-022-02378-x

Wang, C., Elmore, A. J., Numata, I., Cochrane, M. A., Shaogang, L., Huang, J., Zhao, Y., & Li, Y. (2022). Factors affecting relative height and ground elevation estimations of GEDI among forest types across the conterminous USA. GIScience & Remote Sensing, 59(1), 975–999. https://doi.org/10.1080/15481603.2022.2085354

Yang, C., Peng, D., Zhang, N., Chen, M., Zeng, W., Sun, X., Li, L., & Li, W. (2025). Performance evaluation and improvement of ICESat-2 and GEDI forest canopy height retrievals in Northeast China. GIScience & Remote Sensing, 62(1), 2497603. https://doi.org/10.1080/15481603.2025.2497603